UNIVERSITY OF BIRMINGHAM

Preparation, characterisation and secondary crystallisation of PHB based copolymers and carbohydrate blends

By

Annabel Victoria Lucy Fitzgerald

A thesis submitted to the University of Birmingham for the degree of

Doctor of Philosophy

School of Metallurgy and Materials

College of Engineering and Physical Sciences

University of Birmingham

June 2017

Synopsis

Poly(hydroxybutyrate) copolymers are sustainable and biodegradable, but they are known to exhibit secondary crystallisation, a phenomenon that severely reduces the ductility of the material to such an extent that it hinders commercial use of these polymers. Therefore, the main focus of this research was to explore a number of strategies to control the secondary crystallisation behaviour of two Poly(hydroxybutyrate) based copolymers. The over-arching theme was the use of additives that are also biodegradable and non-toxic ie GRAS molecules.

Blends of P(HB-co-HV)(3 wt % HV) with carbohydrate molecules of varying chain lengths (glucose, fructose, maltose, melezitose and CAB) were prepared by melt blending, characterised, and monitored over time to assess the capability of the additives to reduce the secondary crystallisation process. The miscibility, crystallisation kinetics, morphology, rheological, chemical, thermal and mechanical behaviour of the blends were determined. Additives were found to hinder the secondary crystallisation process, with a chain length effect observed within P(HB-co-HV)/ saccharide blends. As the number of monomer units in the saccharide chain increased, the percentage change in E_b following 1 year of storage at ambient temperature was reduced from a 70 % change in the unblended P(HB-co-HV) material, to a 40 % change in blends containing the trisaccharide. All carbohydrate based additives slowed the crystallisation process, most notably in blends containing CAB 15 wt %, which was found to increase the crystallisation half-life from 3 seconds in P(HB-co-HV) to 938 seconds in blends during isothermal crystallisation at 140 ºC.

The effect of storage temperature on the secondary crystallisation behaviour of P(HB-co-HHx)(33 % HHx) was also reported. Samples were stored at a range of storage temperatures (-22, 7, 25, 50, 75 and 100 ºC), and the effects on thermal, chemical and mechanical

properties discussed. Increasing storage temperature caused the secondary process to occur to a greater extent, with greater increases in the melting temperature which increased from 128 ºC to 135 ºC in samples stored at 100 ºC compared minimal changes observed within samples stored at 7 ºC (128 – 128 ºC). Sub-melting point degradation of the material was also noted by a reduction in UTS from 24 MPa to 21 MP following 28 days of storage at 100 ºC, indicative of chain scission, while samples stored at lower temperatures increased in UTS in accordance with the secondary crystallisation process.

In summary, this work has explored two PHB co-polymers with commercial potential, P(HB-co-HV) and P(HB-co-HHx). The work has significance in terms of the applicability of these polymer systems to the field of disposable food packaging materials where the secondary crystallisation process and the associated property deterioration would be highly detrimental. The novel concept of using GRAS additives within P(HB-co-HV) as a measure to control the secondary crystallisation process forms a foundation for further work, with additives of longer chain length at higher concentrations being the most successful at hindering the process. Furthermore, it was shown for the first time that the secondary crystallisation process in P(HB-co-HHx) accelerates with increasing temperature, with sub-melting point degradation becoming apparent as the temperature approaches that of the melting.

Acknowledgements

I would like to thank Dr Mike Jenkins for the opportunity to study for this PhD, and his guidance, support and patience throughout. A special thanks to Dr Catherine Kelly for all of her help, knowledge, advice and friendship which have been invaluable to me during the completion of this work. I am also extremely grateful to Mr Frank Biddlestone for his lab based help and expertise over the years and for the funding received from the EPSRC that made this work possible.

Thank you to my family for always believing in me, and whose love and support has never faltered. Finally, a sincere thank you to my friends who have been with me every step of the way and given me the strength to keep going through what has been an extremely tough four years.

Abbreviations

ATR	Attenuated Total Reflectance
BN	Boron Nitride
BPA	Bisphenol A
C=O	Carbonyl group
CAB	Cellulose Acetate Butyrate
CH_3	Methyl group
CO_2	Carbon dioxide
DCP	Dicumyl Peroxide
DMTA	Dynamic Mechanical Thermal Analysis
DSC	Differential Scanning Calorimetry
E	Young's modulus
E'	Storage modulus
Ea	Activation energy
E_b	Elongation to break
F	Fluorine
FDA	US Food and Drug Administration
FTIR	Fourier Transform Infra-Red Spectroscopy
GRAS	Generally Recognised as Safe
^{1}H NMR	Proton Nuclear Magnetic Resonance Spectroscopy
HA	Hydroxyacid
HB	Hydroxybutyrate
H-bonding	Intermolecular hydrogen bonding

HCAB	High molecular weight Cellulose Acetate Burtyrate
HHx	Hydroxyhexanoate
HMF	Hydroxymethylfurfural
HV	Hydroxyvalerate
3-hydroxyacyl-CoA	3-hydroxyacyl-coenzyme A
IR	Infra-Red
K value	Crystallisation rate constant
K_g	Nucleation factor
LCAB	Low molecular weight Cellulose Acetate Butyrate
mcl	Medium chain length
Mr	Molecular mass
MRR	Melt, re-crystallisation and re-melting
M_w	Molecular weight
N	Nitrogen
O	Oxygen
OH	Hydroxyl groups
P(3HB)	Poly(3-hydroxybutyrate)
P(3HB-co-3HD)	Poly(3-hydroxybutyrate-co-3-hydroxydecanoate)
P(3HB-co-3HHx)	Poly(3-hydroxybutyrate-co-3-hydroxyhexanoate)
P(3HB-co-3HO)	Poly(3-hydroxybutyrate-co-3-hydroxyoctanoate)
P(3HB-co-3HV)	Poly(3-hydroxybutyrate-co-3-hydroxyvalerate)
P(3HD)	Poly(3-hydroxydecanoate)
P(3HHx)	Poly(3-hydroxyhexanoate)
P(3HO)	Poly(3-hydroxyoctanoate)
P(3HV)	Poly(3-hydroxyvalerate)

PEG	Poly(ethylene Glycol)
PET	Polyethylene Terephthalate
PHA	Poly(hydroxyalkanoate)
PLA	Poly(lactic acid)
PP	Polypropylene
PTFE	Polytetrafluoroethylene
scl	Short chain length
SEM	Scanning Electron Microscopy
$\mathbf{t_{1/2}}$	Crystallisation half life
$\mathbf{T_c}$	Melt crystallisation temperature
$\mathbf{T_{cc}}$	Cold crystallisation temperature
$\mathbf{T_g}$	Glass transition temperature
$\mathbf{T_m}$	Melting temperature
$\mathbf{T_m^0}$	Equilibrium melting temperature
UTS	Ultimate tensile stress
wt %	Weight percent
$\mathbf{X_c}$	Degree of crystallinity
$\mathbf{\Delta H_c}$	Enthalpy of crystallisation
$\mathbf{\Delta H_f}$	Enthalpy of fusion

Contents

Chapter 1
Introduction

1.0 Poly(hydroxyalkanoates) 1

1.1 An introduction to Poly(hydroxyalkanoates) 1

1.1.1 Structure of PHAs 3

1.1.1.1 Chemical structure 3

1.1.1.2 Categorisation due to chemical structure 4

1.2 Poly(hydroxybutyrate) 5

1.2.1 Introduction to Poly(hydroxybutyrate) 5

1.2.2 Crystallisation in PHB 6

1.2.3 Properties of PHB 8

1.3 Current barriers to the commercial use of PHB 10

1.3.1 Inherent brittleness 10

1.3.1.1 Chemical structure 10

1.3.1.2 Nucleation density and spherulitic cracking 10

1.3.2 Secondary crystallisation 12

1.3.2.1 The problem of secondary crystallisation 12

1.3.2.2 Mechanisms of secondary crystallisation 13

1.3.3 Thermal stability 14

1.4 Potential application areas of PHB related polymers 15

1.5 Solutions to enhance commercial potential of PHB 16

1.5.1 Nucleating agents 16

1.5.2 Copolymerisation 18

1.5.2.1 Poly(hydroxybutyrate-co-hydroxyvalerate) 20

1.5.2.2 Poly(hydroxybutyrate-co-hydroxyhexanoate) 21

1.5.3 Crosslinking 26

1.5.3.1 Cross-linking by intermolecular by intermolecular hydrogen bonding 27

1.5.3.2 Cross-linking with polysaccharides 28

1.5.3.2.1 Starch 29
1.5.3.2.2 Cellulose Acetate Butyrate 34
1.6 Scope of this work 37
1.7 References 40

Chapter 2

Materials and Methods

2.1 Materials 48
2.1.1 PHB Copolymers 48
2.1.2 Additives 48
2.2 Calculating blend quantities 49
2.2.1 Determination of the amount of cross-linker required 49
2.2.2 Calculation of cross-link ratios in P(HB-co-HV)/saccharide blends 51
2.2.3 Quantities in P(HB-co-HV)/CAB blends 53
2.3 Production of P(HB-co-HV) based blends 54
2.3.1 Experimental Technique 54
2.3.2 Method 55
2.4 Sample preparation 55
2.4.1 Solvent casting versus melt casting 55
2.4.2 Experimental technique 58
2.4.3 Procedure 59
2.4.4 Press cooling rate 60
2.5 Time dependent studies 62
2.5.1 P(HB-co-HV) studies 62
2.5.2 P(HB-co-HHx) studies 62
2.6 Differential Scanning Calorimetry 62
2.6.1 Experimental technique 62
2.6.2 Method 64
2.6.2.1 Dynamic Measurements 64

2.6.2.2 Isothermal Measurements 66
2.7 Dynamic Mechanical Thermal Analysis 68
2.7.1 Experimental technique 68
2.7.2 Method 68
2.8 Rheology 69
2.8.1 Experimental technique 69
2.8.2 Method 69
2.9 Tensile Testing 70
2.9.1 Experimental technique 70
2.9.2 Method 71
2.10 Fourier Transform Infra-Red Spectroscopy: Attenuated Total Reflection 72
2.10.1 Experimental technique 72
2.10.2 Method 72
2.11 Hot stage microscopy 73
2.11.1 Experimental technique 73
2.11.2 Method 73
2.12 Scanning Electron Microscopy 74
2.12.1 Experimental technique 74
2.12.2 Method 74
2.13 References 76

Chapter 3

The effect of incorporating saccharides into P(HB-co-HV) on the secondary crystallisation process

3.0 Introduction 77
3.1 Results and Discussion 81
3.1.1 Characterisation of blend components 81
3.1.2 Sample production 82
3.1.3 Characterisation of the blends – Day 0 86

3.1.3.1 Dynamic DSC analysis - Melting 86
3.1.3.2 Dynamic DSC analysis – Melt Crystallisation 92
3.1.3.3 Fourier-Transform Infra-red Spectroscopy 97
3.1.3.4 Rheology 104
3.1.3.5 Mechanical properties 109
3.1.3.6 Scanning Electron Microscopy 115
3.1.4 Secondary crystallisation behaviour of P(HB-co-HV)/ saccharide blends 117
3.1.4.1 DSC analysis 117
3.1.4.2 Mechanical properties 119
3.2 Conclusions 127
3.3 References 130

Chapter 4

Binary blends of P(HB-co-HV) and CAB: Effects on properties and secondary crystallisation behaviour

4.0 Introduction 134
4.1 Results and Discussion 136
4.1.1 The effect of CAB on the materials properties prior to storage 136
4.1.1.1 Thermal properties 136
4.1.1.1.1 Dynamic measurements 136
4.1.1.1.2 Isothermal measurements 151
4.1.2 Mechanical properties 162
4.1.3 Fourier transform Infra-Red Spectroscopy (FTIR) 168
4.1.4 Morphology 172
4.1.4.1 Hot stage microscopy 172
4.1.4.2 Scanning Electron Microscopy (SEM) 177
4.1.5 Effect of CAB on the materials properties over time 180
4.1.5.1 Thermal Properties 180
4.1.5.2 Mechanical properties 186
4.2 Conclusions 189

4.3 References **192**

Chapter 5

Influence of temperature on the secondary crystallisation behaviour of P(HB-co-HHx)

5.0 Introduction **195**
5.1 Results **198**
5.1.1 Characterisation of P(HB-co-HHx) 198
5.1.1.1 Optimising processing conditions of P(HB-co-HHx) 198
5.1.1.2 Exploring Sample variability 202
5.1.2 Effect of storage temperature on P(HB-co-HHx) over time 208
5.1.2.1 Thermal Properties 208
5.1.2.1.1 Melting 208
5.1.2.1.2 Melt crystallisation 206
5.1.2.1.3 Chemical changes 223
5.1.2.1.4 Visual inspection 226
5.1.2.2 Mechanical Properties 227
5.2 Conclusions **237**
5.3 References **240**

Chapter 6

Conclusions and Further Work

6.1 Conclusions **242**
6.2 Future Work **245**

List of Figures

Chapter 1

Introduction

Figure 1.1.	Accumulation of PHA granules observed by TEM	1
Figure 1.2.	A schematic diagram of the fundamental components of a PHA granule; Green spheres - phospholipids, purple spheres - PHA phasin proteins, blue spheres - PHA synthase proteins	2
Figure 1.3.	Generic chemical structure of PHAs	3
Figure 1.4.	The chemical structure of Poly(3-hydroxybutyrate)	6
Figure 1.5.	A schematic diagram to illustrate the morphology of a polymer spherulite a) whole spherulite b) individual lamellar with amorphous material (blue) and crystalline material (red)	7
Figure 1.6.	A proposed model structure for the lamellar of PHB with a) adjacent re-entry chain folding and b) random re-entry (or 'switchboard') chain folding across lamellar thickness 'l'	8
Figure 1.7.	Change in mechanical properties to PHB with storage from 0 - 300 days	13
Figure 1.8.	Mechanisms of secondary crystallisation a) impinged spherulites b) regular distribution of amorphous and crystalline material c) lamellar thickening d) lamellar insertion	14
Figure 1.9.	Effect of storage time at ambient temperature on the mechanical properties of P(HB-co-HV) (8 mol %)	21
Figure 1.10.	The chemical structure of P(HB-co-HHx)	22
Figure 1.11.	Stress strain behaviour of P(HB-co-HHx) (8.1 mol %) following storage after 11 days	24
Figure 1.12.	Effect on increasing co-monomer content on the T_g of P(HB-co-HHx) over time	25
Figure 1.13.	Chemical structure of Bisphenol A	28
Figure 1.14.	The chemical structures of the two components of natural starch a) amylose b) amylopectin	29
Figure 1.15.	Chemical structure of glucose	33
Figure 1.16.	The chemical structure of CAB	34

Chapter 2

Materials and Methods

Figure 2.1.	A schematic diagram of a counter-rotating twin screw compounder	54
Figure 2.2	Example of layer assembly used to create flat polymer samples by hot pressing	59
Figure 2.3.	Cooling profile of the hydraulic press from 180 ºC to room temperature simulating the cooling conditions undergone by the P(HB-co-HV) samples and blends	61
Figure 2.4.	Cooling profile of the hydraulic press from 170 ºC to room temperature simulating the cooling conditions undergone by the P(HB-co-HHx) samples	61
Figure 2.5.	DSC sample chamber showing the sample (S) and reference (R) cells	63
Figure 2.6.	A typical DSC trace of a semi-crystalline polymer illustrating T_m and X_c were determined	64
Figure 2.7.	DSC trace showing the determination of T_g	66
Figure 2.8.	An example stress strain curve and how it is used to determine mechanical properties of a sample	70

Chapter 3

The effect of incorporating saccharides into P(HB-co-HV) on the secondary crystallisation process

Figure 3.1.	Chemical structures of a) BPA and b) Starch	78
Figure 3.2.	Chemical structures of a) glucose b) fructose c) maltose d) melezitose	80
Figure 3.3.	The melting endotherms of the blend components analysed at 10 ºC/min	81
Figure 3.4.	Photographs of sample plaques produced a) P(HB-co-HV) b) glucose c)fructose d) maltose e) melezitose	82
Figure 3.5.	Reaction mechanism for the thermal dehydration of glucose to HMF	85
Figure 3.6.	DSC traces of P(HB-co-HV) and glucose blends obtained by heating at 10 ºC/min	87
Figure 3.7.	DSC traces of P(HB-co-HV) and fructose blends obtained by heating at 10 ºC/min	88
Figure 3.8.	DSC traces of P(HB-co-HV) and maltose blends obtained by	89

heating at 10 ºC/min

Figure 3.9. DSC traces of P(HB-co-HV) and melezitose blends obtained by heating at 10 ºC/min 90

Figure 3.10. A schematic diagram of the possible locations of impurities showing the rejection of impurities into the inter-spherulitic regions (left) and the presence of the impurity within the amorphous inter-lamellar regions of the spherulite 91

Figure 3.11. DSC traces of P(HB-co-HV) and glucose blends at each concentration obtained by cooling at 10 ºC/min 93

Figure 3.12. DSC traces of P(HB-co-HV) and fructose blends at each concentration obtained by cooling at 10 ºC/min 94

Figure 3.13. DSC traces of P(HB-co-HV) and maltose blends at each concentration obtained by cooling at 10 ºC/min 95

Figure 3.14. DSC traces of P(HB-co-HV) and melezitose blends at each concentration obtained by cooling at 10 ºC/min 96

Figure 3.15. FTIR spectra of P(HB-co-HV)/glucose blends at each composition. Red (P(HB-co-HV)), light (low), middle (medium), dark (high) 98

Figure 3.16. FTIR spectra of P(HB-co-HV)/fructose blends at each composition. Red (P(HB-co-HV)), light (low), middle (medium), dark (high) 99

Figure 3.17. FTIR spectra of P(HB-co-HV)/maltose blends at each composition. Red (P(HB-co-HV)), light (low), middle (medium), dark (high) 99

Figure 3.18. FTIR spectra of P(HB-co-HV)/melezitose blends at each composition. Red (P(HB-co-HV)), light (low), middle (medium), dark (high) 100

Figure 3.19. FTIR spectra of the carbonyl region of saccharide blends at medium concentrations displaying the evolution of crotonic acid 101

Figure 3.20. FTIR spectra of crotonic acid in the carbonyl region 102

Figure 3.21. FTIR spectra of the hydroxyl region in P(HB-co-HV)/glucose blends 103

Figure 3.22. FTIR spectra of D-Glucose in the hydroxyl region 104

Figure 3.23. Rheological data of P(HB-co-HV) and blends with glucose analysed at a frequency of 10 Hz 105

Figure 3.24. Rheological data of P(HB-co-HV) and blends with fructose analysed at a frequency of 10 Hz 106

Figure 3.25. Rheological data of P(HB-co-HV) and blends with maltose analysed at a frequency of 10 Hz 106

Figure 3.26. Rheological data of P(HB-co-HV) and blends with melezitose analysed at a frequency of 10 Hz 107

Figure 3.27. The effect of increasing the number of repeat units in the additive chain on the shear viscosity at medium concentrations 108

Figure 3.28. The stress/strain behaviour of P(HB-co-HV)/maltose blends 110

Figure 3.29. The modes of fracture observed in samples of P(HB-co-HV) with impinged spherulites following tensile testing and etching: Circumferential propagation (a-b), transpherulitic propagation (c-d) and interspherulitic propagation (e-f) 112

Figure 3.30. Effect of increasing unit chain length and increasing concentration on the E_b of the blends at day 0 113

Figure 3.31. Effect of increasing chain length and concentration on the toughness on day 0 113

Figure 3.32. Effect of increasing additive chain length and increasing concentration on the UTS of the blends at day 0 114

Figure 3.33. Effect of increasing additive chain length and increasing concentration on the Young's modulus at day 0 114

Figure 3.34. SEM images of the fracture surfaces of P(HB-co-HV)(a-c) blended with glucose (d-f), fructose (g-i), and maltose (j-l) at 600, 1500 and 6,000 x magnification (from left to right) 116

Figure 3.35. Effect of blending P(HB-co-HV) with glucose on the change in T_m over time 118

Figure 3.36. Effect of blending P(HB-co-HV) with glucose on the change in crystallinity over time 119

Figure 3.37. Change in values for elongation to break upon storage at ambient temperature over time 120

Figure 3.38. Percentage change in elongation to break from the original day 0 values 120

Figure 3.39. Change in values for toughness upon storage at ambient temperature over time 121

Figure 3.40. Percentage change in toughness from original day 0 values 121

Figure 3.41. Change in values for UTS upon storage at ambient temperature over time 122

Figure 3.42. Percentage change in UTS from original day 0 values 122

Figure 3.43. Change in values for Young's modulus following storage at ambient temperature over time 123

Figure 3.44. Percentage change in Young's modulus from original day 0 values 123

Figure 3.45. Effect of additive chain length on the percentage change in E_b following storage at ambient temperature for 336 days 125

Figure 3.46. Effect of additive chain length on the percentage change in toughness following storage at ambient temperature for 336 days 125

Figure 3.47. Effect of additive chain length on the percentage change in UTS following storage at ambient temperature for 336 days 126

Figure 3.48. Effect of chain length on the percentage change in Young's modulus following storage at ambient temperature for 336 days 126

Chapter 4

Binary blends of P(HB-co-HV) and CAB: Effects on properties and secondary crystallisation behaviour

Figure 4.1.	The chemical structure of CAB	135
Figure 4.2.	A DSC trace showing the T_g of amorphous CAB measured at 10 ºC/min	136
Figure 4.3.	A DSC trace showing the T_m of semi-crystalline P(HB-co-HV) measured at 10 ºC/min	137
Figure 4.4.	The effects of blending on the T_m of the blends measured at 10 ºC/min	138
Figure 4.5.	The effects of blending on the thermal transitions of the blends measured at 50 °C/min	139
Figure 4.6.	The effects of CAB content on the degree of crystallinity of P(HB-co-HV)	140
Figure 4.7.	The effect of CAB content on the T_m of P(HB-co-HV) from heating at 10 and 50 ºC/min	140
Figure 4.8.	The effect of CAB content on the T_g of P(HB-co-HV) as measured by the peak in Tan δ measured at 1 Hz	144
Figure 4.9.	DMTA data to show the effect of CAB content on E' of the blends measured at 1 Hz	144
Figure 4.10.	The effect of CAB composition on the loss modulus (E') of the blends	146
Figure 4.11.	The Tan δ data for P(HB-co-HV) used for the calculations of Ea of P(HB-co-HV) and its blends with CAB at each concentration.	148
Figure 4.12.	An Arrhenius plot showing the Ea of P(HB-co-HV) and its blends with CAB	148
Figure 4.13.	The effect of CAB content on the T_c of the blend following cooling at 10 ºC/min	150
Figure 4.14.	Isothermal crystallisation of P(HB-co-HV). Samples held at temperatures between 140 ºC and 148 ºC for 120 minutes	152
Figure 4.15.	Isothermal crystallisation behaviour of P(HB-co-HV)/ CAB blends at 5 wt % CAB. Samples held at temperatures between 132 and 140 ºC for 120 minutes	153
Figure 4.16.	Isothermal crystallisation behaviour of P(HB-co-HV)/ CAB blends at 10 wt % CAB. Samples held at temperatures between 132 and 140 ºC for 120 minutes	153
Figure 4.17.	Isothermal crystallisation behaviour of P(HB-co-HV)/ CAB blends at 15 wt % CAB. Samples held at temperatures between 132 and 140 ºC for 120 minutes	154

Figure 4.18. Effect of CAB content on the isothermal crystallisation behaviour at 140 ºC for 120 minutes 155

Figure 4.19. The effect of CAB content on the $t_{1/2}$ of P(HB-co-HV) at 140 ºC for 120 minutes 157

Figure 4.20. The effect of CAB content on the Avrami exponent of P(HB-co-HV) during isothermal crystallisation at 140 ºC for 120 minutes 159

Figure 4.21. A Hoffman-Weeks plot of P(HB-co-HV) and the CAB blends to establish T_m^0 160

Figure 4.22. The effect of CAB content on the tensile properties of the blends 163

Figure 4.23. The effect of CAB content on the E_b of P(HB-co-HV)/ CAB blends prior to storage 164

Figure 4.24. The effect of CAB content on the Young's Modulus of the P(HB-co-HV)/ CAB blends prior to storage 165

Figure 4.25. The the effect of CAB content on the UTS of P(HB-co-HV)/ CAB blends prior to storage 166

Figure 4.26. The effect of CAB content on the toughness of P(HB-co-HV)/CAB blends prior to storage 167

Figure 4.27. FTIR spectrum showing the effect of blending on the carbonyl peak 169

Figure 4.28. FTIR spectra of the PHB intramolecular hydrogen bonding region 171

Figure 4.29. FTIR spectrum of the region assigned to intramolecular bonding within CAB 172

Figure 4.30. P(HB-co-HV) in the melt at 180 °C 173

Figure 4.31. Fully crystallised P(HB-co-HV) analysed under hot stage. Sample cooled from 180 °C to 25 °C at 50 °C/min 173

Figure 4.32. Cooling of P(HB-co-HV)/CAB (5 wt %) from the melt. a) melt state at 180 °C b) intermediate state at 115 °C and c) fully crystallised at 25 °C. Scale bars represent 25 µm. 174

Figure 4.33. A CAB droplet leaching into the P(HB-co-HV) 175

Figure 4.34. Optical microscopy of a) and d) CAB 10 wt % and b) and c) CAB 15 wt %. The scale bars represent 25 µm 176

Figure 4.35. The fracture surface of P(HB-co-HV) under SEM at 10,000 x magnification 177

Figure 4.36. The fracture surface of CAB under SEM at 10,000 x magnification 178

Figure 4.37. SEM images of CAB blends presenting pull out holes a) CAB 5 wt % b) CAB 10 wt %, c & d) 15 wt % 179

Figure 4.38. The effect of CAB content on the T_m of the blends over time 181

Figure 4.39. The effect of CAB content on the X_c of the blends over time 182

Figure 4.40. Change in the shape of the melting endotherm over time in the P(HB-co-HV) heated at 10 °C/min 183

Figure 4.41. Change in the shape of the melting endotherm over time in the 184

P(HB-co-HV)/ CAB 5 wt % blend heated at 10 ºC/ min

Figure 4.42. Change in the shape of the melting endotherm over time in the P(HB-co-HV)/ CAB 10 wt % blend heated at 10 °C/min 184

Figure 4.43. Change in the shape of the melting endotherm over time in the P(HB-co-HV)/ CAB 15 wt % blend heated at 10 ºC/min 185

Figure 4.44. The effect of increasing CAB concentration on the E_b of the blends over time 186

Figure 4.45. The effect of increasing CAB content on the toughness of the blends over time 187

Figure 4.46. The effect of increasing CAB concentration on the E of the blends over time 187

Figure 4.47. The effect of increasing CAB content on the UTS of the blends over time 188

Chapter 5

Influence of temperature on the secondary crystallisation behaviour of P(HB-co-HHx)

Figure 5.1. The chemical structures of a) P(HB-co-HV) and b) P(HB-co-HHx) 195

Figure 5.2. Cis-elimination reaction of polyesters 196

Figure 5.3. The T_m of P(HB-co-HHx) resulting from the above processing conditions obtained by heating at 10 ºC/min 200

Figure 5.4. The T_m of P(HB-co-HHx) resulting from the above processing conditions obtained by heating at 50 ºC/min 200

Figure 5.5. The T_c of P(HB-co-HHx) following processing at the above conditions by cooling at 10 ºC/min 201

Figure 5.6. Locations of samples within the plaque 202

Figure 5.7. Inter-plaque variation within a sample plaque 203

Figure 5.8. Variability in elongation to break within the same sample plaque 206

Figure 5.9. Variability in toughness within the same sample plaque 206

Figure 5.10. Variability in UTS within the same sample plaque 207

Figure 5.11. Variability in Young's modulus within the same sample plaque 207

Figure 5.12. Effect of storage temperature on the T_{m1} and $T_{m\,2}$ over 28 days in samples stored at -22 ºC (blue), 7 ºC (green), 25 ºC (yellow), 50 ºC (orange), 75 ºC (brown) and 100 ºC (red) 209

Figure 5.13. Change in crystallinity over time at each storage temperature 210

Figure 5.14. Melting temperature of P(HB-co-HHx) stored at -22 ºC over time 212

Figure 5.15. Melting temperature of P(HB-co-HHx) over time at 100 ºC 212

Figure 5.16. DSC experiment examining the effect of partial melting on the annealing peak in P(HB-co-HHx) for samples a) isothermally crystallised at 60 ºC and b) partially melted at 90 ºC for 10 mins following isothermal crystallisation at 60 ºC 214

Figure 5.17. Final melting endotherms following 28 days at each storage temperature 215

Figure 5.18. Effect of storage temperature on the appearance of a shoulder at 25 ºC and above following 28 days of storage 216

Figure 5.19. Change in the shape of the melting endotherm following storage of P(HB-co-HHx) at -22 ºC for 28 days 217

Figure 5.20. Change in shape of the melting endotherm following storage of P(HB-co-HHx) at 100 ºC for 28 days 217

Figure 5.21. Change in T_c over time at each storage temperature 219

Figure 5.22. T_c of P(HB-co-HHx) following storage at -22 ºC over time 220

Figure 5.23. T_c of P(HB-co-HHx) following storage at 100 ºC over time 221

Figure 5.24. Effect of storage temperature on T_c of P(HB-co-HHx) following storage for 28 days 222

Figure 5.25. Effect of storage temperature on the ΔH_c of P(HB-co-HHx) following storage at each temperature for 28 days 222

Figure 5.26. FTIR Spectra of the carbonyl peak for samples stored at -22 ºC over time. Day 0 (blue) Day 28 (red) 223

Figure 5.27. FTIR Spectra of the 1230 – 1160 cm^{-1} range located within the fingerprint region for samples stored at -22 ºC over 28 days. Day 0 (blue) Day 28 (red) 224

Figure 5.28. FTIR spectra of the carbonyl peak for samples stored at 25 ºC over time. Day 0 (blue) Day 28 (red) 224

Figure 5.29. FTIR spectra of the 1230-1160 cm^{-1} range located within the fingerprint region for samples stored at 25 ºC over 28 days. Day 0 (blue) Day 28 (red) 225

Figure 5.30. FTIR spectra of the carbonyl peak for samples stored at 100 ºC over time. Day 0 (blue) Day 28 (red) 225

Figure 5.31. FTIR spectra of the 1240 - 1150 cm^{-1} range located within the fingerprint region for samples stored at 100 ºC over 28 days. Day 0 (blue) Day 28 (red) 226

Figure 5.32. Effect of high temperature storage on the appearance and opacity of P(HB-co-HHx). Comparisons between samples post processing prior to storage (Day 0) and those stored at -22 ºC and 100 ºC for 28 days 227

Figure 5.33. Change in elongation to break over time at each storage temperature 228

Figure 5.34. Percentage change in elongation to break over time at each storage temperature 229
Figure 5.35. Change in toughness over time at each sample temperature 230
Figure 5.36. Percentage change in toughness over time at each storage temperature 231
Figure 5.37. Change in E over time at each storage temperature 233
Figure 5.38. Percentage change in E over time at each storage temperature 234
Figure 5.39. Change in UTS over time at each storage temperature 236
Figure 5.40. Percentage change in UTS over time at each storage temperature 236

List of Tables

Chapter 1

Introduction

Table 1.1.	Examples of the most commonly examined PHA monomers	4
Table 1.2.	Comparisons of PHB with commercial isotactic Polypropylene	9
Table 1.3.	The chemical formulae of the most widely researched PHB based copolymers	18
Table 1.4.	Comparison of mechanical and thermal properties of the main PHB copolymers produced by the solvent casting technique	19

Chapter 2

Materials and Methods

Table 2.1.	Crosslink ratios calculated for this work	50
Table 2.2.	Molecular mass data required for further calculation of required additives	51
Table 2.3.	The quantities of P(HB-co-HV) and additive within each blend	53
Table 2.4.	Comparison of properties obtained via different processing techniques of PHB	57
Table 2.5.	Summary of pressing conditions for all materials used	60

Chapter 3

The effect of incorporating saccharides into P(HB-co-HV) on the secondary crystallisation process

Table 3.1.	The melting temperatures of the blend components analysed at 10 ^{o}C/min	82
Table 3.2.	The caramelisation temperatures of the saccharides used within this work	84
Table 3.3.	Thermal properties of P(HB-co-HV) and glucose blends	87
Table 3.4.	Thermal properties of P(HB-co-HV) and fructose blends	88

Table 3.5.	Thermal properties of P(HB-co-HV) and maltose blends	89
Table 3.6.	Thermal properties of P(HB-co-HV) and melezitose blends	90
Table 3.7.	Thermal properties obtained upon melt crystallisation in P(HB-co-HV) and glucose blends	94
Table 3.8.	Thermal properties obtained upon melt crystallisation of P(HB-co-HV) and fructose blends	95
Table 3.9.	Thermal properties obtained upon melt crystallisation of P(HB-co-HV) and maltose blends	96
Table 3.10.	Thermal properties obtained upon melt crystallisation of P(HB-co-HV) and melezitose blends	97
Table 3.11.	Effect of blending on the position of the carbonyl peak	100
Table 3.12.	A summary of the possible interactions occurring between the blend components identified by a range of characterisation techniques. Green: interaction observed. Red: interaction not observed. Grey: not obtainable with this technique	128

Chapter 4

Binary blends of P(HB-co-HV) and CAB: Effects on properties and secondary crystallisation behaviour

Table 4.1.	The effect of CAB content on the thermal properties of P(HB-co-HV) binary blends	141
Table 4.2.	The effect of CAB content on the T_g of the blends at 1 Hz	145
Table 4.3.	The effect of CAB content on the loss modulus of the blends at 40 ºC	146
Table 4.4.	The effect of CAB content on the Ea of the blends	149
Table 4.5.	The effect of CAB content on the T_c of the blends	151
Table 4.6.	Effect of CAB content on the induction time for isothermal crystallisation at 140 ºC over 120 minutes	155
Table 4.7.	The effect of CAB content on the $t_{1/2}$ during isothermal crystallisation at 140 ºC for 120 minutes	158
Table 4.8.	The effect of CAB content in the Avrami exponent (n) and Rate constant (z) during isothermal crystallisation at 140 ºC for 120 minutes	159
Table 4.9.	The effect of CAB on the T_m^0 of P(HB-co-HV)	161
Table 4.10.	A summary of the mechanical properties of the P(HB-co-HV)/CAB blends prior to storage	168
Table 4.11.	Values for the position of the carbonyl peak in each blend	169
Table 4.12.	A summary of the change in T_m over time for each blend	181

Table 4.13. A summary of the change in X_c over time for each blend 182

Table 4.14. A summary of the percentage change in values following 168 days of storage at 25 ºC 188

Chapter 5

Influence of temperature on the secondary crystallisation behaviour of P(HB-co-HHx)

Table 5.1. A summary of the thermal properties of the P(HB-co-HHx) material 201

Table 5.2. Change in T_g over time at each storage temperature 211

Table 5.3. Initial and final values for E_b at each storage temperature after 28 days 230

Table 5.4. Initial and final values for toughness at each storage temperature after 28 days 232

Table 5.5. Initial and final values for E at each storage temperature after 28 days 235

Table 5.6. Initial and final values for UTS at each storage temperature after 28 days 237

Chapter 1
Introduction

1.0 Poly(hydroxyalkanoates)

1.1 An introduction to Poly(hydroxyalkanoates)

Poly(hydroxyalkanoates)(PHAs) are a family of aliphatic bio-polyesters that are naturally synthesised by a variety of bacterial strains (e.g. *Cupravidis necator*) as an intracellular energy reserve, under conditions where nitrogen is limited, but an excess of carbon sources (such as fructose) are provided (Taidi, Mansfield et al. 1995). Limiting nitrogen encourages the bacteria to utilise as much of the carbon source as possible and turn it into a PHA, which it can then access as its energy source when required. Industrially, this is achieved via bacterial fermentation. The polymer accumulates as discrete, water-insoluble granules (White granules, Figure 1.1), with some bacteria accumulating up to 80 % of their dry cell mass (Bucci, Tavares et al. 2005). The number of granules per cell and the approximate size can vary among different bacterial species, however up to 13 granules ranging from 0.2 to 0.5 μm in diameter have been observed in *Cupravidis necator* (Lee 1996).

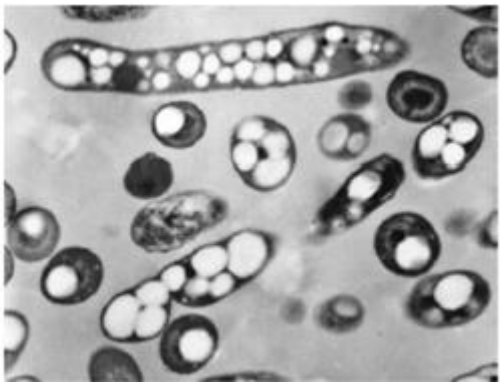

Figure 1.1. Accumulation of PHA granules observed by Transmission electron microscopy (Taidi, Mansfield et al. 1995)

According to bioaccumulation studies, these granules consist of an outer coating of phospholipids, and other proteins known as PHA synthases and PHA phasins surrounding the amorphous polymer in the centre (Figure 1.2). PHA synthase enzymes are responsible for the synthesis of PHAs (Tian, Sinskey et al. 2005). There are two proposed mechanisms (micelle and budding models) for the formation of these granules within the cytoplasm, but the correct mechanism is still unclear and remains a topic for further research (Tian, Sinskey et al. 2005).

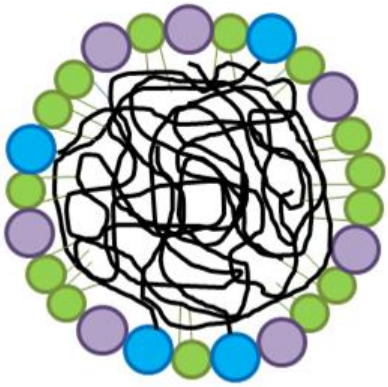

Figure 1.2. A schematic diagram of the fundamental components of a PHA granule; Green spheres - phospholipids, purple spheres - PHA phasin proteins, blue spheres - PHA synthase proteins

In addition, PHAs possess the ability to biodegrade fully within biologically active environments into harmless molecules such as water and CO_2 as a result of its hydrolysable backbone (Lee 1996). PHAs can be completely biodegraded by a variety of microorganisms within a year depending on the conditions used, unlike their synthetic counterparts which can take several decades to degrade, if at all (Suriyamongkol, Weselake et al. 2007). This natural and renewable production method, coupled with their inherent biodegradability gives PHAs a distinct advantage over their non-renewable, non-biodegradable competitors as sustainability becomes an issue of global importance.

1.1.1 Structure of PHAs

1.1.1.1 Chemical structure

The general chemical structure of PHAs can be seen in Figure 1.3. They are linear molecules with isotactic stereoregularity, which results from the stereospecificity of the biosynthetic enzymes found within the bacteria. This leads to the monomer hydroxyacid (HA) units occurring exclusively in the D(-) configuration (Lee 1996).

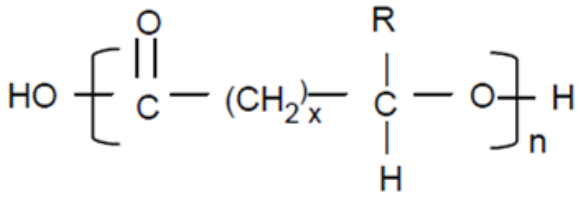

Figure 1.3. Generic chemical structure of PHAs (Lee 1996)

With reference to Figure 1.3, the structures of the main members of the PHA family can be described (Table 1.1). The -R group is commonly located on the 3rd carbon in these materials (on the 3rd Carbon away from the ester functional group), indicated by the '3' located in the naming of each material. In most commercially relevant polymers, x = 1, while the –R group varies in length, allowing for PHAs with a diverse range of properties to be produced. The molecular weights of the polymers are in the range of 2×10^5 to 3×10^6 Daltons, depending on the microorganism and the growth conditions used (Lee 1996).

Table 1.1. Examples of the most commonly examined PHA monomers

PHA	Abbreviation	x	-R
Poly(3-hydroxybutyrate)	P(3HB)	1	$-CH_3$
Poly(3-hydroxyvalerate)	P(3HV)	1	$-CH_2CH_3$
Poly(3-hydroxyhexanoate)	P(3HHx)	1	$-CH_2CH_2CH_3$
Poly(3-hydroxyoctanoate)	P(3HO)	1	$-(CH_2)_4CH_3$
Poly(3-hydroxydecanoate)	P(3HD)	1	$-(CH_2)_6CH_3$

1.1.1.2 Categorisation due to chemical structure

Bacterial PHAs can be sub-categorised by chain length into short chain length (scl-), and medium chain length (mcl-) PHAs. Short chain length PHAs contain 3-5 Carbon atoms within each repeat unit of the chain, whereas medium chain length PHAs contain between 6-14 Carbon atoms (Mittendorf, Robertson et al. 1998, Ashby, Solaiman et al. 2002). This therefore means polymers with a diverse range of properties can be produced. For example, the mcl-PHAs tend to be semi-crystalline elastomers with a low melting point, low tensile strength and high elongation to break, whereas scl-PHAs have higher melting points and are more brittle due to higher degrees of crystallinity (Lee 1996). The properties of scl-PHAs more closely resemble those of conventional petrochemical polymers, whereas mcl-PHAs are generally classed as elastomers and rubbers (Suriyamongkol, Weselake et al. 2007).

The category of PHA produced is determined by the bacterial strain used in the fermentation process. This is due to the PHA synthase enzyme in different bacteria species possessing different substrate specificities, meaning they can only metabolise certain feedstock materials to produce polymer. For example, the PHA synthase enzyme in *Cupravidis necator* only reacts with a narrow range of substrates, with chain lengths of C3-C5, and prefers C4

substrates (Suriyamongkol, Weselake et al. 2007). This means that mcl-PHAs cannot be produced within this species without genetic modification. Strains such as *Pseudomonas oleovorans* and *Pseudomonas aeruginosa* however allow incorporation of larger units as they directly utilise intermediates from the fatty acid β-oxidation pathway, thus allowing them to form larger molecules of 3-hydroxyacyl-CoA, leading to increased polymer chain length (Suriyamongkol, Weselake et al. 2007). Examples of currently available PHAs can be seen in Table 1.1, where P(3HB)and P(3HV) are scl-PHAs, while P(3HHx), P(3HO) and P(3HD) are classified as mcl-PHAs. Of these PHA's, P(3HB) is the most broadly studied, and thus is one of the very few PHAs that has been produced on a large enough scale for commercial use (Bugnicourt, Cinelli et al. 2014).

1.2 Poly(hydroxybutyrate)

1.2.1 Introduction to Poly(hydroxybutyrate)

Poly(hyroxybutyrate) (P(3HB)) is a linear semi-crystalline polymer with high isotactic regularity (Figure 1.4). It was first characterised by Lemoigne in the 1920's, and then later commercialised in 1981 by ICI under the trade name Biopol. *Cupravidis necator* is a common bacterial species used to produce P(3HB) due to its ability to produce high yields (Dawes 1988). Glucose or fructose can be used as the excess carbon source in the fermentation process to produce the monomer (Chanprateep 2010, Keshavarz and Roy 2010, Batcha, Prasad et al. 2014). Due to ongoing concerns over diminishing petrochemical resources, there is a need to find sustainable alternatives to synthetic polymers for the future of plastic products. Thus, P(3HB), as naturally produced and biodegradable material, has received much attention across varying applications, namely packaging. Approximately 30 % of all plastics used worldwide are for packaging applications (Shah, Hasan et al. 2008), meaning there is a market for sustainable materials, especially in high volume, single use,

disposable products which currently contribute to a large amount of plastic waste (Bucci, Tavares et al. 2005). A feature of P(3HB) that makes it attractive for this application as well as its natural accumulation and clean biodegradation is its low water permeability, an inherent property resulting from its high degree of crystallinity. However, despite its obvious advantages regarding sustainability, P(3HB) has never made it into widely used commercial products.

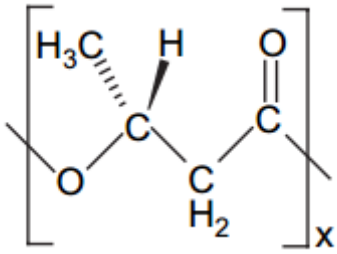

Figure 1.4. The chemical structure of Poly(3-hydroxybutyrate) (Hu, Zhang et al. 2007)

1.2.2 Crystallisation in P(3HB)

As P(3HB) is a semi-crystalline material, it has regions of disordered chains (amorphous regions), as well as highly ordered regions of tightly packed chains (crystalline regions) that arrange themselves into structures known as spherulites (Figure 1.5a) during cooling from the melt following processing. Crystallisation is the process by which, upon cooling, an ordered (i.e., crystalline) solid phase is produced from a liquid melt. In this process, intramolecular hydrogen bonding causes chain folding, resulting in the highly ordered lamellar structure (Figure 1.5b). The crystallisation of a molten polymer occurs by nucleation and growth processes. On cooling through the melting temperature, (assuming a purely homogenous material) nuclei form from chain entanglements. These nuclei grow and interactions occur causing the chains to align into the ordered lamellar structures, which subsequently grow out radially and branch creating the spherulitic structures characteristic of semi-crystalline

materials. P(3HB) forms large banded spherulites on crystallisation from the melt, sometimes reaching diameters of several millimetres due to a low nucleation density (El-Hadi, Schnabel et al. 2002). In semi-crystalline polymers, the proportion of each phase varies between polymers, and processing conditions, but the crystallinity of P(3HB) generally resides between 60% and 80 % (Barham, Barker et al. 1992)

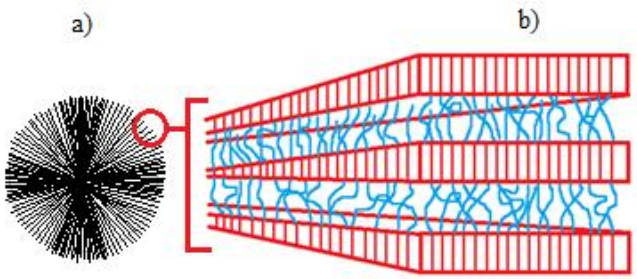

Figure 1.5. A schematic diagram to illustrate the morphology of a polymer spherulite a) whole spherulite b) individual lamellar with amorphous material (blue) and crystalline material (red)

During the formation of lamellar crystals, the chains align perpendicularly to the lamellar base and, due to space restriction, the chains fold back on themselves to fit into the area (Figure 1.6a). The switchboard model (Figure 1.6b) describing a degree of random chain re-entry to the melt crystallised lamellae is thought to be most likely, although some adjacent re-entry may also be present with loose and tight folds (Harris 1995). When P(3HB) crystallises, it is held in a crystal lattice via intramolecular hydrogen bonding between the methyl ($-CH_3$) group in one helical structure, and the carbonyl (C=O) group in the other helical structure. The polymer adopts a 2/1 helical structure in an orthombic unit cell ($P2_12_12_1$) with crystallographic dimensions a = 5.76 Å, b = 13.20 Å, and c = 5.96 Å determined by X-ray crystallographic analysis (Harris 1995).

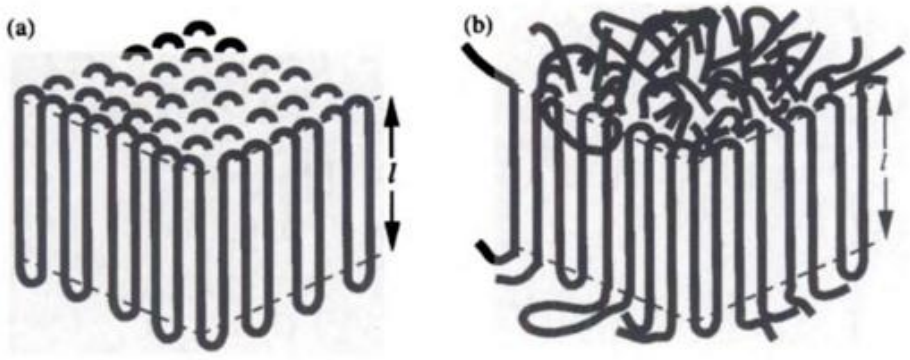

Figure 1.6. A proposed model structure for the lamellar of P(3HB) with a) adjacent re-entry chain folding and b) random re-entry (or 'switchboard') chain folding across lamellar thickness 'l' (Wilkinson 1998)

Aggregation of chains, and thus crystallisation is therefore favoured by symmetry and linearity within the chains, and is further encouraged by groups which allow intermolecular interactions. These intermolecular interactions hold the chains together in a lattice, and are significant in maintaining chain confirmation. In contrast, branching and high molar mass inhibits the development of crystallinity through their exclusion from the lattice. Chain tacticity, bulkiness of side groups and polarity also affect crystallinity and ease of crystallisation through restriction of the close packing of the chains required for crystallisation to occur. The isotacticity of P(3HB) results in the monomer units being able to align which forms a highly ordered structure responsible for its materials properties, which are discussed below.

1.2.3 Properties of P(3HB)

Another advantage of P(3HB) is that it possesses thermal properties comparable to synthetic polymers, in particular Polypropylene (PP) (Table 1.2) (Thompson 2003, Gunaratne, Shanks et al. 2004, Bregg 2006, Callister and Rethwisch 2008, Calhoun 2010, Robertson 2012, Ineos 2013). Similarities observed in melting temperature (T_m) and tensile strength are particularly

advantageous. Furthermore, P(3HB) is also water insoluble. Due to the high crystallinity of P(3HB), it has an excellent resistance to solvents, and the oxygen permeability is very low in comparison to other commercial packaging materials such as PP and Low density polyethylene (LDPE)(Table 1.2), making P(3HB) a suitable material for oxygen sensitive products. P(3HB) also has low water vapour permeability compared to other bio-based polymers.(Shen 2009).

Table 1.2. Comparisons of P(3HB) with commercial isotactic Polypropylene

Property	P(3HB)	PP	LDPE
Melting point (°C)	170-180	160-165	115
Glass transition (°C)	0-5	-18	-110
Crystallinity (%)	60-80	40-70	55-70
Tensile strength (MPa)	40	31-41	8-31
Elongation to break (%)	6	100-600	100-650
Young's Modulus (MPa)	3500	1300	170-280
O_2 diffusion (cm^3 m^{-2} atm^{-1} d^{-1})	45	1700	3900-13000
Water diffusion (g mm m^{-2} d^{-1})	1.16	0.59	6.0-23.2

Investigations into bioaccumulation of P(3HB) have reported that the native granules exist within the cytoplasm in a metastable amorphous state (Tian, Sinskey et al. 2005, Jendrossek

2009). However, once isolated from the bacterial cell, a semi-crystalline material forms with a high degree of crystallinity residing between 60 and 80 %. Whilst this degree of crystallinity provides P(3HB) with excellent barrier properties, this results in a stiff and brittle material, giving rise to low values for elongation to break (E_b) of around 6 % and high values for Young's modulus compared to PP and LDPE (Table 1.2) (Lee 1996). These properties present significant barriers to the commercialisation, and these will be explored in more detail in the following section.

1.3 Current barriers to the commercial use of P(3HB)

1.3.1 Inherent brittleness

1.3.1.1 Chemical structure

P(3HB) once extracted, is a naturally brittle material as shown in Table 1.2. This occurs as a result of its chemical structure. The chains are completely linear and the chiral centres are 100 % stereospecific (only possessing the –D stereochemical configuration) resulting in polymer that is completely isotactic, and therefore capable of crystallising readily through close packing of chains via intramolecular hydrogen bonding (de Koning and Lemstra 1993). The high degree of crystallinity therefore produces a rigid material that is inherently brittle leading to the low values for elongation at break observed (Table 1.2). This is currently a major barrier to the commercial use of P(3HB). It is therefore of importance to over-come this inherent brittleness found within P(3HB) for it to be able to compete with its petrochemical counterparts.

1.3.1.2 Nucleation density and spherulitic cracking

P(3HB) and its copolymers crystallise slowly, creating large brittle spherulites following crystallisation from the melt, as a result of its inherently low nucleation density. Furthermore,

commercially these polymers are produced by batch fermentation to give an extremely pure material, which results in a general absence of impurities that could act as nucleating agents. Lower nucleation density leads to decreased crystallisation rate, and thus larger spherulites which have less mechanical stability. This can however be influenced by the super-cooling of the material during processing, which will be discussed in a later section. The slow crystallisation also has implications for the processing of the material, as it will remain tacky for longer causing the material to stick to itself during the processing of a film, for example.

Furthermore, it has been found that cracks (crazes) appear in the spherulites upon growth during cooling from the melt using hot stage microscopy (Bassett 1988). These cracks grow and join together under tension, contributing to the mechanical failure of P(3HB). They have been found to run circumferentially around the edges of the spherulites, as well as running radially through them depending on the crystallisation temperature used. There is dispute however regarding the conditions that create each type of crack. In one study (cited in Bassett, 2012), it was reported that the cracks run radially in spherulites grown at temperatures below 120 ºC, and circumferentially in those produced at temperatures greater than 120 ºC. For the latter, the cracks only appeared when the spherulites had grown at least 35 μm in diameter. In contrast, Hobbs et al. (1996) found that circumferential cracks did occur at temperatures below 120 ºC (Hobbs, McMaster et al. 1996). The occurrence of such cracks could be attributed to the difference in radial and circumferential thermal expansion coefficients observed by Martinez – Salazar et al. (1989), which act to generate internal stresses on cooling. The radial co-efficient was found to be much larger than the circumferential one, leading to large tensile stresses in the radial direction, which is consequently relieved through circumferential cracking of the spherulite (Martinez-Salazar, Sanchez-Cuesta et al. 1989). Despite the inconsistency in the literature concerning the

mechanisms of formation of these cracks, it is apparent that they are present and further act to decrease the mechanical strength of the material.

1.3.2 Secondary crystallisation

1.3.2.1 The problem of secondary crystallisation

The properties of any new materials will need to match those of currently used materials within their applications, and remain stable over the products life time. This is where P(3HB) is at a distinct disadvantage. Following completion of the primary crystallisation process (impingement of spherulites), a secondary process termed 'secondary crystallisation' is widely reported to occur within the amorphous phase of the material during storage at ambient temperature. This occurs due to the low glass transition temperature (T_g) of P(3HB) (~4 ^{0}C), meaning that at ambient temperature, the polymer chains have sufficient mobility to allow the amorphous regions to re-organise, and thus crystallise over time, made easier by their highly regular chemical structure allowing close compaction of chains. This acts to progressively increase the overall degree of crystallinity, and causes embrittlement of the material (de Koning and Lemstra 1993, Biddlestone, Harris et al. 1996) as illustrated in Figure 1.7 by a significant decrease in elongation to break and increasing Young's modulus over 300 days at room temperature (de Koning and Lemstra 1993). The effects of this are apparent within the first day following storage, greatly limiting the applications of the polymer.

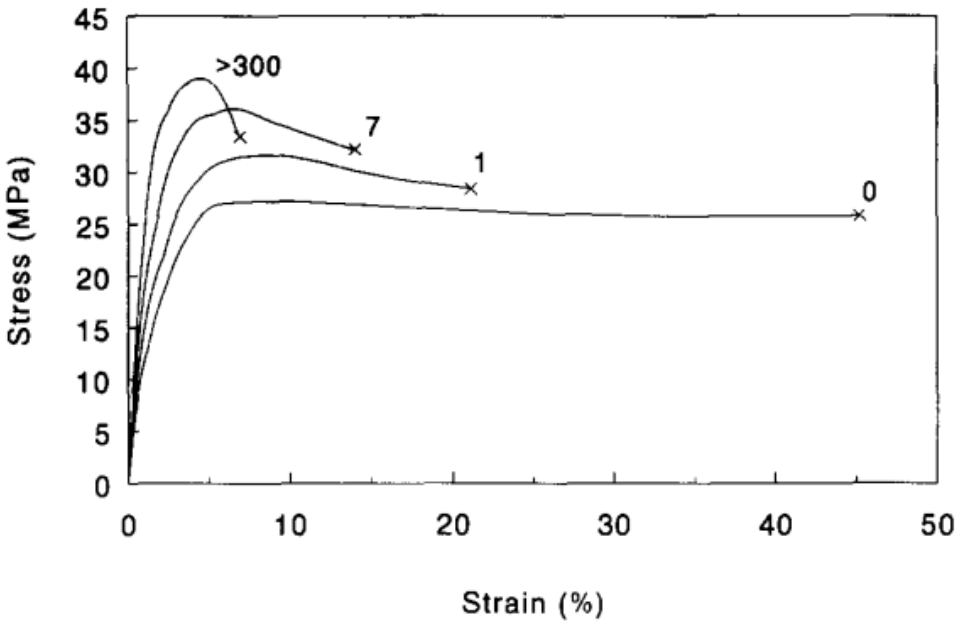

Figure 1.7. Change in mechanical properties to P(3HB) with storage from 0 - 300 days (de Koning and Lemstra 1993)

1.3.2.2 Mechanisms of secondary crystallisation

There are two dominant mechanisms of secondary crystallisation within P(3HB) as illustrated in Figure 1.8. Some studies report thickening of the original crystalline lamellar (Figure 1.8c), where the amorphous region is consumed in the process (Kolb, Wutz et al. 2001, Sics, Ezquerra et al. 2001). This has been characterised by a reduction in the intensity of α-relaxations within the amorphous polymer chains as crystallisation ensues (Sics, Ezquerra et al. 2001). The second mechanism is the growth of new thinner lamellae within the amorphous regions between dominant lamellar stacks formed during primary crystallisation (lamellar insertion – Figure 1.8d) (Wang, Hsiao et al. 1999, Kolb, Wutz et al. 2001, Sics, Ezquerra et al. 2001). Both of these mechanisms lead to an increase in crystal perfection, resulting in a further decrease in the ductility of the material via an increase in crystallinity.

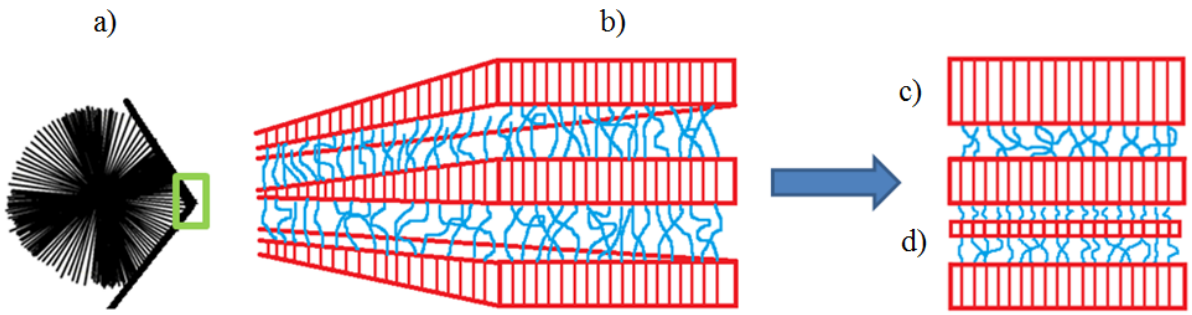

Figure 1.8. Mechanisms of secondary crystallisation a) impinged spherulites b) regular distribution of amorphous and crystalline material c) lamellar thickening d) lamellar insertion

Considering elastic properties are controlled by the amorphous fraction (bridge molecules) in semi-crystalline polymers (Špitalský and Bleha 2004) a reduction in the amorphous regions over time as they progressively secondary crystallise, inevitably leads to the aforementioned increases in brittleness and rigidity observed within the material upon storage (Bergmann and Owen 2004). It is therefore apparent that to enhance the commercial application of P(3HB), hindrance of secondary crystallisation is required.

De Koning and Lemstra (1992) while investigating the causes of embrittlement in P(3HB) monitored molecular weight during storage at room temperature. No reduction in molecular weight was observed throughout storage, ruling out chain scission as the cause of embrittlement.

1.3.3 Thermal instability

Another fundamental issue with P(3HB) is its thermal instability at elevated temperatures. It has been reported to degrade at temperatures around the T_m (180 ºC) into products such as crotonic acid (Grassie, Murray et al. 1984). Furthermore, with a decomposition temperature of around 220 ºC, this gives rise to a narrow processing window. Thermal degradation occurs

as a result of heating for a sustained period of time above the T_m, which has detrimental effects on the final properties of the material during melt processing. This therefore affects the processability and viability of the polymer, further hindering its larger industrial use.

Thermal instability and degradation of P(3HB) has been noted by a few studies (Grassie, Murray et al. 1984, Aoyagi, Yamashita et al. 2002, Abe 2006) which have reported P(3HB) to be susceptible to chain scission at elevated temperatures, suggesting degradation on processing as a possible cause of the brittleness of the material. Thermal degradation reduces the molecular weight (M_w) which then has a knock on effect on the materials properties (Grassie, Murray et al. 1984, Nguyen, Yu et al. 2002, Bugnicourt, Cinelli et al. 2014). For example, thermal degradation of P(3HB) has been quantified by drastic reductions in melt viscosity of more than 50 % when held at 180 °C for 5 minutes as a result of significant molecular weight decrease (Arakawa, Yokohara et al. 2008). It is therefore important to pay attention to the processing conditions of the material to avoid degradation as much as possible. This includes minimising the time the material is at elevated temperatures above the melting point and reducing the number of high temperature processing steps.

1.4 Potential application areas of P(3HB) related polymers

One application of particular interest for sustainable polymers is that of food packaging materials. P(3HB) looks to have great potential as a sustainable alternative due to its natural production and clean biodegradation. However, it is apparent from the above section, that currently, P(3HB) does not possess the thermal or mechanical properties to rival its petrochemical counterparts for such applications. Therefore, solutions to improve the properties of this polymer are required to improve its commercial viability, and any solutions used need to comply with strict food safety regulations and be Generally Recognised as Safe (GRAS) according to the FDA. The ISA-Pack project was a European funded research

project working towards the creation of novel sustainable food packaging using P(3HB) copolymers as the base material. The following work was conducted in conjunction with ISA-Pack, focusing on the research and development of sustainable and food safe materials as a viable alternative for food packaging applications.

1.5 Solutions to enhance commercial potential of P(3HB)

1.5.1 Nucleating agents

As previously mentioned, P(3HB) and copolymers crystallise slowly, creating large brittle spherulites due to a low nucleation density (Kai, He et al. 2005). This is because commercially these polymers are produced by a batch fermentation process to give an extremely pure material, which results in a general absence of heterogeneities that could act as nucleating agents. Furthermore, due to thermal instability of the material, the long dwell times required during processing to obtain a higher degree of crystal perfection are impractical and detrimental to the material (Withey and Hay 1999). Therefore, to achieve a greater rate of crystallisation, a nucleating agent must be added (Withey and Hay 1999).

In general, the addition of a nucleating agent has been found to be effective for accelerating crystallisation of polymers. Usually, a good nucleating agent provides a surface that reduces the free energy barrier to the primary nucleation process (hence lowering the Gibbs free energy), and thus nucleation density and rate is increased. Therefore, by adding a nucleating agent (heterogenous nucleation), the nucleation density increases and spherulite size decreases leading to more mechanically stable spherulites, and therefore an increase in strength and ductility of the material (Kai, He et al. 2005).

Kai et al. (2005) investigated the effect of two well-known nucleating agents (Talc and Boron Nitride (BN)) on the crystallisation kinetics of a common copolymer of P(3HB), P(3HB-co-

3HV) (6.9 mol% HV). They concluded that both agents improved the crystallisation with no changes to the crystal form of P(3HB-co-3HV), with BN being the most effective of the two (Kai et al, 2005; Liu et al, 2001). Upon Differential Scanning Calorimetry (DSC) analysis, they found that with the addition of both agents, the melt crystallisation temperature (T_{mc}) shifted to a higher temperature region, and the crystallisation peak became much sharper indicating that the crystallisation rate had increased, and that the diversity of the crystalline morphologies within (such as size and perfection of the spherulites and lamellar thickness) becomes narrower. The shifting of T_{mc} towards a higher temperature means that the polymer can crystallise more easily at lower supercooling, resulting in a reduction in the energy required to drive the crystallisation process (Liu, Yang et al. 2002).

Furthermore, upon examination of the isothermal crystallisation of blends with both nucleating agents, the K values (representing the crystallisation rate constant) increased dramatically at all crystallisation temperatures tested, while $t_{1/2}$(representing half the time required for maximum crystallisation to be achieved), decreased with the inclusion of nucleating agents. This indicates that the crystallisation rate of P(3HB-co-3HV) in the blends is much faster than without the nucleating agents at the same crystallisation temperature. BN was again the most effective nucleating agent crystallising P(3HB-co-3HV) 1.5 times faster than the blend supplemented with talc (Kai, He et al. 2005). Isothermal experiments conducted by Liu et al. (2001) showed the crystallisation temperatures had to be higher for BN blends than with the unblended material otherwise it would crystallise too fast, thus demonstrating the nucleating effect of BN. However a direct comparison between pure and blended material at the same temperature was not made in order to compare the rates.

Kai et al. (2005) used optical microscopy analysis to establish that the nucleation density of P(3HB-co-3HV) increases significantly upon blending with BN, demonstrating its ability to effectively enhance the crystallisation process and increase nucleation sites. Blends with talc

however produced results comparable to the unblended P(3HB-co-3HV), thus it was concluded that talc has a relatively low activity in initiating the crystallisation of P(3HB-co-3HV) (Kai, He et al. 2005). It can therefore be concluded that BN produces a greater effect on the nucleation of P(3HB) polymers than talc, and therefore to produce the most effective material as possible, material pre-nucleated with BN will be used in this work.

1.5.2 Copolymerisation

One way to alleviate the problem of secondary crystallisation whilst maintaining sustainability has been to copolymerise P(3HB) with other HA monomers described previously (Section 1.1.2) into the polymer backbone. Most of these have been produced on a laboratory scale, however a few of them have attracted industrial interest and been commercialised in the past decade (Shen, Zhang et al. 2009). Copolymers of P(3HB) with other PHAs are the most commercially important PHA copolymers, examples of which can be seen in Table 1.3.

Table 1.3. The chemical formulae of the most widely researched P(3HB) based copolymers

P(3HB) copolymer	R_1	R_2
P(3HB)	$-CH_3$	x
P(3HB-co-3HV)	$-CH_3$	$-CH_2CH_3$
P(3HB-co-3HHx)	$-CH_3$	$-CH_2CH_2CH_3$
P(3HB-co-3HO)	$-CH_3$	$-(CH_2)_4CH_3$
P(3HB-co-3HD)	$-CH_3$	$-(CH_2)_6CH_3$

These copolymers are formed by adding additional alternative feedstocks to the bacteria growth medium. This generally produces random copolymers, however by alternating the feedstock at regular timings, block copolymers can also be produced. Random copolymers have been found to improve the properties of P(3HB), thereby producing materials more suitable for commercial applications.

The properties of the resulting copolymers depend on the type, length and distribution of the other PHA monomer in the polymer backbone. The additions of 3HV and 3HHx units have been found to significantly alter the properties of P(3HB), as seen in Table 1.4 (Balaji, Gopi et al. 2013). These are the most widely studied of the P(3HB) copolymers and have attracted the most interest in food packaging applications as a result of their properties, and are therefore the two focus materials of this thesis.

Table 1.4. Comparison of mechanical and thermal properties of the main P(3HB) copolymers produced by the solvent casting technique (Balaji, Gopi et al. 2013)

Property	P(3HB)	P(3HB-co-3HV)	P(3HB-co-3HHx)
Melting point (º C)	177	145	127
Glass transition(º C)	2	-1	-1
Crystallinity (%)	60	56	34
Tensile strength (MPa)	43	20	21
Elongation to break (%)	5	50	400

The addition of the longer pendant groups acts to improve the properties significantly, allowing some to approach, if not exceed properties of PP (Table 1.2). As shown in Table 1.4, the elongation to break increases with the addition of these pendant groups, approaching values comparable to those of PP (100-600 %) and LDPE (100-650 %), as a result of

decreasing values for crystallinity to below those of PP (40-70 %) and LDPE (55-70 %). Furthermore, values for T_m decrease below that of PP (160-165 ºC), allowing for lower processing temperatures of these materials. This therefore makes these materials attractive alternatives for the future of sustainable packaging, and will be discussed in more detail in the following sections.

1.5.2.1 Poly(hydroxybutyrate-co-hydroxyvalerate)

One of the most commonly studied of the P(3HB) copolymers is P(3HB-co-3HV). Adding the slightly longer HV units onto the side chain has been shown to improve the properties of P(3HB) considerably. As the concentration of HV within the copolymer is increased from 0 to 25 mol %, the melt temperature has been shown to reduce by as much as 42 ºC (Lee 1996). This is extremely advantageous to the polymer, as it broadens the initially very narrow processing window, thus minimising the risk of thermal degradation upon processing. The ethyl group of HV reduces the packing of chains during crystallisation due to steric hindrance, however co-crystallisation of the two monomers has been reported to occur due to their structural similarity (isodimorphism), resulting in little change to the crystallinity (Bluhm, Hamer et al. 1986). The elongation to break is significantly increased above that of the homopolymer making it more ductile and therefore a more commercially viable material. P(3HB-co-3HV) has been shown to completely degrade after 6, 75 and 350 weeks in anaerobic sewage, soil and sea water respectively (Lee 1996). However, the material has been observed to undergo secondary crystallisation, and therefore this is an avenue that still prompts further research to stabilise the mechanical properties. For example, in a study by Biddlestone et al (1995) on P(3HB-co-3HV) (8 % HV), storage of the amorphous material over time lead to significant changes to the mechanical properties as observed in Figure 1.9.

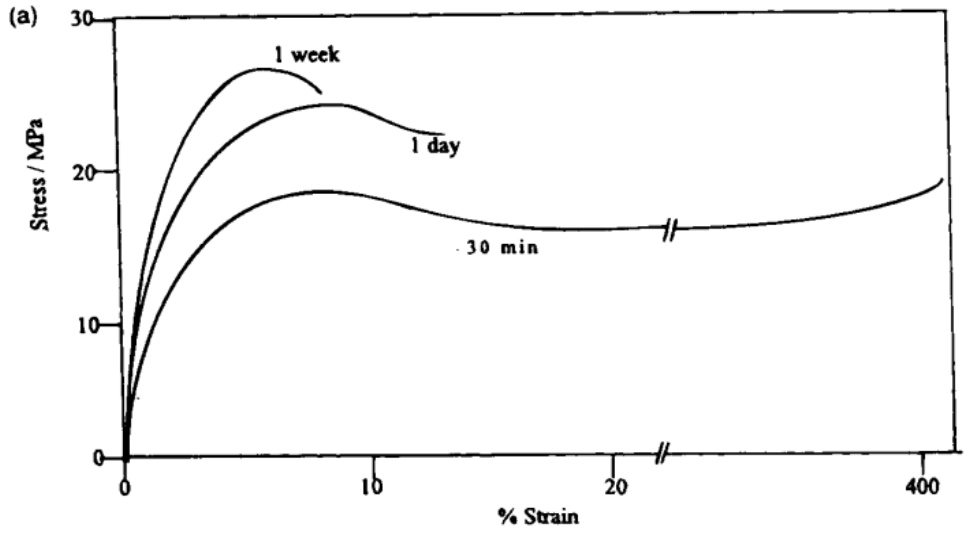

Figure 1.9. Effect of storage time at ambient temperature on the mechanical properties of P(3HB-co-3HV) (8 mol %) (Biddlestone, Harris et al. 1996)

In this study, the E_b of the material drastically decreased from 400 % to below 10 % following storage at room temperature for one week. In addition, the yield stress which originally started at a fairly low value of 18 MPa, increased to 28 MPa within the same time frame. The changes continued to a lesser extent over 100 days of storage. Using Fourier Transfer Infrared Spectroscopy (FTIR), Luo and Netravali (2002) also found an increase in crystallinity via a crystallinity index method. In this method, the band at 1182 cm^{-1} which decreases with decreasing crystallinity was normalised with respect to the intensity at band 1378 cm^{-1}, a band that is the most insensitive to changes in crystallinity. The value for crystallinity index was found to increase following storage at room temperature over time, indicative of an increase in crystallinity of the surface of the P(3HB-co-3HV) films at ambient temperature (Luo and Netravali 2003).

1.5.2.2 Poly(3-hydroxybutyrate-co-3-hydroxyhexanoate)

P(3HB-co-3HHx) has not been as widely studied, but offers improvements to mechanical properties above those of P(3HB-co-3HV). It can be seen in Figure 1.10 and Table 1.3, that

the HHx component possesses a longer side chain than the HB component. This longer pendant group present in P(3HB-co-3HHx) is a key factor in the improvement in properties above the P(3HB) homopolymer and P(3HB-co-3HV). The presence of the group affects the ability of the polymer chains to pack together closely due to the larger volume and lower spatial symmetry of the branching propyl group, thus making tight compaction of chains during crystallisation more difficult. The HHx units are therefore not incorporated into the HB lattice upon crystallisation and thus there is a greater distance between chains, hindering the likelihood of isodimorphism, as previously reported in P(3HB-co-3HV), and any long range packing. This results in greater segmental mobility of P(3HB-co-3HHx) and lowers the T_g values below those of P(3HB-co-3HV) at the same monomer content, with the added advantage of increasing the ductility and toughness of the material. This exclusion of the HHx units from the crystalline lattice of P(3HB) also results in decreased crystallinity, melting temperature and reduced rate of crystallisation which will be discussed further in the next section.

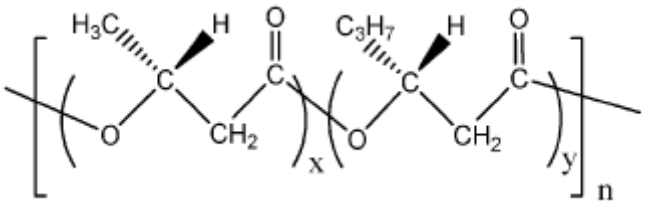

Figure 1.10. The chemical structure of P(3HB-co-3HHx)

It can be seen in Table 1.4 that the addition of HHx into the copolymer reduces crystallinity by almost half, resulting in a significant increase in elongation to break from 5 % in P(3HB) to 400 % in the HHx copolymer (Balaji, Gopi et al. 2013). The reduction in T_m of the material means it can be processed at lower temperatures, leading to a broader processing window, which is an important commercial consideration when processing polymeric

materials. It has attracted much attention in the biomedical field due to its excellent cytocompatibility with most bodily cells, where it has been tested in many areas of tissue engineering including cartilage, tendon, vascular and nerve tissue engineering (Chang, Wang et al. 2014). Packaging applications also look promising due to the increased ductility and transparency of the material, making it suitable for film lids which are currently unrecyclable.

Based upon the above observations that the pendant group acts to reduce crystallinity and ease of crystallisation in P(3HB-co-3HHx) compared to the homopolymer, it is interesting to consider the effect of the pendant group on the ability of the material to secondary crystallise. Based on limited literature, it was found that despite the presence of the bulkier pendent group hindering crystallisation within P(3HB-co-3HHx), secondary crystallisation and therefore ongoing embrittlement still occurred within the material at room temperature, but to a lesser extent as the HHx content is increased. In a study by (Asrar, Valentin et al. 2002), the elongation to break of P(3HB-co-3HHx) (8.1 mol %) was found to decline from 31.6 % to 12 % with an increase in strength from 18.8 MPa to 22.8 MPa, following 11 days storage at room temperature, as observed previously in P(3HB) and P(3HB-co-3HV). Annealing at 130 ºC for 30 minutes restored the properties, but re-aging occurs again upon subsequent storage (Figure 1.11).

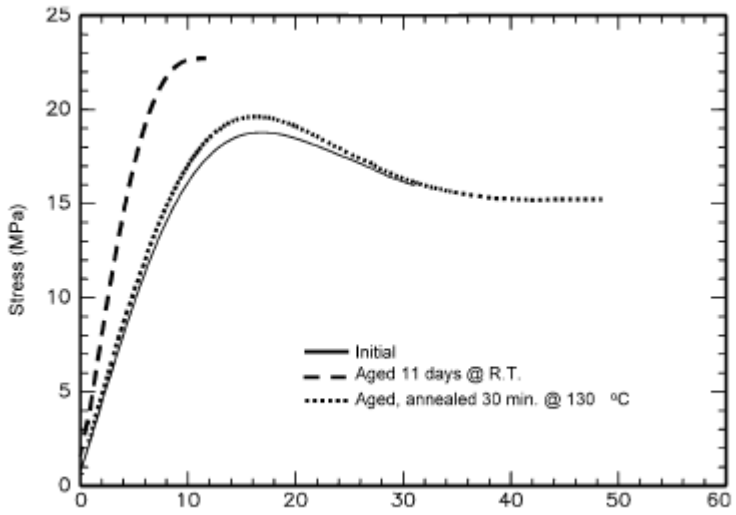

Figure 1.11. Stress strain behaviour of P(3HB-co-3HHx) (8.1 mol %) following storage after 11 days (Asrar, Valentin et al. 2002)

In a paper by Alata et al (2007), a broader range of HHx contents were examined from 5-18 mol % in solution cast films. They subsequently found that the secondary process only significantly occurred in copolymers with HHx contents lower than 10 mol %, in agreement with Asrar et al (2002)(Alata, Aoyama et al. 2007). They found similar trends in the decrease of elongation to break with storage and concurrent increase in the tensile strength of the material. For example, for 7 mol % HHx, the initial elongation to break and tensile strength were 381.4 % and 15. 3 MPa respectively. Following 60 days of storage at room temperature, the elongation to break dropped to 73.4 % and the tensile strength increased to 20.2 MPa. They did however establish that as the co-monomer content increased up to 18.5 %, the change in materials properties was significantly less, offering percentage reduction in elongation to break of 18.0 % in 18.5 mol % HHx, in comparison to an 80.8 % change in 7 mol % HHx. The presence of HHx units therefore does retard the secondary crystallisation ability of HHx by disrupting chain compaction due to the steric hindrance created by the pendant group (Alata, Aoyama et al. 2007).

Furthermore, crystallinity, indicated by X-Ray (Alata, Aoyama et al. 2007), and enthalpy of fusion (ΔH_f) (Asrar, Valentin et al. 2002, Alata, Aoyama et al. 2007) were found to increase with storage time at room temperature. Consequently, this affects the T_g and its behaviour over time. It is apparent from Figure 1.12, that the copolymers with 5 and 7 mol % fraction, as well as possessing higher values for T_g initially, also increase to a greater degree over time than those of the copolymers of fraction 10, 12 and 18 mol %. This indicates that the mobility of the amorphous region of the copolymers with HHx molar fractions lower than 10 mol % decreases much more significantly than the other copolymers with HHx fraction higher than 10 mol % with storage at room temperature over time, indicating greater ease of secondary crystallisation at lower HHx concentrations.

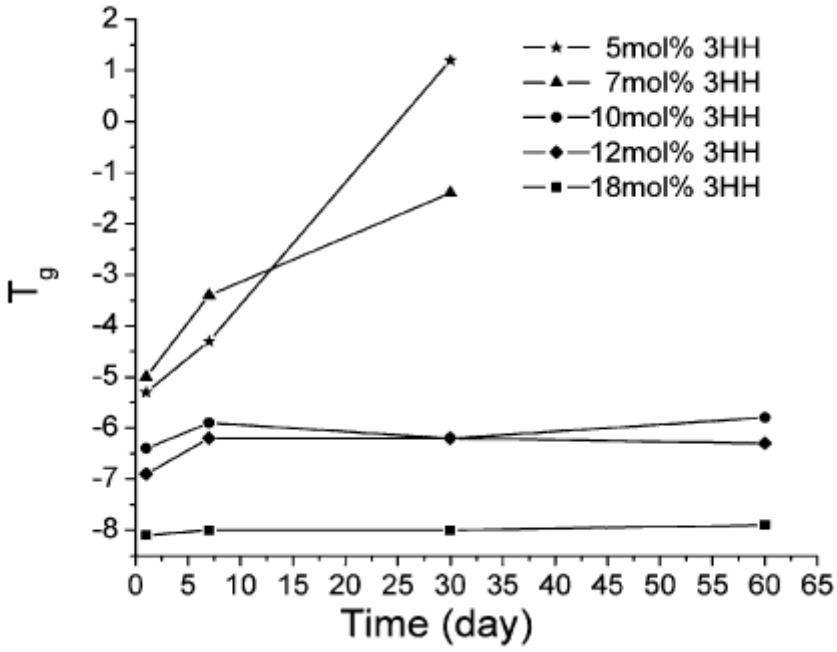

Figure 1.12. Effect on increasing co-monomer content on the T_g of P(3HB-co-3HHx) over time (Alata, Aoyama et al. 2007)

It is apparent from the above evidence that secondary crystallisation also occurs within P(3HB-co-3HHx) at room temperature over time, but to what extent depends upon the composition. It is therefore expected that at higher percentages of HHx (above 10 mol %), the

secondary crystallisation process is minimal based on these findings, and thus, it can be concluded that minimal changes to the P(3HB-co-3HHx) used in this work are expected under ambient conditions.

Furthermore, despite the extensive research into thermal stability and degradation of P(3HB) (Grassie, Murray et al. 1984, Nguyen, Yu et al. 2002, Luo and Netravali 2003, Gonzalez, Irusta et al. 2005, Abe 2006, Ariffin, Nishida et al. 2008), no work on the thermal stability and effects of thermal degradation of P(3HB-co-3HHx) copolymer has been conducted. As a result, an aim of this work is to analyse the effects of higher temperature storage on the secondary crystallisation behaviour and thermal stability of P(3HB-co-3HHx) copolymer.

1.5.3 Crosslinking

Polymer crystallisation is related to the mobility of the polymer chains. Therefore, in order to reduce secondary crystallisation within P(3HB), a restriction in chain mobility would be advantageous. Crosslinking is a means of achieving this, with three dominant methods appearing amongst research. Crosslinking via chemical initiators, such as Dicumyl Peroxide (DCP) has been successfully carried out resulting in improvements to the mechanical properties of P(3HB) (Fei, Chen et al. 2003, Fei, Chen et al. 2004, Fei, Chen et al. 2004, Semba, Kitagawa et al. 2006). However, this method introduces toxic materials into the system, and thus would not be suitable for food packaging applications. Other attempts via ultra violet (Rupp, Ebner et al. 2010, Sadi, Fechine et al. 2010), and gamma (Mitomo, Watanabe et al. 1995, Parra, Rodrigues et al. 2005, Oliveira, Araújo et al. 2006) irradiation to induce crosslinking have yielded mixed results. Crosslinking in this way is advantageous because it can be achieved without the use of harmful additives. However, irradiation has also been described to simultaneously cause chain scission, which ultimately leads to increased

molecular mobility, and therefore no real improvements to overall crystallinity of the material (Mitomo, Watanabe et al. 1995, Parra, Rodrigues et al. 2005, Oliveira, Araújo et al. 2006). The third mechanism, intermolecular hydrogen bonding, offers a more natural approach and is discussed below in more detail.

1.5.3.1 Cross-linking by intermolecular hydrogen bonding

A method that avoids the above problems is intermolecular hydrogen bonding (H-Bonding). H-bonding is a naturally occurring crosslinking mechanism, made possible by the electronegative oxygen present in the carbonyl groups of P(3HB-co-3HV). In general, the hydrogen bond is an attractive interaction between electron deficient hydrogen and a region of high electron density. Most frequently, a hydrogen bond is of the X-H…Y type, where X and Y are electronegative elements and Y possesses one or more lone pair of electrons. In most cases, X and Y are predominantly F, O or N atoms. The hydrogen bonds are generally much weaker than covalent bonds or other polar bonds, but much stronger than the Van der Waals interaction (He, Zhu et al. 2004).The hydrogen bond is a fundamental component of the structure and function of biomolecules, such as polysaccharides, proteins and nucleic acids. Furthermore, the formation of inter-associated H-bonds not only promotes miscibility of the components, but also improves compatibilisation of polymer blends (He, Zhu et al. 2004).

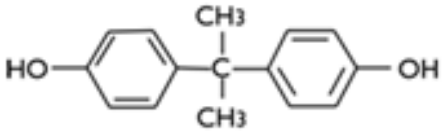

Figure 1.13. Chemical structure of Bisphenol A

Crosslinking P(3HB-co-3HV) with Bisphenol A (BPA) (Figure 1.13) (Fei et al, 2003; Fei et al, 2004) has produced promising results. In blends containing 20 wt% BPA, ductility was enhanced significantly, with E_b increasing from 11 % to 370 % (Fei, Chen et al. 2003). This was attributed to two features of BPA; the hydroxyl functional groups allowing for the formation of the hydrogen bond network restricting chain mobility; and the bulky phenyl rings which prevent close packing of P(3HB-co-3HV) chains during primary crystallisation. A depression in T_m of 24 °C is also observed upon cross-linking, broadening the originally narrow processing window (Fei, Chen et al. 2003). However, BPA is considered to be a toxic material, and therefore not considered to be a GRAS substance, discounting it from the use within food packaging materials. Thus, biocompatible and bio-friendly alternative cross-linking agents are required should this strategy be employed within food packaging materials.

1.5.3.2 Cross-linking with polysaccharides

Consequently, recent attention has been directed towards natural polymers such as starch, chitosan and cellulose derivatives due to their similar bulky ring structures and their potential to form intermolecular hydrogen bonds . In addition, as these substances are naturally sourced and abundant in nature, the blends maintain their biocompatibility and sustainability whilst remaining cost effective.

1.5.3.2.1 Starch

Starch is considered to be an attractive biopolymer due to its low cost, high availability, low density, non-abrasive nature, and biodegradability. It is composed of 2 polymers, a linear polymer known as amylose and a highly branched polymer, amylopectin (amylopectin). Both components are composed of α-D-glucose repeating units, with amylose joined together solely by α-(1-4) ester linkages creating the linear chain (Figure 1.14a), while amylopectin also contains α-(1-6) ester linkages, creating its branched structure (Figure 1.14b). Thermoplastic starch can also be obtained by mixing starch powder, water, and or plasticisers such as polyols, mono-, di-, or oligosaccharides, fatty acids, lipids and derivatives through a gelatinisation process (Zhang and Thomas 2010). As starch is abundantly and cheaply available, its use in blending with P(3HB) will result in a completely biodegradable material which can have desired physical properties with concomitant reduction in cost (Godbole, Gote et al. 2003).

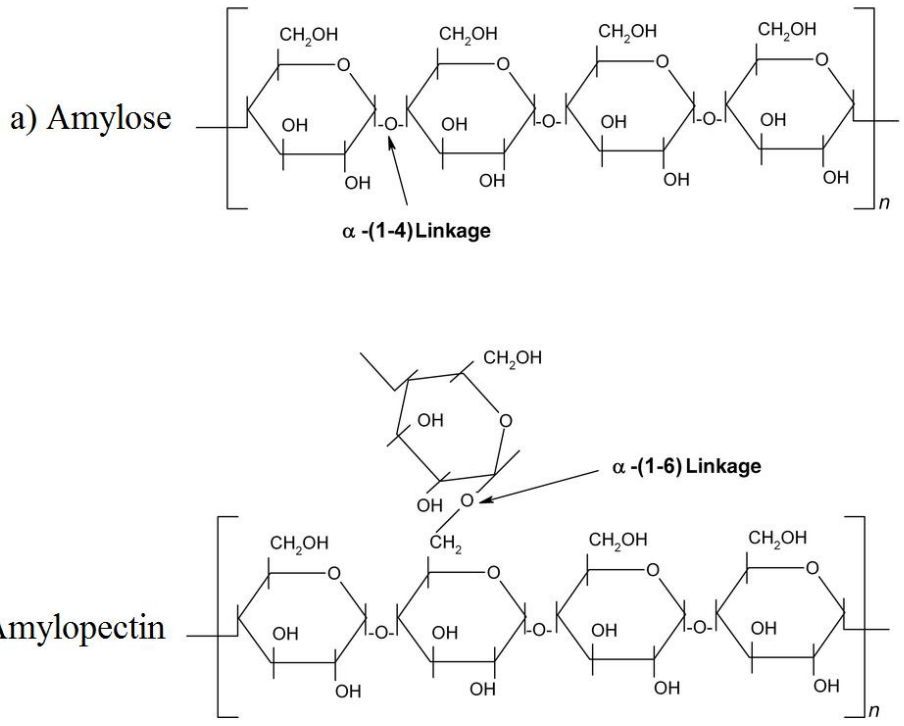

Figure 1.14. The chemical structures of the two components of natural starch a) amylose b) amylopectin (Visakh P M 2012)

Starch is not only completely biodegradable in nature, allowing for a completely biofriendly material, but its presence within P(3HB) blends acted to increase the biodegradation rate. Films (150 μm thick) containing 50 wt % starch had 100 % weight loss in fewer than 8 days, whereas a month was required for total weight loss in the pure unblended P(3HB-co-3HV) held under controlled aerobic conditions in a chemostat (Ramsay, Langlade et al. 1993). However, due to starch being an extremely large network polymer, it has a high melting temperature. It was therefore observed in Scanning Electron Microscopy (SEM) analysis that the starch granules did not melt during processing, and therefore remained un-uniformly dispersed throughout the material as discrete inclusions, thus acting as a filler (Ramsay, Langlade et al. 1993, Thiré, Ribeiro et al. 2006, Zhang and Thomas 2010). This lead to the appearance of pull out holes upon analysis of the fracture surface using SEM, and this was attributed to low interfacial adhesion between the two components (Thiré, Ribeiro et al. 2006). As a result, Thire et al (2005) reported a reduction in E_b with the addition of starch from 5.25 % in P(3HB) to 1.25 % at 40 wt % starch in compression moulded films. This was accompanied by a reduction in modulus from 1317 MPa to 366 MPa resulting in a less ductile, yet more flexible material. Tensile strength also decreased with increasing starch content and becomes as low as 5 MPa at 50 wt % starch.

Conversely, a study by Godbole et al (2003) reported that as natural starch content increased, the E_b increased from 3.32 % in pure P(3HB), to 9.4 % with the addition of 30 wt % starch. A further increase in E_b to 11.7 % was also observed using thermoplastic starch instead of natural starch. Tensile strength also increased with the addition of natural starch up to 30 wt %, while Young's Modulus decreases from 1708 MPa to 949 MPa, indicating a stronger and more flexible material following the addition of the starch, however samples were produced by the solvent casting technique which generally produces a more homogenous distribution of starch within the blend (Godbole, Gote et al. 2003).

In an alternative study by Reis et al (2008) using solvent cast starch blends it was found that the Young's modulus decreased as starch content increased, in agreement with Godbole et al. (2003)(Reis, Pereira et al. 2008). However, they also found that, in contrast to Godbole, the strength decreased as the starch content increased. Similarly to Thire et al (2005), this was attributed to low interfacial interaction between the two components, leading to mechanical rupture at the blend interface during tensile testing. Elongation to break also exhibited a significant decrease with the introduction of starch. Similar findings were also reported by Ramsay et al (1993) who found that the addition of starch up to 50 % lead to reductions in elongation to yield and break, yield stress, and strength at break, whilst also increasing the Young's modulus significantly.

Zhang and Thomas (2010) found that starch improved the thermal stability by reducing the effect of thermal degradation within P(3HB) upon blending due to hydrogen bonding between the hydroxyl groups of starch and the carbonyl groups of P(3HB) (Zhang and Thomas 2010). P(3HB) is known to have low thermal stability as previously mentioned in Section 1.3.3. P(3HB)/starch blends (Blend 1: starch containing 70 % amylose, Blend 2: starch containing 72 % amylopectin) were heated at 10 ºC/min for two runs by DSC. In the first run, the melting temperatures of P(3HB) and P(3HB)/starch blends were similar at about 171 ºC. However, during the second heating run the T_m for P(3HB) shifted to a significantly lower temperature due to chain scission. The T_m of blend 2 was not reduced by as much as pure P(3HB), and blend 1 shows virtually no degradation, although double melting was present. This improvement in the thermal stability of P(3HB) was attributed to the hydrogen bonding between the hydroxyl groups of starch and the carbonyl groups of P(3HB). According to the work of Grassie et al. (1984) amongst other authors, thermal degradation of P(3HB) is due to chain scission through a widely accepted ring ester decomposition mechanism involving a 6 membered ring transition state. It was suggested that H-bonding

between starch and P(3HB) inhibited the formation of the ring structure and hence improve the thermal stability of P(3HB) (Zhang and Thomas 2010).

Thire et al (2005) also found via X-ray diffraction, that the crystallinity of the blends decreased as the starch content increased without disrupting the crystal lattice. The crystallinity of pure P(3HB) was found to be 44.9 %, and this decreased to 32.3 % in blends containing 30 wt % starch.

The presence of hydrogen bonding between P(3HB) and starch was confirmed using FTIR (Zhang and Thomas 2010). Pure starch presents a broad band at 3400 cm^{-1} which relates to hydroxyl vibrations. In P(3HB)/starch blends, this band decreases in intensity compared to that of pure starch, and the peak of this band shifts to a higher wavenumber (not quantified) compared to pure starch. Furthermore, the peak of the band at 1709 cm^{-1}, which is attributed to the vibration of the H-bonded carbonyl groups increases with the addition of starch causing the carbonyl peak to broaden. These results suggest that intermolecular H-bonding occurs between the two components, whereby the hydroxyl groups of the starch chains participate in intermolecular H-bonding with the carbonyl groups on P(3HB) (Zhang and Thomas 2010). Furthermore, the change observed in the peak shoulder at 1750 cm^{-1}, attributed to the P(3HB) amorphous carbonyl vibration, indicates that the intermolecular H-bonding is predominantly due to the interactions between P(3HB) and starch in the amorphous phase (Zhang and Thomas 2010).

However, despite starch showing promise as a property modifier and cost reducer, the high T_m of the material makes it difficult to be fully incorporated into the blend via melt blending which is the chosen route for processing that will conducted within this work. This is because, the processing temperatures required to minimise degradation within P(3HB) materials are not high enough to melt polysaccharides such as starch. The starch particles

therefore remained discretely dispersed within the polymer where they act as inclusions as previously discussed. It is therefore apparent that an alternative solution should contain similar chemical features, whilst having the ability to be fully incorporated into the material by melt blending through appropriate thermal properties. Starch itself is a long chain polymer of the monosaccharide glucose. With melt temperature of 162 °C, glucose has a low enough melting temperature to be incorporated into the blend during melt processing, whilst offering a similar chemical structure giving it the capability to form H- bonds. Its chemical structure is shown in Figure 1.15.

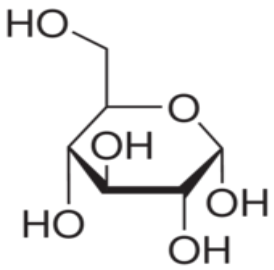

Figure 1.15. Chemical structure of glucose

Similar structures are also available in increasing chain lengths of glucose units. Disaccharides and trisaccharides such as maltose and melezitose are also available. These therefore offer a greater number of hydroxyl units for H-bonding whilst being a longer chain to hinder the crystallisation process. Furthermore, they also possess the desired thermal properties required to be melt blended as their T_ms are below that of P(3HB-co-3HV). It is therefore the intention to incorporate a series of mono, di and trisaccharides into P(3HB-co-3HV) via melt blending to see if they improve the materials properties and have any effect on reducing the secondary crystallisation process within P(3HB-co-3HV). They are also GRAS, widely available and cost effective additives, and would therefore be suitable for use in food packaging materials.

1.5.3.2.2 Cellulose Acetate Butyrate

Another seemingly fitting alternative based upon these criteria is the addition of cellulose Acetate Butyrate (CAB) into the blends. CAB is derived from the esterification of the natural polymer, cellulose. It possesses similar functional groups and a T_g in the region of 100 °C and thus would be suitable to be incorporated into a blend with P(3HB-co-3HV) by either solvent blending or melt blending. Many different grades of CAB are available due to fact that variations of the substitute groups are available. Differences in butyryl, acetyl, and hydroxyl groups create CAB grades with different mechanical and thermal properties. It can come in both semi-crystalline and amorphous grades making it a very versatile product with properties that can be selected based on the required application. The structure of CAB can be seen in Figure 1.16, with 'R' indicating the possible locations for the different substitute groups.

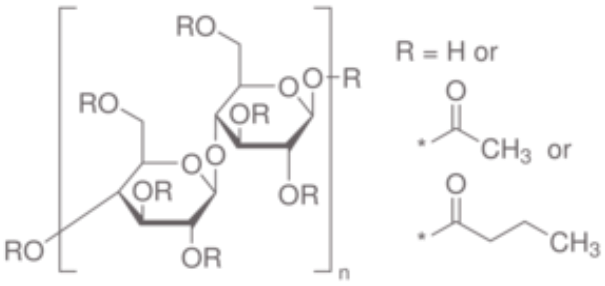

Figure 1.16. The chemical structure of CAB

Evidence for composition dependent intermolecular interactions between P(3HB) and CAB have been observed by FTIR (Park, Tanaka et al. 2005, Suttiwijitpukdee, Sato et al. 2011, Suttiwijitpukdee, Sato et al. 2011). Suttiwijitpukdee et al (2011) studied the effects of intermolecular hydrogen bonding in blends of P(3HB) and CAB during isothermal crystallisation of solvent cast blends. A strong peak at ~3435 cm^{-1} assigned to the first

overtone of the stretching mode of the C=O groups involved in intramolecular hydrogen bonding within P(3HB) was observed. With the addition of CAB, a shift of this peak to 3450 cm^{-1} was observed in 50/50 blends. It was suggested that this was due to interruption of the existing P(3HB)-P(3HB) interactions by the formation of H-bonds between the carbonyl groups of P(3HB) and the hydroxyl groups in CAB, thus creating physical crosslinks within the material. Furthermore, Suttiwijitpukdee et al (2011), reported the appearance of a new peak at 1738 cm^{-1} in the second derivative spectra for the 50/50 HCAB (high molecular weight CAB) blend, also attributed to the presence of H-bonding. HCAB had a greater number of hydroxyl (OH) groups present on the chain than LCAB (low molecular weight CAB) by an order of magnitude, which resulted in a greater extent of H-bonding. This clearly demonstrates the importance of hydroxyl groups on the ability of the CAB to hydrogen bond. A peak shift and decrease in magnitude of the carbonyl group was also observed with the addition of 40 % CAB and greater indicating intermolecular interactions, and decreasing crystallinity of the resulting materials as the concentration is increased (Suttiwijitpukdee, Sato et al. 2011).

Miscibility was confirmed between the two components via thermal analysis of the blends. Wang et al (2002) found that the T_m of the blend decreases with the addition of CAB over a broad composition range (Wang, Cheng et al. 2003). Park et al (2005) also found the T_m to reduce with up to 30 % CAB before the samples became completely amorphous and no longer showed a T_m (Park, Tanaka et al. 2005). It was also established that that T_g increased with the addition of CAB towards higher temperatures as measured by DSC (Buchanan, Gedon et al. 1992, Pizzoli, Scandola et al. 1994, El-Shafee, Saad et al. 2001). El Shaffee et al (2001) also found a shift in T_g measured by DSC for all samples, and at high levels of CAB there was a strong dependence of the measured T_g on composition. This was quantified by Buchanan (1992) where the T_g was found to increase from 1 ºC in 20 % CAB to 10 ºC in 80

% CAB. In addition, a reduction in the equilibrium melting point (Tm^0) was observed with the addition of CAB in solution cast blends up to 50 wt % CAB (El-Shaffe et al, 2001).

Upon analysis of the crystallisation kinetics of the blends, it was shown that the nucleation factor (K_g) is significantly lower in the blends than in the homopolymer, leading to a higher nucleation density during the primary crystallisation process (El-Shaffee et al, 2001). This, in combination with a decreased crystallisation rate (El Shaffee et al., 2001; Suttiwijitpukdee et al, 2011) with increasing CAB content produces numerous, well ordered, perfectly formed spherulites during crystallisation and a reduction in crystallinity (El-Shaffee et al, 2001). In addition, compared to pure P(3HB), the cold crystallisation temperatures (T_{cc}) increase with greater CAB content, highlighting the increased difficulty of crystallisation of P(3HB) in the blends (El Shafee et al., 2001; Suttiwijitpukdee et al., 2011).

Research into the effect of CAB on the mechanical properties of P(3HB) and copolymers is limited. Wang et al (2002) found the tensile strength to decrease from 26 MPa in 100 % P(3HB) to 13 MPa in a 50/50 binary blend. They found elongation to break to increase from 2 % to 7 % with 50 % CAB while the impact strength increases from 20 kg/m^2 to 59 kg/m^2. Tensile strength and tear strength decreased while elongation to break increased on raising the CAB (Buchanan, 1992).Yamaguchi and Arakawa (2006) also found that E_b increased with the addition of CAB, but improvements were most prominent with the addition of cellulose acetate propionate due to its higher molecular weight (Yamaguchi and Arakawa 2007).

Its H-bonding capabilities, along with increasing ductility and reduced crystallinity render CAB a useful addition to P(3HB). However, the effect of CAB on the secondary crystallisation process in P(3HB) or copolymers has not currently been assessed. It is therefore the intention to assess the influence of CAB on the secondary crystallisation

behaviour of P(3HB-co-3HV) to see if it is a possible strategy to gain control of the deterioration of properties, and thus improve its commercial potential.

1.6 Scope of this work

There is a commercial need for biodegradable and sustainable polymeric materials. As a result, there has been increasing interest in biopolymers, especially for single use disposable products such as food packaging materials. In particular, research has focused on P(3HB), a bacterially produced and cleanly biodegradable material for such applications. However, P(3HB) is an inherently brittle polymer due to its chemical structure creating a high degree of crystallinity. Furthermore, it undergoes secondary crystallisation at ambient temperature over time as a result of its low T_g, leading to increased embrittlement upon storage, with significant effects observed within the first day. This affects the commercial use of the polymer. To improve the properties and reduce the ability of the material to secondary crystallise, strategies such as the addition of nucleating agents, copolymerisation, polymer-polymer blending and cross-linking have been employed. Whilst nucleating agents and copolymerisation to produce P(3HB-co-3HV) and P(3HB-co-3HHx) have acted to improve the initial thermal and mechanical properties of the P(3HB) polymers, these materials still secondary crystallise upon storage under ambient conditions. It is of commercial importance to stabilise the properties of P(3HB) based materials to ensure a suitable shelf life for use in commercial products.

The ability of polymers to secondary crystallise results from the mobility of the polymer chains. Therefore, a strategy to prevent the secondary process from occurring should restrict chain mobility hindering the chain interactions that lead to crystallisation. Previous studies have cross-linked P(3HB) via chemical initiators such as Dicumyl peroxide and Bisphenol A, resulting in improved mechanical properties, however these materials are toxic and are

therefore not classified as GRAS molecules according to FDA regulations, which is a fundamental requirement for food packaging materials.

As a result, the addition of polysaccharides such as starch and CAB to P(3HB) and copolymers had been previously researched with promising results. The presence of intermolecular hydrogen bonding has been confirmed in both systems whilst the blends maintain their biocompatibility and sustainability with the added benefit of being cost effective. They have been found to reduce the crystallinity of the blends and in some cases improve the mechanical properties of the materials. Their success in interacting and influencing the properties of P(3HB) was due to their multi-hydroxyl, bulky ring chemical structures. Despite its influence, starch has a much higher T_m than that of P(3HB) and thus, upon melt blending, created discrete inclusions within the P(3HB) matrix with low interfacial adhesion affecting the mechanical properties of the blends. Therefore, additives with a similar chemical structure to allow interaction, but possessing lower processing temperatures to allow it to be successfully incorporated into the blend are desirable. On this basis, the first aim of this work was therefore to incorporate mono, di and trisaccharides in addition to the cellulose derivative CAB into P(3HB) to assess their interaction with the material and effect on the materials properties. In addition to this, discovering the effect of the additives on the secondary crystallisation process at ambient temperatures over time was also a key aim and a novel approach. The effect of these additives both on initial properties and following storage will be analysed and discussed in Chapters 3 (saccharides) and 4 (CAB).

In addition, thermal instability is another key issue preventing the wide-scale use of P(3HB) and its copolymers. There has been a large amount of research into the thermal stability and degradation of P(3HB) and P(3HB-co-3HV), however to date there is no research investigating the effects of thermal stability/degradation of P(3HB-co-3HHx), or the effect of storage temperature on the secondary crystallisation behaviour of P(3HB-co-3HHx). From

the literature, it was observed that copolymers containing higher HHx contents (above 10 mol %) show minimal secondary crystallisation in terms of changes to T_g and mechanical properties at ambient temperature, brought about by the steric hindrance created by the longer pendant group. The final aim of the work, covered in Chapter 5, was therefore to analyse the effects of high temperature storage on the secondary crystallisation behaviour and thermal stability of P(3HB-co-3HHx) copolymer containing 33 wt % HHx. The possibility of sub T_m degradation was also analysed, and is a topic that hasn't been previously investigated to the authors' knowledge.

1.7 References

Abe, H. (2006). "Thermal degradation of environmentally degradable poly(hydroxyalkanoic acid)s." Macromol Biosci **6**(7): 469-486.

Alata, H., et al. (2007). "Effect of Aging on the Mechanical Properties of Poly(3-hydroxybutyrate-co-3-hydroxyhexanoate)." Macromolecules **40**(13): 4546-4551.

Aoyagi, Y., et al. (2002). "Thermal degradation of poly[(R)-3-hydroxybutyrate], poly[ε-caprolactone], and poly[(S)-lactide]." Polymer Degradation and Stability **76**(1): 53-59.

Arakawa, K., et al. (2008). "Enhancement of melt elasticity for poly(3-hydroxybutyrate-co-3-hydroxyvalerate) by addition of weak gel." Journal of Applied Polymer Science **107**(2): 1320-1324.

Ariffin, H., et al. (2008). "Determination of multiple thermal degradation mechanisms of poly(3-hydroxybutyrate)." Polymer Degradation and Stability **93**(8): 1433-1439.

Ashby, R. D., et al. (2002). "The synthesis of short- and medium-chain-length poly(hydroxyalkanoate) mixtures from glucose- or alkanoic acid-grown Pseudomonas oleovorans." J Ind Microbiol Biotechnol **28**(3): 147-153.

Asrar, J., et al. (2002). "Biosynthesis and properties of poly(3-hydroxybutyrate-co-3-hydroxyhexanoate) polymers." Biomacromolecules **3**(5): 1006-1012.

Balaji, S., et al. (2013). "A review on production of poly β hydroxybutyrates from cyanobacteria for the production of bio plastics." Algal Research **2**(3): 278-285.

Barham, P. J., et al. (1992). "Physical properties of poly(hydroxybutyrate) and copolymers of hydroxybutyrate and hydroxyvalerate." FEMS Microbiology Letters **103**(2): 289-298.

Bassett (1988). Developments in Crystalline Polymers - 2. Essex, England, Elsevier Applied Publishers Ltd.

Batcha, A. F., et al. (2014). "Biosynthesis of poly(3-hydroxybutyrate) (PHB) by Cupriavidus necator H16 from jatropha oil as carbon source." Bioprocess Biosyst Eng **37**(5): 943-951.

Bergmann, A. and A. Owen (2004). "Dielectric relaxation spectroscopy of poly[(R)-3-hydroxybutyrate] (PHB) during crystallization." Polymer International **53**(7): 863-868.

Biddlestone, F., et al. (1996). "The physical ageing of amorphous poly(hydroxybutyrate)." Polymer International **39**(3): 221-229.

Bluhm, T. L., et al. (1986). "Isodimorphism in bacterial poly(β-hydroxybutyrate-co-β-hydroxyvalerate)." Macromolecules **19**(11): 2871-2876.

Bregg (2006). New Frontiers in Polymer Research, Nova Science Publishers

Bucci, D. Z., et al. (2005). "PHB packaging for the storage of food products." Polymer Testing **24**(5): 564-571.

Buchanan, C. M., et al. (1992). "Cellulose acetate butyrate and poly(hydroxybutyrate-co-valerate) copolymer blends." Macromolecules **25**(26): 7373-7381.

Bugnicourt, E., et al. (2014). "Polyhydroxyalkanoate (PHA): Review of synthesis, characteristics, processing and potential applications in packaging." Express Polymer Letters **8**(11): 791-808.

Calhoun, A. (2010). Chapter 3 - Polypropylene A2 - Wagner, John R. Multilayer Flexible Packaging. Boston, William Andrew Publishing**:** 31-36.

Callister, W. D. and D. G. Rethwisch (2008). Fundamentals of Materials Science and Engineering. An Intergrated Approach. Asia, John Wiley and Sons.

Chang, H. M., et al. (2014). "Poly(3-hydroxybutyrate-co-3-hydroxyhexanoate)-based scaffolds for tissue engineering." Brazilian Journal of Medical and Biological Research **47**(7): 533-539.

Chanprateep, S. (2010). "Current trends in biodegradable polyhydroxyalkanoates." J Biosci Bioeng **110**(6): 621-632.

Dawes, E. A. (1988). "Polyhydroxybutyrate: an intriguing biopolymer." Biosci Rep **8**(6): 537-547.

de Koning, G. J. M. and P. J. Lemstra (1993). "Crystallization phenomena in bacterial poly[(R)-3-hydroxybutyrate]: 2. Embrittlement and rejuvenation." Polymer **34**(19): 4089-4094.

El-Hadi, A., et al. (2002). "Correlation between degree of crystallinity, morphology, glass temperature, mechanical properties and biodegradation of poly (3-hydroxyalkanoate) PHAs and their blends." Polymer Testing **21**(6): 665-674.

El-Shafee, E., et al. (2001). "Miscibility, crystallization and phase structure of poly(3-hydroxybutyrate)/cellulose acetate butyrate blends." European Polymer Journal **37**(10): 2091-2104.

Fei, B., et al. (2004). "Crosslinking of poly[(3-hydroxybutyrate)-co-(3-hydroxyvalerate)] using dicumyl peroxide as initiator." Polymer International **53**(7): 937-943.

Fei, B., et al. (2003). "Quantitative FTIR study of PHBV/bisphenol A blends." European Polymer Journal **39**(10): 1939-1946.

Fei, B., et al. (2004). "Modified poly(3-hydroxybutyrate-co-3-hydroxyvalerate) using hydrogen bonding monomers." Polymer **45**(18): 6275-6284.

Godbole, S., et al. (2003). "Preparation and characterization of biodegradable poly-3-hydroxybutyrate–starch blend films." Bioresource Technology **86**(1): 33-37.

Gonzalez, A., et al. (2005). "Application of pyrolysis/gas chromatography/Fourier transform infrared spectroscopy and TGA techniques in the study of thermal degradation of poly (3-hydroxybutyrate)." Polymer Degradation and Stability **87**(2): 347-354.

Grassie, N., et al. (1984). "The thermal degradation of poly(-(d)-β-hydroxybutyric acid): Part 1—Identification and quantitative analysis of products." Polymer Degradation and Stability **6**(1): 47-61.

Gunaratne, L. M. W. K., et al. (2004). "Thermal history effects on crystallisation and melting of poly(3-hydroxybutyrate)." Thermochimica Acta **423**(1–2): 127-135.

Harris (1995). Ageing of Poly(3-hydroxybutyrate) and its copolymers. Metallurgy and Materials. Birmingham, University of Birmingham. **PhD**.

He, Y., et al. (2004). "Hydrogen bonds in polymer blends." Progress in Polymer Science **29**(10): 1021-1051.

Hobbs, J. K., et al. (1996). "Cracking in spherulites of poly(hydroxybutyrate)." Polymer **37**(15): 3241-3246.

Hu, Y., et al. (2007). "Multiple melting behavior of poly(3-hydroxybutyrate-co-3-hydroxyhexanoate) investigated by differential scanning calorimetry and infrared spectroscopy." Polymer **48**(16): 4777-4785.

Ineos (2013). "Typical engineering properties of polyproylene." from http://www.ineos.com/globalassets/ineos-group/businesses/ineos-olefins-and-polymers-usa/products/technical-information--patents/ineos-engineering-properties-of-pp.pdf

Jendrossek, D. (2009). "Polyhydroxyalkanoate granules are complex subcellular organelles (carbonosomes)." J Bacteriol **191**(10): 3195-3202.

Kai, W., et al. (2005). "Fast crystallization of poly(3-hydroxybutyrate) and poly(3-hydroxybutyrate-co-3-hydroxyvalerate) with talc and boron nitride as nucleating agents." Polymer International **54**(5): 780-789.

Keshavarz, T. and I. Roy (2010). "Polyhydroxyalkanoates: bioplastics with a green agenda." Curr Opin Microbiol **13**(3): 321-326.

Kolb, R., et al. (2001). "Investigation of secondary crystallization of polymers by means of microbeam X-ray scattering." Polymer **42**(12): 5257-5266.

Lee, S. Y. (1996). "Bacterial polyhydroxyalkanoates." Biotechnology and Bioengineering **49**(1): 1-14.

Liu, W. J., et al. (2002). "Effect of nucleating agents on the crystallization of poly(3-hydroxybutyrate-co-3-hydroxyvalerate)." Journal of Applied Polymer Science **86**(9): 2145-2152.

Luo, S. and A. N. Netravali (2003). "A study of physical and mechanical properties of poly(hydroxybutyrate-co-hydroxyvalerate) during composting." Polymer Degradation and Stability **80**(1): 59-66.

Martinez-Salazar, J., et al. (1989). "Thermal expansion and spherulite cracking in 3-hydroxybutyrate/3-hydroxyvalerate copolymers." Journal of Materials Science Letters **8**(4): 490-492.

Mitomo, H., et al. (1995). "Radiation effect on polyesters." Radiation Physics and Chemistry **46**(2): 233-238.

Mittendorf, V., et al. (1998). "Synthesis of medium-chain-length polyhydroxyalkanoates in Arabidopsis thaliana using intermediates of peroxisomal fatty acid β-oxidation." Proceedings of the National Academy of Sciences of the United States of America **95**(23): 13397-13402.

Nguyen, S., et al. (2002). "Thermal Degradation of Poly(3-hydroxyalkanoates): Preparation of Well-Defined Oligomers." Biomacromolecules **3**(1): 219-224.

Oliveira, L. M., et al. (2006). "Gamma irradiation effects on poly(hydroxybutyrate)." Polymer Degradation and Stability **91**(9): 2157-2162.

Park, J. W., et al. (2005). "Uniaxial drawing of poly[(R)-3-hydroxybutyrate]/cellulose acetate butyrate blends and their orientation behavior." Macromol Biosci **5**(9): 840-852.

Parra, D. F., et al. (2005). "Use of gamma-irradiation technology in the manufacture of biopolymer-based packaging films for shelf-stable foods." Nuclear Instruments and Methods in Physics Research Section B: Beam Interactions with Materials and Atoms **236**(1–4): 563-566.

Pizzoli, M., et al. (1994). "Crystallization Kinetics and Morphology of Poly(3-hydroxybutyrate)/Cellulose Ester Blends." Macromolecules **27**(17): 4755-4761.

Ramsay, B. A., et al. (1993). "Biodegradability and mechanical properties of poly-(beta-hydroxybutyrate-co-beta-hydroxyvalerate)-starch blends." Appl Environ Microbiol **59**(4): 1242-1246.

Reis, K. C., et al. (2008). "Characterization of polyhydroxybutyrate-hydroxyvalerate (PHB-HV)/maize starch blend films." Journal of Food Engineering **89**(4): 361-369.

Robertson, G. L. (2012). Food Packaging: Principles and Practice. Florida, USA, CRC Press.

Rupp, B., et al. (2010). "UV-induced crosslinking of the biopolyester poly(3-hydroxybutyrate)-co-(3-hydroxyvalerate)." Green Chemistry **12**(10): 1796-1802.

Sadi, R. K., et al. (2010). "Photodegradation of poly(3-hydroxybutyrate)." Polymer Degradation and Stability **95**(12): 2318-2327.

Semba, T., et al. (2006). "The effect of crosslinking on the mechanical properties of polylactic acid/polycaprolactone blends." Journal of Applied Polymer Science **101**(3): 1816-1825.

Shah, A. A., et al. (2008). "Biological degradation of plastics: a comprehensive review." Biotechnol Adv **26**(3): 246-265.

Shen, F., et al. (2009). "Surface bio-modification of poly(hydroxybutyrate-co-hydroxyhexanoate) and its aging effect." Colloids and Surfaces B: Biointerfaces **73**(2): 302-307.

Shen, H., and Patel (2009). Product overview and market projection of emerging bio-based plastics. The Netherlands, Utrecht University.

Sics, I., et al. (2001). "On the relationship between crystalline structure and amorphous phase dynamics during isothermal crystallization of bacterial poly(3-hydroxybutyrate-co-3-hydroxyvalerate) copolymers." Biomacromolecules **2**(2): 581-587.

Špitalský, Z. and T. Bleha (2004). "Elastic Properties of Poly(hydroxybutyrate) Molecules." Macromolecular Bioscience **4**(6): 601-609.

Suriyamongkol, P., et al. (2007). "Biotechnological approaches for the production of polyhydroxyalkanoates in microorganisms and plants — A review." Biotechnology Advances **25**(2): 148-175.

Suttiwijitpukdee, N., et al. (2011). "Effects of Intermolecular Hydrogen Bondings on Isothermal Crystallization Behavior of Polymer Blends of Cellulose Acetate Butyrate and Poly(3-hydroxybutyrate)." Macromolecules **44**(9): 3467-3477.

Suttiwijitpukdee, N., et al. (2011). "Intermolecular interactions and crystallization behaviors of biodegradable polymer blends between poly (3-hydroxybutyrate) and cellulose acetate butyrate studied by DSC, FT-IR, and WAXD." Polymer **52**(2): 461-471.

Taidi, B., et al. (1995). "Turnover of poly(3-hydroxybutyrate) (PHB) and its influence on the molecular mass of the polymer accumulated by Alcaligenes eutrophus during batch culture." FEMS Microbiology Letters **129**(2): 201-205.

Thiré, R. M. S. M., et al. (2006). "Effect of starch addition on compression-molded poly(3-hydroxybutyrate)/starch blends." Journal of Applied Polymer Science **100**(6): 4338-4347.

Thompson, A. K. (2003). Fruit and Vegetables: Harvesting, Handling and Storage. Oxford, UK, Blackwell Publishing.

Tian, J., et al. (2005). "Kinetic studies of polyhydroxybutyrate granule formation in Wautersia eutropha H16 by transmission electron microscopy." J Bacteriol **187**(11): 3814-3824.

Visakh P M, M. A. P., Oksman K, Thomas S (2012). Polysaccharide building blocks. L. L. A. Habibi Y. New Jersey, USA, John Wiley & Sons.

Wang, T., et al. (2003). "Crystallization behavior, mechanical properties, and environmental biodegradability of poly(β-hydroxybutyrate)/cellulose acetate butyrate blends." Journal of Applied Polymer Science **89**(8): 2116-2122.

Wang, Z. G., et al. (1999). "The nature of secondary crystallization in poly(ethylene terephthalate)." Polymer **40**(16): 4615-4627.

Wilkinson, R. (1998). Polymer Processing and Structural Development. Cornwall, Kluwer Academic Publishers.

Withey, R. E. and J. N. Hay (1999). "The effect of seeding on the crystallisation of poly(hydroxybutyrate), and co-poly(hydroxybutyrate-co-valerate)." Polymer **40**(18): 5147-5152.

Yamaguchi, M. and K. Arakawa (2007). "Control of structure and mechanical properties for binary blends of poly(3-hydroxybutyrate) and cellulose derivative." Journal of Applied Polymer Science **103**(5): 3447-3452.

Zhang, M. and N. L. Thomas (2010). "Preparation and properties of polyhydroxybutyrate blended with different types of starch." Journal of Applied Polymer Science **116**(2): 688-694.

Chapter 2
Materials and Methods

2.1 Materials

2.1.1 P(3HB) Copolymers

Two P(3HB) based co-polymers were used in this work. Poly(3-hydroxybutyrate-co-3-hydroxyvalerate) P(3HB-co-3HV) containing 3 wt% HV (Tianan ENMAT Y1000P) was obtained from Helian Polymers (Venlo, Netherlands) and used as received. The material was nucleated with 1 % Boron Nitride nucleating agent, as well as containing 1 wt % Irganox 1010 as a thermal stabiliser. Poly(hydroxybutyrate-co-hydroxyhexanoate) (P3HB-co-3HHx) containing 33 wt % HHx (obtained by ^{1}H NMR from the school of Chemistry, University of Birmingham) HHx was provided by Pera Technology (Melton Mowbray, UK) and used as received.

2.1.2 Additives

The following additives were blended into the P(3HB-co-3HV). D-(+)-Glucose, D-(-)-Fructose, D-(+)-Maltose monohydrate, and D-(+)-Melezitose monohydrate were purchased from Sigma Aldrich (Dorset, UK) and used as received. Cellulose Acetate Butyrate (CAB) (butyryl 37 %, acetyl 13 % and hydroxyl 1.5 %) (Mn: 30,000 g/mol) was provided by Pera Technology (Melton Mowbray, UK) and used as received.

2.2 Calculating blend quantities

2.2.1 Determination of the amount of cross-linker required – saccharide blends

In order for comparisons to be made between the different saccharide additives, the quantities required to keep the possible number of cross-links achievable the same was calculated based on their chemical structures. This was done for three concentrations of each saccharide additive. The three ratios required for each saccharide blend were 87.94, 41.66, and 25.78, and the weight percentages required to achieve these ratios were calculated according to the molecular mass (Mr) of each saccharide , also taking into account the maximum capacity of the compounder (50g). The determination of these cross-linking ratios is outlined below.

Previous studies on the blending of poly(lactic acid) (PLA) and Polyethylene glycol (PEG) showed a region of high miscibility to occur between PEG concentrations of 8 and 25 wt% (Kelly, Naylor et al. 2012). In light of this, it was decided to begin by using concentrations of 5, 10 and 15 wt% for the middle molecular weight PEG, PEG 400. As these concentrations worked well previously with PEG, the same concentrations were used in the calculations for saccharide molecules. This also ensured that the resulting blends still predominantly consisted of P(3HB-co-3HV). As the main focus of the blending studies performed in this work is to determine the effect of crosslinking P(3HB-co-3HV), it is important that the number of crosslinks remains consistent between additives and therefore the mass of additive was adjusted accordingly. An example of how this was determined for PEG is given below.

Crosslink ratios for P(3HB-co-3HV)/PEG blends were determined using Mr. Hydroxybutyrate repeat unit has an Mr of 86 and hydroxyvalerate has an Mr of 100. As the P(3HB-co-3HV) used in this work (ENMAT Y1000P) consists of 3 % hydroxyvalerate, this gives an average repeat unit mass of 86.42 g/mol.

To determine the ratio of HB/HV repeat units to full PEG chains in the 5 wt% blend for example, the mole ratios of the two must be compared based on a total mass of 1 g:

$$\text{Moles} = \frac{\text{mass (g)}}{Mr} \qquad [2.1]$$

Therefore, for a 5% concentration of PEG 400:

Moles PEG chain= 0.05/400 = 0.000125

Moles HB/HV units = 0.95/86.42 = 0.010993

Ratio of HB/HV units to PEG chains 0.010993/0.000125 = 87.94:1

Ratio of PEG units to HB/HV chains = 0.000125/0.010993 = 0.0114

This calculation was repeated on the 10 and 15 wt% PEG 400 blends with the results given in (Table 2.1).

Table 2.1. Crosslink ratios calculated for this work

Crosslinker content	PEG equivalent	HB/HV: PEG 400	PEG 400: HB/HV
Low	5	87.9	0.0114
Medium	10	41.7	0.0240
High	15	25.8	0.0388

2.2.2 Calculation of crosslink ratios in P(3HB-co-3HV)/saccharide blends

The molecular masses of the carbohydrate molecules can be seen in Table 2.2.

Table 2.2. Molecular mass data required for further calculation of required additives

Component	Chemical Formula	Molecular Mass (g/mol)
P(3HB-co-3HV)	$[COCH_2CH(CH_3)O)$-co-$(COCH_2CH(C_2H_5)O]$	86.42
Glucose	$C_6H_{12}O_6$	180.00
Fructose	$C_6H_{12}O_6$	180.00
Maltose	$C_{12}H_{22}O_{11}$	342.00
Melezitose	$C_{18}H_{32}O_{16}$	504.00

In order to keep the results consistent the ratios detailed above in Table 2.2 are used for each of the additives unless otherwise stated. The mass of cross-linker required can therefore be calculated as detailed below.

Example: Lowest concentration of Glucose

As the low cross-linker content requires a ratio of 87.9 this means that for every mole of Glucose present, 87.9 moles of HB/HV are required. Therefore, using the mole equation (Equation 2.1), the mass of each material based on the presence of 1 mole of glucose can be calculated:

Glucose low: mass = moles x M_r = 1 x 180 = 180

P(3HB-co-3HV): mass = moles x M_r = 87.9 x 86.42 = 7596

The wt % of cross-linker required can then be calculated using Equation 2.2.

$$\text{Crosslinker (wt \%)} = \frac{\text{mass}_{\text{1 mole crosslinker}}}{(\text{mass}_{\text{1 mole crosslinker}} + \text{mass}_{\text{required moles P(3HB-co-3HV)}})} \times 100\% \quad [2.2]$$

Thus (Glucose low):

$$\text{Crosslinker (wt \%)} = \frac{180}{(180 + 7596)} \times 100\% = 2.31\%$$

The masses required for each percentage to create 50 g of each blend were then calculated like so:

Glucose low: (2.31/100) x 50 = 1.15 g

P(3HB-co-3HV): ((100 – 2.31)/100) x 50 = 48.85 g

To give the following quantities required for each additive, at each crosslinking ratio that were used in this work (Table 2.3).

Table 2.3. The quantities of P(3HB-co-3HV) and additive within each blend

Sample	Structure	% Additive required
Glucose	Monosaccharide 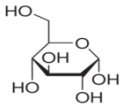	2.31 4.76 7.48
Fructose	Monosaccharide 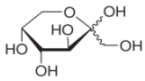	2.31 4.76 7.48
Maltose	Disaccharide 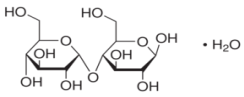	4.31 8.68 13.31
Melezitose	Trisaccharide 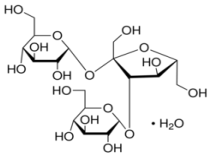	6.43 12.66 18.98

2.2.3 Quantities in P(3HB-co-3HV)/CAB blends

At the time of blending, the molecular weight of the Cellulose Acetate Butyrate required for similar calculations was unknown, and it was therefore not possible to calculate the required

masses in the same way. Thus, taking into account that the blends should be predominantly P(3HB-co-3HV) material, compositions of 5, 10 and 15 wt% CAB were used in this work.

2.3 Production of P(3HB-co-3HV) based blends

2.3.1 Experimental Technique

A HaakePolylab QC (Haake, Massachusettes, USA) mechanical compounder was used to create the required blends. This mechanical mixer is a counter rotating twin screw compounder with intermeshing screws that sit inside a heated chamber (Figure 2.1). The temperature of the chamber can be adjusted and is constantly controlled throughout by temperature sensors. To start the process, the polymer is fed in to the mixing chamber through the hopper where the combination of heat inside the chamber and shear from the screws act to melt the polymer and ensure thorough mixing of the components. It is mixed for the required processing time and extracted by manually scraping the material from the chamber once complete.

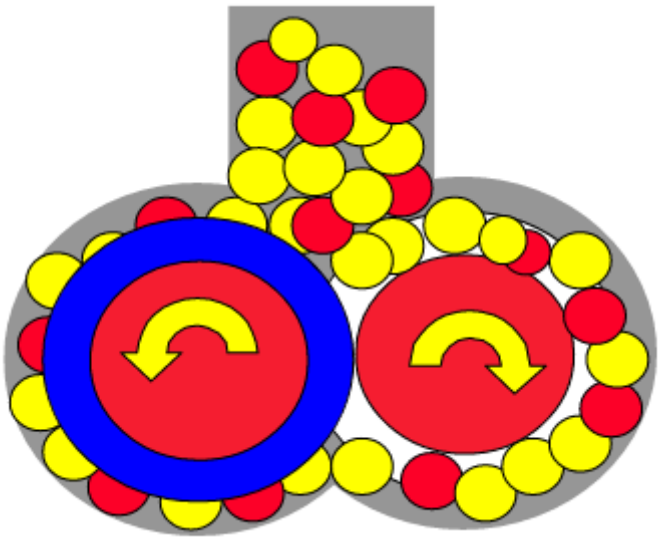

Figure 2.1. A schematic diagram of a counter-rotating twin screw compounder (Thermo 2017)

2.3.2 Method

The P(3HB-co-3HV) material was dried prior to processing for 2 hours at 80 °C to eliminate surface and internally bound water within the material. The pellets were returned to the oven between production of blends to ensure they didn't regain any moisture. The required quantities of P(3HB-co-3HV) and additives were weighed out according to pre-established crosslinking ratios (Table 2.1) which were determined to keep the number of cross-links the same across all saccharides. The materials were combined by hand before being placed into the compounder where they were mixed at 170 °C for 10 minutes with a screw speed of 100 rpm. These conditions were monitored and controlled throughout the process by Haake Polysoft OS Software, while an extractor was used simultaneously to remove any harmful fumes and dust produced during mixing. Once produced, the samples were allowed to cool and stored in a freezer at -22 °C until required.

2.4 Sample preparation

2.4.1 Solvent casting versus melt casting

There are two current methods of processing P(3HB) into sample materials; solvent casting and hot pressing, each with their own advantages and disadvantages. Solvent casting produces more ductile material with better mechanical properties. This occurs as a result of the comparatively low crystallisation temperature (25 °C) used to produce solvent cast materials which ensures its nucleation density is maximised due to a higher supercooling. As a result, the spherulite size is reduced with respect to the melt cast samples, creating a more ductile material. However, it is difficult to dissolve highly crystalline P(3HB) in solvents, and high temperatures over a significant period of time are usually required. In addition to this, there is a high chance of residual trapped solvent in the blend, rendering the material un-pure.

There is also argument that the solvents could act as a plasticiser within the material (Bassett 1988).

The advantage of hot pressing compared to solution casting is the avoidance of the use of solvents. The material is pressed as a powder or pellets without any additional substances. However, it does expose the material to high temperatures, which as previously discussed (Section 1.3.3), could lead to the initiation of thermal degradation. It seems logical that increasing the number of processing steps via this process is likely to further influence the resulting properties of the material, however this hasn't been quantified in the literature. Work has been conducted previously to analyse the different sample preparation techniques and how this affects the final properties of the materials. Table 2.4 displays the properties of P(3HB) resulting from both solvent blending and melt blending, with the additional effect of nucleating agents (1 wt % Boron Nitride) on the moulding process also being examined (Bassett, 2012).

Table 2.4. Comparison of properties obtained via different processing techniques of P(3HB) (Bassett, 2012)

Parameter	Solution cast	Hot pressed (Un-nucleated)	Hot pressed (Nucleated)
Processing temperature (º C)	25	195	195
Average spherulite diameter (µm)	1	200	10
Young's modulus (GPa)	2.8	3.5	3.2
Notched I-zod impact strength (Jm^{-1})	-	20	65
Falling weight Impact strength (J)	17	0.5	3.5
Extension to break (%)	20	2	8

Here it can be observed that the difference between the two processes on spherulite diameter is significant (199 µm). This directly relates to the ductility of the samples where it can be seen that the un-nucleated moulded P(3HB) shows a 90 % reduction in elongation to break compared to the solution cast samples due to the much larger spherulites. The solution cast plaques also demonstrate superior impact strength, with a reduced stiffness. However, it can be seen that although un-nucleated moulded P(3HB) is far inferior to solution cast samples upon testing, this can to an extent be rectified by nucleating the P(3HB) which sees a dramatic decrease in spherulite size, reduced stiffness, increased impact strength and elongation to break compared to the un-nucleated samples. As a result, to maintain pure,

solvent free and completely biodegradable materials suitable for food packaging applications, nucleated P(3HB) co-polymers will be used and produced via hot pressing in this thesis.

2.4.2 Experimental technique

Hot pressing is a technique combining heat and pressure to produce flat polymer samples for characterisation across a wide range of techniques. It has a top and a bottom plate which are heated via the passage of heated oil that circulates through the system. The polymer is sandwiched within a suitable mould between two thinner steel plates and composite Polytetrafluoro ethylene (PTFE) glass fibre sheets to create a smooth sample finish before being mounted into the press (Figure 2.2). Pressure is applied manually by a hydraulic ram. Once the sample has been produced, the system is cooled via the circulation of cold water. The size and thickness of the samples can be controlled by the size and thickness of the mould used, and the processing time, temperature and pressure applied can be varied depending on optimum processing conditions for the material.

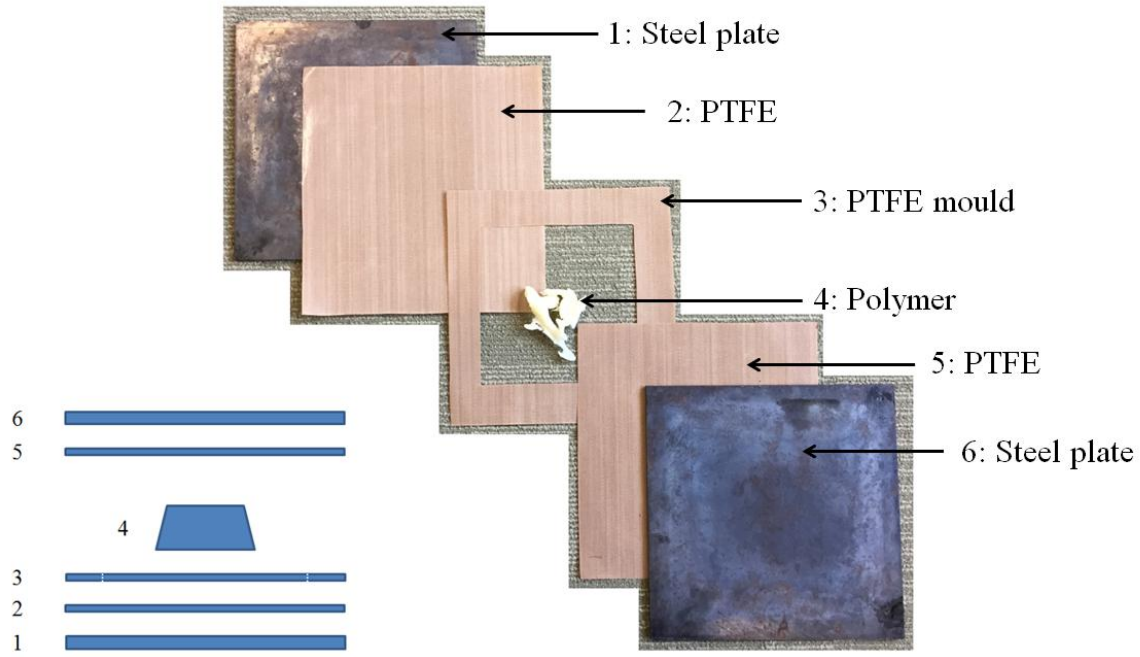

Figure 2.2. Example of layer assembly used to create flat polymer samples by hot pressing

2.4.3 Procedure

The polymer blends were hot pressed into plaques using a Moore Hydraulic Press (George E. Moore & Sons Ltd, Birmingham, UK). The polymer was weighed (9 g) and placed into the appropriate mould, which was sandwiched between two PTFE glass fibre and steel sheets (Figure 2.2) and mounted into the press. It was allowed to warm through for 3 minutes before being compressed by a mass of 10 tonnes for 5 minutes (Table 2.5). The conditions for P(3HB-co- 3HV) were chosen based on previous work within the research group in order to fully melt the samples whilst keeping the time that the materials spends at elevated temperatures to a minimum. The conditions for P(3HB-co-HHx) differ as this material possesses a lower melting point, and therefore optimal conditions were explored and decided upon accordingly. The press was cooled by flushing water through the system while the pressure was maintained, before the plaque was extracted. Plaques of each blend were

prepared for mechanical testing and DSC (150 x 150 x 0.215 ± 0.03 mm), and rheology (75 x 75 x 1.131 ± 0.02 mm).

Table 2.5. Summary of pressing conditions for all materials used

Co-polymer	Additive	Temperature (^{o}C)	Hold time (mins)	Compression time (mins)	Pressure (tonnes)	Cool time (mins)
P(3HB-co-3HV)	N/A	180	3	5	10	20
P(3HB-co-3HV)	Glucose	180	3	5	10	20
P(3HB-co-3HV)	Fructose	180	3	5	10	20
P(3HB-co-3HV)	Maltose	180	3	5	10	20
P(3HB-co-3HV)	Melezitose	180	3	5	10	20
P(3HB-co-3HV)	CAB	180	3	5	10	20
P(3HB-co-3HHx)	N/A	170	2	2	10	15

2.4.4 Press cooling rate

Due to the fact that mechanical properties of polymers are heavily influenced by crystallisation conditions, it is important to understand the cooling rate that the samples are subjected to, in order to predict the effect on the crystallisation of the samples and therefore understand this in relation to mechanical properties. The cooling rate of the press was determined using a TC-08 thermocouple data logger attached to a type K (NiCr/NiAl conductors) thermocouple using PicoLog software. The pressing conditions used to produce the samples were simulated. From this, an approximate cooling rate of 20 º C/ min was established for all samples produced in the hot press by an approximation from the linear portion of the cooling curves (Figures 2.2 and 2.3).

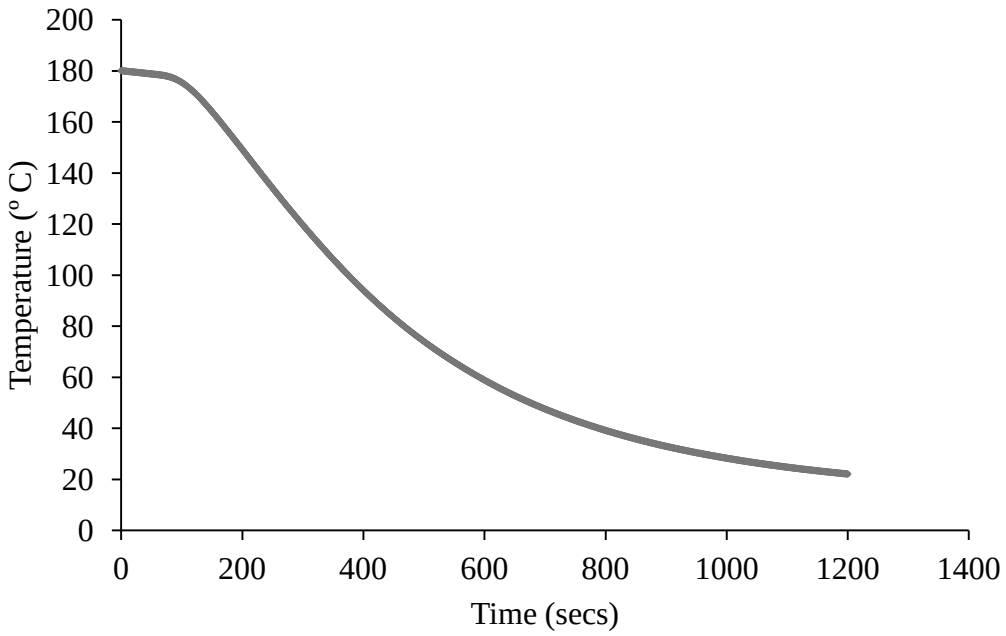

Figure 2.3. Cooling profile of the hydraulic press from 180 ºC to room temperature simulating the cooling conditions undergone by the P(3HB-co-3HV) samples and blends

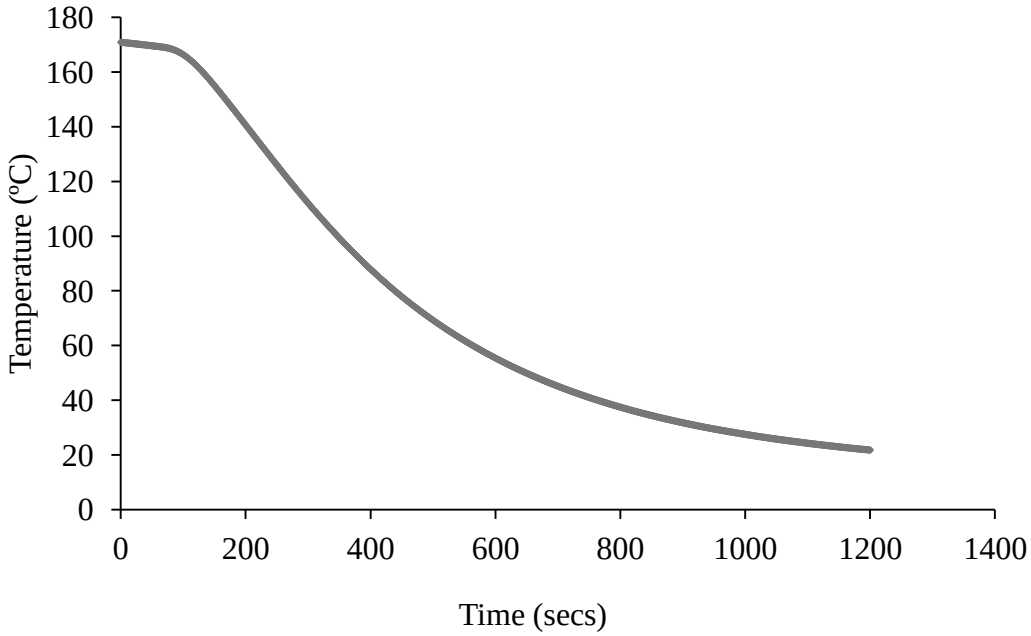

Figure 2.4. Cooling profile of the hydraulic press from 170 ºC to room temperature simulating the cooling conditions undergone by the P(3HB-co-3HHx) samples

2.5 Time dependent studies

2.5.1 P(3HB-co-3HV) studies

The rate of secondary crystallisation and resulting change in mechanical properties within the blends were analysed by conducting time studies. Once cut into the desired shape, the samples were stored at room temperature (25 °C) and analysed after 0, 7, 14, 21, 28, 56, 84, 168, 266 and 336 days, via mechanical testing, and differential scanning calorimetry (DSC) as discussed below.

2.5.2 P(3HB-co-3HHx) studies

P(3HB-co-3HHx) samples were analysed over a period of 28 days on the following time points; Day 0, 1, 2, 3, 4, 5, 6, 7, 14, 21 and 28 days. This was due to the fact that this work was conducted later on in the thesis after the finding that the majority of change within the P(3HB-co-3HV) happens within the first 28 days, and therefore changes following this were negligible. The samples were examined by storage at varying temperatures within a Gallenkamp (Size one) oven (-22, 7, 25, 50, 75 and 100 ° C) to observe the effects of storage temperature on the secondary crystallisation process. Oven temperature was monitored throughout the experiments via a thermocouple. The samples were analysed via DSC, tensile testing, mass loss, visual inspection and FTIR using the methods outlined below.

2.6 Differential Scanning Calorimetry

2.6.1 Experimental technique

Differential Scanning Calorimetry (DSC) is a useful technique to analyse a broad range of thermal properties within polymeric samples by changes in heat capacity. Differences in heat flow in a sample arise when it absorbs or releases heat due to thermal effects such as melting and crystallisation amongst other processes, allowing the measurement of thermal properties

such as the glass transition temperature (T_g), melting temperature (T_m), and crystallisation temperature (T_c) to be recorded. Additionally miscibility of polymer blends, crystallisation kinetics and morphology of a material can also be established via this technique. Semi-crystalline materials will present a T_g, T_m and T_c, while amorphous materials only produce a T_g.

A power compensated DSC was used in this work. The sample chamber contains a sample (S) and reference (R) cell shown in Figure 2.4. A pan is placed on each sensor with the reference pan being empty, and the sample pan containing the sample to be measured. The power compensated DSC works by varying the power input to ensure both the sample and reference cells remain at the same temperature as the system is heated or cooled. The differential heating power required to do so is measured and plotted as heat flow versus temperature or time. The temperature of each cell is monitored and controlled independently by thermocouples and ceramic sensors on the base of the furnace.

Figure 2.5. DSC sample chamber showing the sample (S) and reference (R) cells

2.6.2 Method

2.6.2.1 Dynamic Measurements

DSC was used to analyse the thermal behaviour and crystallinity of the raw materials and resulting blends using a METTLER Toledo DSC 1 (Mettler Toledo, Schwerzenbach, Switzerland) calorimeter. The DSC was calibrated using Zinc and Indium standards, and all experiments were conducted under nitrogen flow maintained at 1 bar. Samples (2-6 mg) were punched from the relevant plaques using a small borer (5 mm diameter), weighed and secured inside a 40 µl aluminium pan. To establish melting points of the blends, the samples were run from - 40 to 200 ºC at 10 ºC/min to minimise thermal lag within the samples, but also from -40 to 200 ºC at 50 ºC/min to reduce the effect of recrystallization upon heating. The T_m was taken as the peak on the resulting trace (Figure 2.5).

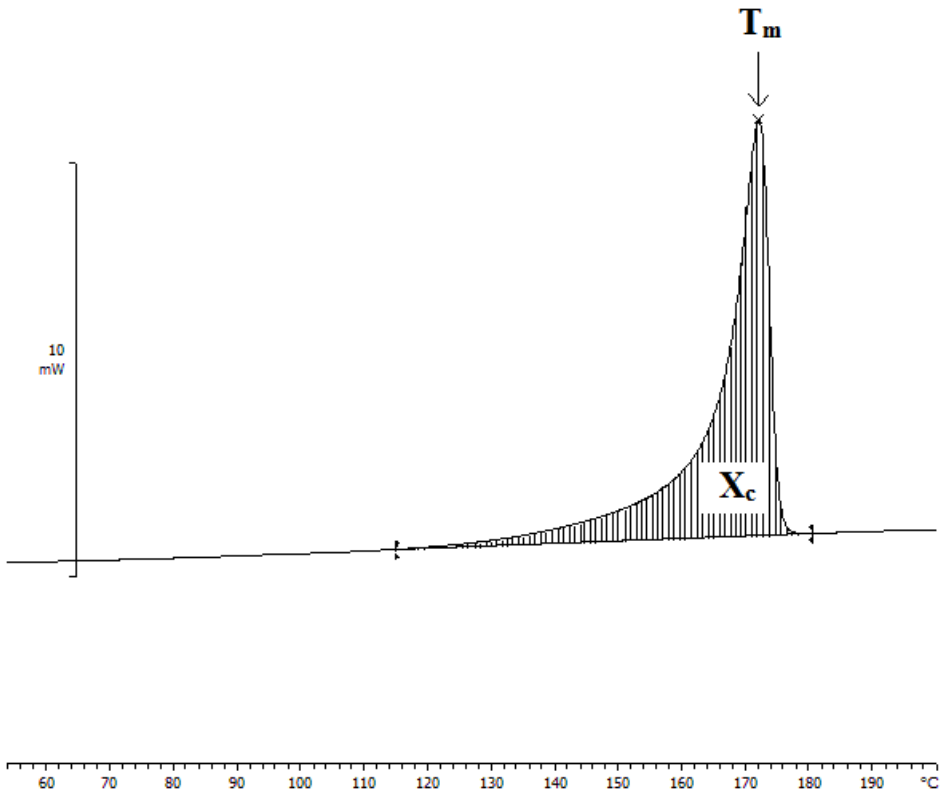

Figure 2.6. A typical DSC trace of a semi-crystalline polymer illustrating T_m and X_c were determined

The degree of crystallinity (X_c) was obtained via heating the samples from -40 to 200 ºC at 50 ºC/min and calculated using Equation 2.3, where $\Delta H_f(T_m)$is the enthalpy of fusion measured at the melting point, and $\Delta H_f^{\circ}(T_m^{\circ})$ is the enthalpy of fusion for 100% crystalline P(3HB). A value of 146 Jg^{-1} obtained from the literature was used in this case (de Koning and Lemstra 1993, Modi, Koelling et al. 2011).

$$Xc = \frac{\Delta H_f(T_m)}{\Delta H_f^{\circ}(T_m^{\circ})} x\ 100 \qquad [2.3]$$

The crystallinity of the P(3HB-co-3HV) component within each blend was calculated using Equation 2.4 in combination with the DSC trace as shown in Figure 2.5. X_c is the crystallinity value of the whole blend, and $W_{\%}$ is the percentage weight of P(3HB-co-3HV) within the blend.

$$Xc_{(PHB-co-HV)} = \frac{Xc}{W_{\%}} x\ 100 \qquad [2.4]$$

The melt crystallisation temperature (T_c) was obtained by cooling from 200 to -40 ºC at 10 ºC/min and reported as the peak of the transition. The enthalpy of crystallisation (ΔH_c) was determined by the area under the melt crystallisation peak.

The T_g of P(3HB-co-3HHx) and CAB were established via drawing tangents (orange lines) at the transitions to determine the onset, , midpoint and endset (Figure 2.6). The T_g was recorded as the midpoint of the transition.

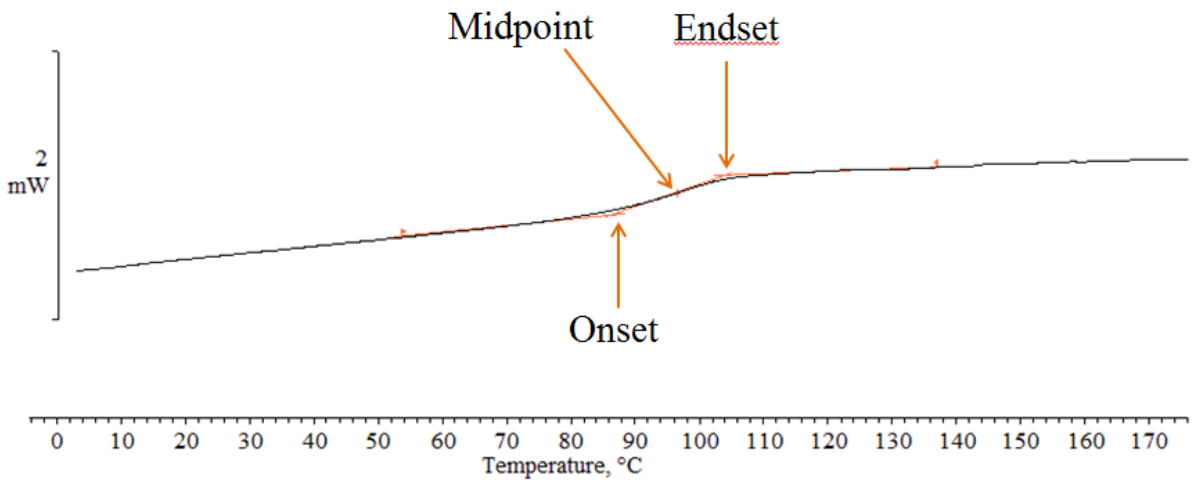

Figure 2.7. DSC trace showing the determination of T_g

The effects of secondary crystallisation and physical aging can be melted out on heating of the sample to above its melting temperature, and thermal degradation is induced by multiple heat cycling of the same material sample. Therefore, the thermal characteristics of the materials are determined from the first run, and using a new sample stored under the appropriate conditions each time.

2.6.2.2 Isothermal Measurements

The crystallisation kinetics of the P(3HB-co-3HV)/CAB blends were analysed via isothermal experiments.. Samples were heated to 180 ºC, held at this temperature for 5 mins to ensure the sample was fully melted, then dropped down to the appropriate crystallisation temperature at 50 ºC/ min and held for 120 minutes to allow the material to crystallise. The appropriate crystallisation temperature that worked across all blends was determined experimentally to be 140 ºC following numerous trials. This was used to establish values for induction time to

crystallisation, $t_{1/2}$, and to conduct Avrami analysis. The Avrami equation is shown in Equation 2.5.

$$X_c(t) = 1 - \exp(-Kt^n) \qquad [2.5]$$

In this equation, $X_c(t)$ represents the fraction transformed at time (t), t is the time from the start of the phase transformation, K represents the shape of the growing crystallites (rods, spheres or discs) and n provides information on nucleation type and crystal growth geometry. The parameters in this equation are usually determined by taking the double logarithm plot, given in Equation 2.6.

$$ln\big(-\ln\big(1 - X_c(t)\big)\big) = nlnt + lnK \qquad [2.6]$$

Experiments to establish equilibrium melting temperature (T_m^0) were also conducted on P(3HB-co-3HV) and its blends with CAB. These were subjected to a heat from the crystallisation temperature (140 to 148 ºC for P(3HB-co-3HV) and 132 to 140 ºC for CAB blends) following isothermal crystallisation to 220 ºC at 50 ºC/min. The peak in the endotherm was recorded on the abscissa scale to obtain the T_m. These values were subsequently plotted against the crystallisation temperature (T_c). A linear trend line was applied to the results for each blend, and the intercept of that line with the line of $T_m = T_c$ was used to determine the equilibrium melting point for each material.

2.7 Dynamic Mechanical Thermal Analysis

2.7.1 Experimental technique

Dynamic Mechanical Thermal Analysis (DMTA) is a dynamic thermal analysis technique that can be used to characterise viscoelastic properties of polymers by the application of sinusoidal stress at a set frequency to the sample as it is heated. The resulting changes in stiffness (modulus) and damping (Tan δ) are recorded. Because a sinusoidal force is applied, this creates an in-phase (storage modulus) and out of phase (loss modulus) component. The storage modulus (E') is the measure of a samples elastic behaviour. The ratio of the loss modulus to the storage modulus is Tan δ, which is often also referred to as damping. It is a measure of the energy dissipation of a material, allowing for thermal transitions such as T_g to be measured. T_g is seen as a large drop (a decade or more) in the storage modulus when plotted on a log scale against a linear temperature scale. The T_g is therefore measured by the temperature at which this drop occurs and also by the peak in Tan δ, both of which were conducted in this work.

2.7.2 Method

DMTA was carried out to observe the miscibility of the blends by observation of T_g shift as this wasn't apparent on the DSC traces due to high levels of crystallinity within the samples. Samples were cut into rectangular shapes (10 x 55 x 1.1 ± 0.07 mm) using scissors. These were loaded into the DMTA (NETZCH DMA 242 cell linked to TASC 414/3 controller) containing a 3 point bend accessory and the temperature lowered to -40 ºC via liquid nitrogen feed into the chamber. The temperature was then raised at 1º C per minute to 70 ºC and measured at varying frequencies of 1, 10 and 33 Hz. From this, the T_g, Loss modulus (E') and Activation energy (Ea) were calculated. Ea was calculated using the Arrhenius equation from results obtained from an Arrhenius plot (ln(f) vs 1/T). The Arrhenius equation is given below

in Equation 2.7, where Ea is the activation energy, M is the gradient of the line for ln(f) vs 1/T and R is the universal gas constant (8.31 J mol^{-1} K^{-1}).

$$Ea = MR \qquad [2.7]$$

2.8 Rheology

2.8.1 Experimental technique

Rheology is the study of deformation and flow of soft matter under applied forces. The rheological properties of a polymer, such as melt viscosity, have important implications for the processing of the material. A rotational rheometer with parallel plates was used in this work. In this technique, the heads rotate at a set frequency at the appropriate temperature and the flow behaviour of the material is measured. Rheology allows the determination of melt viscosity of the polymer and classification of Newtonian or Non-Newtonian behaviour by its response to shear rate or strain.

2.8.2 Method

The melt viscosity of the blends were analysed using the ARES Rheometric Scientific Rheometer (Rheometric Scientific, New Castle, USA), with TA orchestrator software controlling the process. The samples were cut into discs (25 x 1.131 ± 0.02mm) and placed into the Rheometer. The system was held for 5 minutes at 180 °C to melt the sample before analysing at a frequency of 10 Hz with the strain increasing logarithmically from 1 to 327 %. Ten readings were plotted per decade, with the shear viscosity determined at an offset of 10% strain. Three repeats were conducted for each sample to obtain an average for each blend.

2.9 Tensile Testing

2.9.1 Experimental technique

Tensile testing is a destructive testing procedure used to determine the mechanical properties of a material. Uniaxial tensile testing applies stress to the material and records the materials response along one axis until fracture. The specimen is mounted at each end into the grips of the testing apparatus. The testing machine elongates the specimen along its long axis at a constant rate whilst measuring the instantaneous applied load (with a load cell) and the resulting elongation (with an extensometer). The output of such a tensile test is recorded as load versus extension, or stress versus strain, which is presented graphically. The resulting stress/strain curves can be analysed to produce results for elongation to break (E_b), ultimate tensile stress (UTS) Young's modulus (E), and Toughness as shown in Figure 2.7.

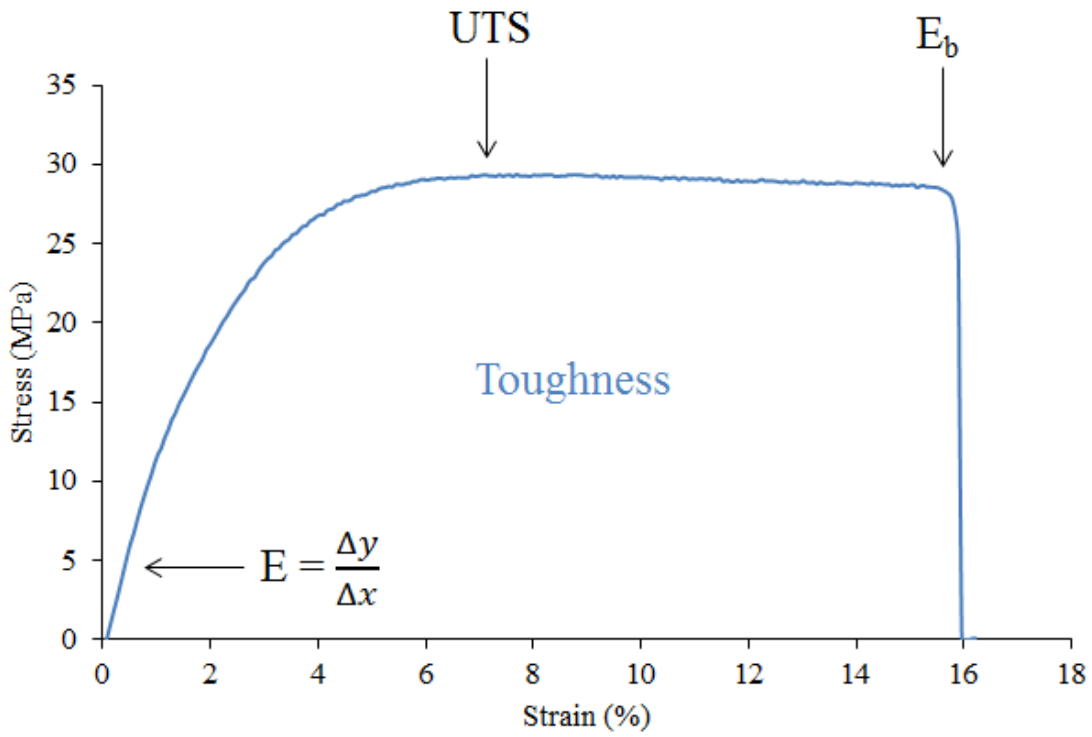

Figure 2.8. An example stress strain curve and how it is used to determine mechanical properties of a sample

2.9.2 Method

Tensile testing was carried out on the samples to analyse the mechanical properties of the blends using an Instron 5566 mechanical tester (Instron, High Wycombe, UK) in combination with Merlin software. Using a Wallace cutter,dog-bone shaped samples with a gauge length of 26 mm, width of 4 mm and thickness of 0.215 ± 0.03 mm were cut from the hot pressed plaques. This size was used in order to produce as many test samples as possible out of the material available, as well as making it possible to draw comparisons with previous work within the research group. Thin samples were produced as the application of interest for this work was thin films for food packaging. Before testing, the edges of each dog-bone were smoothed using P800 emery paper. Three repeats for each polymer blend were tested at each time point, with the experimental parameters set to a load cell of 10 kN, cross head speed of 2 mm/min, and 500 ms time intervals. Tests were conducted at ambient temperature (21 ºC), and proceeded until failure of the sample. Three repeats were tested for P(3HB-co-3HV)/ Carbohydrate blends, while five repeats were tested for P(3HB-co-3HV)/CAB blends and P(3HB-co-3HHx) material as this was determined to produce more accurate results in later work.

Due to the fact that mechanical performance of polymers is affected by temperature, care was taken to ensure that samples stored in the freezer (necessary across all samples), or at the elevated temperatures (in the case of P(3HB-co-3HHx)), were at room temperature before proceeding with mechanical testing. Increasing temperature gives rise to a decrease in modulus of elasticity and tensile strength, while increasing the ductility of the material. Reducing the temperature will therefore cause the opposite effects. Therefore, to reduce any effect of storage conditions on the mechanical performance of the polymers and get the true change in mechanical properties over time based on the secondary process, the samples were

left outside of the storage condition for 10 minutes to return the sample to ambient temperature inside the lab.

2.10 Fourier Transform Infra-Red Spectroscopy: Attenuated Total Reflection

2.10.1 Experimental technique

Fourier Transform Infra-Red spectroscopy (FTIR) is a non-destructive characterisation technique used for determining any chemical changes occurring within the material via an infra-red laser beam. In the attenuated total reflectance (ATR) technique, an infra-red beam is directed towards an interfereometer which splits the beam into two paths. One is directed via a mirror towards the sample an optically dense crystal (with a high refractive index) at a certain angle, whilst the other is directed towards a reference. This creates an evanescent wave that penetrates the surface of the sample that is in contact with the crystal, causing certain molecules within the sample to vibrate. It is therefore important that there is good contact between the crystal and the sample which can be achieved by clamping the sample in place. In regions of the infra-red spectrum where the sample absorbs energy from bond vibration, the evanescent wave will be attenuated or altered. The attenuated energy from each evanescent wave is passed back to the other IR beam and combined, which then exits the opposite end of the crystal and is passed to the detector in the IR spectrometer. This results in the production of an FTIR spectrum.

2.10.2 Method

Analysis was performed on the blends over time on a Thermo Nicolet 380 FTIR with Smart Orbit ATR accessory running Omnic software. The accessory had a ratchet system in place so that the pressure applied to each sample was consistent. A blank spectrum was taken

before each run to eliminate any noise from the environment and to obtain a pure sample spectrum. Samples were run at an optical velocity of 0.6329 $cm.s^{-1}$, with 100 scans per minute at a resolution of 4 nm from wavelengths of 4000-700 cm^{-1} using 2 levels of zero filling. All runs were conducted at ambient temperature. Due to equipment issues, FTIR spectra for each time point in P(3HB-co-3HV) samples could not be run on the same piece of material over time. Therefore, spectra were taken from different regions of the same plaque, and as a result this opens up the potential for inter-sample variability.

2.11 Hot stage microscopy

2.11.1 Experimental procedure

Hot stage microscopy was used to analyse the crystal morphology of P(3HB-co-3HV) and its blends with CAB in the melt, and following crystallisation from the melt. This was to detect any obvious lack of miscibility through the addition of CAB and to create a visual picture of any changes occurring to the spherulite morphology upon blending. The use of a polarising optical microscope with cross-polars in this technique means that it is only suitable for semi-crystalline polymers, as it requires refraction of this polarised light by crystalline structures to generate an image. Amorphous polymers would therefore not be visible using this technique. The colourful images are created due to different refractive indices of the crystals within the samples resulting from differences in orientation and alignment, known as birefringence. This therefore allows spherulite morphology to be observed.

2.11.2 Method

Samples with a thickness of 10 µm were produced using a Biocut 2035 microtome (Reichert-Jung). They were heated from ambient temperature (~25 ºC) to 180 ºC at 50 ºC/min, and held for 2 minutes, before being cooled back down to room temperature at 50 ºC/min. Samples

were analysed at 50 x magnification on an Olympus microscope fitted with a Pixelink camera. This was connected to a Linkam THMS 600 hot stage, and controlled by Linksys 32 software.

2.12 Scanning Electron Microscopy

2.12.1 Experimental technique

Scanning electron microscopy (SEM) is a method for high resolution imaging of surfaces, and in this work was used to analyse the fracture surfaces of the material to assess mode of fracture and miscibility. In this technique, an electron beam is scanned across the sample surface (which is coated with an electrically conductive material) resulting in the production of low energy secondary electrons and back scattered electrons which are collected by their respective detectors. The secondary electrons that escape from the sample surface provide topographical information. The backscattered electrons produce contrast within the sample, based on the atomic number of the elements. Elements with higher atomic number appear brighter, while those with a lower atomic number appear darker.

2.12.2 Method

All samples were taken from plaques of 1 mm thickness. Samples with a width of 7 mm were cut using scissors and submerged in liquid nitrogen for 30 seconds. They were then removed, fractured using pliers and trimmed to an approximate height of 5mm from the fracture surface using scissors. The samples were then mounted in the upright position on SEM stubs (30 mm diameter) using double sided circular SEM adhesive labels to expose the fracture surface before being sputter coated in platinum.

P(3HB-co-3HV)/ Carbohydrate blends were analysed on a HITACHI S-4000 SEM, at 1,000, 3,000 and 10,000 magnification while P(3HB-co-3HV)/ CAB blends were analysed using a JEOL ESEM at 1,000, 3,000 and 10,000 magnification due to availability of equipment.

2.13 References

Bassett (1988). Developments in Crystalline Polymers - 2. Essex, England, Elsevier Applied Publishers Ltd.

de Koning, G. J. M. and P. J. Lemstra (1993). "Crystallization phenomena in bacterial poly[(R)-3-hydroxybutyrate]: 2. Embrittlement and rejuvenation." Polymer **34**(19): 4089-4094.

Kelly, C. A., et al. (2012). "Supercritical CO2: A Clean and Low Temperature Approach to Blending PDLLA and PEG." Advanced Functional Materials **22**(8): 1684-1691.

Modi, S., et al. (2011). "Assessment of PHB with varying hydroxyvalerate content for potential packaging applications." European Polymer Journal **47**(2): 179-186.

Thermo (2017, 20/04/2017). "Feeding material into twin-screw extruders." Retrieved 20/04/2017, from http://slideplayer.com/slide/5793117/

Chapter 3
The effect of incorporating saccharides into P(HB-co-HV) on the secondary crystallisation process

3.0 Introduction

It has been established from the literature that intermolecular hydrogen bonding (H-bonding) is a successful means of improving the mechanical and thermal properties of P(3HB) and P(3HB-co-3HV) (which will now be referenced as PHB and P(HB-co-HV) in the remaining chapters). Molecules such as BPA (Figure 3.1a) contain hydroxyl groups and therefore capable of hydrogen bonding with the oxygen present on the carboxylic acid groups of PHB and copolymers. This was found to significantly improve the mechanical properties of P(HB-co-HV), and reduce the crystallinity due to its bulky chemical structure hindering the chain interaction required for crystallisation (Fei, Chen et al. 2003, Fei, Chen et al. 2004, Fei, Chen et al. 2004, Semba, Kitagawa et al. 2006). However, BPA is toxic, and therefore it cannot be incorporated into food packaging materials making it unsuitable for investigation in this project. Suitable molecules for these applications have to be classified as 'Generally Regarded as Safe' (GRAS) under regulations outlined by the FDA.

An additive that fits the GRAS criteria is starch. Starch is a polymeric carbohydrate, with its repeat unit shown in Figure 3.1b. It has a bulky chemical structure, with hydroxyl groups present, and therefore possesses the key functional groups outlined for a potentially sustainable alternative to BPA. In addition, the presence of hydroxyl groups makes it capable of hydrogen bonding in a similar fashion. The presence of H-bonding between PHB and natural starch was reported by Zhang and Thomas (2010) whereby changes to the width,

intensity and shift of the carbonyl peak were observed as a result of the formation of H-bonds.

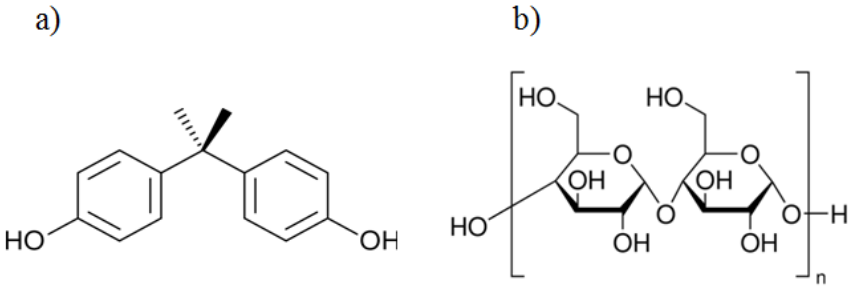

Figure 3.1. Chemical structures of a) BPA and b) Starch

Starch was found to be an advantageous addition to PHB, with benefits to thermal properties such as a reduction in degree of crystallinity (X_c)(Thiré, Ribeiro et al. 2006), in addition to increased biodegradation rate (Ramsay, Langlade et al. 1993) and enhanced thermal stability (Zhang and Thomas 2010). Furthermore starch is naturally sourced, biodegradable, cheap and widely available, making it a sustainable and cost effective additive for PHB polymers. However, natural starch was found to reduce mechanical properties in most cases in melt blended samples (Ramsay, Langlade et al. 1993, Thiré, Ribeiro et al. 2006, Zhang and Thomas 2010). This was because the T_m of natural starch is in excess of 200 ºC. As the T_m of P(HB-co-HV) is around 170 ºC, the starch did not melt and disperse upon processing. It was therefore present as discrete granules of starch within the P(HB-co-HV) matrix as observed by SEM, with pull out holes indicating low interfacial adhesion between the two components (Thiré, Ribeiro et al. 2006, Reis, Pereira et al. 2008). This produced a brittle material with reduced strength and toughness.

This was improved by the incorporation of thermoplastic starch (Godbole, Gote et al. 2003), where the mechanical properties were found to increase. Thermoplastic starch is produced by the gelatinisation of natural starch with heat and shear to disrupt the native starch granules,

and the addition of water and plasticisers such as glycerol. Another polymer such as poly(vinyl alcohol), poly(oxyethylene), or poly(vinylpyrrolidone) which is capable of forming hydrogen bonds is also incorporated into the starch to stabilise the amorphous phase and prevent the material crystallising (Shanks and Kong 2012). This gives it thermoplastic type properties that allow it to be easily and homogenously incorporated into a polymer blend for food packaging applications whilst improving the mechanical properties.

It is therefore apparent that molecules that can be thoroughly and homogenously incorporated into the melt may help to improve the properties of P(HB-co-HV), and therefore substances with melting temperatures that are lower that P(HB-co-HV) are desirable. In light of starch looking like a promising material, the monomer of starch, glucose was considered. This contains a bulky six carbon ring capable of chain disruption during crystallisation, plus the hydroxyl groups that allow the material to form H-bonds. Other structures present in nature that possess similar structures to glucose are, fructose, maltose and melezitose. The chemical structures of these units can be seen in Figures 3.2 a-d.

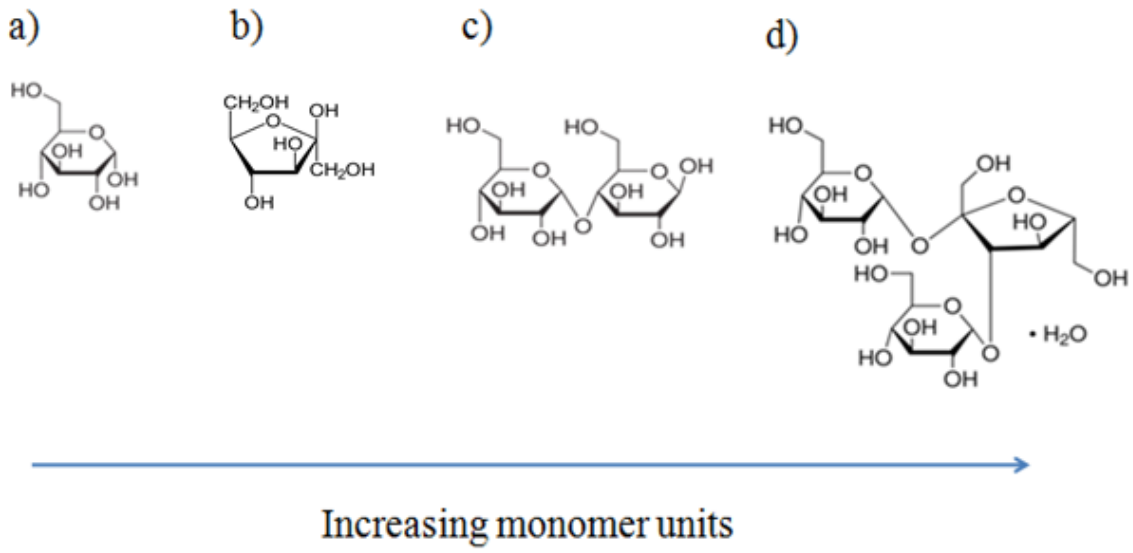

Figure 3.2. Chemical structures of a) glucose b) fructose c) maltose d) melezitose

All of the substances presented above present the two key structural requirements previously mentioned in that they all possess bulky ring structures and hydroxyl groups. Furthermore, the melting temperatures of all of these are below that of P(HB-co-HV), thus facilitating dispersion of the saccharides into the blends. Therefore, the above saccharides were incorporated into P(HB-co-HV) to analyse the effect of each of the additives on the initial mechanical properties of P(HB-co-HV). Furthermore, as previously discussed in Chapter 1 (Section 1.3.2), P(HB-co-HV) is known to secondary crystallise, which is brought about by mobility of the polymer chains within the amorphous region when the material is stored at room temperature. Crosslinks restrict chain mobility, and therefore the effect of incorporating the above hydrogen bonding substances on their ability to restrict the secondary crystallisation behaviour of P(HB-co-HV) was also assessed.

3.1 Results and Discussion

3.1.1 Characterisation of blend components

The melting temperatures of the blend components were analysed by Differential Scanning Calorimetry (DSC). Knowledge of the properties of the blend components is important as it determines their suitability to be combined, and provides an indication regarding interactions between the blend components. The thermal properties of the blend components used in this work are illustrated in Figure 3.3, and detailed in Table 3.1.

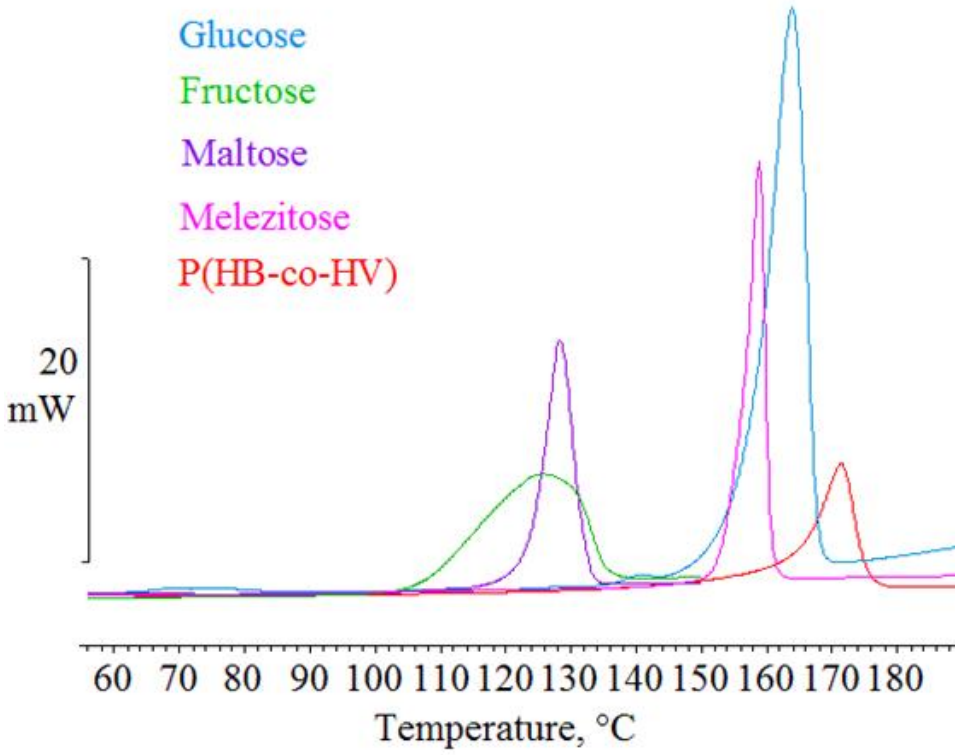

Figure 3.3. The melting endotherms of the blend components analysed at 10 ºC/min

Table 3.1. The melting temperatures of the blend components analysed at 10 ºC/min

Component	T_m (ºC)
P(HB-co-HV)	171
Glucose	162
Fructose	125
Maltose	128
Melezitose	157

It can be observed that the melting temperatures of all of the saccharides were below that of P(HB-co-HV). This confirmed that they would be suitable additives to be fully incorporated via melt blending into P(HB-co-HV).

3.1.2 Sample production

Each saccharide was blended in three concentrations with P(HB-co-HV) in the quantities outlined in Chapter 2 (Section 2.2.1.2). The concentrations will be denoted as 'low,' 'medium' and 'high' in this work, and equate to the crosslink ratios of 87.94, 41.66 and 25.78 respectively. Examples of the resulting sample plaques are shown in Figure 3.4 (a-e) and contain the lowest concentration of each additive.

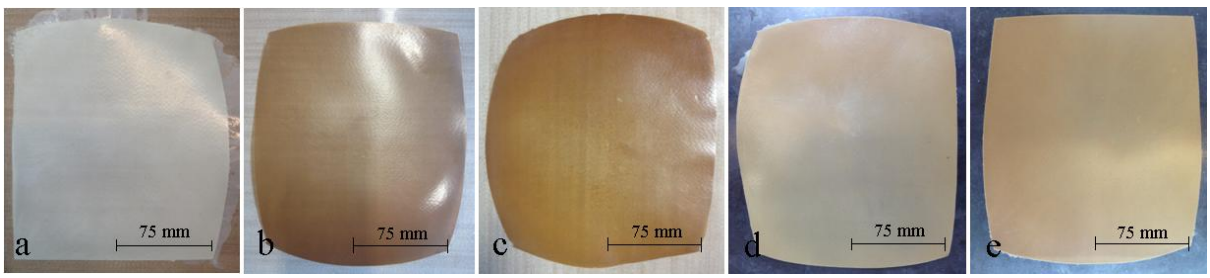

Figure 3.4. Photographs of sample plaques produced a) P(HB-co-HV) b) glucose c)fructose d) maltose e) melezitose

Unblended P(HB-co-HV) is shown in Figure 3.4a, where it is a milky white colour. As observed from Figures 3.4 b-e, the addition of all saccharides renders the samples a shade of brown. This colour change is either indicative of degradation of the polymer, or caramelisation of the sugars. As the samples were all processed under the same conditions, the fact that the unblended material is the only sample that isn't brown indicates that the colour change observed in P(HB-co-HV)/saccharide blends is a product of the caramelisation of the sugars during melt processing. The extent of the colour change varies between samples. There does not appear to be a link between melting temperature and the degree of colour change, however the additives composed of larger units (maltose and melezitose) show a reduced colour change than the monosaccharides glucose and fructose despite there being a larger weight percentage within the blends. This therefore indicates that the observed differences arise from differences in chemical structure. This could result from the presence of glycosidic bonds within maltose and melezitose which are responsible for the joining of two or more saccharide molecules (Figure 3.2c and d). This renders the materials more thermally stable by creating additional steps in the chemical decomposition of disaccharides and trisaccharides (Kroh 1994). These structures therefore do not break down as much during melt processing. There are also more bonds to break in the larger chains for complete degradation of the molecule. This leads to a higher caramelisation temperature in disaccharides and trisaccharides (Table 3.2)(Food-Info 2014). Furthermore, unlike glucose and fructose, the caramelisation temperature for maltose is above that of its T_m. It is also above that of the temperature used to blend the materials (170 ºC), and is the same as the temperature used to process the materials into plaques. As a result, the material caramelises at a later stage and to a lesser extent than the blends containing glucose and fructose, leading to the reduced colour change observed in these blends.

Table 3.2. The caramelisation temperatures of the saccharides used within this work

Saccharide	Caramelisation temperature (ºC)
Glucose	160
Fructose	110
Maltose	180
Melezitose	n.d*

* n.d: not determined

Caramelisation is a heat initiated decomposition process resulting in dehydration of the molecule, breakdown of the ring structure, and free radical polymerisation. The first step typically involves internal reorganisations within the carbohydrates known as enolisations (Ramsay, Langlade et al. 1993, Tian, Sinskey et al. 2005, Zhang and Thomas 2010), followed by the elimination of water molecules (Claude and Ubbink 2006). The composition of the sugar determines the following set of reactions, but the main reaction product obtained from the thermal decomposition of glucose, maltose and melezitose is Hydroxymethylfurfural (HMF) (Sugisawa 1966, Fagerson 1969, Kroh 1994, Gamble 2002, Venderbosch and Heeres 2011, Woo, Kim et al. 2015). Other products such as formic acid, lactic acid and levulinic acid have also been reported (Venderbosch and Heeres 2011, Woo, Kim et al. 2015). Sugisawa (1966) established that these volatiles were already formed in glucose during thermal decomposition at 150 ºC (Sugisawa 1966), a factor which should be taken into consideration in this work. This degradation product is one of the contributing factors to the colour change observed in glucose and maltose (Woo, Kim et al. 2015). The mechanism of thermal degradation of glucose into HMF can be seen in Figure 3.5 (Venderbosch and Heeres 2011).

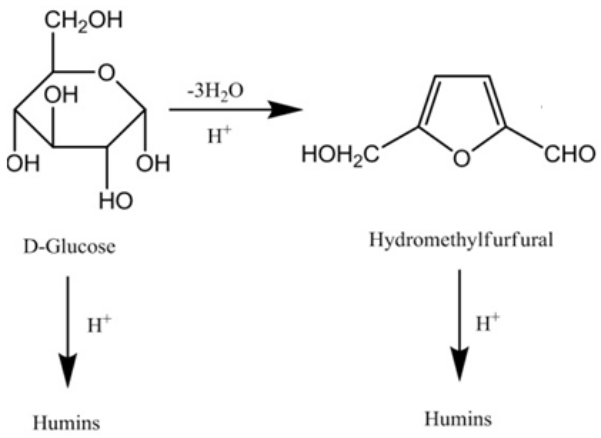

Figure 3.5. Reaction mechanism for the thermal dehydration of glucose to HMF. Adapted from (Venderbosch and Heeres 2011)

This resulting removal of hydroxyl groups from the structure in the form of water could have had an effect on the hydrogen bonding capabilities of the material by reducing the number sites that are available for interaction between the two components of the blends as the number of hydroxyl groups present has reduced. Furthermore, P(HB-co-HV) has a hydrolysable backbone and is therefore sensitive to the presence of water. The production of water would therefore act to degrade the P(HB-co-HV) by hydrolysis of the ester linkages during processing. The implications of these possibilities with regards to properties will be discussed in future sections within this work.

In a study by Eggleston and Vercellotti (2000), the rate of fructose degradation was found to be higher in degraded fructose solution than glucose solution. The observed colour change was 3 fold higher in degraded fructose than glucose after 2 hours at 80 ºC. This was attributed to the higher the rate of enolisation in fructose due to conformational differences between the structures (Eggleston and Vercellotti 2000) which could also be responsible for its markedly lower caramelisation temperature. This would explain the slightly darker colour observed for

fructose samples than the glucose samples, although this is not immediately obvious from Figure 3.4c, but was established by visual observations of the samples.

3.1.3 Characterisation of the blends – Day 0

3.1.3.1 Dynamic DSC analysis - Melting

DSC is a useful technique to characterise the thermal properties of polymers, and assess the level of interaction between the blend components. The results for the incorporation of each sugar into P(HB-co-HV) at each concentration are given below in Figures 3.6-3.9 and quantified in Tables 3.3-3.5 with colour intensity increasing from light to dark with increasing saccharide content from low to high. The melting temperatures (T_m), degree of crystallinity of the blend ($X_{c\ Blend}$) and the P(HB-co-HV) component of the blend (X_c), as well as heat of fusion of the blend (ΔH_f) were determined.

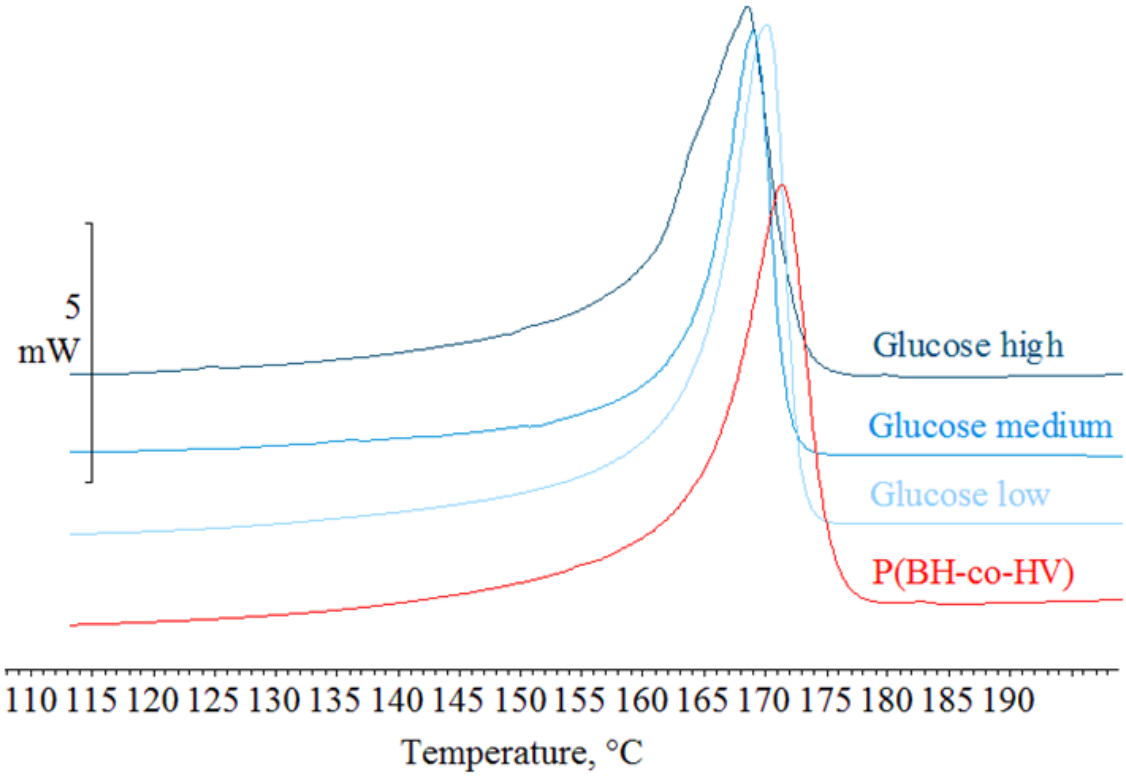

Figure 3.6. DSC traces of P(HB-co-HV) and glucose blends obtained by heating at 10 ºC/min

Table 3.3. Thermal properties of P(HB-co-HV) and glucose blends

Sample	T_m (ºC)	$X_{c\ Blend}$ (%)	X_c (%)	ΔH_f (Jg^{-1})
P(HB-co-HV)	171.2	62.0	62.0	89.9
Glucose low	168.0	62.0	63.0	89.7
Glucose medium	166.1	57.0	60.0	83.6
Glucose high	163.9	52.0	56.0	75.2

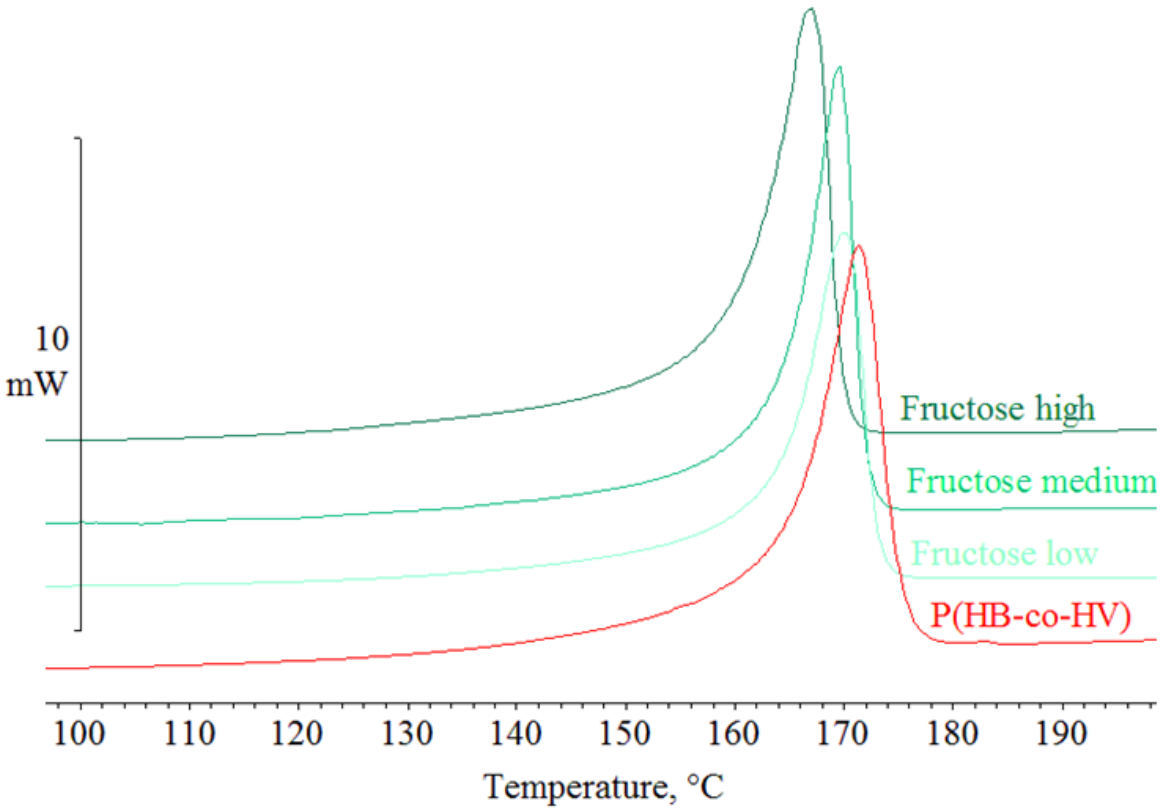

Figure 3.7. DSC traces of P(HB-co-HV) and fructose blends obtained by heating at 10 ºC/min

Table 3.4. Thermal properties of P(HB-co-HV) and fructose blends

Sample	T_m (ºC)	$X_{c\ Blend}$ (%)	X_c (%)	ΔH_f (Jg^{-1})
P(HB-co-HV)	171.2	62.0	62.0	89.9
Fructose low	168.7	60.0	61.0	87.2
Fructose medium	167.7	58.0	61.0	85.3
Fructose high	165.9	56.0	61.0	81.1

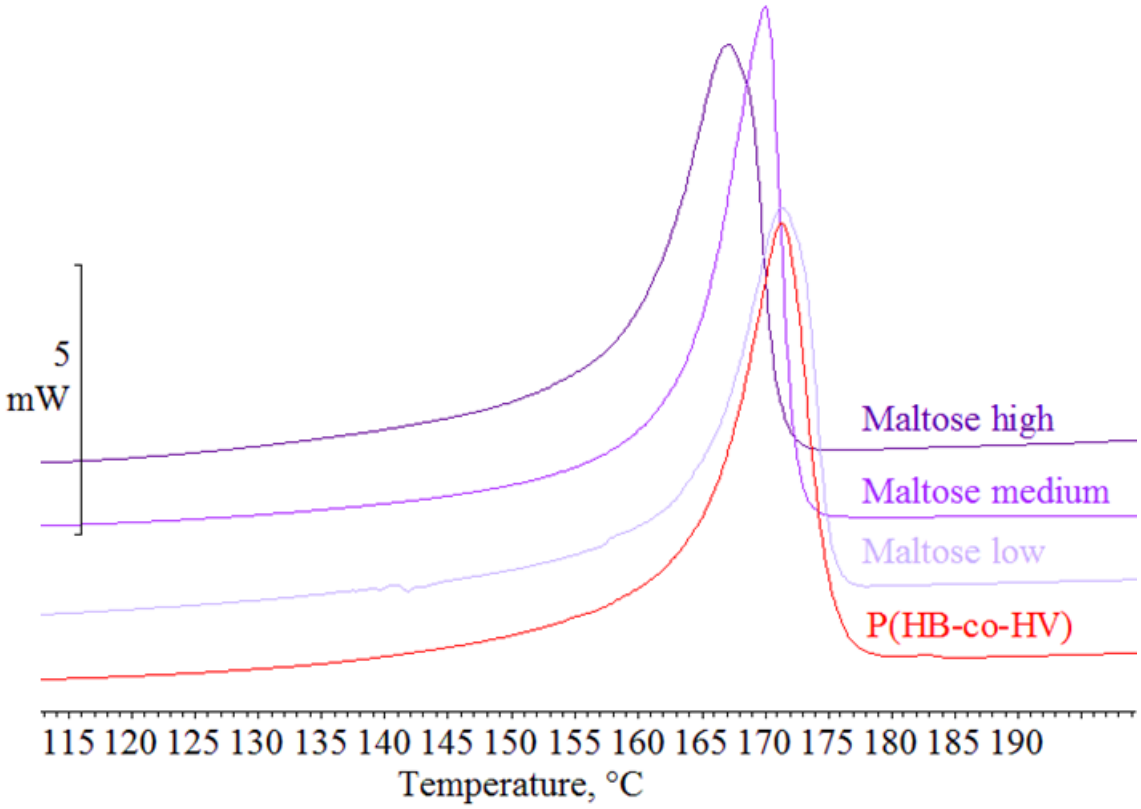

Figure 3.8. DSC traces of P(HB-co-HV) and maltose blends obtained by heating at 10 ºC/min

Table 3.5. Thermal properties of P(HB-co-HV) and maltose blends

Sample	T_m (ºC)	$X_{c\ Blend}$ (%)	X_c (%)	ΔH_f (Jg^{-1})
P(HB-co-HV)	171.2	62.0	62.0	89.9
Maltose low	167.4	59.0	61.0	86.4
Maltose medium	167.4	59.0	65.0	85.8
Maltose high	166.5	50.0	58.0	73.5

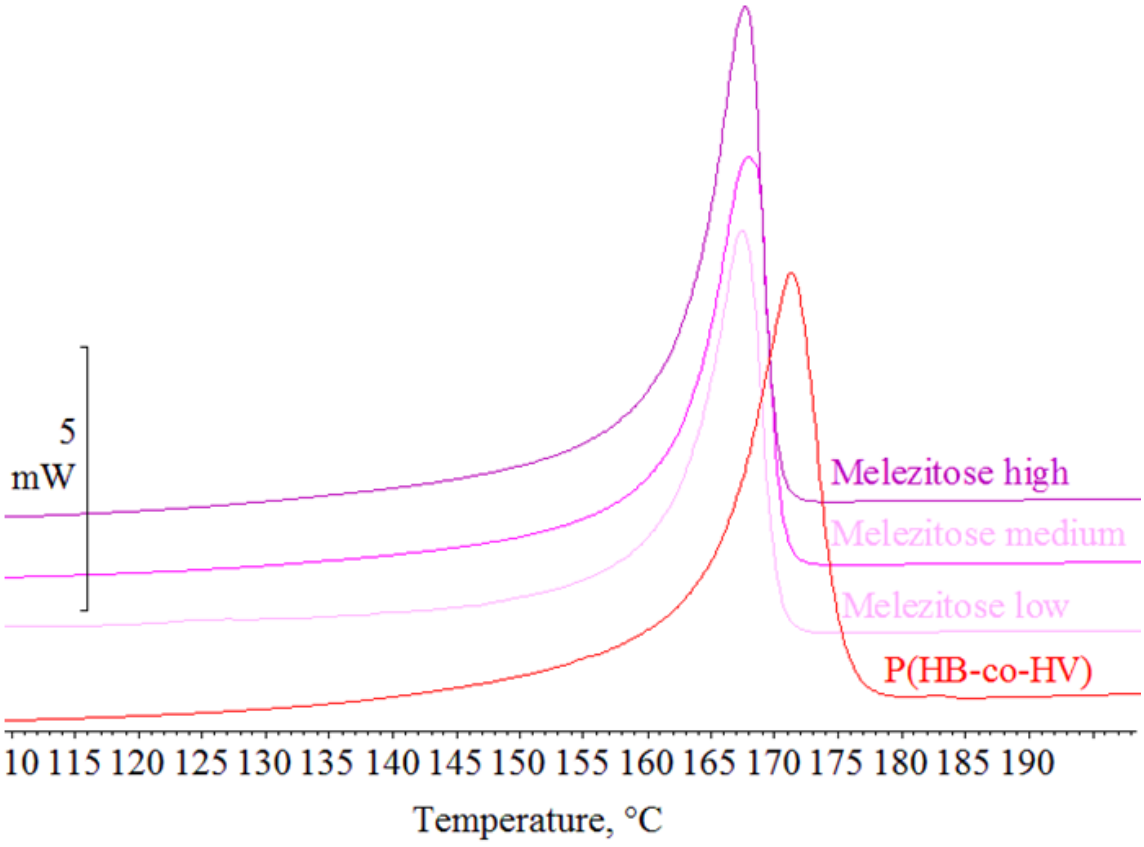

Figure 3.9. DSC traces of P(HB-co-HV) and melezitose blends obtained by heating at 10 ºC

Table 3.6. Thermal properties of P(HB-co-HV) and melezitose blends

Sample	T_m (ºC)	$X_{c\ Blend}$ (%)	X_c (%)	ΔH_f (Jg^{-1})
P(HB-co-HV)	171.2	62.0	62.0	89.9
Melezitose low	164.4	55.0	59.0	79.5
Melezitose medium	162.0	55.0	63.0	79.6
Melezitose high	163.4	52.0	64.0	76.3

In Figures 3.6-3.9 a single endotherm is observed in all cases with no evidence of the presence of the corresponding T_ms of the sugar components. This suggests that the blend is homogenous and the components are compatible, if not miscible. A schematic diagram of the possible locations of the additives within the crystalline morphology is shown in Figure 3.10. It can also be seen that the presence of each additive induces melting point depression, in addition to a reduction in ΔH_f. This suggests that the saccharides are present within the spherulites, as they would not be influencing the T_m if they had been rejected to the inter-spherulitic regions.

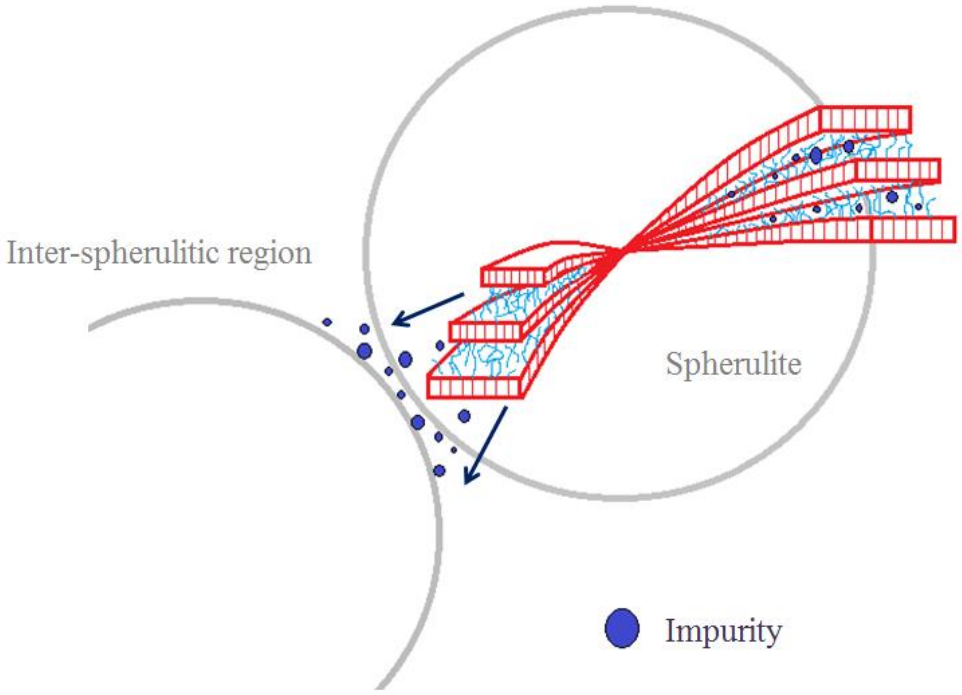

Figure 3.10. A schematic diagram of the possible locations of impurities showing the rejection of impurities into the inter-spherulitic regions (left) and the presence of the impurity within the amorphous inter-lamellar regions of the spherulite

Here, the saccharides could be actively forming intermolecular H-bonds with the P(HB-co-HV). This would act to disrupt the chain interactions and prevent the close packing of chains

required for crystallisation of the material from the melt. This hindrance of crystallisation would lead to reduced crystallinity, which would result in a decrease in T_m. This is because more energy is required to overcome interactions within crystalline regions to transform it to the liquid state. Thus, with fewer crystalline regions present, the energy required to melt the polymer is reduced. However, upon analysis of crystallinity within the samples (Tables 3.3-3.6), the crystallinity of the P(HB-co-HV) component is only found to reduce in glucose blends (Table 3.3).A reduction of 6 % is observed when the concentration is increased from pure P(HB-co-HV) to the blend containing the highest concentration of glucose (Table 3.3). There is no significant reduction in crystallinity of the P(HB-co-HV) components in other blend systems (Tables 3.4-3.6), therefore making this explanation unlikely.

This T_m depression could also be occurring as a result of colligative properties of impurities within the matrix. This is where the addition of another component increases the entropy of the system therefore resulting in a decreased chemical potential and as a result , less energy is required to melt the polymer. Alternatively, the reduction in T_m within the blends could be due to the thermal degradation of the polymer upon processing. Hydrolysis of the ester linkages produced by the degradation of sugars at elevated temperatures could induce chain scission of P(HB-co-HV), leading to a reduction in the M_w of the material and production of acidic reaction products (Saeki, Tsukegi et al. 2005). Decreased molecular weight decreases the melting temperature, as shorter chains required less energy to melt. It is clear that the saccharide additives could be having a number of effects on the P(HB-co-HV) material. The likelihood of each case will be discussed in more detail throughout the chapter as other findings are reported.

3.1.3.2 Dynamic DSC analysis – Melt Crystallisation

The effect of each additive on the melt crystallisation behaviour was observed by cooling the samples following the heating run. From the resulting traces, the melt crystallisation

temperature (T_c) was obtained by measuring the peak of the transition, and the enthalpy of crystallisation (ΔH_c) by the area underneath the peak. This allows for analysis of nucleation and growth processing during crystallisation to be assessed where the nucleation process is indicated by the position of the onset and of crystallisation, and growth behaviour can be observed by breadth of the peak.

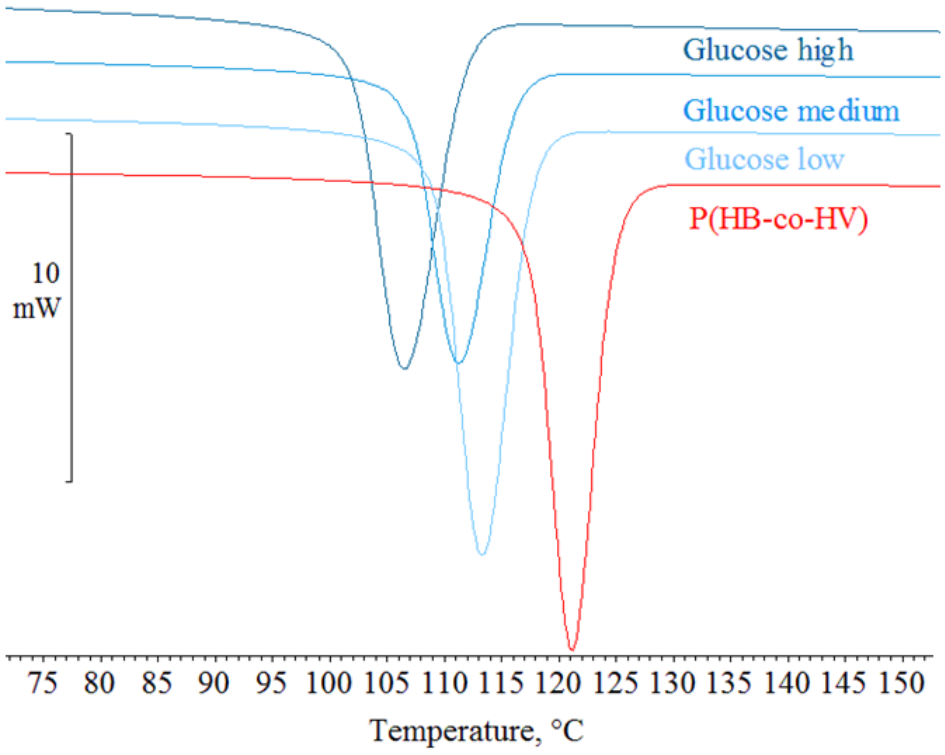

Figure 3.11. DSC traces of P(HB-co-HV) and glucose blends at each concentration obtained by cooling at 10 ºC/min

Table 3.7. Thermal properties obtained upon melt crystallisation in P(HB-co-HV) and glucose blends

Sample	T_c (ºC)	ΔH_c (Jg^{-1})
P(HB-co-HV)	121.8	-77.5
Glucose low	113.9	-78.0
Glucose medium	111.6	-74.6
Glucose high	107.0	-70.5

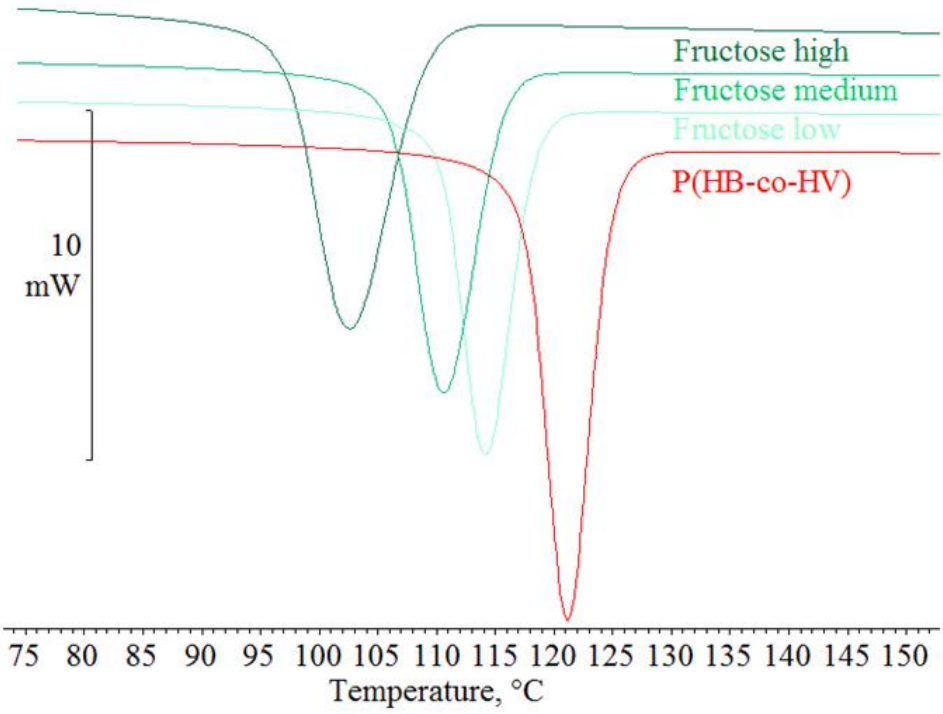

Figure 3.12. DSC traces of P(HB-co-HV) and fructose blends at each concentration obtained by cooling at 10 ºC/min

Table 3.8. Thermal properties obtained upon melt crystallisation of P(HB-co-HV) and fructose blends

Sample	T_c (ºC)	ΔH_c (Jg^{-1})
P(HB-co-HV)	121.8	-77.5
Fructose low	114.6	-77.3
Fructose medium	110.9	-73.5
Fructose high	103.0	-69.1

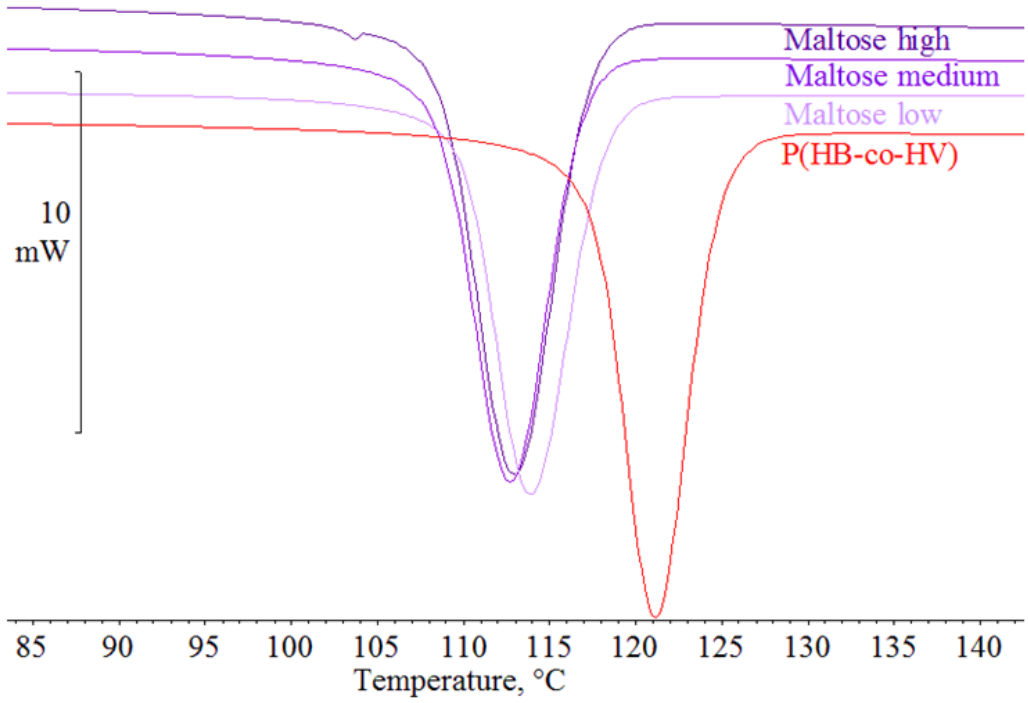

Figure 3.13. DSC traces of P(HB-co-HV) and maltose blends at each concentration obtained by cooling at 10 ºC/min

Table 3.9. Thermal properties obtained upon melt crystallisation of P(HB-co-HV) and maltose blends

Sample	T_c (ºC)	ΔH_c (Jg^{-1})
P(HB-co-HV)	121.8	-77.5
Maltose low	114.4	-75.7
Maltose medium	113.2	-72.0
Maltose high	113.6	-69.2

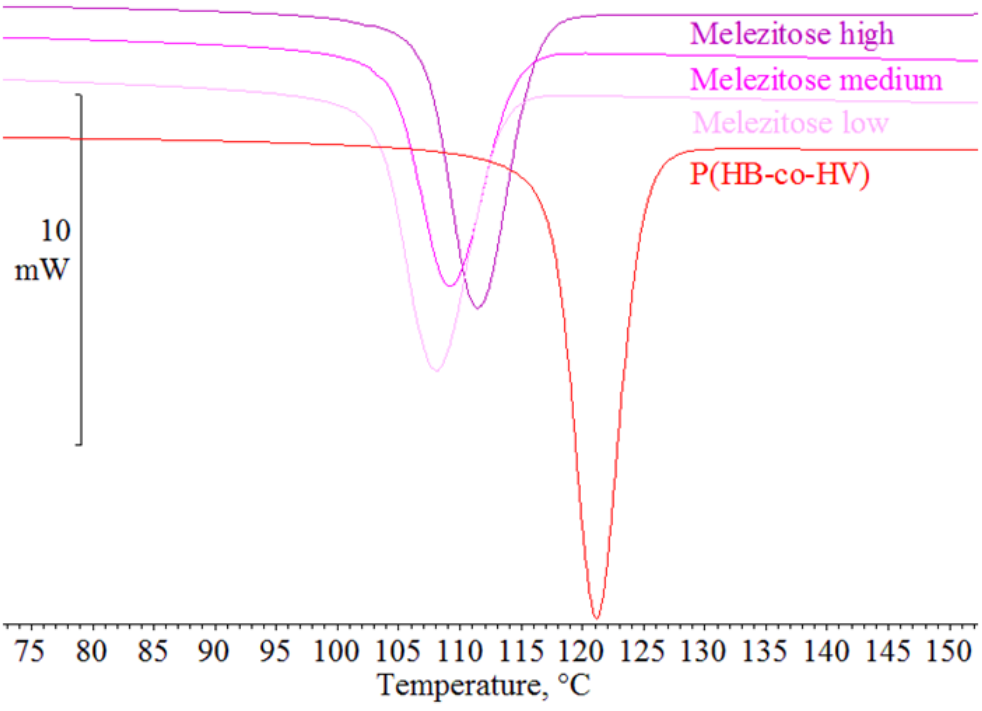

Figure 3.14. DSC traces of P(HB-co-HV) and melezitose blends at each concentration obtained by cooling at 10 ºC/min

Table 3.10. Thermal properties obtained upon melt crystallisation of P(HB-co-HV) and melezitose blends

Sample	T_c (ºC)	ΔH_c (Jg^{-1})
P(HB-co-HV)	121.8	-77.5
Melezitose low	108.4	-70.8
Melezitose medium	109.5	-68.59
Melezitose high	116.43	-63.73

It is apparent from Figures 3.11-3.14 that the presence of sugars has an effect on the melt crystallisation behaviour of P(HB-co-HV). In all cases, the ΔH_c decreases with the addition of each saccharide, and then as more of the saccharide is incorporated into the blend. The T_c also decreases with increasing concentration in all but one case. As shown in Table 3.10, with the addition of the lowest concentration of melezitose, the T_c drops by 4 ºC. Then as the concentration is increased, the T_c begins to increase and approaches that of pure P(HB-co-HV) in the highest concentration of melezitose. The onset of crystallisation is also delayed as the concentration of each additive is increased. This is because, as the polymer crystallises, low M_w additives are excluded from the crystal lattice into inter-lamellar amorphous regions, which therefore hinders the onset and duration of the crystallisation process. The more additive that is present, the more there is to be excluded and therefore a greater hindrance to the process. The reduction in ΔH_c as concentration increases is likely to be a concentration effect, as there is less available polymer in the system to crystallise.

3.1.3.3 Fourier-Transform Infra-red Spectroscopy

To investigate whether intermolecular interactions were occurring within the P(HB-co-HV) saccharide blends, Fourier Transform Infra-red spectroscopy (FTIR) was conducted as it is a

well-established technique used to determine chemical changes occurring within a material. The identification of intermolecular hydrogen bonding would appear as a shift in the carbonyl peak to higher wavenumbers. The spectra for each set of blends can be seen in Figures 3.15–3.18 below, and a summary of peak positions outlined in Table 3.11. The spectra are labelled from light to dark colours indicating low to high concentrations of each additive within the blends.

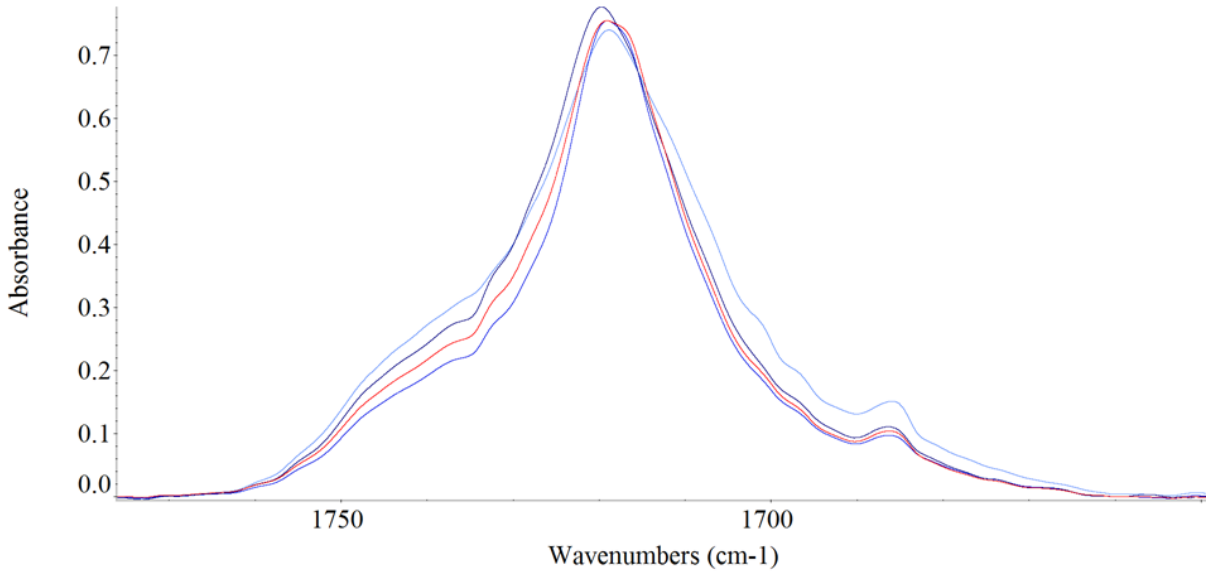

Figure 3.15. FTIR spectra of P(HB-co-HV)/glucose blends at each composition. Red (P(HB-co-HV)), light (low), middle (medium), dark (high)

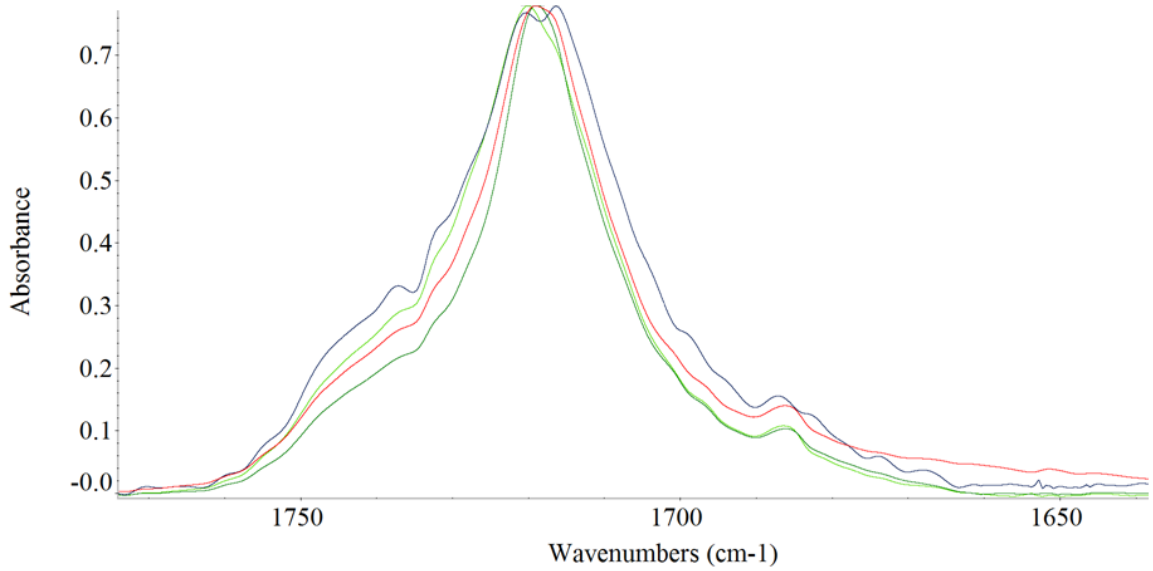

Figure 3.16. FTIR spectra of P(HB-co-HV)/fructose blends at each composition. Red (P(HB-co-HV)), light (low), middle (medium), dark (high)

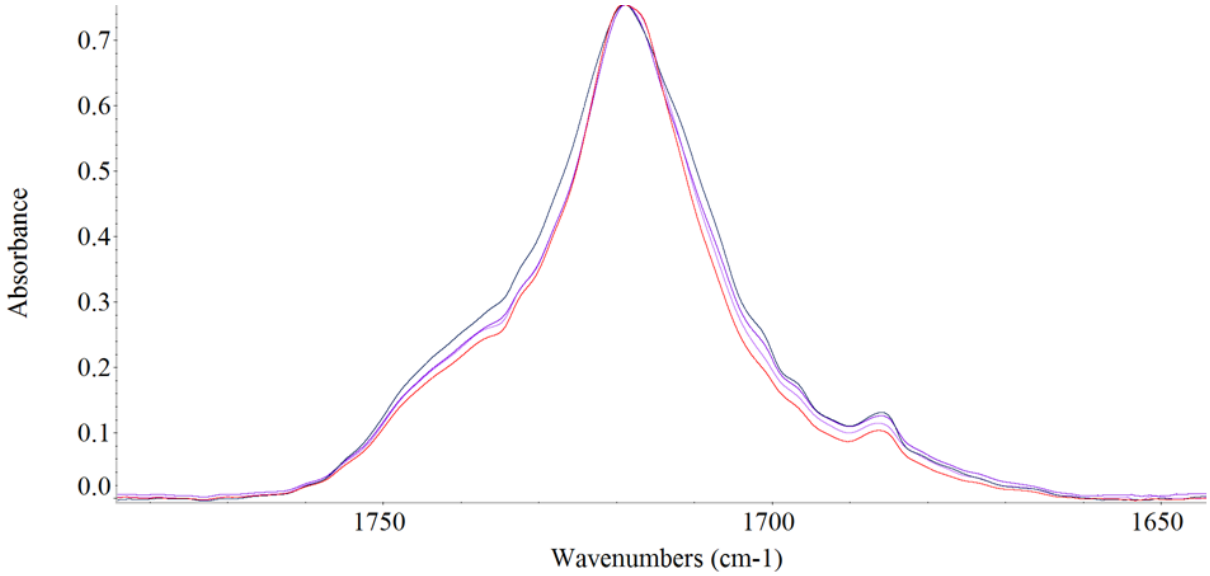

Figure 3.17. FTIR spectra of P(HB-co-HV)/maltose blends at each composition. Red (P(HB-co-HV)), light (low), middle (medium), dark (high)

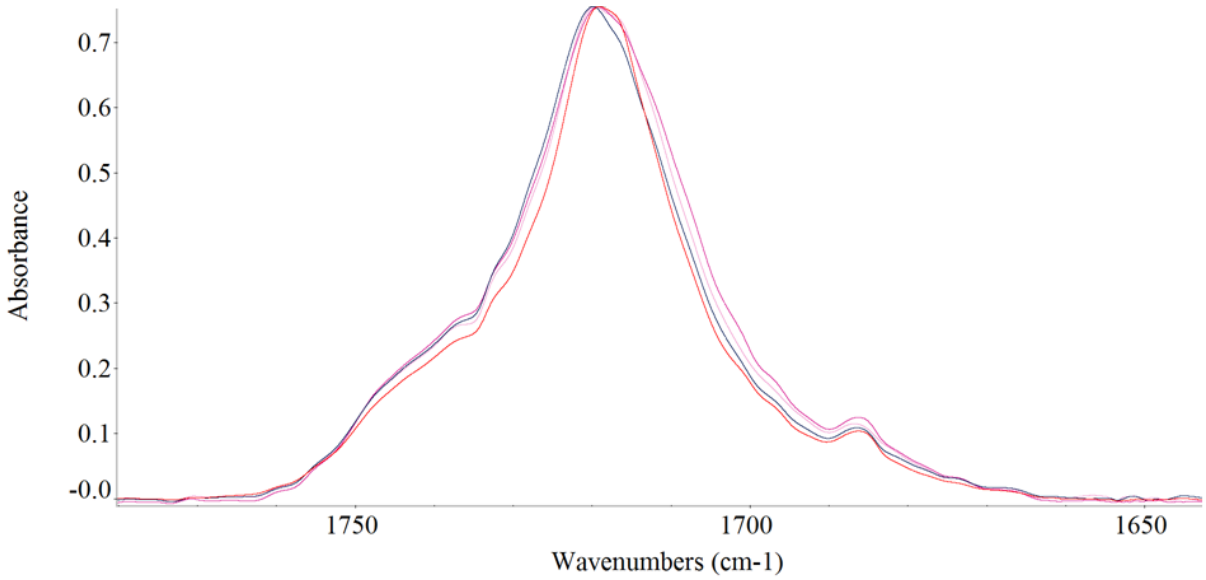

Figure 3.18. FTIR spectra of P(HB-co-HV)/melezitose blends at each composition. Red (P(HB-co-HV)), light (low), middle (medium), dark (high)

Table 3.11. Effect of blending on the position of the carbonyl peak

Additive	Concentration of blend component			P(HB-co-HV)
	Low (cm^{-1})	Medium (cm^{-1})	High (cm^{-1})	(cm^{-1})
Glucose	1719	1719	1720	1719
Fructose	1720	1719	1716 1721	1719
Maltose	1719	1719	1719	1719
Melezitose	1720	1719	1720	1719

It can be seen that there is minimal shift in the carbonyl groups for each set of additives indicatingthat there is minimal interaction between the additives. Furthermore, the highest concentration of fructose leads to a double peak on the carbonyl peak. The carbonyl band consists of two well separated peaks at 1716 and 1721 cm^{-1}. The separation of the carbonyl

has been previously reported to have occurred in pyrolysis of PHB and attributed to the formation of S-trans and S-cis confirmations of the PHB degradation product, crotonic acid (Gonzalez, Irusta et al. 2005). This suggests that the presence of a high composition of fructose within the blends is acting to cause the production of crotonic acid within the blends. This was also observed in blends containing all other additives at points during the time study. Figure 3.19 shows examples of splitting of the carbonyl peaks in blends containing additives at medium concentrations. These spectra were collected from different regions of the polymer samples at varying time points throughout the study. There was no correlation between time point and the occurrence of the split carbonyl peak.

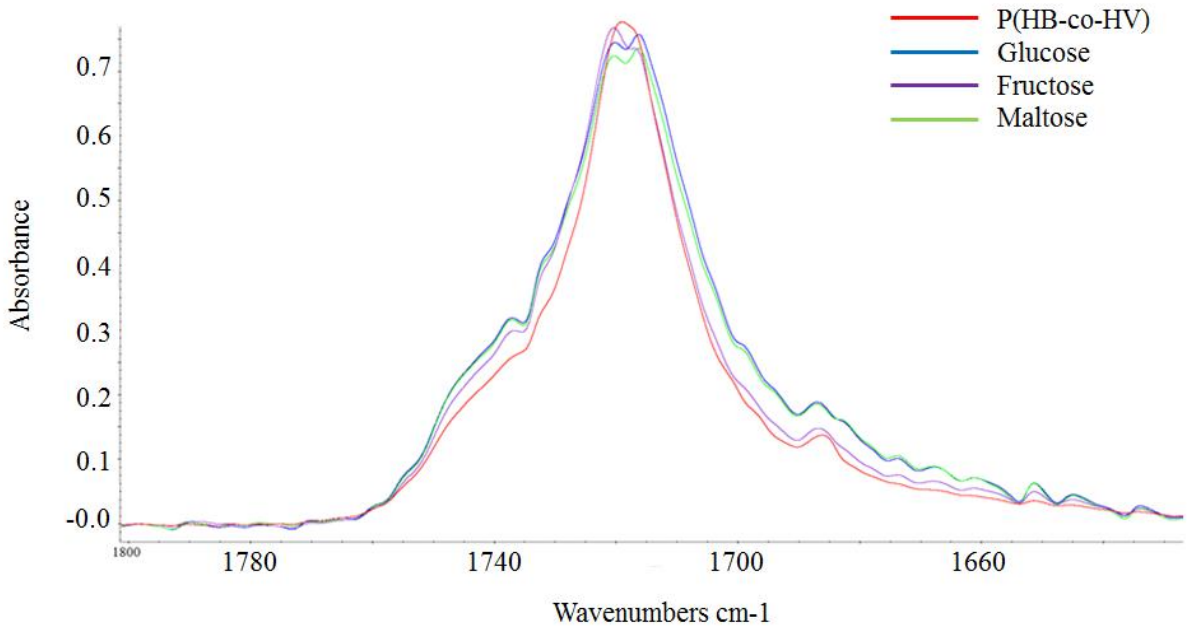

Figure 3.19. FTIR spectra of the carbonyl region of saccharide blends at medium concentrations displaying the evolution of crotonic acid

This is a strong indication that thermal degradation is occurring within all P(HB-co-HV)/ saccharide blends due to hydrolysis. As previously discussed, glucose thermally degrades by a dehydration reaction producing water at temperatures around 150 ºC and above. P(HB-co-

HV) possesses a hydrolysable backbone (Saeki, Tsukegi et al. 2005). Crotonic acid is a reaction product of the alkaline hydrolysis of PHB (Yu, Plackett et al. 2005). It therefore seems reasonable to conclude that a possible explanation for this behaviour could be due to the thermal degradation of saccharides at 150 ºC leading to a production of water, which in turn hydrolyses the ester bonds of the P(HB-co-HB) chains, resulting in the production of crotonic acid as observed on the FTIR spectra above.

This is therefore a strong argument for the concurrent degradation of both blend components upon melt processing. Figure 3.20 shows the relevant region of the IR spectra of crotonic acid in the region associated with the carbonyl peak of P(HB-co-HV) (NIST 2012). It displays a broad peak at approximately 1710 cm^{-1}. It is therefore probable that the peak at 1716 cm^{-1}, is a product of crotonic acid formation, in addition to the fact that the peaks broaden with the addition of the saccharides from P(HB-co-HV).

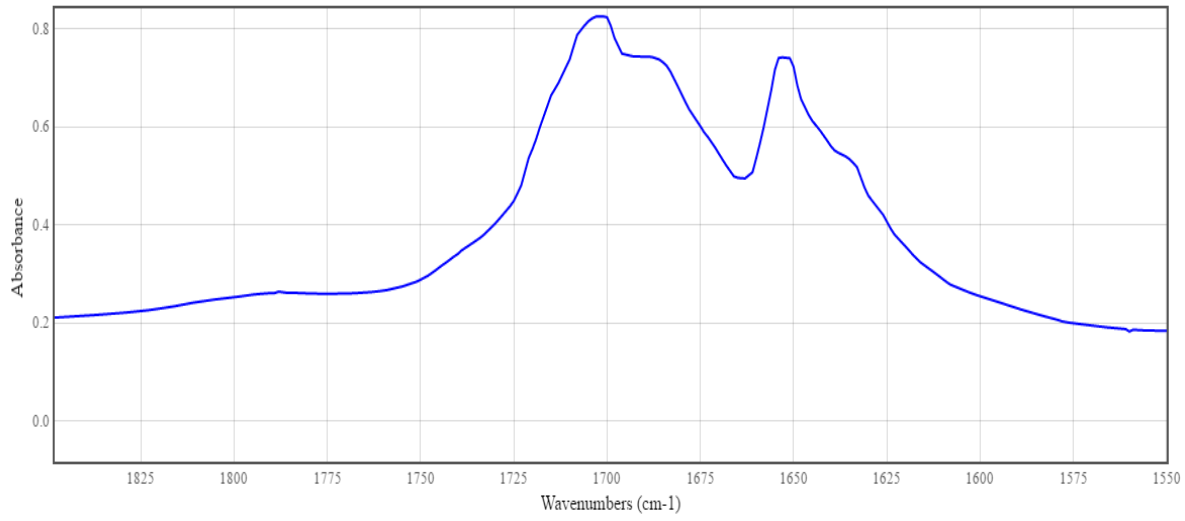

Figure 3.20. FTIR spectra of crotonic acid in the carbonyl region

To double check that the saccharides were being detected by the FTIR technique, the OH bonding region was observed. The presence of an increasing intensity within the 3600 – 3000 cm^{-1} region in Figure 3.21 is indicative of increasing amounts of OH molecules as the glucose concentration is increased, based on the FTIR spectra of D-glucose within this region (Figure 3.22). This occurs across all additives, with the highest intensity occurring in blends containing melezitose, in accordance with a greater number of hydroxyl groups present. It is therefore apparent that the FTIR is detecting signals from the saccharides , and therefore a lack of peak shift is a product of limited interactions between the components rather than the presence of saccharides not being registered in the system.

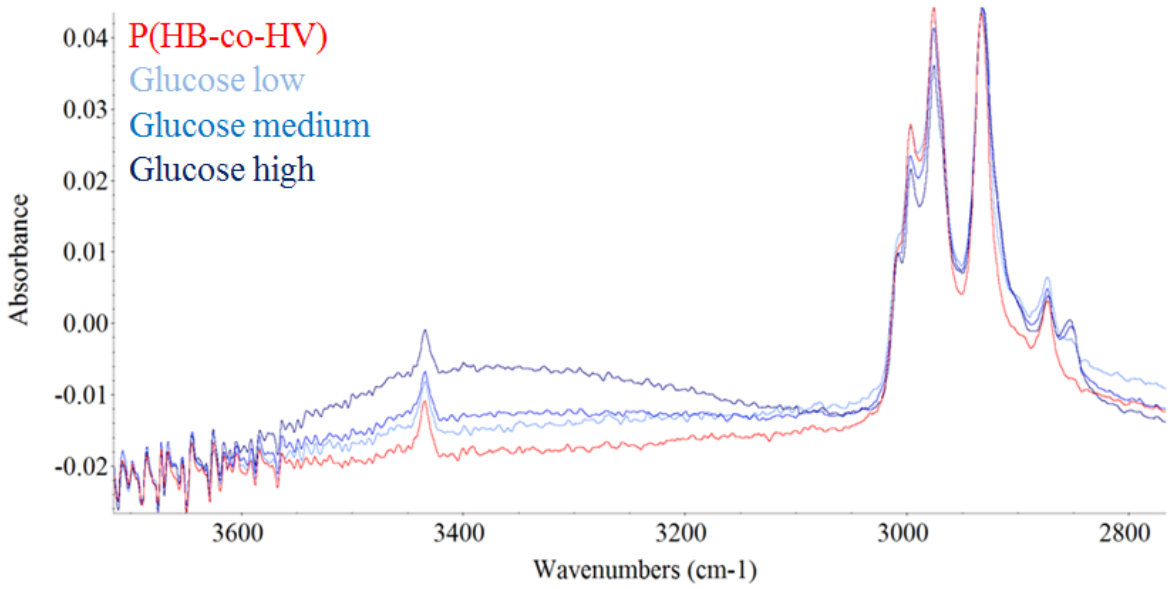

Figure 3.21. FTIR spectra of the hydroxyl region in P(HB-co-HV)/glucose blends

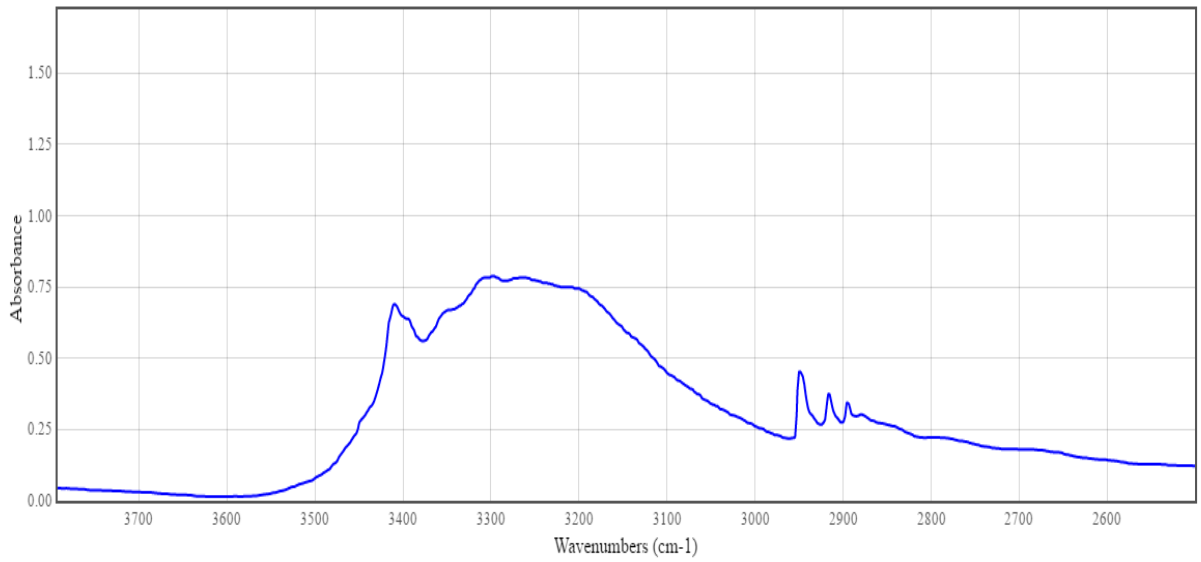

Figure 3.22. FTIR spectra of D-Glucose in the hydroxyl region

3.1.3.4 Rheology

Rheology is a useful technique to establish melt flow characteristics of polymers which is important to understand for the melt processing of the materials. Important parameters that influence the rheology of the polymer melts are molecular weight, molecular weight distribution and branching. The property measured in this work was shear viscosity (ŋ) which is determined using Equation 3.1 where τ represents the shear stress (force per area) and γ is the shear rate.

$$ŋ(Pa.s) = \frac{\tau}{\gamma} \qquad [3.1]$$

Shear stress and shear rate are calculated using Equations 3.2 and 3.3 respectively where σ represents shear stress, F represents force, A equates to area dγ is change in strain and dt is change in time.

$$\sigma(Pa) = \frac{F}{A} \qquad [3.2]$$

$$\gamma\ (s^{-1}) = \frac{d\gamma}{dt} \qquad [3.3]$$

The rheological data for the blends can be observed in Figures 3.23-3.26All samples exhibit Newtonian behaviour in the first portion of the traces where they possess a flat region. As the strain is increased, shear thinning begins to occur, characterised by the downwards slope on the traces where viscosity decreases with increasing shear. This is a characteristic trait for polymeric materials where the chains begin to unravel and align with the direction of motion. This is an indicator of elasticity within the melt (Gupta 2000). All blends for all samples display this behaviour (Figures 3.23-3.26). Furthermore PHB has been found to decrease in molecular weight with increasing residency time in the rheometer at 180 ºC which could also be another contribution to the observed melt flow behaviours (Yamaguchi and Arakawa 2006).

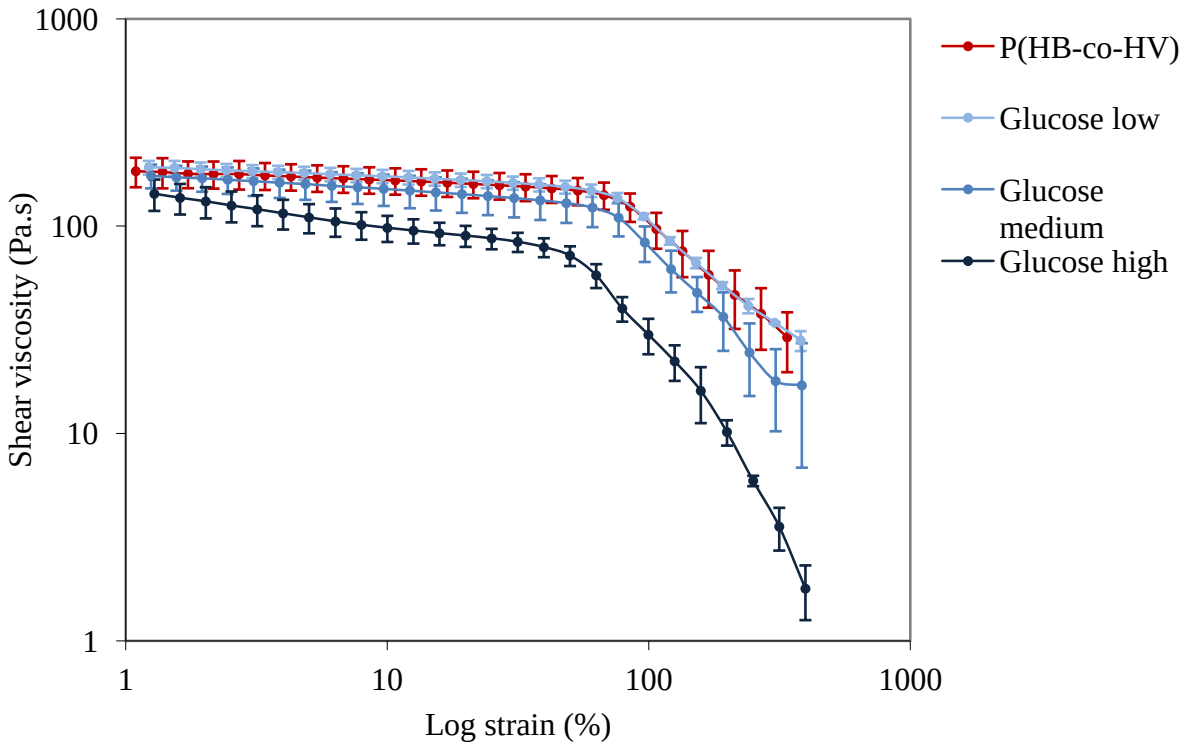

Figure 3.23. Rheological data of P(HB-co-HV) and glucose blends analysed at a frequency of 10 Hz

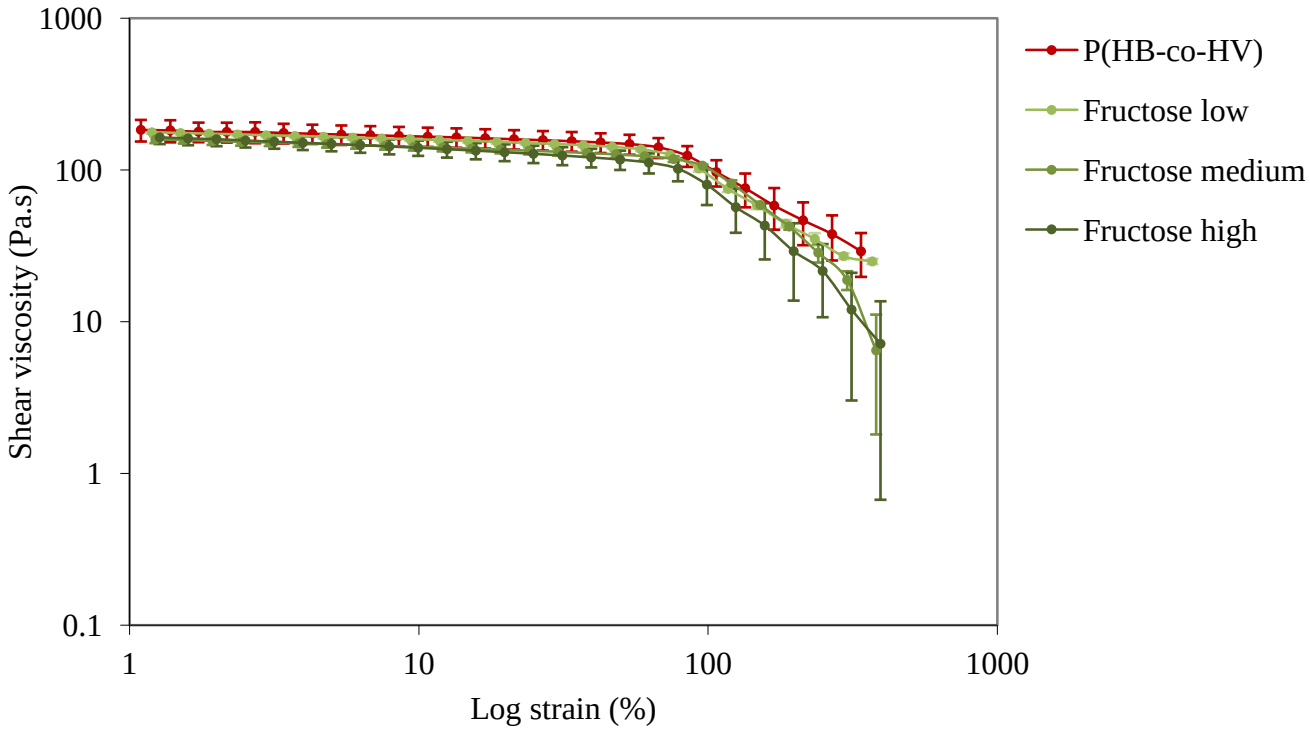

Figure 3.24. Rheological data of P(HB-co-HV) and fructose blends analysed at a frequency of 10 Hz

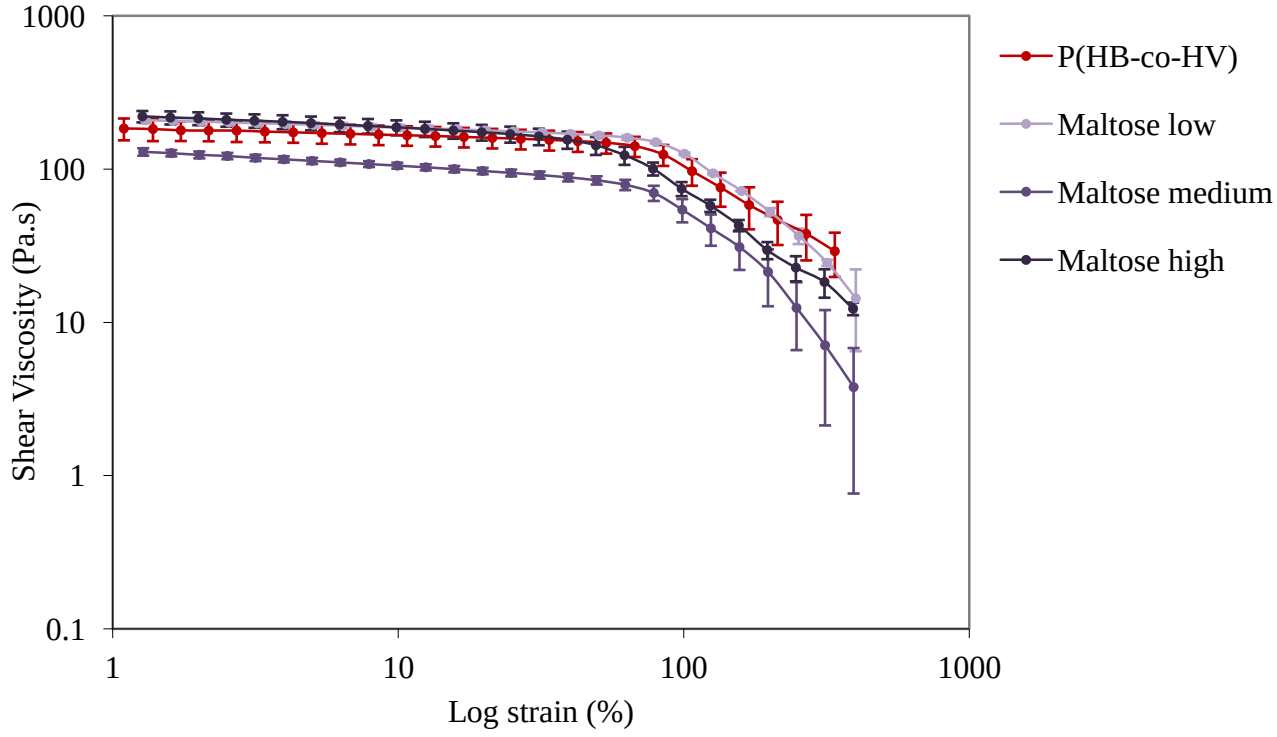

Figure 3.25. Rheological data of P(HB-co-HV) and maltose blends analysed at a frequency of 10 Hz

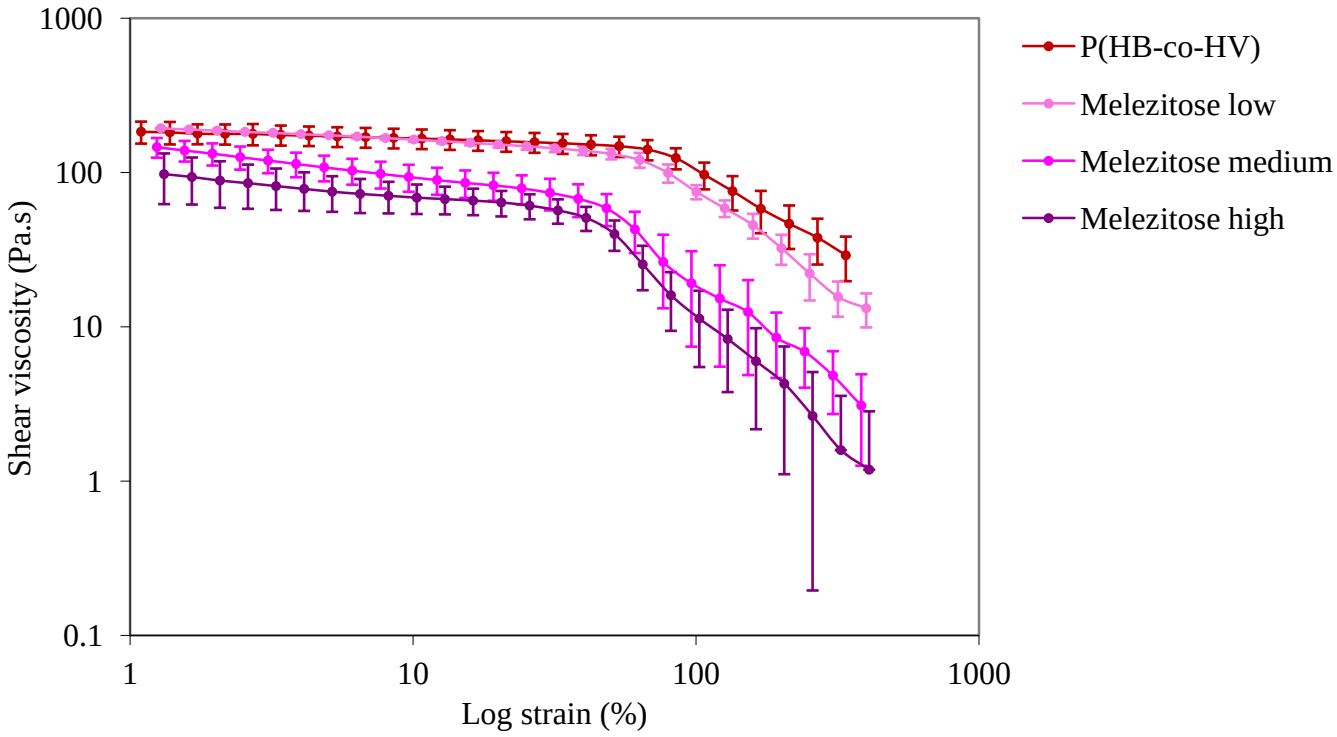

Figure 3.26. Rheological data of P(HB-co-HV) and melezitose blends analysed at a frequency of 10 Hz

The shear viscosity in these samples was quantified at an offset of 10 % strain. This position was chosen to standardise the position of the reading taken for each blend. Typically, as the concentration of additive is increased in each case, the shear viscosity decreased. This could be an indicator of one of two things. The saccharides occupy positions between the chains, which acts to plasticise the material by creating less resistance to flow of the melt(Gil, Saska et al. 2006). This occurs due to the disruption of chain interactions and the creation of more free volume within the material, leading to a reduced melt viscosity. Decreasing viscosity is also observed with increasing chain length of the additive (Figure 3.27). This could imply that the larger the molecule, the more inter-chain spacing is created between P(HB-co-HV) chains. This would to reduce the melt viscosity by increasing the free volume, thus creating less resistance to flow. The data point located at 0 on the horizontal axis represents the values for pure P(HB-co-HV).

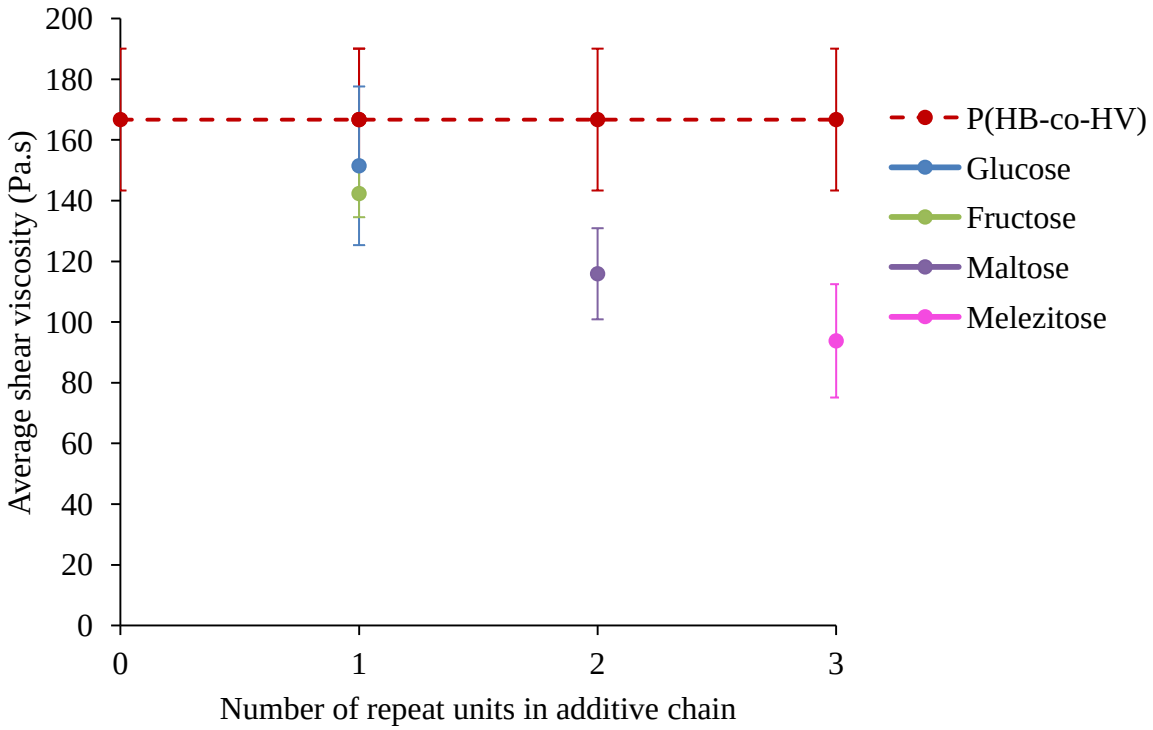

Figure 3.27. The effect of increasing the number of repeat units in the additive chain on the shear viscosity: medium concentrations

This could also be a concentration effect whereby there is less P(HB-co-HV) material in blends of longer chains as a result of more of the additive being present at the same crosslinking ratio. There is therefore less of the high viscosity component and thus creating less resistance to flow. This effect could also be due to the rheological properties of the sugars. In a study by Montanez-Soto et al (2013) studying the effect of the Fructose on the rheological behaviour of syrups, it was established that all syrups displayed Newtonian behaviour, but intermolecular interactions were stronger between molecules of glucose or sucrose (a glucose bound to a fructose molecule by a glycosidic bond). This meant that a higher content of fructose reduced the viscosity of the solutions, while a higher content of glucose increased the viscosity of the solutions. This was due to increased chain interactions

of glucose within the bulk solution, while fructose was more soluble in the solution leading to the decreased viscosity observed(Montanez-Soto, Gonzalez-Hernandez et al. 2013). This could be why the average viscosity within P(HB-co-HV)/glucose blends is higher than in fructose blends, and may therefore explain the behaviours of the other sugars.

It could also be degradation occurring within both materials as previously discussed. Degradation leads to a reduction in M_w (Yamaguchi and Arakawa 2006). With lower M_w the chains are shorter and therefore fewer chain entanglements are possible. This acts to reduce the melt viscosity by creating less resistance to flow(Gupta 2000).

3.1.3.5 Mechanical properties

Figure 3.28 shows an example of the effect of maltose at each concentration on the stress/strain behaviour of the blends produced and tested by uniaxial tensile testing. The same behaviour was observed in all other P(HB-co-HV)/saccharide blends, and therefore for more concise explanations, the following results will be discussed for P(HB-co-HV)/maltose blends but apply to all P(HB-co-HV)/saccharide blends. Tensile properties including elongation to break (E_b), toughness, ultimate tensile strength (UTS), and Young's modulus were reported and subsequently compared across all P(HB-co-HV)/saccharide blends.

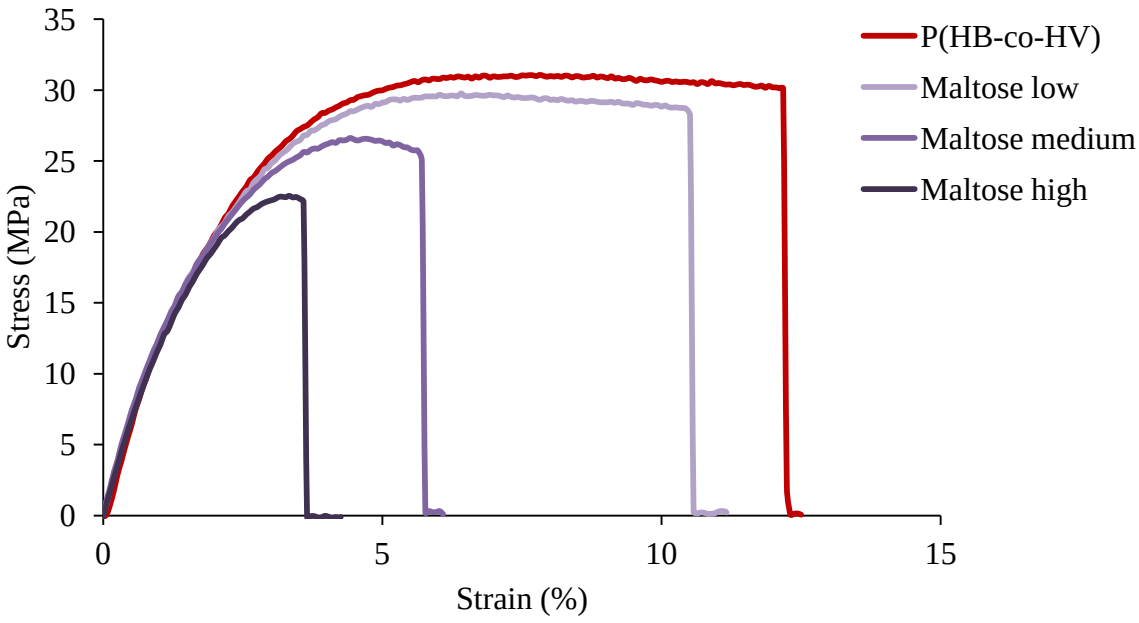

Figure 3.28. The stress/strain behaviour of P(HB-co-HV)/maltose blends

The stress/strain behaviour observed in all curves is characteristic of brittle polymers. The samples do not exhibit any necking or drawing behaviour, which is likely to be due to the high degree of crystallinity within the materials, as the proportion of amorphous chains that are available for alignment during this process is low(Callister and Rethwisch 2008).

Elongation to break is the percentage increase in length before the specimen breaks under tension, and is determined by Equation 3.4, where l_f is the final length of the sample and l_o is the original length of the sample(Callister and Rethwisch 2008).

$$E_b = \frac{(l_f - l_o)}{l_o} x\ 100 \qquad [3.4]$$

It can be seen in Figure 3.28 that the most significant difference between the mechanical properties of the blends is values for E_b. P(HB-co-HV) possesses the highest value for E_b at 12 %. As the maltose is added, the values for E_b reduce, dropping to 4 % at the highest concentration of maltose. Elongation to break is governed by the ability of the amorphous chains to elongate and align, and therefore a reduction in E_b indicates that the presence of the additives is disrupting the ability of the chains to do so. It is therefore not plasticising the material as this would lead to an increased E_b. Toughness is the ability of a material to absorb energy up to fracture and is therefore directly affected by E_b. Values for toughness therefore give similar trends upon analysis, whereby toughness decreases with increasing concentrations of the additives. The presence of the additives therefore reduced the ductility of the material, which is opposite to the desired effect.

Additional changes observed are within UTS. The UTS drops with increasing additive content, indicative of a weaker material with increasing concentration. This is another argument for the lack of crosslinks within the material, as the presence of crosslinks would act to increase the UTS of the material. This could be an indication of degradation as this would produce lower M_w chains. UTS is governed by chain entanglements and thus with shorter chains the material will possess less strength.

The fracture mechanisms of P(HB-co-HV) (12 % HV) under tension were studied by Hermida et al. (2009). Samples of compression moulded P(HB-co-HV) were tensile tested, and subsequently etched to reveal the crystalline morphology present for analysis under polarised light microscopy. Modes of crack propagation were observed in samples with fully impinged spherulites following primary crystallisation. Three modes were observed within the samples; propagation along the circumferential planes, transpherulitic cracking along radial planes or a combination of radial and circumferential planes, and inter-spherulitic crack propagation. It was established that the dominant mechanism was propagation along radial

cracks of impinged morphology in P(HB-co-HV)(12 % HV). This is therefore likely to be the mode of fracture within the samples used within this work. Visual representations of each mechanism can be observed in Figure 3.29 (Hermida and Casariego 2009).

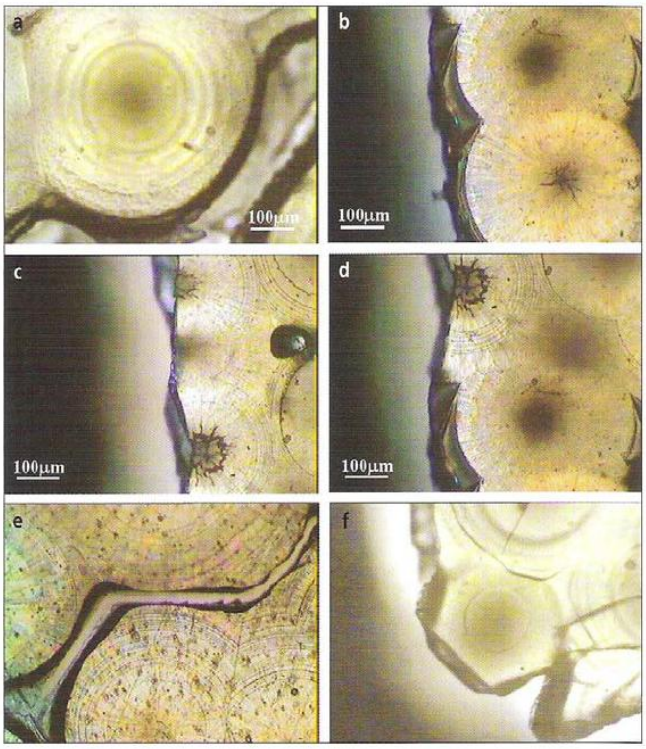

Figure 3.29. The modes of fracture observed in samples of P(HB-co-HV) with impinged spherulites following tensile testing and etching: Circumferential propagation (a-b), transpherulitic propagation (c-d) and inter-spherulitic propagation (e-f)(Hermida and Casariego 2009).

The effect of on increasing the chain length on the initial mechanical properties on day 0 can be seen in Figures 3.30-3.33. Here, a clear concentration dependence and chain size dependence on the resulting properties for E_b, toughness and UTS. There is no effect on Young's modulus (Figure 3.33). It is important to note that the increasing crosslinking ratio represents a decreasing concentration of additive and therefore the concentration of additive is decreasing as the horizontal axis is read from left to right. This was done to allow all of the additives across all of the concentrations to be presented on the same graph to allow for direct comparisons between the crosslinking ratios .

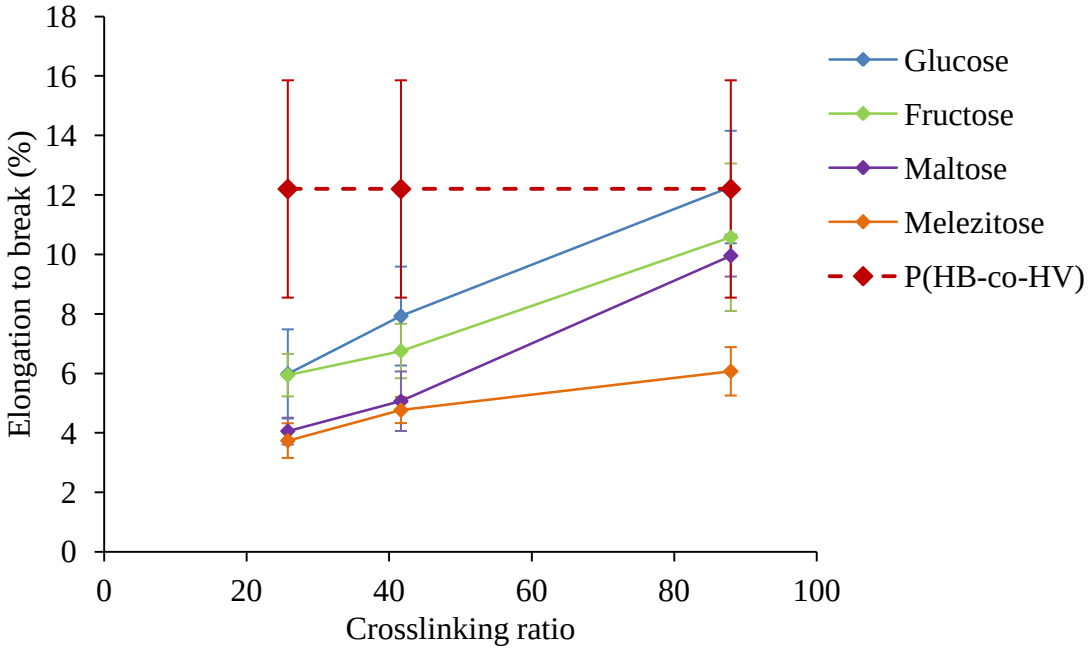

Figure 3.30. Effect of increasing additive chain length and increasing concentration on the E_b of the blends at day 0

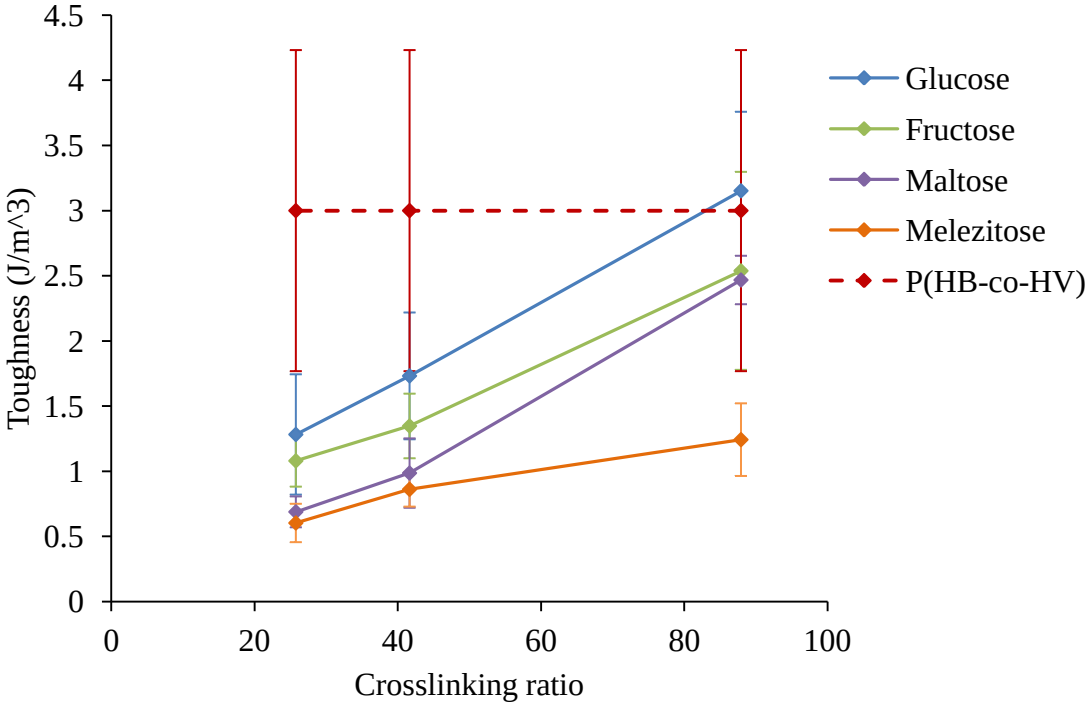

Figure 3.31. Effect of increasing additive chain length and increasing concentration on the toughness of the blends on day 0

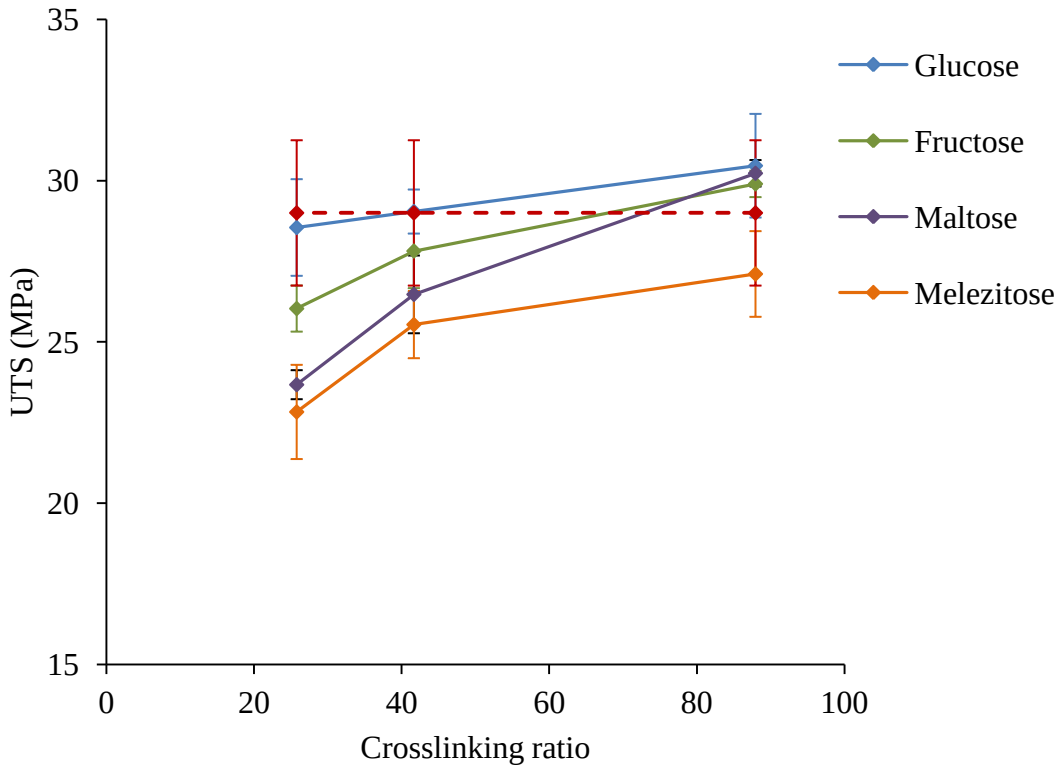

Figure 3. 32. Effect of increasing additive chain length and increasing concentration on the UTS of the blends at day 0

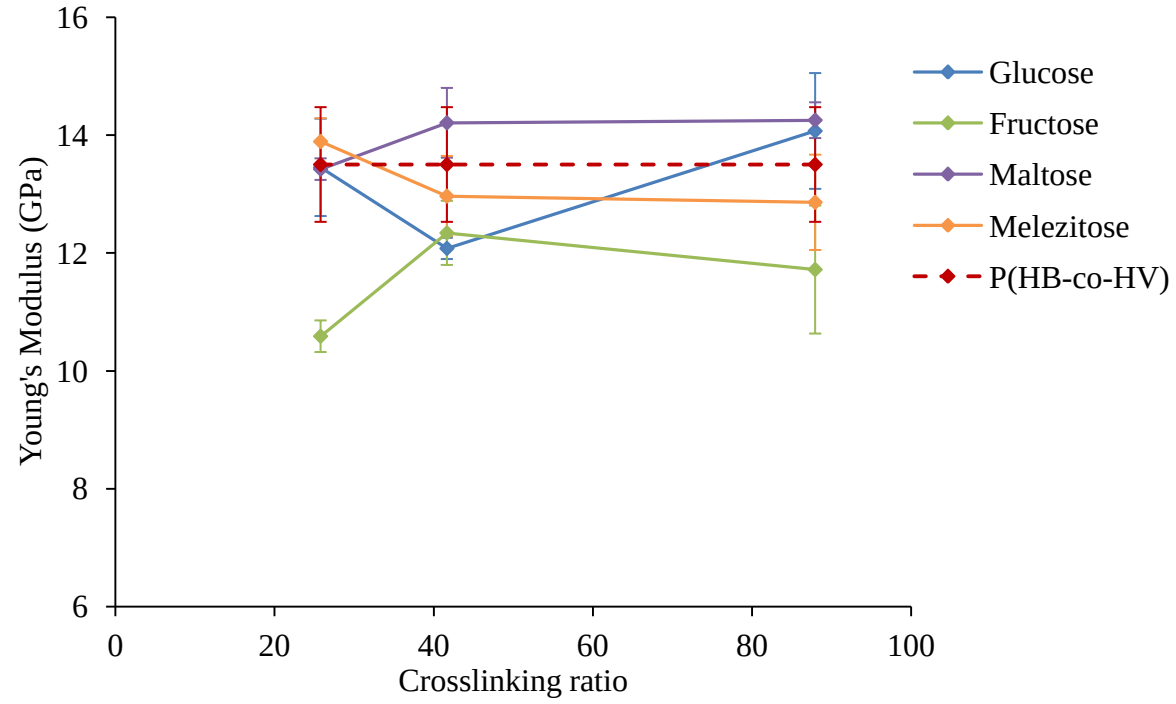

Figure 3. 33. Effect of increasing additive chain length and increasing concentration on the Young's modulus at day 0

The graphs show that as the concentration of additive is decreased (left to right) and as number of units in the additive chain increases (top to bottom), values for E_b, toughness and UTS increase . From previous observations within this work , the likely cause of the apparent reduction in mechanical properties is degradation within the material as the wt % of the additive is increased. It can therefore be observed that the highest concentration of the trisaccharide melezitose presents the worst mechanical properties. This is because, due to its molecular mass, from the crosslinking calculation, this blend contains the highest weight percent of saccharide, and therefore the lowest percentage of PHB. For example, the highest concentration of melezitose is 18.98 wt % in comparison to the highest concentration of glucose required being 7.48 wt %. Not only does that open up the potential for increased hydrolytic degradation of P(HB-co-HV) with the increased quantity of melezitose, but it also reduces the percentage of polymer to resist deformation under tension. No clear trends were observed with increasing chain length or concentration for Young's modulus, however the highest concentration (lowest crosslink ratio) of fructose leads to a significantly lower Young's modulus. This could be related to the lower melting temperature and significantly lower caramelisation temperature of this additive.

3.1.3.6 Scanning Electron Microscopy

Scanning Electron Microscopy (SEM) was used to analyse the fracture surfaces and assess whether the cause of the reduced mechanical properties could be observed visually via changes in morphology of the fracture surface. The medium concentration was picked for the blends and analysed at 600, 1500 and 6,000 x magnification. The results of these experiments can be observed below in Figures 3.3a-l. Attempts to analyse the samples at higher magnifications were made, but were unsuccessful due to beam damage.

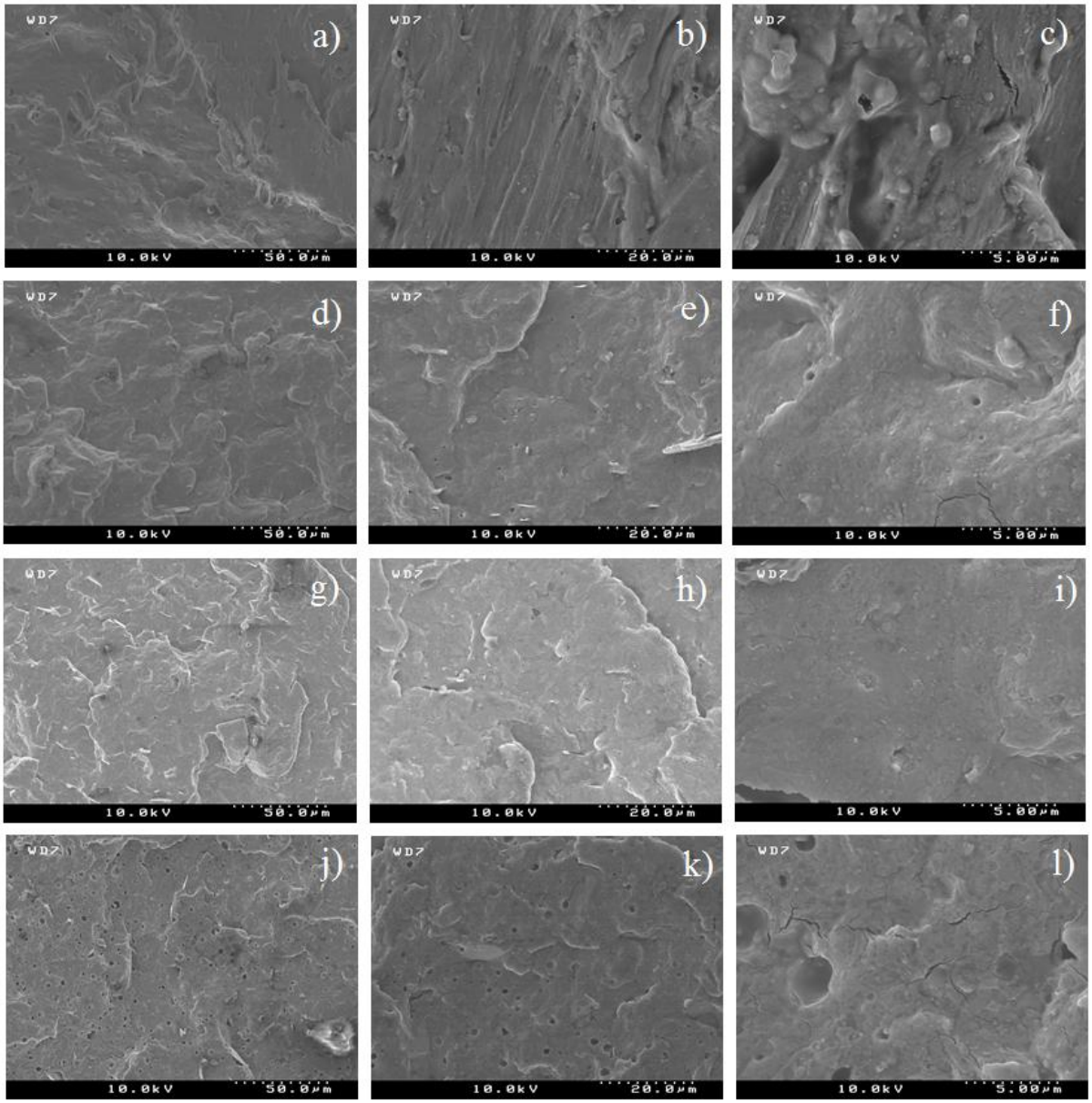

Figure 3. 34. SEM images of the fracture surfaces of P(HB-co-HV)(a-c) blended with glucose (d-f), fructose (g-i), and maltose (j-l) at 600, 1500 and 6,000 x magnification (from left to right)

Figure 3.34 (a-c) shows the morphology of the fracture surface in pure P(HB-co-HV). The surface shows a typical fracture surface of a brittle polymer. It is apparent that as glucose is added in a medium concentration (Figure 3.34 d-f), a more brittle fracture surface is observed by an increasingly angled and smooth morphology. Small pores can be observed in Figure 34f but are not widely observed throughout the morphology. No pores are observed on fructose blends (Figure 3.34 g-i), but as maltose is added a large number of pores are

observed within the material throughout the entire fracture surface (Figure 3.34 j-l). These pores are likely to be a result of degradation within the material, and more prevalent throughout the surface due to the higher wt % of maltose within the blend than glucose and fructose. This could occur as a result of hydrolytic degradation of the P(HB-co-HV), and evaporation of degradation by-products at elevated temperatures during processing. Similar pores have been observed by de Paula et al (2015) following hydrolytic degradation of Poly(L-lactic acid) (PLLA) in a phosphate buffer solution (Paula, Mano et al. 2015). These pores could act as stress concentration sites, where cracks form between the pores causing them to propagate more quickly, resulting in the decreasing ductility and strength observed within the samples as the concentration of saccharide increases.

3.1.4 Secondary crystallisation behaviour of P(HB-co-HV)/saccharide blends

3.1.4.1 DSC analysis

The T_m and X_c are properties that are known to increase as a result of the secondary crystallisation process and were therefore monitored over time in all blends to analyse the effect of each saccharide on the secondary crystallisation behaviour. The secondary process presents itself by an increase in lamellar thickness (Kolb, Wutz et al. 2001, Sics, Ezquerra et al. 2001) and the formation of smaller subsidiary lamellae within the amorphous regions between the original lamellar stacks (Wang, Hsiao et al. 1999, Kolb, Wutz et al. 2001, Sics, Ezquerra et al. 2001). This acts to increase the crystalline fraction of the polymer, thus increasing the T_m and degree of crystallinity.

An example of the behaviour observed with the addition of glucose can be seen in Figure 3.29 below. For clarity of trends, only data from the first 28 days is included as minimal change is observed after these time points. It is apparent from Figures 3.35 and 3.36 that

secondary crystallisation is occurring within all blends. There is minimal change in the highest concentration for T_m, however the value for crystallinity increases to above that of the pure P(HB-co-HV). This indicates the additives have a minimal effect on the secondary process. All other blends at their respective compositions displayed similar behaviour and were therefore unsuccessful at stopping the secondary process.

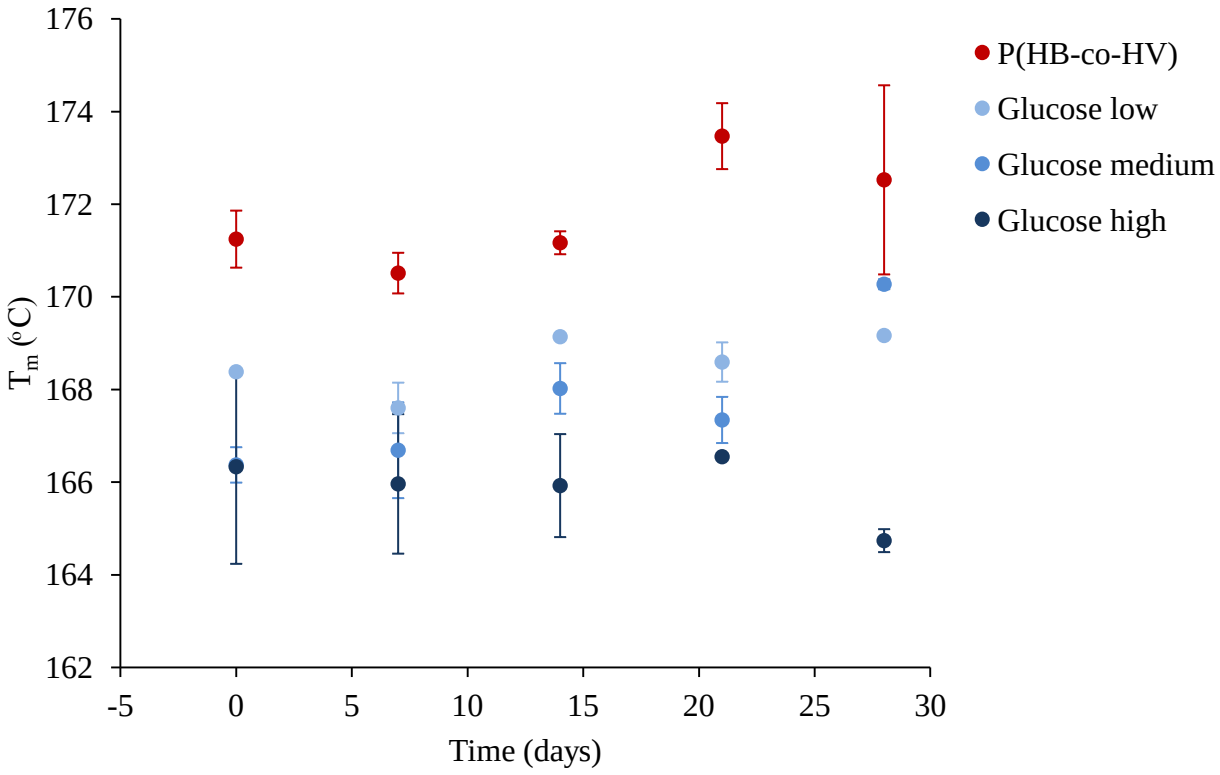

Figure 3.35. Effect of blending P(HB-co-HV) with glucose on the change in T_m over time

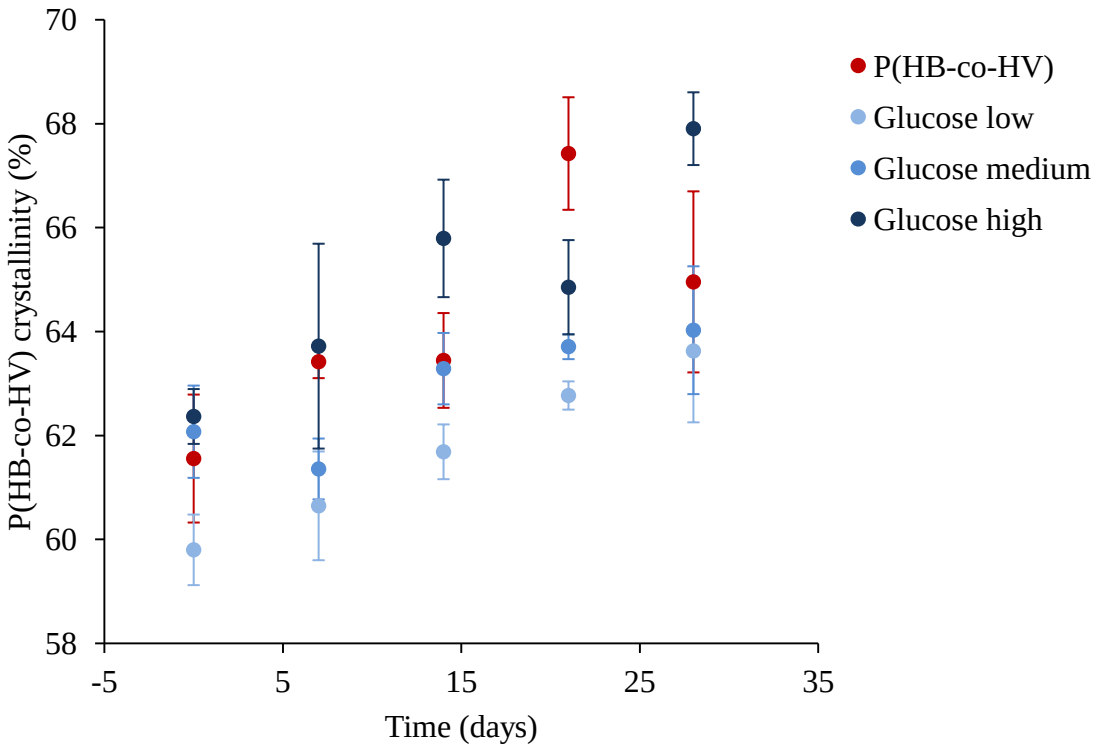

Figure 3.36. Effect of blending P(HB-co-HV) with glucose on the change in crystallinity over time

3.1.4.2 Mechanical properties

Changes in mechanical properties have also been used to identify the secondary process with the most significant change occurring within values for E_b. (de Koning and Lemstra 1993, Biddlestone, Harris et al. 1996). The change in mechanical properties within this study were analysed and shown below for P(HB-co-HV)/glucose blends. As the curves for all properties follow the same line as P(HB-co-HV) from day 7, for clarity of results, the blends containing the medium concentration of glucose are displayed for each property to give a visual representation of its behaviour with respect to that of the pure P(HB-co-HV) (Figures 3.37, 3.39, 3.42 and 3.44). The behaviour was identical in all of the saccharide blends whereby the data points were almost superimposed on top of one another. However, as different concentrations produced significantly different starting properties, the amount that each blend

had changed as a percentage of its starting value was also calculated (Figures 3.38, 3.40, 3.42 and 3.44).

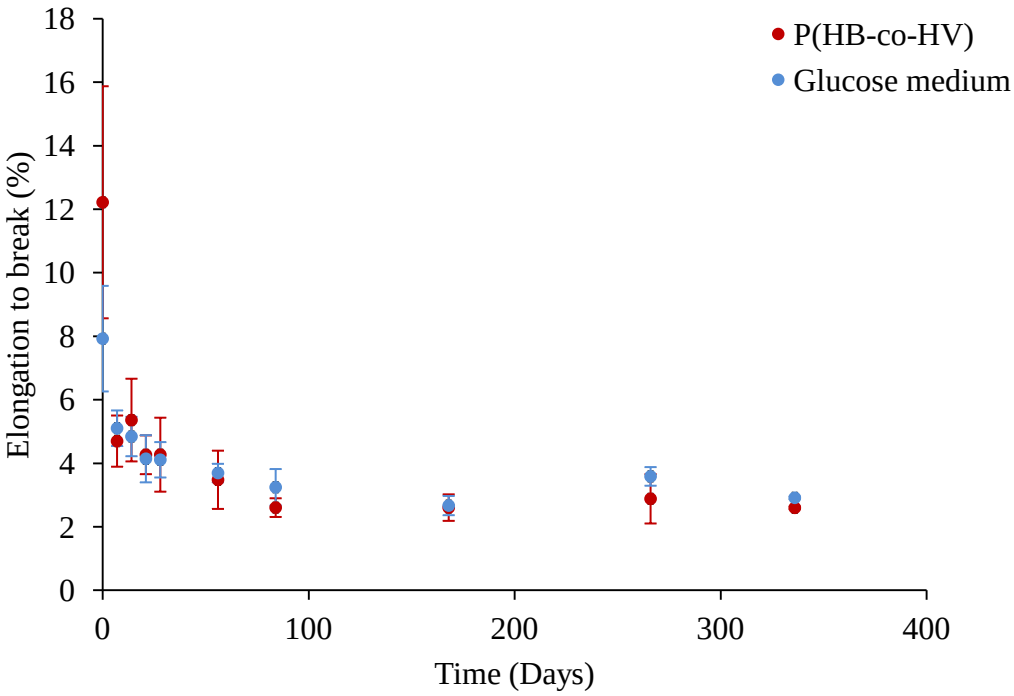

Figure 3.37. Change in values for elongation to break upon storage at ambient temperature over time

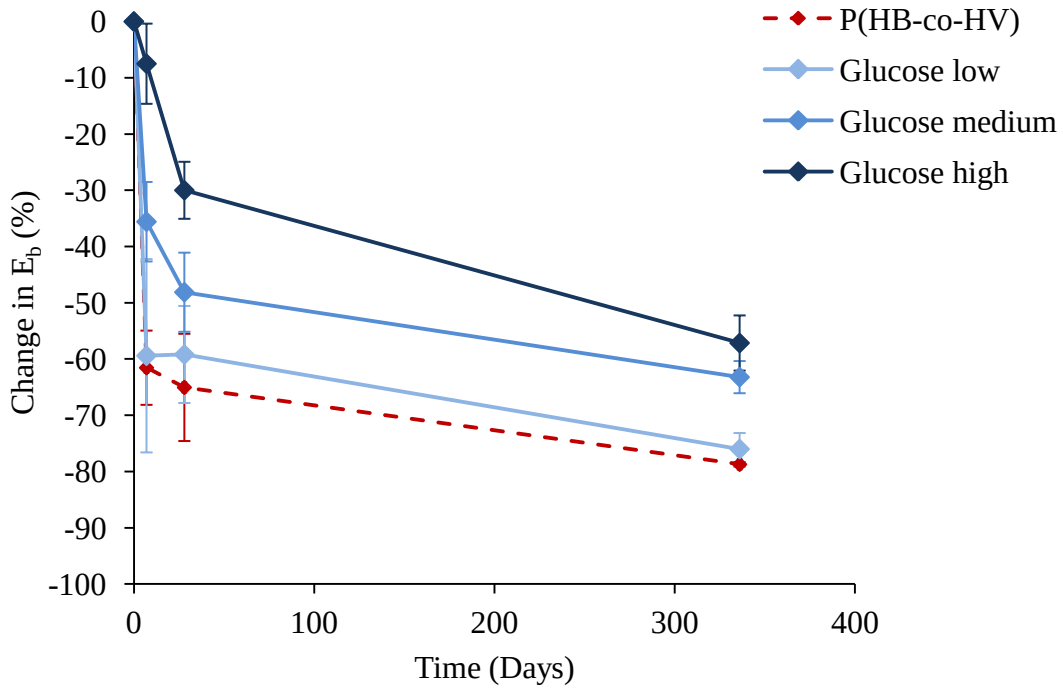

Figure 3.38. Percentage change in elongation to break from the original day 0 values

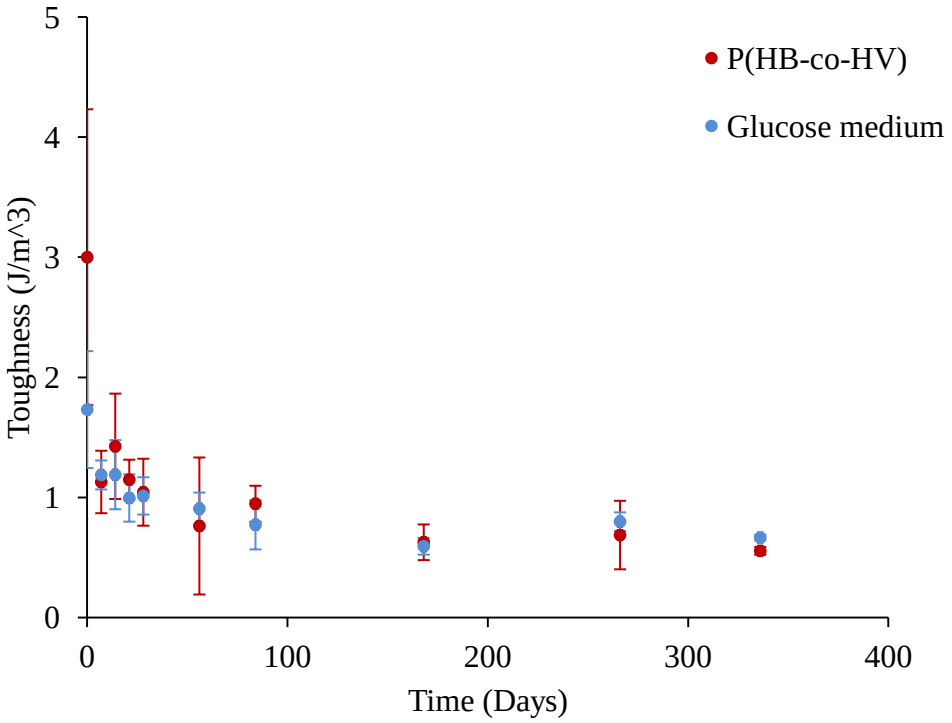

Figure 3. 39. Change in values for toughness upon storage at ambient temperature over time

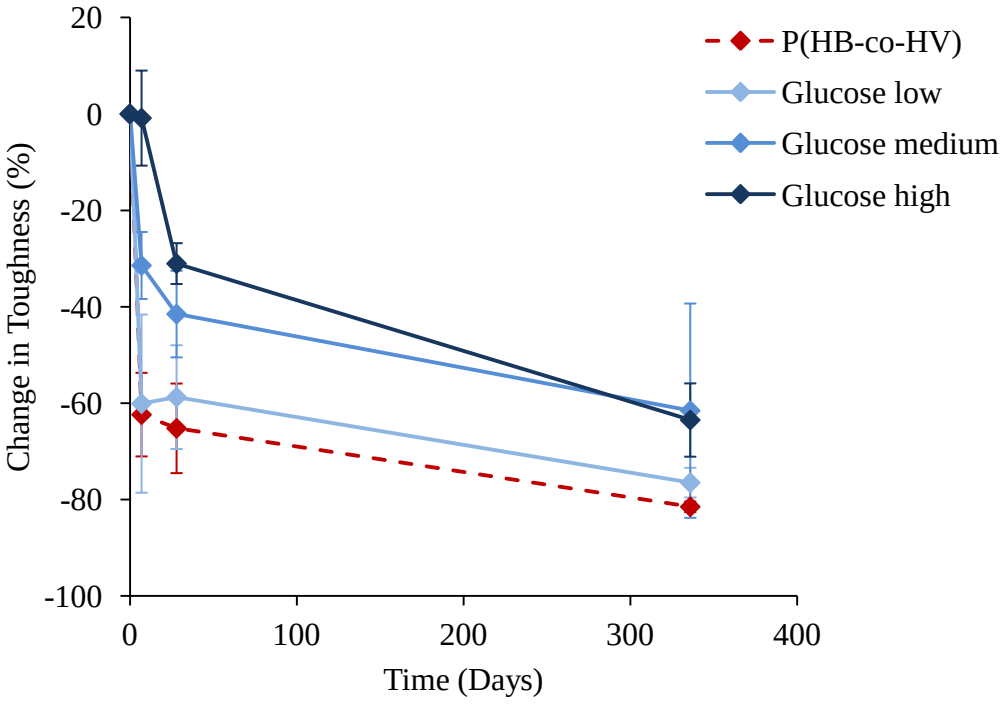

Figure 3. 40. Percentage change in toughness from original day 0 values

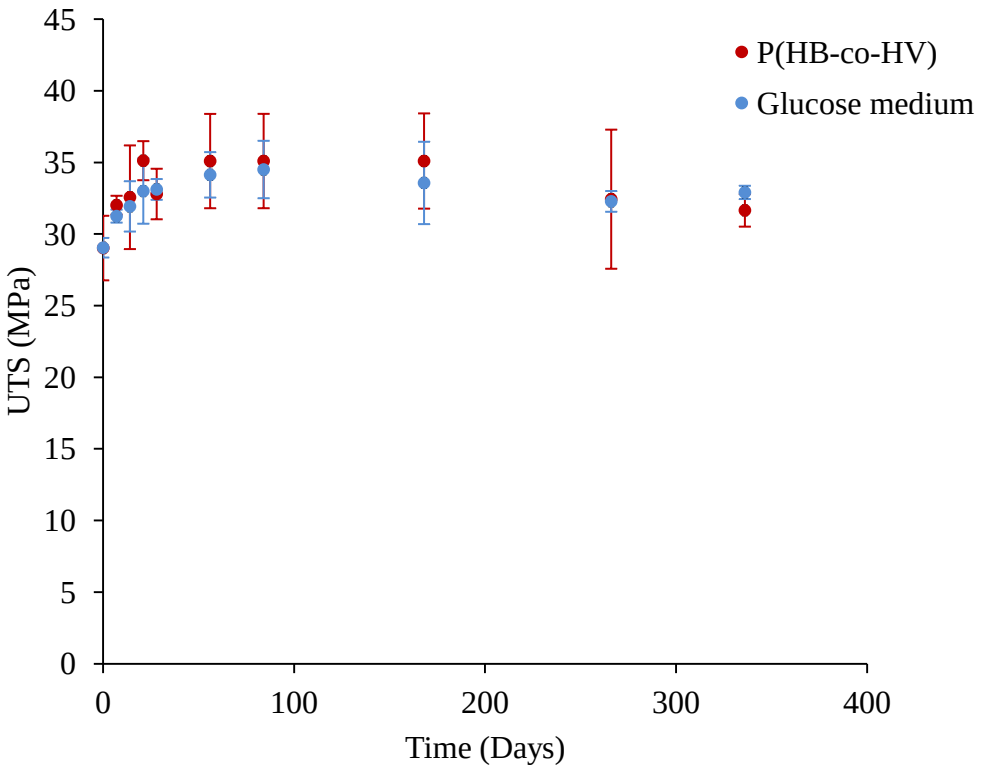

Figure 3.41. Change in values for UTS upon storage at ambient temperature over time

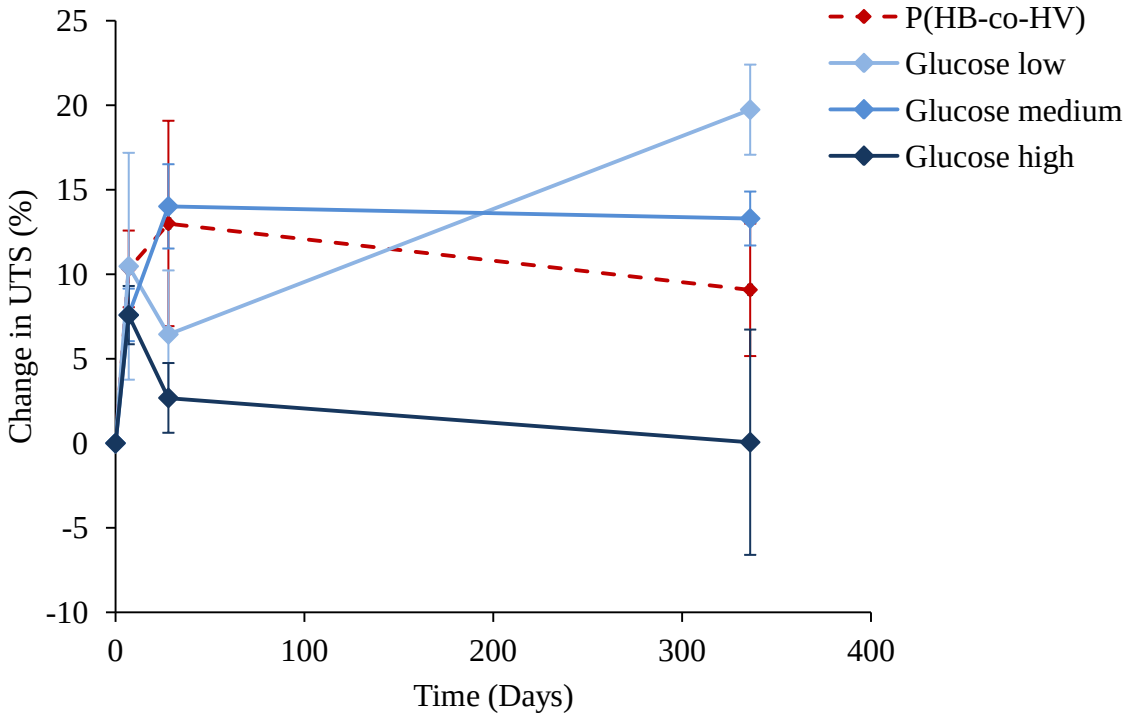

Figure 3.42. Percentage change in UTS from original day 0 values

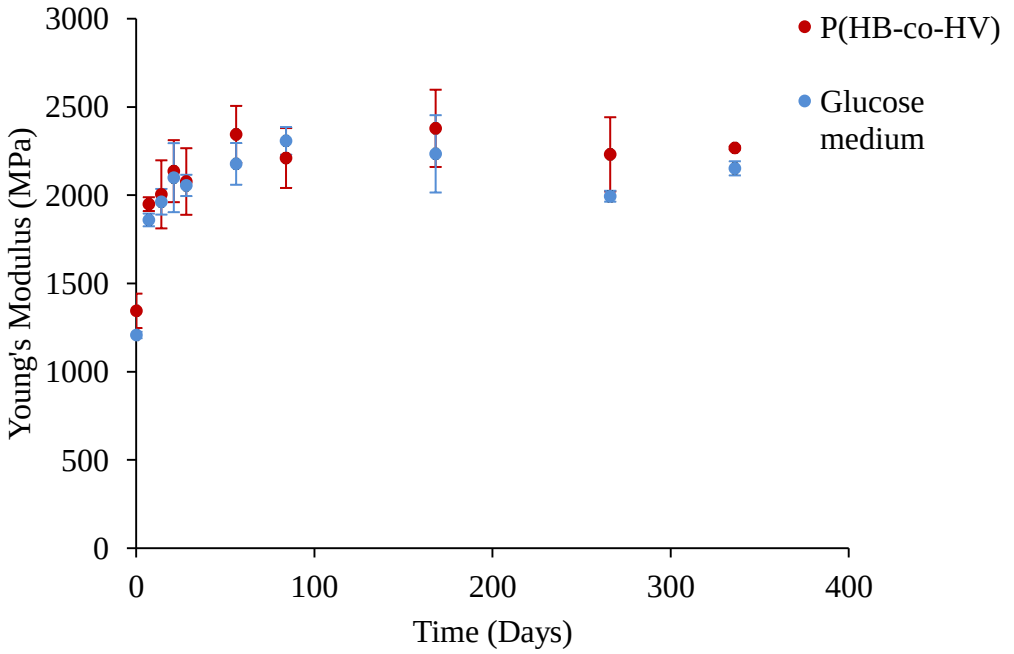

Figure 3.43. Change in values for Young's modulus over time following storage at ambient temperature over time

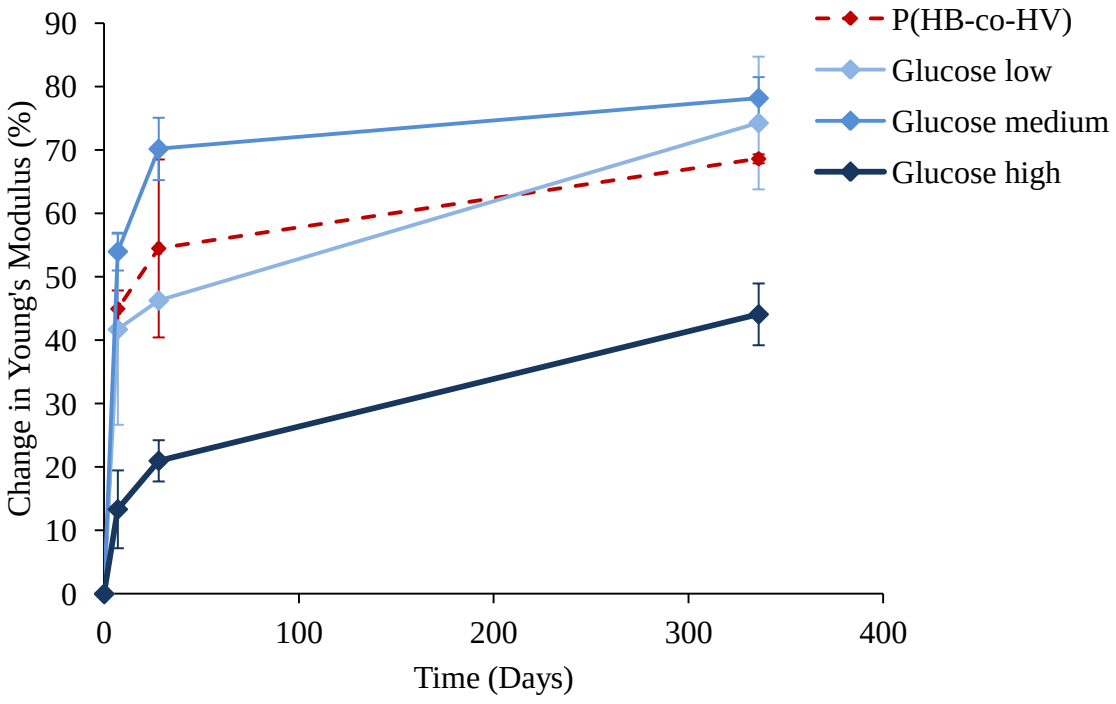

Figure 3.44. Percentage change in Young's modulus from original day 0 values

It can be clearly observed from Figures 3.38, 3.40, 3.42 and 3.44 that although the secondary crystallisation process still occurs within samples blended with glucose, that as you increase the concentration of glucose, the mechanical properties change by less over 336 days. This is the case for all properties measured and the same trends were observed for all additives. It is therefore apparent that the secondary process is hindered by the presence of the additive in higher quantities as the material does not change as much. However, it is important to note that the value for each property is lower on day 0 at higher concentrations of each sugar (Figure 3.28).

There also appears to be an effect of additive chain length on the secondary process at medium concentrations as reported in Figures 3.45–3.48. It can be seen that as the additive chain length is increased from monosaccharide (glucose and fructose) to trisaccharide (melezitose) that the percentage change in E_b, toughness and E is reduced. This could therefore indicate that the longer chain additives help to reduce the secondary process within the blends. The bulkier additive chains could have acted to prevent close compaction of the P(HB-co-HV) chains during the secondary crystallisation process. However, it could also be a product of composition of the blends. As chain length increases, there is a greater wt % of additive within the blend at each crosslink ratio. It could therefore also be the case that the reduced secondary crystallisation occurs as there is less of the P(HB-co-HV) in the blend to undergo secondary crystallisation. Conversely, the change in UTS is seen to increase upon increasing the chain length of the additive, so this effect does not carry across all properties.

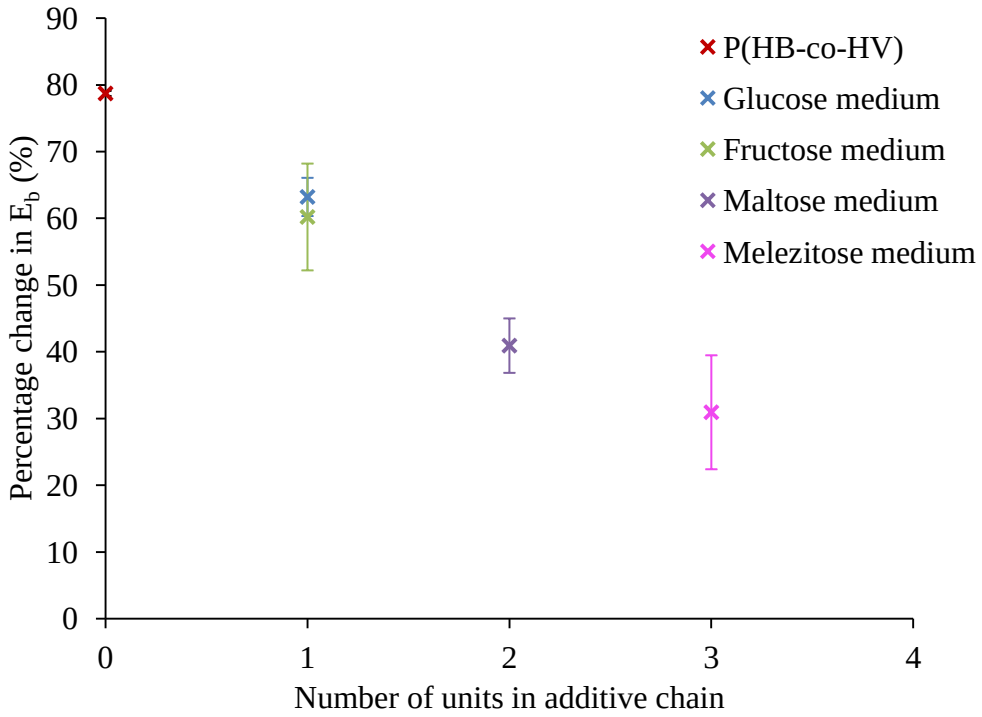

Figure 3.45. Effect of additive chain length on the percentage change in E_b following storage at ambient temperature for 336 days

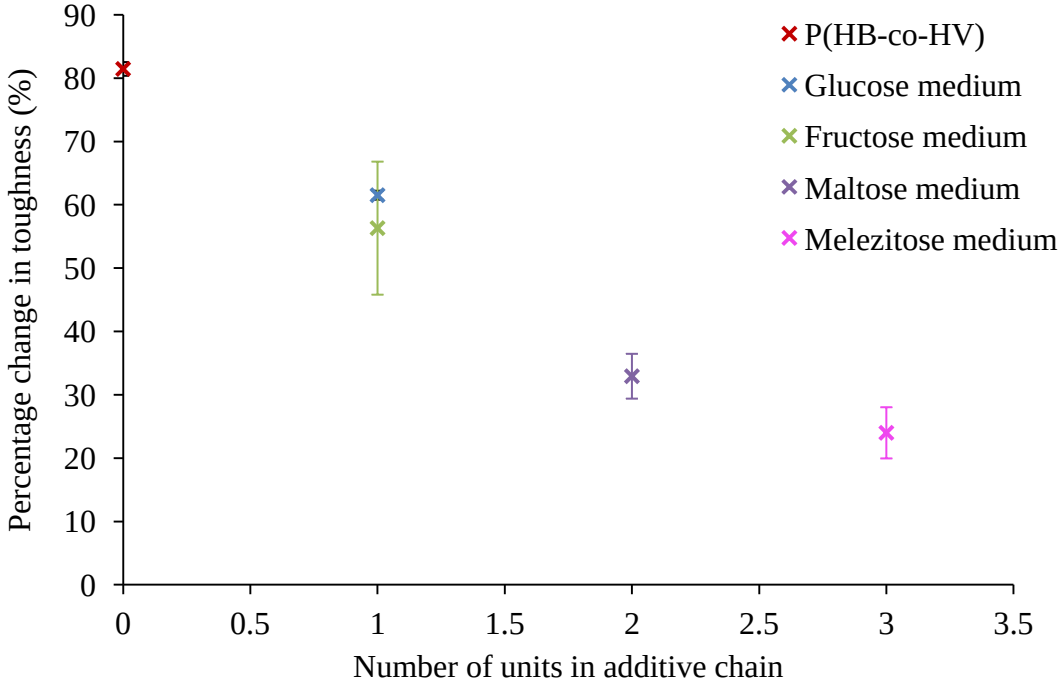

Figure 3.46. Effect of additive chain length on the percentage change in toughness following storage at ambient temperature for 336 days

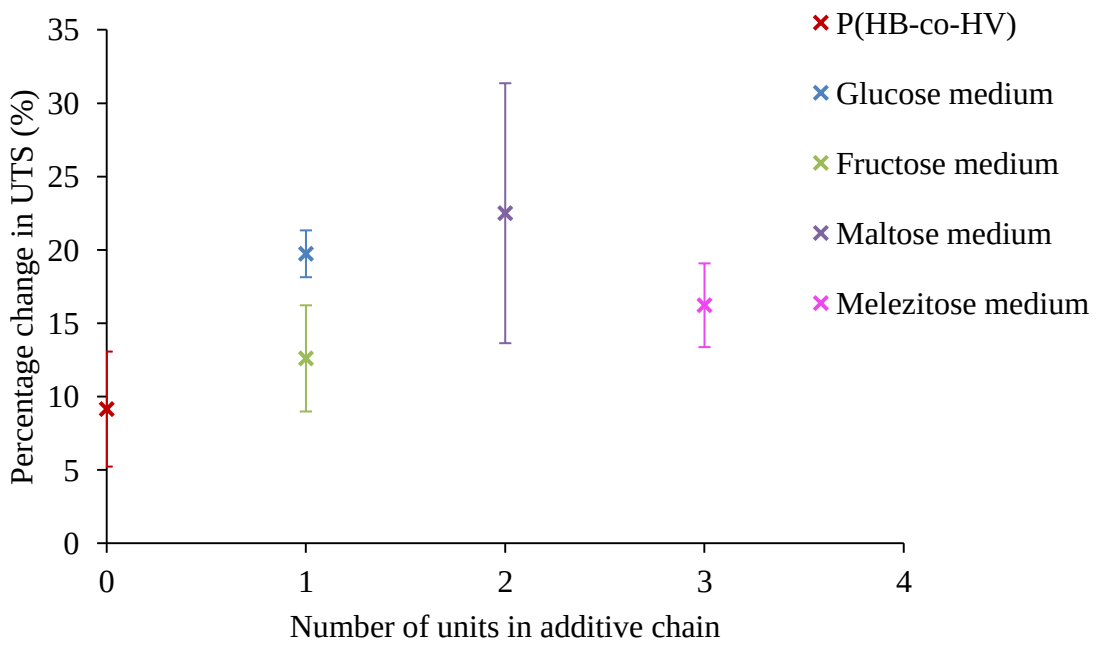

Figure 3.47. Effect of additive chain length on the percentage change in UTS following storage at ambient temperature for 336 days

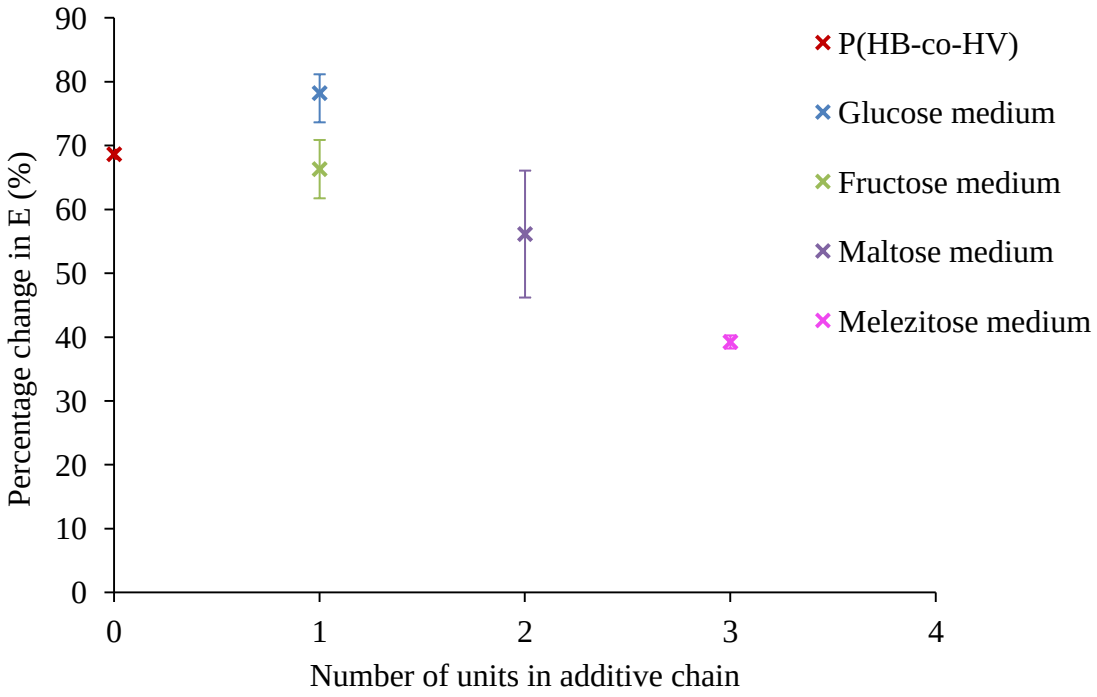

Figure 3.48. Effect of chain length on the percentage change in Young's modulus following storage at ambient temperature for 336 days

3.2 Conclusions

P(HB-co-HV) (3 wt %) was melt blended with glucose, fructose, maltose and melezitose. Characterisation of the resulting blends was conducted by DSC, FTIR, rheology, mechanical testing and SEM. Caramelisation occurred in all saccharide blends, resulting in brown material, with the degree of colour change linked to the respective caramelisation temperature of each saccharide. Crosslinking between saccharides and P(HB-co-HV) did not seem to occur as expected, and the effect of the additives was found to be detrimental to the mechanical properties of P(HB-co-HV), with increasing concentrations of additive and number of chains in the repeat unit found to have the greatest effect. These additives are therefore not recommended for use with P(HB-co-HV) as commercially viable options for food packaging materials.

The effects that may have led to the resulting properties have been discussed and are summarised in Table 3.12. Following consideration of all possibilities across all techniques, the deterioration in materials properties has been concluded to be due to degradation of the P(HB-co-HV) that was likely to have been induced by the decomposition of saccharides during caramelisation upon processing. Evidence for this effect was seen across all characterisation techniques (Table 3.12). This caramelisation reaction produces water as a reaction product. P(HB-co-HV) is known to have a hydrolysable backbone and is therefore sensitive to the presence of water. This could have led to hydrolysis of the ester linkages in P(HB-co-HV) resulting in chain scission, and thus lower molecular weight chains.

The result of this was T_m depression, reduction in melt viscosity, E_b, toughness and UTS as the concentration increased which are characteristic behaviours associated with decreasing M_w. Furthermore, an additional peak was observed on the carbonyl spectra at 1716 cm^{-1} which was attributed to the presence of crotonic acid from the degradation process. SEM

indicated that the presence of sugars created pores in the fracture surface of the blends which are not observed in the unblended material, another factor which would undoubtedly act to deteriorate mechanical properties through the creation of weaknesses in the material. Furthermore, no evidence of H-bonding was observed within this work. This effect would have led to an increase in T_m via DSC, peak shifts in FTIR, in addition to increased mechanical properties and melt viscosity. This is a likely result of melt processing the blend, where exposing the material to elevated temperatures altered the chemical structures of the components, thus making H-bonding less favourable between them.

Table 3.12. A summary of the possible interactions occurring between the blend components, identified by a range of characterisation techniques. Green: interaction observed. Red: interaction not observed. Grey: Not obtainable with this technique

	Miscibility	H-bonding	Colligative	Degradation
DSC	T_m depression	T_m depression	T_m depression	T_m depression
FTIR	No peak shift	No peak shift		New peaks Split carbonyl
Rheology	Decreased viscosity	Decreased viscosity		Decreased viscosity
Mechanical testing	Decreased E_b and UTS	Decreased E_b and UTS		Decreased E_b and UTS
SEM	Pores present in material			Pores present in material

Moreover, the blends were found to secondary crystallise and therefore the presence of additives did not hinder the process. This was characterised by increasing values for T_m, X_c, Young's modulus and UTS while the E_b and toughness of the materials decreased. The properties were found to change to a lesser extent in samples containing the highest concentrations of additives and those with the longer chain lengths. However, this is most likely due to the fact that a greater amount of degradation will have occurred in these samples as a result of higher concentrations of additive creating more water in the caramelisation process, therefore having a greater detrimental effect on the properties at day 0. This was observed in SEM images of the blends, where a large number of pores which were attributed to the degradation of maltose were created due to a higher concentration of the substance. Fewer pores were observed in blends containing less of the saccharide.

In summary, the effect of novel additives as a sustainable, GRAS and cost effective property modifier of P(HB-co-HV) was assessed. Despite limited success in achieving enhanced mechanical properties of P(HB-co-HV), this novel approach to achieving control over the secondary crystallisation behaviour was conducted for the first time and forms a foundation for future work within this area, where more ductile and thermally stable additives with hydrogen bonding capabilities would be desirable.

3.3 References

Biddlestone, F., et al. (1996). "The physical ageing of amorphous poly(hydroxybutyrate)." Polymer International**39**(3): 221-229.

Callister, W. D. and D. G. Rethwisch (2008). Fundamentals of Materials Science and Engineering. An Intergrated Approach. Asia, John Wiley and Sons.

Claude, J. and J. Ubbink (2006). "Thermal degradation of carbohydrate polymers in amorphous states: A physical study including colorimetry." Food Chemistry**96**(3): 402-410.

de Koning, G. J. M. and P. J. Lemstra (1993). "Crystallization phenomena in bacterial poly[(R)-3-hydroxybutyrate]: 2. Embrittlement and rejuvenation." Polymer**34**(19): 4089-4094.

Eggleston, G. and J. R. Vercellotti (2000). "Degradation of Sucrose, Glucose and Fructose in Concentrated Aqueous Solutions Under Constant pH Conditions at Elevated Temperature." Journal of Carbohydrate Chemistry**19**(9): 1305-1318.

Fagerson, I. (1969). "Thermal degradation of carbohydrates." J Agr Food Chem.

Fei, B., et al. (2004). "Crosslinking of poly[(3-hydroxybutyrate)-co-(3-hydroxyvalerate)] using dicumyl peroxide as initiator." Polymer International**53**(7): 937-943.

Fei, B., et al. (2003). "Quantitative FTIR study of PHBV/bisphenol A blends." European Polymer Journal**39**(10): 1939-1946.

Fei, B., et al. (2004). "Modified poly(3-hydroxybutyrate-co-3-hydroxyvalerate) using hydrogen bonding monomers." Polymer**45**(18): 6275-6284.

Food-Info (2014, 14 August 2014). "Caramelization." Retrieved 18/12/16, from http://www.food-info.net/uk/colour/caramel.htm

Gamble, G. R. (2002). "Thermochemical degradation of melezitose and trehalulose as related to cotton stickiness." Textile Research Journal**72**(2): 174.

Gil, N., et al. (2006). "Evaluation of the effects of biobased plasticizers on the thermal and mechanical properties of poly(vinyl chloride)." Journal of Applied Polymer Science**102**(2): 1366-1373.

Godbole, S., et al. (2003). "Preparation and characterization of biodegradable poly-3-hydroxybutyrate–starch blend films." Bioresource Technology**86**(1): 33-37.

Gonzalez, A., et al. (2005). "Application of pyrolysis/gas chromatography/Fourier transform infrared spectroscopy and TGA techniques in the study of thermal degradation of poly (3-hydroxybutyrate)." Polymer Degradation and Stability**87**(2): 347-354.

Gupta, R. K. (2000). Polymer and composite rheology. United States, Marcel Dekker, Inc.

Hermida and Casariego (2009). Morphology of plastic deformation fracture of a biodegradable biopolymer. Microscopy and Analysis Digital Cameras and Image Analysis Supplement Buenos Aires, Argentina, John Wiley and Sons

Kolb, R., et al. (2001). "Investigation of secondary crystallization of polymers by means of microbeam X-ray scattering." Polymer**42**(12): 5257-5266.

Kroh, L. W. (1994). "Caramelisation in food and beverages." Food Chemistry**51**(4): 373-379.

Montanez-Soto, et al. (2013). "Effect of the fructose and glucose concentration on the rheological behaviour of high fructose syrups." African Journal of Biotechnology**12**(12): 1401-1407.

NIST (2012). "Material Measurement Laboratory, Crotonic Acid." Retrieved 18/12/16, from http://webbook.nist.gov/cgi/cbook.cgi?ID=C3724650&Mask=80

Paula, E. L. d., et al. (2015). "HYDROLYTIC DEGRADATION BEHAVIOR OF PLLA NANOCOMPOSITES REINFORCED WITH MODIFIED CELLULOSE NANOCRYSTALS." Química Nova**38**: 1014-1020.

Ramsay, B. A., et al. (1993). "Biodegradability and mechanical properties of poly-(beta-hydroxybutyrate-co-beta-hydroxyvalerate)-starch blends." Appl Environ Microbiol**59**(4): 1242-1246.

Reis, K. C., et al. (2008). "Characterization of polyhydroxybutyrate-hydroxyvalerate (PHB-HV)/maize starch blend films." Journal of Food Engineering**89**(4): 361-369.

Saeki, T., et al. (2005). "Hydrolytic degradation of poly[(R)-3-hydroxybutyric acid] in the melt." Polymer**46**(7): 2157-2162.

Semba, T., et al. (2006). "The effect of crosslinking on the mechanical properties of polylactic acid/polycaprolactone blends." Journal of Applied Polymer Science**101**(3): 1816-1825.

Sics, I., et al. (2001). "On the relationship between crystalline structure and amorphous phase dynamics during isothermal crystallization of bacterial poly(3-hydroxybutyrate-co-3-hydroxyvalerate) copolymers." Biomacromolecules**2**(2): 581-587.

Sugisawa, H. (1966). "The Thermal Degradation of Sugars. II. The Volatile Decomposition Products of Glucose Caramel." Journal of Food Science**31**(3): 381-385.

Thiré, R. M. S. M., et al. (2006). "Effect of starch addition on compression-molded poly(3-hydroxybutyrate)/starch blends." Journal of Applied Polymer Science**100**(6): 4338-4347.

Tian, J., et al. (2005). "Kinetic Studies of Polyhydroxybutyrate Granule Formation in Wautersia eutropha H16 by Transmission Electron Microscopy." Journal of Bacteriology**187**(11): 3814-3824.

Venderbosch, R. H. and H. J. Heeres (2011). Pyrolysis Oil Stabilisation by Catalytic Hydrotreatment.

Wang, Z. G., et al. (1999). "The nature of secondary crystallization in poly(ethylene terephthalate)." Polymer**40**(16): 4615-4627.

Woo, K. S., et al. (2015). "Characteristics of the Thermal Degradation of Glucose and Maltose Solutions." Preventive Nutrition and Food Science**20**(2): 102-109.

Yamaguchi, M. and K. Arakawa (2006). "Effect of thermal degradation on rheological properties for poly(3-hydroxybutyrate)." European Polymer Journal**42**(7): 1479-1486.

Yu, J., et al. (2005). "Kinetics and mechanism of the monomeric products from abiotic hydrolysis of poly[(R)-3-hydroxybutyrate] under acidic and alkaline conditions." Polymer Degradation and Stability**89**(2): 289-299.

Zhang, M. and N. L. Thomas (2010). "Preparation and properties of polyhydroxybutyrate blended with different types of starch." Journal of Applied Polymer Science**116**(2): 688-694.

Chapter 4
Binary blends of P(HB-co-HV) and CAB: Effects on properties and secondary crystallisation behaviour

4.0 Introduction

Work conducted in the previous chapter investigated the effect of blending saccharides of increasing chain length with P(HB-co-HV) to examine their effects on the initial properties and secondary crystallisation behaviour. The blends were found to decrease initial 'day 0' properties below those of pure P(HB-co-HV) which was attributed to hydrolytic degradation of P(HB-co-HV) induced by the production of water during caramelisation of the saccharides during processing (Sugisawa 1966, Kroh 1994, Woo, Kim et al. 2015). Furthermore, caramelisation results in the formation of 5- Hydroxymethylfurfural (HMF), which possesses fewer hydroxyl groups in comparison to saccharides. This therefore also limited its hydrogen bonding capabilities and any intermolecular interactions between the additives and the P(HB-co-HV). As a result, it was identified that additives with improved thermal stability would be advantageous. However a middle ground is needed, as starch was found to remain as a solid in the melt due to its high melting temperature (~200 ºC) and was therefore detrimental to the mechanical properties of the blends (Ramsay, Langlade et al. 1993, Tian, Sinskey et al. 2005, Zhang and Thomas 2010).

Another abundant and naturally sourced polymer is cellulose, which is another polymer of glucose. However, the melting point of natural cellulose also exceeds that of PHB, and therefore its addition in the natural form would incur the same problems as natural starch. A seemingly suitable alternative based on cellulose, but with thermoplastic properties is Cellulose Acetate Butyrate (CAB). This is a cellulose ester where different combinations of

acetyl, butyryl and hydroxyl groups give rise to many grades of CAB with a range of different properties. Maximising hydroxyl groups would maximise hydrogen bonding capabilities. The chemical structure of CAB is shown in Figure 4.1.

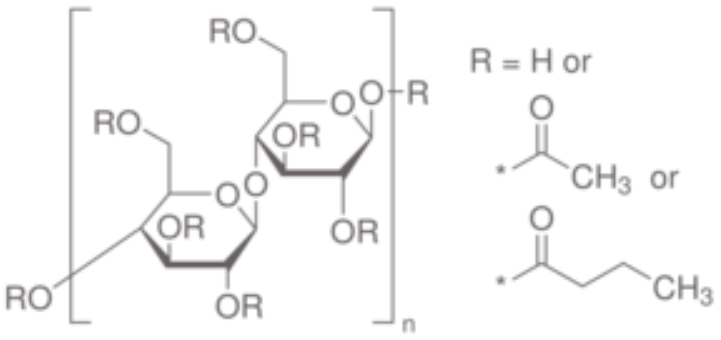

Figure 4.1. The chemical structure of CAB

It has been previously reported that incorporating CAB into blends of PHB has improved the mechanical properties, and reduced crystallinity via alterations to the crystallisation kinetics (Chapter 1). There have been a number of studies reporting this in PHB, however there is limited work on the effect of blending CAB with the P(HB-co-HV) copolymer (Buchanan, Gedon et al. 1992). One study investigates blending with P(HB-co-HV), but only high concentrations (greater than 20 %) of CAB are considered. In addition, there are no studies to date assessing the effect of CAB on the secondary crystallisation behaviour of PHB or its copolymers. Considering that crosslinks within a material hinder chain mobility, the ability of cellulose esters to crosslink via intermolecular hydrogen bonding has the potential to restrict chain mobility present within P(HB-co-HV) chains at room temperature, and therefore hinder the secondary process. The aim of this work was therefore to analyse the effects of incorporating CAB into P(HB-co-HV) on the initial properties, and secondary crystallisation

behaviour of the material, in order to investigate the possibility of hindering the secondary process with the formation of intermolecular hydrogen bonds and thus improve the potential of PHB copolymers for food packaging materials.

4.1 Results and Discussion

4.1.1 The effect of CAB on the materials properties prior to storage

4.1.1.1 Thermal properties

4.1.1.1.1 Dynamic measurements

Figures 4.2 and 4.3 show the thermal properties of the individual components of the blends investigated by DSC. Figure 4.2 displays the glass transition temperature (T_g) of amorphous CAB, while Figure 4.3 shows the melting temperature (T_m) of semi-crystalline P(HB-co-HV). The T_m of P(HB-co-HV) was found to be 171 °C, while the T_g of CAB was found to be 100 °C. P(HB-co-HV) typically possesses a T_g in the region of 0-4 ºC (Gunaratne, Shanks et al. 2004, Balaji, Gopi et al. 2013), however, this transition could not be observed upon analysis of the DSC trace due to the high crystallinity of the polymer.

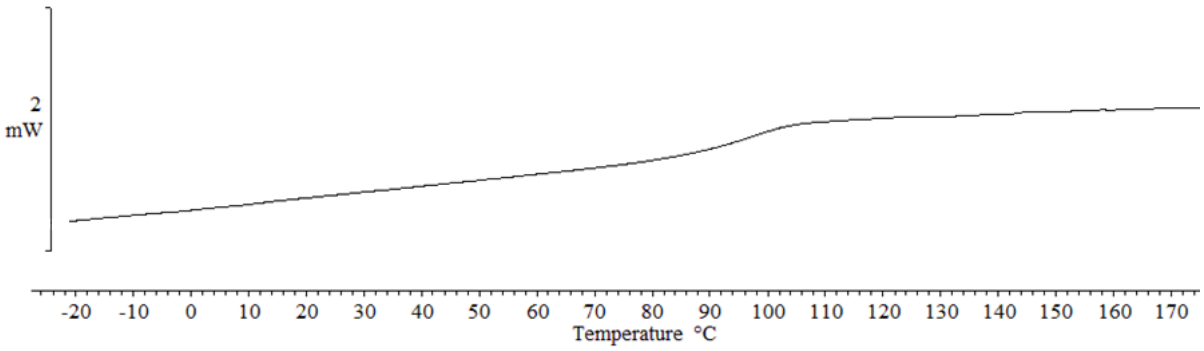

Figure 4.2. A DSC trace showing the T_g of amorphous CAB measured at 10 ºC/min

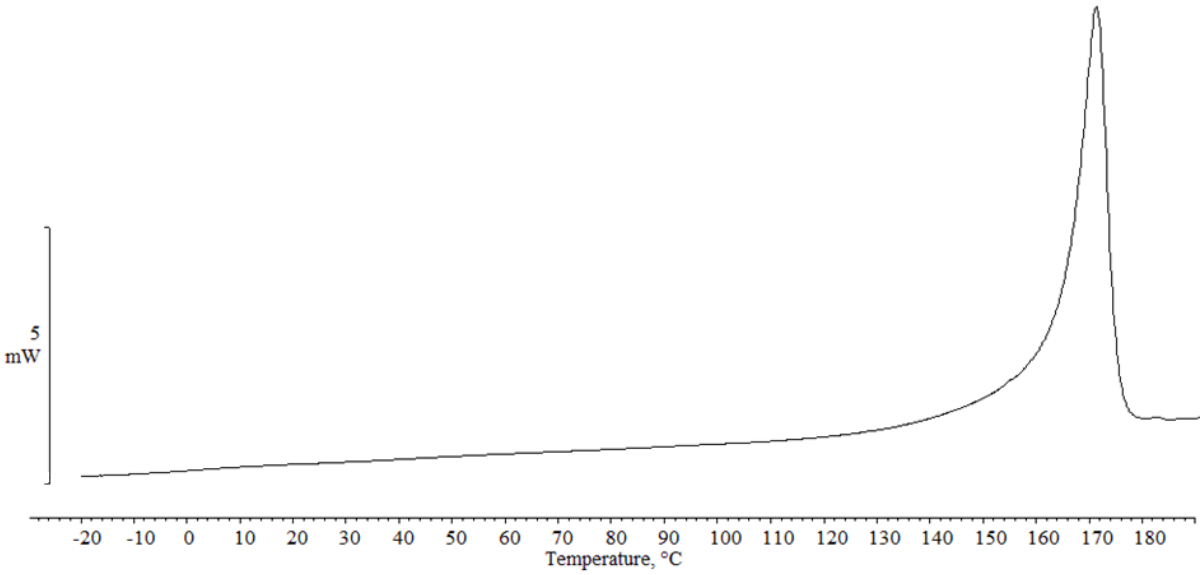

Figure 4.3.A DSC trace showing the T_m of semi-crystalline P(HB-co-HV)measured at 10 ºC/min

As previously described in Chapter 2, CAB was added in three concentrations; 5, 10 and 15 wt %. The blends were analysed by DSC at both 10 ºC/minute (Figure 4.4) and 50 ºC/minute (Figure 4.5). The faster heating rate was used to analyse the blends with a smaller risk of re-crystallisation upon heating, while 10 ºC/min was used to minimise the occurrence of thermal lag through the sample. It is apparent under both sets of conditions that as the concentration of CAB is increased, the T_m of P(HB-co-HV) decreases (Figures 4.4 and 4.5). The T_m is observed to reduce by 7 ºC as the CAB content is increased up to 15 wt % in samples run at 10 ºC/min. This melting point depression implies interaction and miscibility between the two components. This is in agreement with previous studies on P(HB-co-HV) and CAB binary blends (Wang et al, 2002; Park et al, 2005). Furthermore, in a study by Park et al (2002), investigating binary blends of PHB and CAB, it was established that the T_m of the blends decreased with increasing CAB content from 0-100 wt % CAB. A reduction of 4 ºC was observed in hot pressed films between 0 and 20 wt % from 174.6 ºC in unblended PHB, to 170.6 ºC in blends containing 20 wt % CAB at a heating rate of 10 ºC/min (Park, Tanaka et

al. 2005). The hydroxyl content of the CAB was not disclosed, but the T_m depression is comparable with results presented in Table 4.1 for a heating rate of 10 ºC/min. Reductions in the T_m of 3ºC were also observed by El-Shaffee et al. (2001) in solution cast blend films containing 20 % CAB, heated at 20 ºC/min (El-Shafee, Saad et al. 2001).

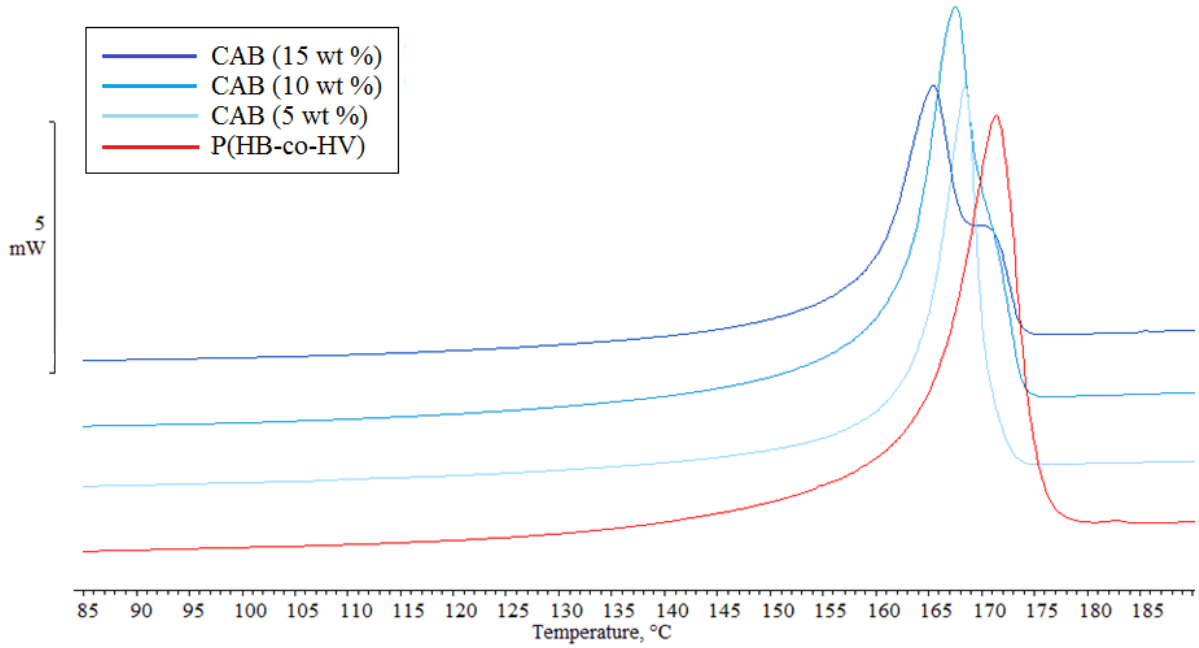

Figure 4.4. The effects of blending on the T_m of the blends measured at 10 ºC/min

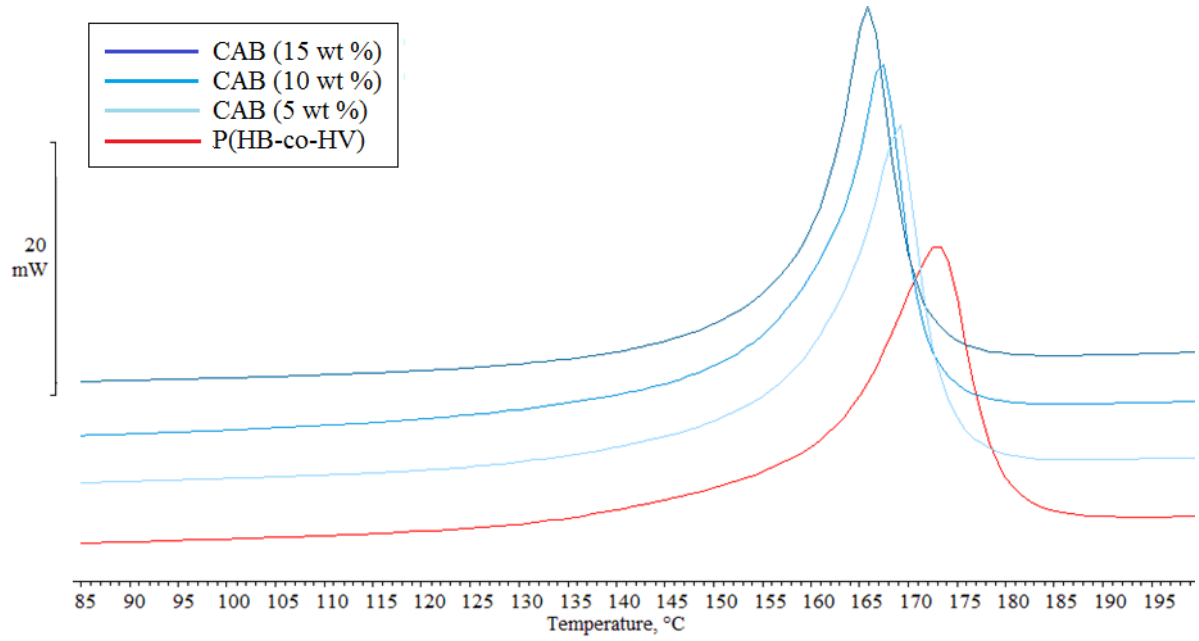

Figure 4.5. The effects of blending on the thermal transitions of the blends measured at 50 °C/min

This reduction in T_m is composition dependent and indicates the rejection of CAB from the crystalline regions during crystallisation into the inter-lamellar amorphous regions (Suttiwijitpukdee, Sato et al. 2011, Suttiwijitpukdee, Sato et al. 2012). Therefore, the more CAB present, the more there is to be rejected, thus resulting in a delayed onset of crystallisation as well as slowing the process. Here, the CAB could act as an impurity within the chains, thus preventing chain organisation required for crystallisation by the formation of intermolecular hydrogen bonds (H-bonds). This would lead to the reduction in crystallinity, as observed in Figure 4.6, which would in turn reduce the melting point of the material (Figure 4.7). Table 4.1 summarises the changes observed to thermal properties upon blending. This shift in T_m and crystallinity is an early indicator of miscibility and interaction between the two systems.. Suttiwijitpukdee, Sato et al. (2011) suggested that the presence of CAB creates less perfect spherulites, with distortions of the intramolecular hydrogen bonding with PHB itself (Suttiwijitpukdee, Sato et al. 2011).

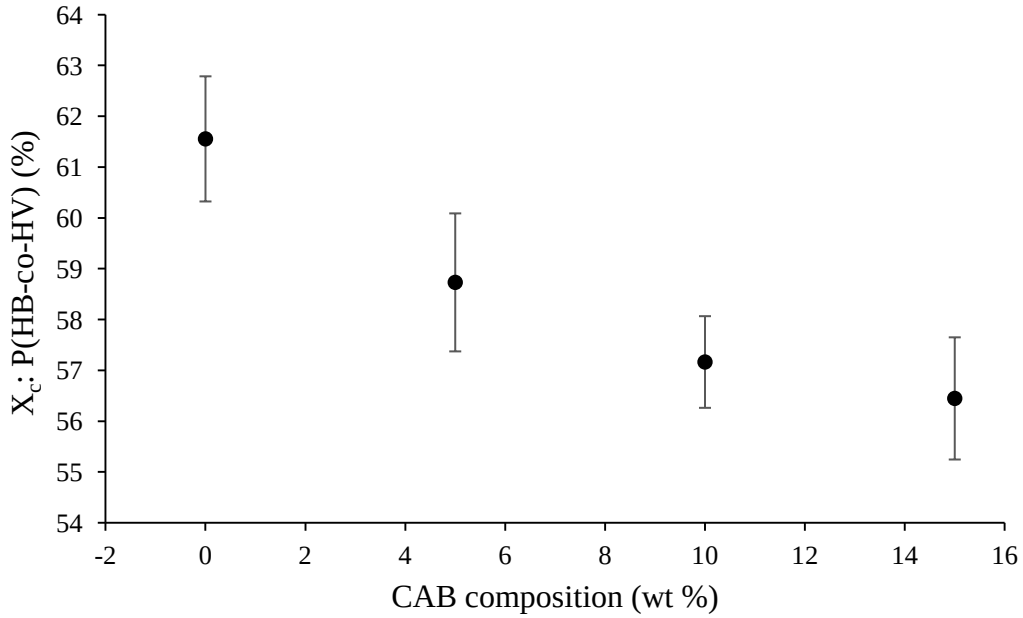

Figure 4.6. The effects of CAB content on the degree of crystallinity of P(HB-co-HV)

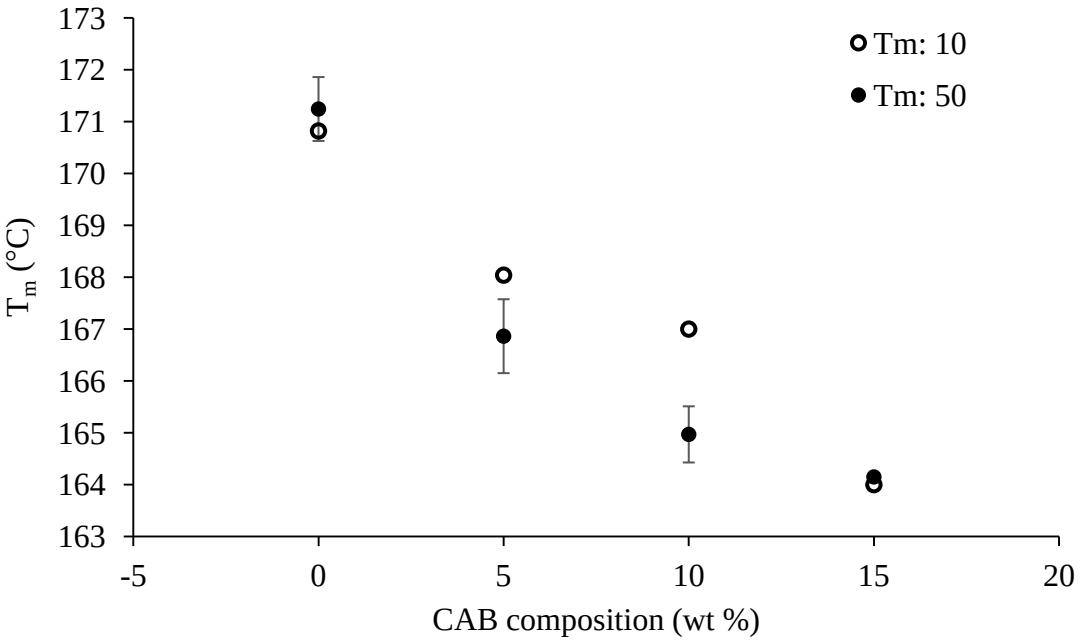

Figure 4.7. The effect of CAB content on the T_m of P(HB-co-HV) from heating at 10 and 50ºC/min

Table 4.1. The effect of CAB content on the thermal properties of P(HB-co-HV) binary blends

Sample	T_m (°C) (50 ºC/min)	T_m (ºC) (10 º/min)	X_c P(HB-co-HV)(%)
P(HB-co-HV)	171.2	170.8	61.6
5 % wt %	166.9	160.0	58.7
10 wt %	165.0	167.0	57.2
15 wt %	164.2	165.0	56.5

Another explanation for the decreasing crystallinity as proposed by Wang et al (2002) relates to the drastically different T_g values between the two blend components during crystallisation. Room temperature is above the T_g of P(HB-co-HV), but below that of CAB. Therefore, the CAB molecules do not have any mobility as they are stuck in the glassy state, whereas the amorphous P(HB-co-HV) chains do have mobility. Therefore some of the P(HB-co-HV) chains in the amorphous state could be trapped by a glassy CAB environment. This reduces the crystallinity by reducing the chains available to crystallise whilst also affecting the regularity and continuity of the P(HB-co-HV) crystalline phase with increasing CAB content(Wang, Cheng et al. 2003).

The shape of the melting endotherms remains consistent for all but one of the transitions. As observed in Figure 4.4, with increasing concentration of CAB to 15 wt %, a shoulder develops on the high temperature side of the endotherm from heating at 10 ºC/min. This bimodal shape was also observed by El-Shaffee et al. (2001) upon heating at 20 ºC/min. This could be due to the fact that the first heating run was used, and therefore could be a product

of thermal history from processing leading to recrystallization upon heating. This would produce a high temperature shoulder corresponding to the melting of the recrystallized crystals at higher temperatures (Suttiwijitpukdee et al. 2011, El-Shaffee et al. 2001). However, it could also suggest a possible lack of miscibility between the two polymers at this composition resulting from the high M_w of both components. P(HB-co-HV)(Tianan ENMAT Y1000P) has a M_w of 215,505 g/mol (Kate Robbins, UoB) while CAB possesses a M_w of 30,000 (Chapter 2, section 2.1.2). High M_w can produce an upper critical solution temperature (UCST) within the blends whereby lowering the temperature below the UCST causes the blend components to phase separate (Ni'mah and Woo 2013). This effect is composition dependent. In this case, it could therefore be that at this blend composition, upon cooling from the melt, the UCST isn't met, causing the two components to phase separate during crystallisation, and therefore presenting themselves individually on a subsequent heating run of the blend. This would cause the emergence of the high temperature peak in line with that of P(HB-co-HV) at 171 ºC, however the presence of the lower temperature peak (166 ºC) suggests some level of interaction whereby the CAB is causing some of the P(HB-co-HV) crystals to melt out at lower temperatures. It is therefore likely that the two components are partially miscible, and this will be discussed further in later sections. .

T_g is another good indicator of miscibility and interaction in a polymer blend system. However, as the T_g of P(HB-co-HV) cannot be seen from the DSC traces, Dynamic Mechanical Thermal Analysis (DMTA) was employed to probe any changes to T_g with the addition of CAB. An upwards shift in T_g in this work would have indicated interaction and miscibility between the two components as the T_g of P(HB-co-HV) would approach that of CAB. The T_g of P(HB-co-HV) was determined via two methods; the peak in Tan δ, and from the convergence point of two tangents; one drawn from the initial flat portion of the trace, and one from the linear portion of the downward slope of the storage modulus (E´) curves.

These two methods give conflicting results. From Figure 4.8, there is a slight reduction in the peak values upon the addition of 5 wt % CAB. However, this does not appear to be composition dependent, as no further shift is observed with increasing the concentration to 10 and 15 wt %. However when obtaining the T_g from tangents of the E´ curves, it can be seen that the T_g decreases from 0 ºC in P(HB-co-HV) to -9 ºC in blends containing 15 wt % CAB (Figure 4.9). The fact that there is a shift of the T_g of P(HB-co-HV) is a good indicator that the two components show some level of interaction, however the shift is not in the expected direction. The T_g of CAB was not analysed using this method as it is an amorphous polymer, and therefore above its T_g is wouldn't have the structural stability to be analysed using this 3 point bend method.

The fact that the T_g is found to decrease in this work, disagrees with some findings on PHB/CAB blends which indicate an increase in T_g with the addition of CAB (Wang, Cheng et al. 2003, Park, Tanaka et al. 2005). However, similar findings have been reported by Pizzoli et al. (1994) reporting a decrease in the T_g with the addition of CAB. In both cases compositional dependence was strongest at higher concentrations of CAB within the blends (above 30 wt %), therefore meaning at lower concentrations (below 30 wt % CAB), minimal changes either way were observed (Pizzoli, Scandola et al. 1994, Park, Tanaka et al. 2005). The downward shift in the present data could be a result of the decreased X_c rather than interaction with the addition of CAB, creating mobility in the chains somewhat like a plasticiser, which in turn reduces the T_g.

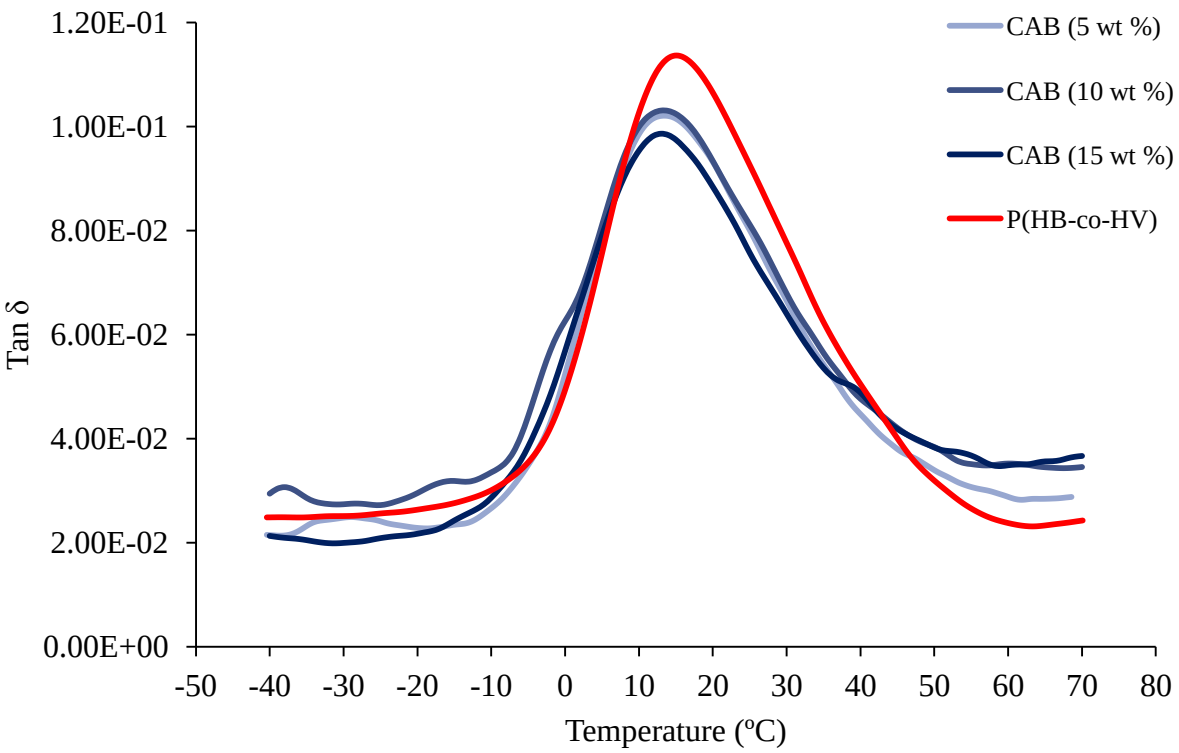

Figure 4.8. The effect of CAB content on the T_g of P(HB-co-HV) as measured by the peak in Tan δ measured at 1 Hz

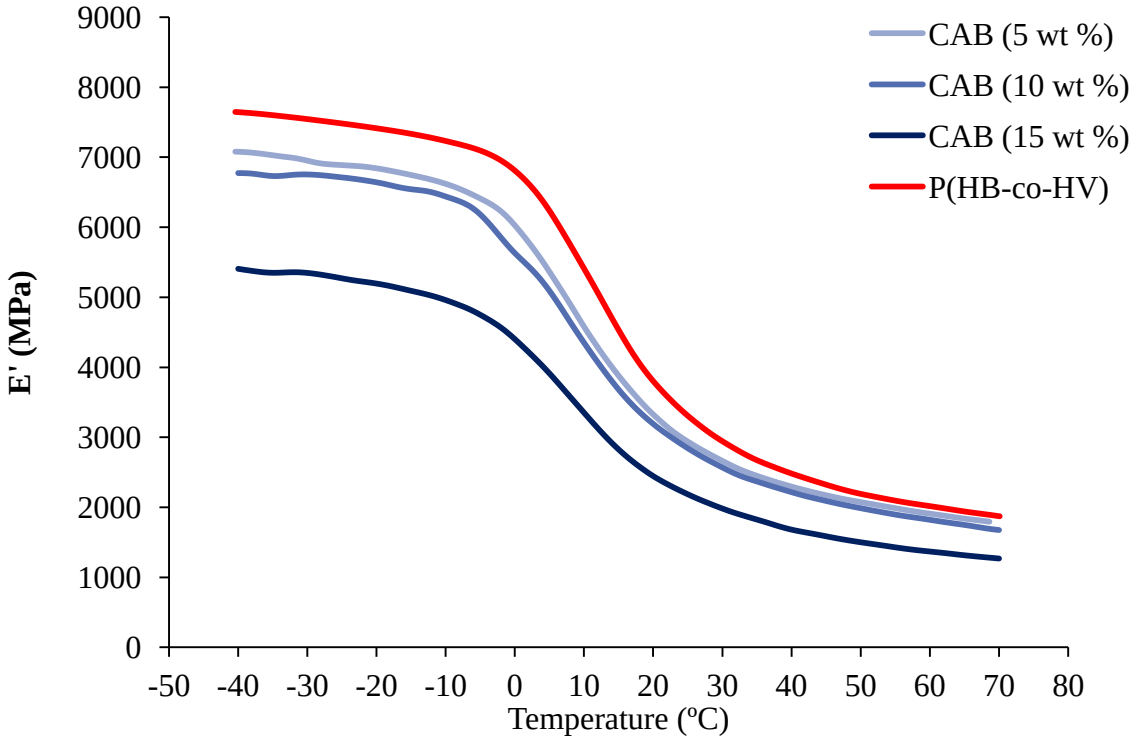

Figure 4.9. DMTA data to show the effect of CAB content on E' of the blends measured at 1 Hz

Table 4.2. The effect of CAB content on the T_g of the blends at 1 Hz

Sample	T_g (°C): Tan δ	T_g (°C): E´
P(HB-co-HV)	15	0
5 % wt %	13	-3
10 wt %	13	-5
15 wt %	13	-9

Figure 4.10 and Table 4.3 also give information regarding the mechanical properties of the blends obtained via DMTA. It can be seen that the initial loss modulus is decreasing as the CAB content increases from 7648 to 5408 MPa, indicative of the material becoming more flexible. The increase in flexibility results from the decreasing crystallinity. The crystalline phase dictates the stiffness of a material, and therefore a reduction in crystallinity, as observed in Figure 4.7, results in concurrent reduction in stiffness, as there are more flexible amorphous chains present and fewer rigid crystalline phases. Increasing flexibility of the polymer would be advantageous for food packaging applications. More detail on the effect of CAB on the mechanical properties of the blends will be discussed in later sections (Chapter 4, Section 4.1.2).

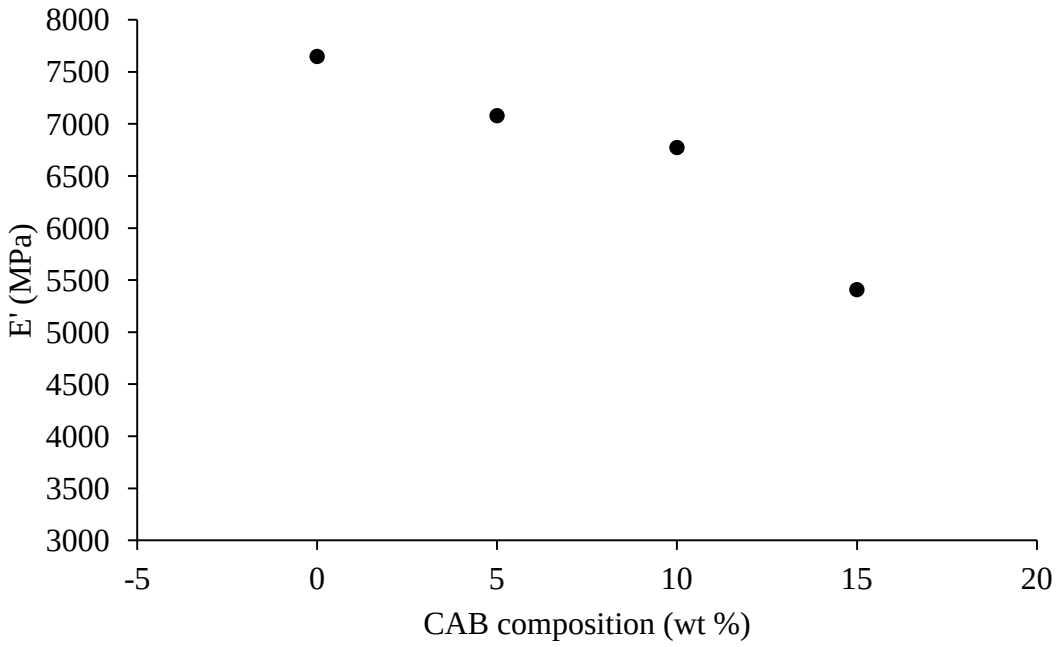

Figure 4.10.The effect of CAB composition on the loss modulus (E) of the blends

Table 4.3.The effect of CAB content on the loss modulus of the blends at 40 ºC

Sample	E´ (MPa)
P(HB-co-HV)	7648
5 % wt %	7098
10 wt %	6773
15 wt %	5408

The activation energy is defined as the minimum energy required for a thermally activated process, in this case the thermal transition from the glass to rubber phase to occur. DMTA was also used to examine the activation energy (Ea) of the blends using the Arrhenius equation (Equation 4.1). This can be rearranged to give Equation 4.2. In these equations, f is the frequency, Ea is the activation energy, R is the universal gas constant (8.31 J mol^{-1} K^{-1}), T is time and M is the gradient of the line for ln(f) vs 1/T.

$$\ln f = \frac{Ea}{RT} \qquad [4.1]$$

$$Ea = MR \qquad [4.2]$$

The blends and the unblended P(HB-co-HV) were analysed at three frequencies as outlined in Chapter 2, and an example of the data collected is shown in Figure 4.11, which is the data for unblended P(HB-co-HV) at 1, 10 and 33 Hz. The Arrhenius equation was then applied to calculate the activation energies of the blends using Equation 4 above (Table 4.4).

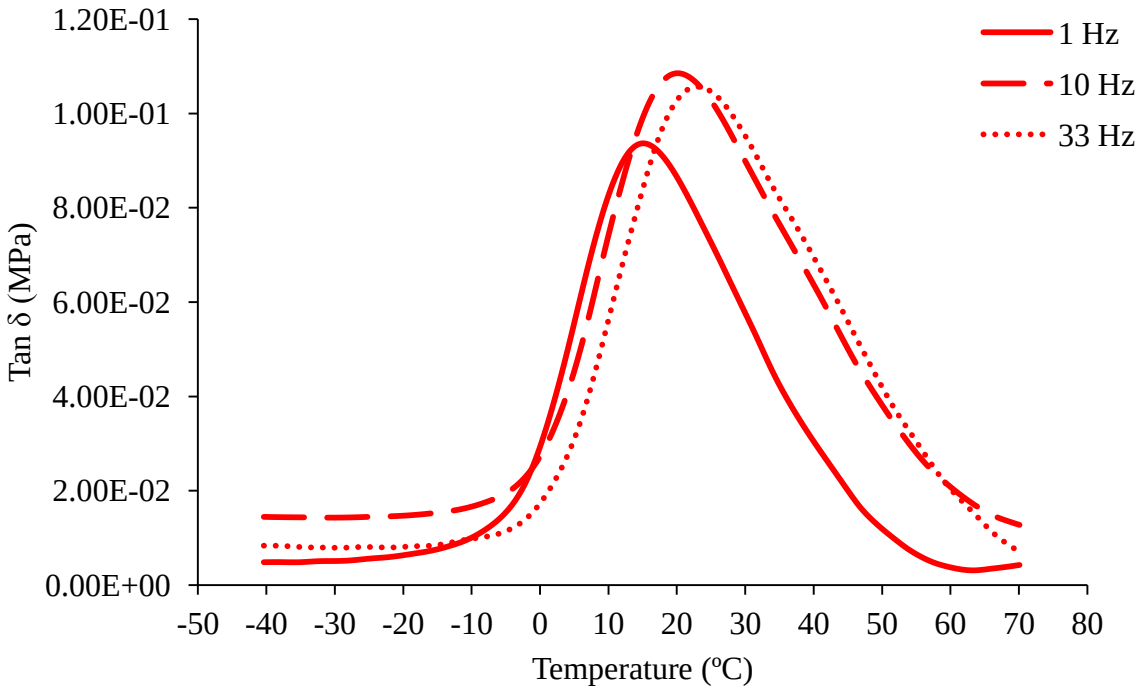

Figure 4.11. The Tan δ data for P(HB-co-HV) used for the calculations of Ea of P(HB-co-HV) and its blends with CAB at each concentration at 1, 10 and 33 Hz.

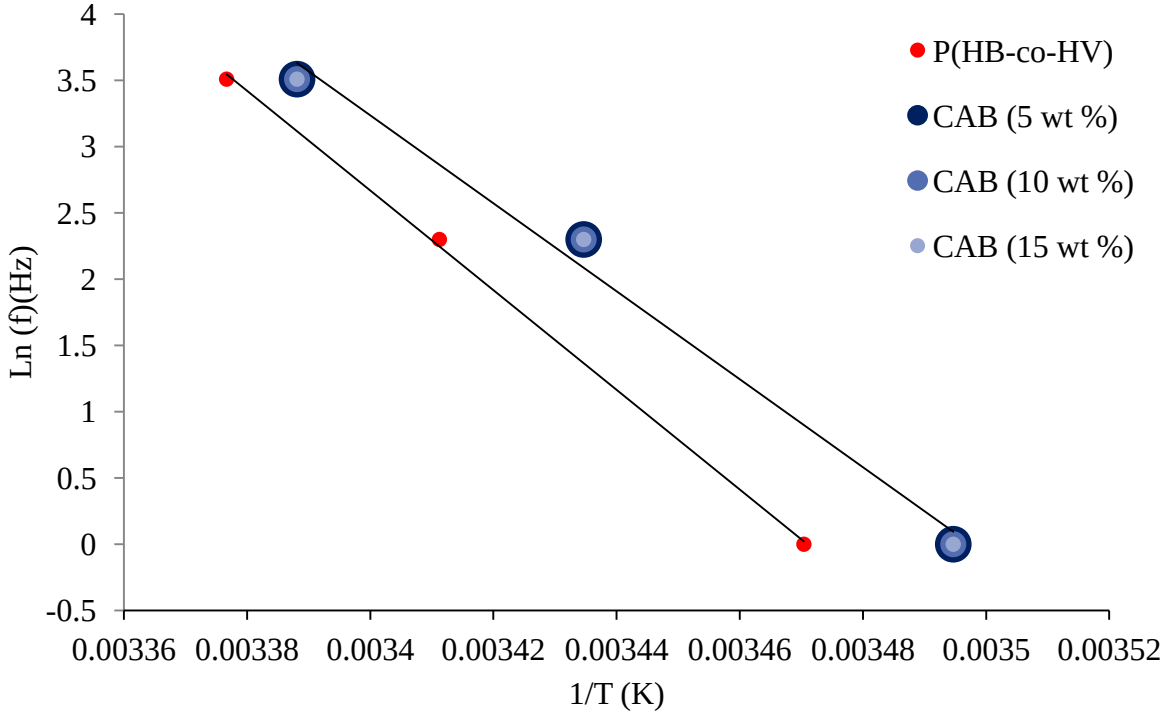

Figure 4.12. An Arrhenius plot showing the Ea of P(HB-co-HV) and its blends with CAB

Table 4.4.The effect of CAB content on the Ea of the blends

Sample	Ea (kJ/mol)
P(HB-co-HV)	312.6
5 wt %	276.0
10 wt %	276.0
15 wt %	276.0

It can therefore be seen from Figure 4.12 and Table 4.4 that the presence of CAB helps to reduce the Ea initially at 5 wt %, and therefore, less energy is required for the thermal transition. This suggests that the CAB may be overcoming interactions within the P(HB-co-HV) such that the T_g is activated sooner in the blends, meaning crystallisation takes place more easily within the blends, however this effect is not composition dependent and therefore is not linked to the wt % of CAB present.

To probe the thermal transitions further, the effect of blending on the melt crystallisation temperature and behaviour was also analysed. This was analysed by non-isothermal crystallisation from the melt using DSC. Un-blended P(HB-co-HV) displays a large sharp peak at 122 ºC (Figure 4.13). As the CAB content is increased, the peaks become smaller, more rounded and the transition broader, as well as the peak temperature shifting to lower temperatures (Table 4.5). A difference of 22 ºC is observed between P(HB-co-HV) and CAB 15 wt %. This suggests that the presence of CAB is retarding the crystallisation process, and causing it to occur at a lower temperature as well as a slower rate. These reductions are in agreement with findings from other studies (Pizzoli, Scandola et al. 1994, Suttiwijitpukdee,

Sato et al. 2011). Pizzoli et al (1994) established that with the introduction of up to 50 % CAB, the spherulitic growth rate is significantly reduced, leading to the broader transitions. They attributed this to a dilution effect which reduces the number of crystallisable elements at the growing lamellar front. In addition to this, the rate of depression could have been caused by the high viscosity of the melt(Pizzoli, Scandola et al. 1994). This reduces the segmental mobility of the crystallising macromolecules, and therefore makes the onset of crystallisation more difficult. Suttiwijitpukdee et al. (2012) related this effect to miscibility whereby the addition of a miscible, non-crystallisable polymer causes the depression of spherulite growth rate of the crystallisable component. These results indicate a level of miscibility within the blend system as there is a clear influence of CAB on the P(HB-co-HV).

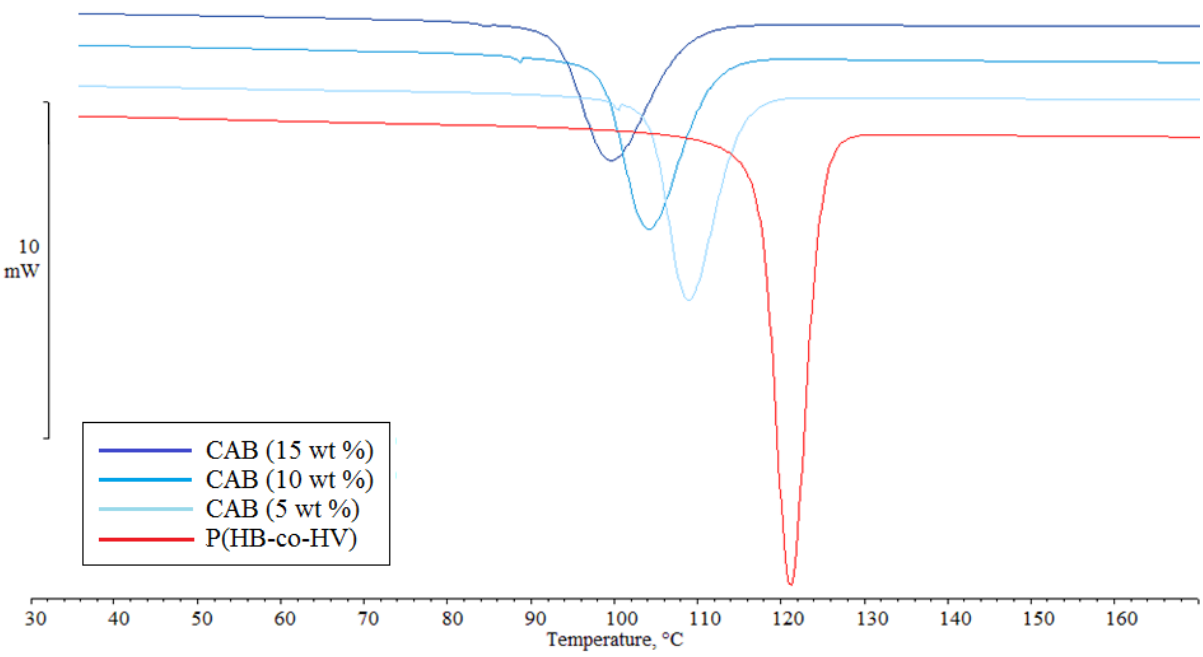

Figure 4.13.The effect of CAB content on the T_c of the blend following cooling at 10 ºC/min

Table 4.5. The effect of CAB content on the T_c of the blends

Sample	T_c (ºC)
P(HB-co-HV)	121
5 wt %	109
10 wt %	104
15 wt %	100

4.1.1.1.2 Isothermal measurements

Isothermal measurements were taken to assess the effect of CAB on the crystallisation kinetics of P(HB-co-HV). Five samples were run per blend. It should be noted that the temperatures explored for unblended P(HB-co-HV) were different to those used for the blends due to the fact that the P(HB-co-HV) used in this work is heavily nucleated causing it to crystallise very quickly, whereas the presence of CAB slowed down this process significantly. Therefore, the P(HB-co-HV) was crystallised from 140 to 148 ºC as 140 º C was the lowest temperature where the start of the process could be observed. The resulting curves for un-blended P(HB-co-HV) are presented in Figure 4.14.

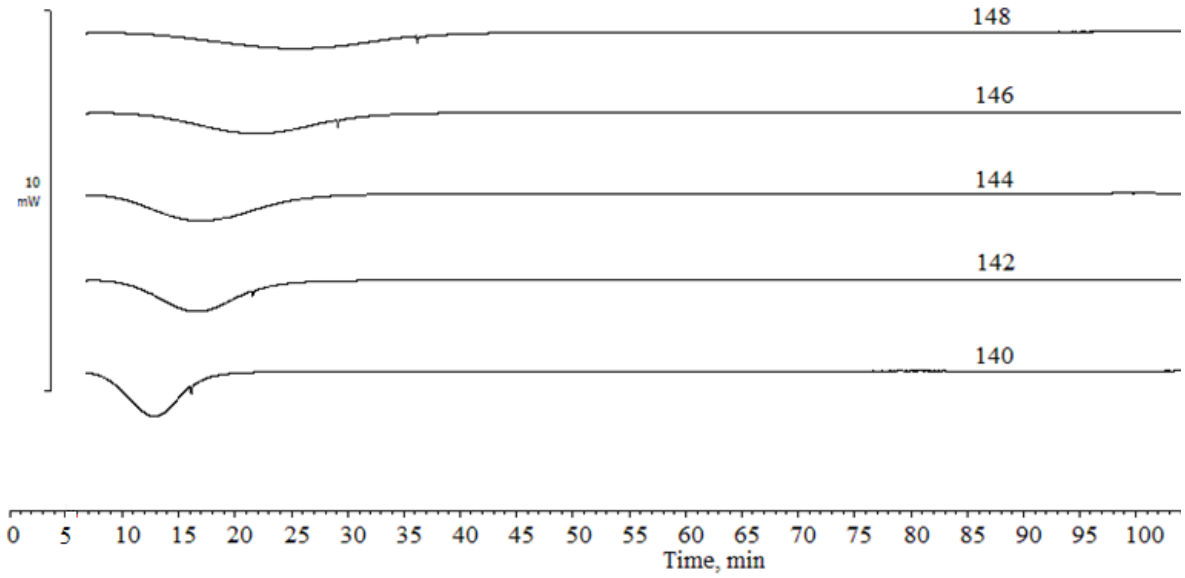

Figure 4.14. Isothermal crystallisation of P(HB-co-HV). Samples held at temperatures between140 ºC and 148 ºC for 120 minutes

The isothermal curves for the different CAB compositions can be seen below in Figures 4.15, 4.16 and 4.17. It is evident from these curves that the isothermal crystallisation process of the blends is significantly affected by the presence of CAB in agreement with the non-isothermal data. This is particularly apparent at a T_c of 140 ºC, where for unblended P(HB-co-HV), crystallisation happens at a very rapid rate, and is the lowest temperature possible to capture the whole crystallisation process. However, for the CAB blends at all compositions, the crystallisation process happens extremely slowly, and is the highest temperature possible to ensure the crystallisation process went through to completion within the 120 minute time frame set for all samples.

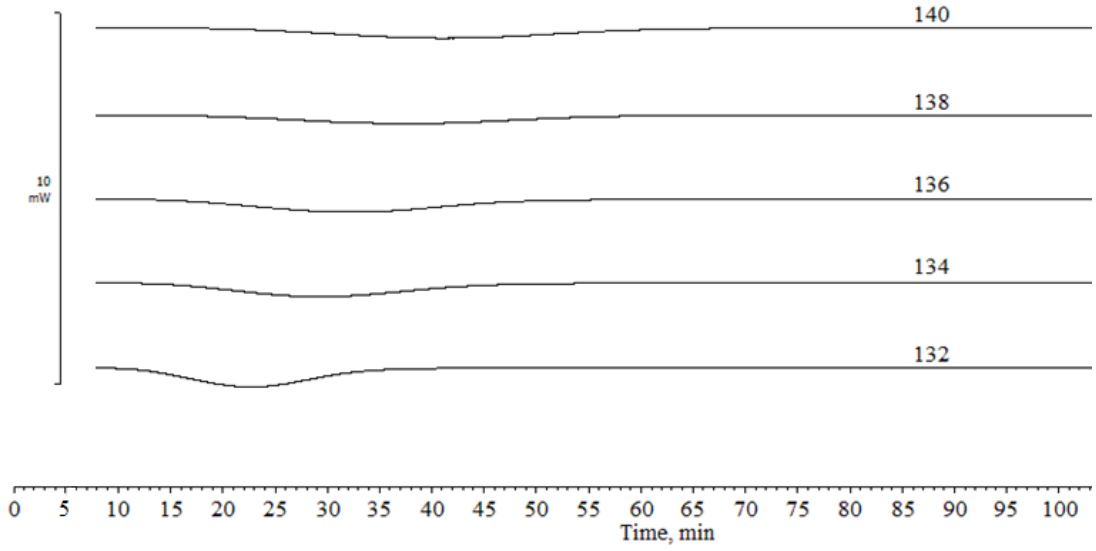

Figure 4.15. Isothermal crystallisation behaviour of P(HB-co-HV)/ CAB blends at 5 wt % CAB. Samples held at temperatures between 132 and 140 ºC for 120 minutes

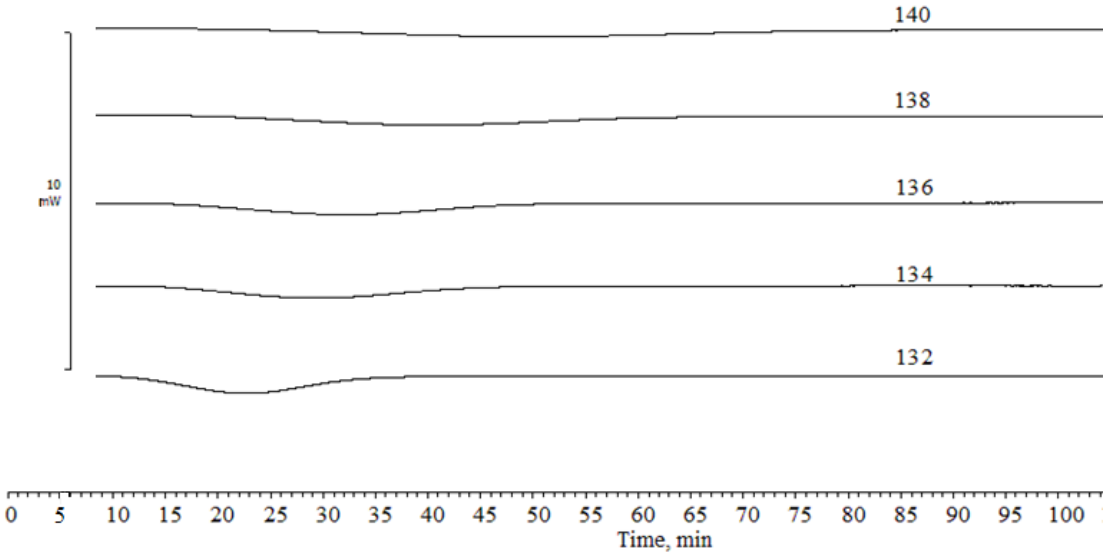

Figure 4.16. Isothermal crystallisation behaviour of P(HB-co-HV)/ CAB blends at 10 wt % CAB. Samples held at temperatures between 132 and 140 ºC for 120 minutes

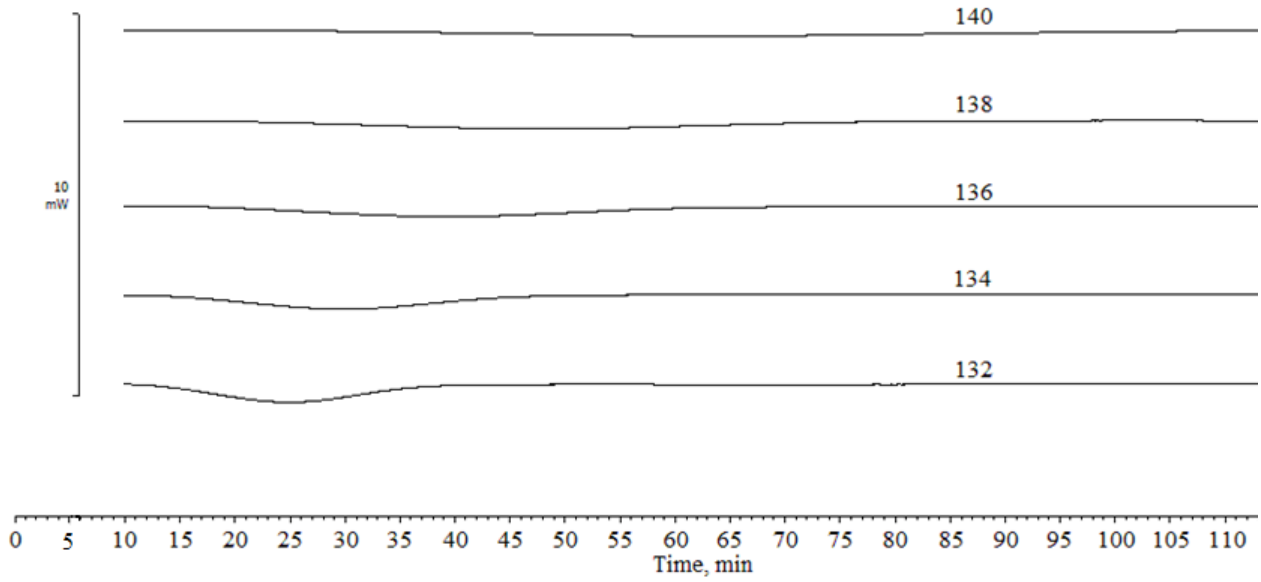

Figure 4.17. Isothermal crystallisation behaviour of P(HB-co-HV)/ CAB blends at 15 wt % CAB. Samples held at temperatures between 132 and 140 ºC for 120 minutes

Avrami analysis was conducted on samples run at 140 ºC to draw comparisons of the effect of the CAB on the crystallisation behaviour as this was the only common temperature possible across all of the blends. Figure 4.18 displays the comparison of crystallisation behaviour between the compositions at 140 ºC. From this graph, it can be clearly observed that the CAB has a significant effect on slowing down the crystallisation process, even at compositions as low as 5 wt%. The induction time to crystallisation is slowed dramatically, from 3 seconds in the unblended material, to 938 seconds in the 15 wt % CAB blend (Table 4.6). Not only is the onset of crystallisation slowed and moved to a lower temperature, but the process itself is slowed, as illustrated by the increasing breadth and reducing magnitude of the crystallisation peaks with increasing concentration of CAB.

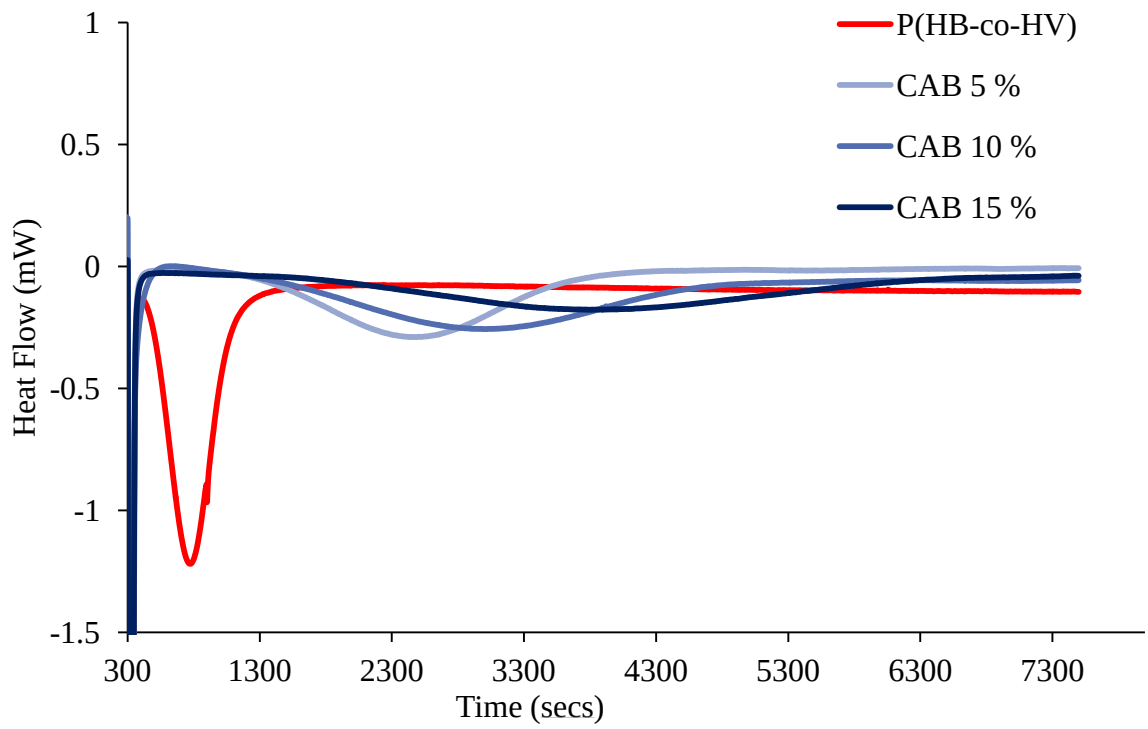

Figure 4.18. Effect of CAB content on the isothermal crystallisation behaviour at 140 ºC for 120 minutes

Table 4.6. Effect of CAB content on the induction time for isothermal crystallisation at 140 º over 120 minutes

Sample	Induction time (secs)
P(HB-co-HV)	3
5 % wt %	211
10 wt %	626
15 wt %	938

This agrees with other studies reporting that the incorporation of a second, high T_g material into the blend significantly reduces the rate of PHB crystallisation by reducing the spherulite growth rate (Pizzoli, Scandola et al. 1994, El-Shafee, Saad et al. 2001). The CAB has been reported to be incorporated into the growing PHB spherulites in the inter-lamellar and inter-fibrullar regions where it is able to retard the crystallisation process by the disruption of intramolecular hydrogen bonding within the PHB (El-Shafee, Saad et al. 2001, Suttiwijitpukdee, Sato et al. 2011). It could also be a result of a dilution effect, where due to the increasing presence of CAB, there is a decreasing quantity of P(HB-co-HV), and therefore less crystallisable material(Pizzoli, Scandola et al. 1994). Alternatively, these results could be indicative of the presence of crosslinks formed between the carbonyl groups present in P(HB-co-HV) and the hydroxyl groups in CAB, acting to reduce the rate of crystallisation and crystallinity of the material as previously observed in blends of PHB and CAB(Suttiwijitpukdee, Sato et al. 2012).

A way of quantifying the rate of crystallisation is the calculation of $t_{1/2}$that can be denoted from the isothermal crystallisation data. This is the time taken for the polymer to reach half of its attainable crystallinity. Figure 4.19 shows the graphs obtained for the calculation of $t_{1/2}$ for each of the blends. The decreasing gradient with increasing composition of CAB indicates that the time taken to reach half the attainable crystallinity is increasing, and therefore the rate of crystallisation is slowing significantly with this addition. These results agree with those obtained from Avrami analysis of PHB/CAB blends where $t_{1/2}$ increased from 29 minutes to 59 minutes in low molecular weight CAB (M_n = 1.2 x 10^4), and more significantly from 29 minutes to 200 minutes in a high molecular weight CAB (M_n = 7.0 x 10^4) (Suttiwijitpukdee, Sato et al. 2011) indicating the influence of molecular weight on retarding the crystallisation process. A possible reason for the significantly different values in comparison to those obtained in this work could be the presence of nucleating agents within the P(HB-co-HV)

used within this work, which may act to significantly reduce $t_{1/2}$ by increasing crystallisation rate of the base material significantly as pure un-nucleated PHB is naturally a very slow crystalliser due to its low nucleation density.

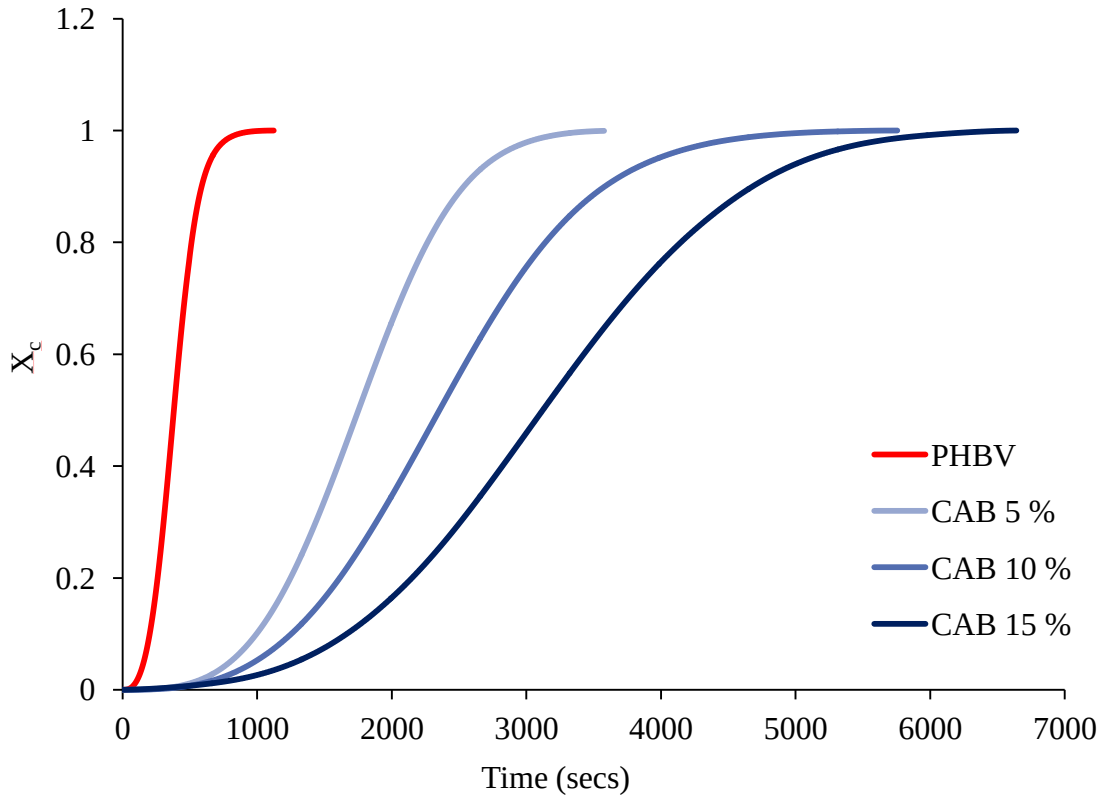

Figure 4.19.The effect of CAB content on the $t_{1/2}$of P(HB-co-HV) at 140 ºC for 120 minutes

Table 4.7.The effect of CAB content on the $t_{1/2}$ during isothermal crystallisation at 140 ºC for 120 minutes

Sample	$t_{1/2}$(secs)
P(HB-co-HV)	3
5 wt %	211
10 wt %	626
15 wt %	938

Avrami analysis provides information on the crystallisation regime in terms of nucleation and growth. This was therefore conducted to analyse the effect of the presence of CAB on the blends. Through application of the Avrami equation a double log plot was produced (Equations 4.3 and 4.4, outlined in Chapter 2), leading to the determination of the Avrami exponent (n). The results are provided in Figure 4.20 and Table 4.8 .

$$X_c(t) = 1 - \exp(Kt^n) \qquad [4.3]$$

$$\ln\left(-ln\left(1 - X_c(t)\right)\right) = n \ln t + \ln K \qquad [4.4]$$

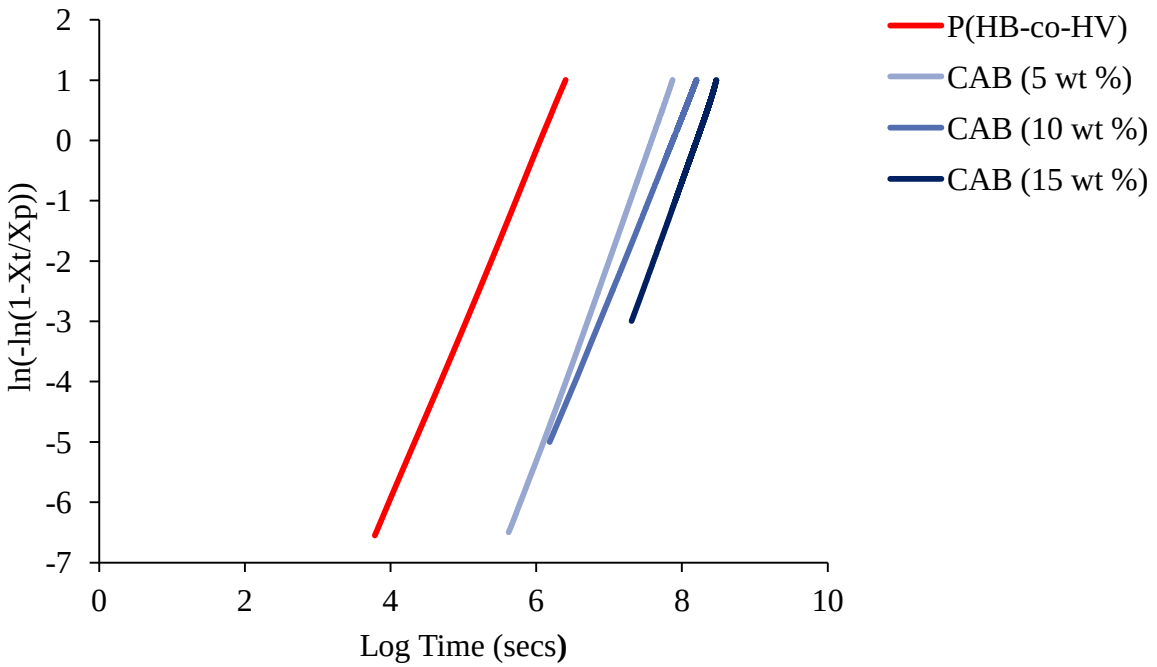

Figure 4.20.The effect of CAB content on the Avrami exponent of P(HB-co-HV) during isothermal crystallisation at 140 ºC for 120 minutes

Table 4.8. The effect of CAB content in the Avrami exponent (n) during isothermal crystallisation at 140 ºC for 120 minutes

Sample	n
P(HB-co-HV)	2.9
CAB (5 wt %)	3.4
CAB (10 wt %)	3.0
CAB (15 wt %)	3.4

The Avrami exponent (n) provides information on the crystal growth during crystallisation. From Table 4.8, it can be seen that the Avrami exponent for all samples is 3. This indicates 3D crystal growth creating a spherical shape in all samples and therefore the mode of crystal growth is unaffected by the presence of CAB.

Another way to analyse the effect of blend components is via depression of the equilibrium melting point (T_m^0) which can be analysed in polymer blends via a Hoffman-Weeks plot. A depression in T_m^0 indicates interaction within the polymer blend components and thus a miscible system. This was applied to the isothermal data to assess any melting point depression with the addition of CAB. T_m^0 was obtained by heating the sample to 220 ºC following isothermal crystallisation to obtain a melting peak. This melting peak (T_m) was plotted against the temperature the sample had been crystallised at (T_c) (Figure 4.21) at five crystallisation temperatures for each blend, and a linear trend line applied. T_m^0 was determined by the intercept of the trend line with the line of $T_m = T_c$.

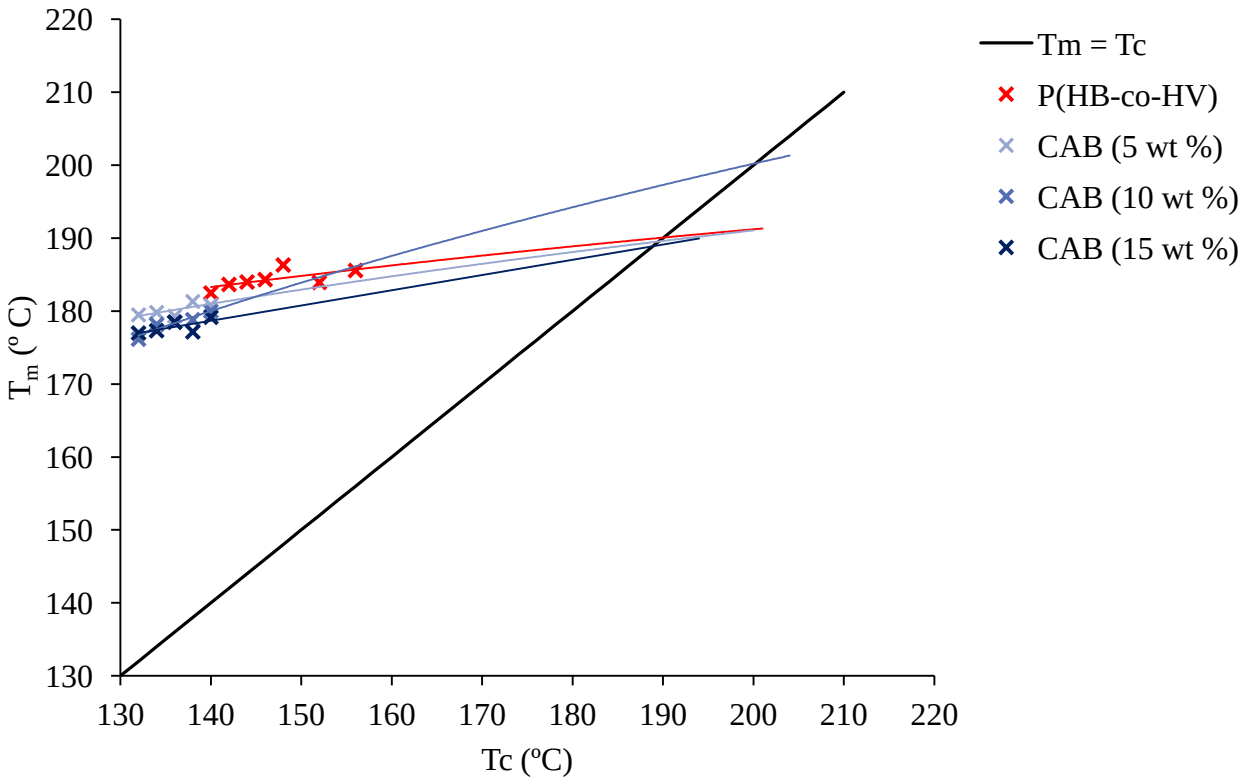

Figure 4.21. A Hoffman-Weeks plot of P(HB-co-HV) and the CAB blends to establish T_m^0

Table 4.9.The effect of CAB on the T_m^0 of P(HB-co-HV)

Sample	T_m^0(ºC)
P(HB-co-HV)	196.0
5 wt %	186.5
10 wt %	200.0
15 wt %	189.0

This Hoffman-Weeks analysis indicates that there is a change in T_m^0 with the addition of CAB, however this does not seem to be composition dependent as no trends are observed, and the blend containing 10 wt % CAB presents an increased value for T_m^0. The T_m^0 depression in the 5 and 15 wt % concentrations indicates that the CAB is getting into the amorphous phase of the P(HB-co-HV) and disrupting its crystal structure, thus affecting its thermal properties, however lack of trends renders the results inconclusive. More data points for each blend should be obtained and subjected to Nishi Wang analysis to draw more accurate conclusions.

From changes in T_m, crystallinity and T_g, it is apparent that the two components of the blend are at least partially miscible, and some level of interaction is occurring. This is brought about by interactions of the chains with each other, and is as a result of the hydroxyl groups on the CAB which, as well as being reported to allow crosslinking by intermolecular hydrogen bonding, also help to induce miscibility in polymer-polymer blend (He, Zhu et al. 2004). This results in the slowing of the crystallisation kinetics of the material, meaning the P(HB-co-HV) crystallises more slowly. This has also previously been reported in other grades of CAB to date, but not in the one used in this work. This retarding of the

crystallisation process could therefore also have an effect on reducing the rate secondary process if not halting it completely, and will be discussed further on in this work.

4.1.2 Mechanical properties

Based upon the significant changes to crystallisation kinetics observed above, changes to mechanical properties as a result are expected. Mechanical properties of materials can be well characterised by uniaxial tensile testing, which has been conducted here to analyse the effects of CAB content on the blends and therefore analyse the suitability of such blends as food packaging materials.

It can be seen from Figure 4.22, that P(HB-co-HV) shows the characteristic curve of a brittle polymer, as it shows elastic behaviour, followed by plastic yielding and then minimal necking/ drawing before fracture at 12 % strain. This is significantly lower than that of polypropylene, which demonstrates values of E_b in the region of 100-600 % (Callister and Rethwisch 2008), classifying it as a ductile polymer. It is apparent from Figure 4.22 that significant changes to mechanical properties are observed upon blending. The most obvious change that can be observed is the change in elongation to break (E_b). The material becomes less ductile as 5 and 10 wt% CAB is added, but then as the CAB content is increased to 15 wt %, the E_b begins to increase and the blend becomes a more ductile material than pure P(HB-co-HV). This can be observed more clearly in Figure 4.23 where a U shaped curve is present. This could indicate that at higher percentages of CAB, the mechanical properties may exceed those of unblended P(HB-co-HV) which has been reported previously in other work(Buchanan, Gedon et al. 1992, Wang, Cheng et al. 2003, Yamaguchi and Arakawa 2006). However, it should be noted that there is a large error within the results conducted

within this work, and therefore within error the change may not be significant despite the apparent trend of data points.

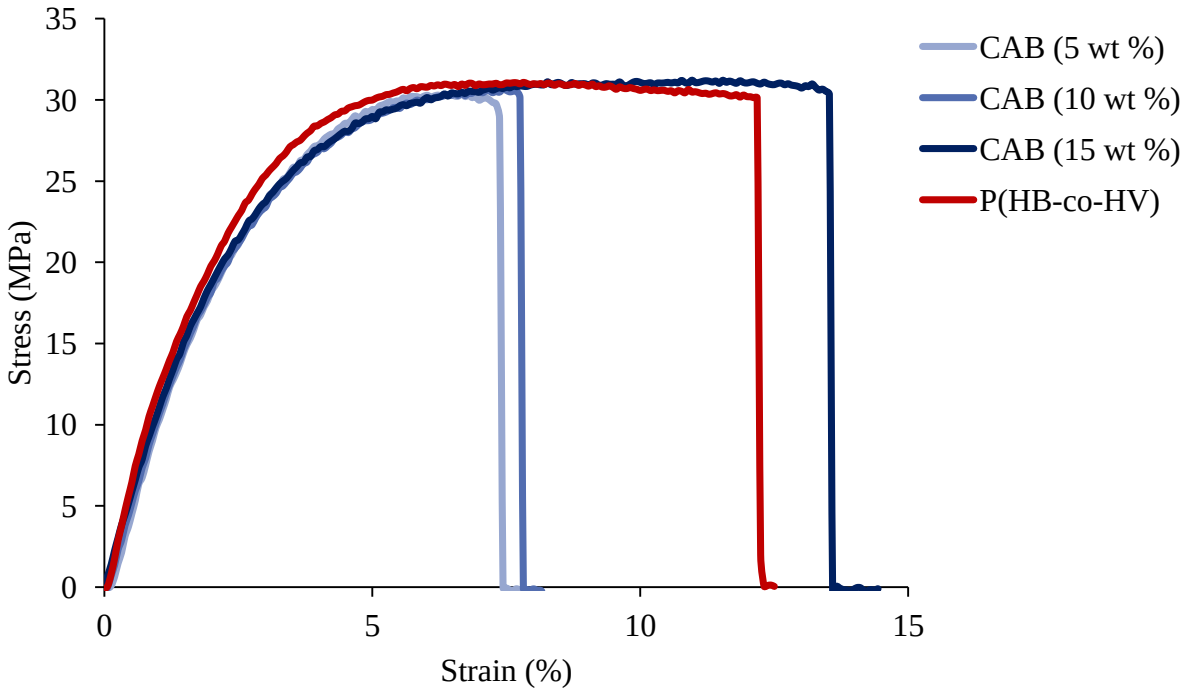

Figure 4.22.The effect of CAB content on the tensile properties of the blends

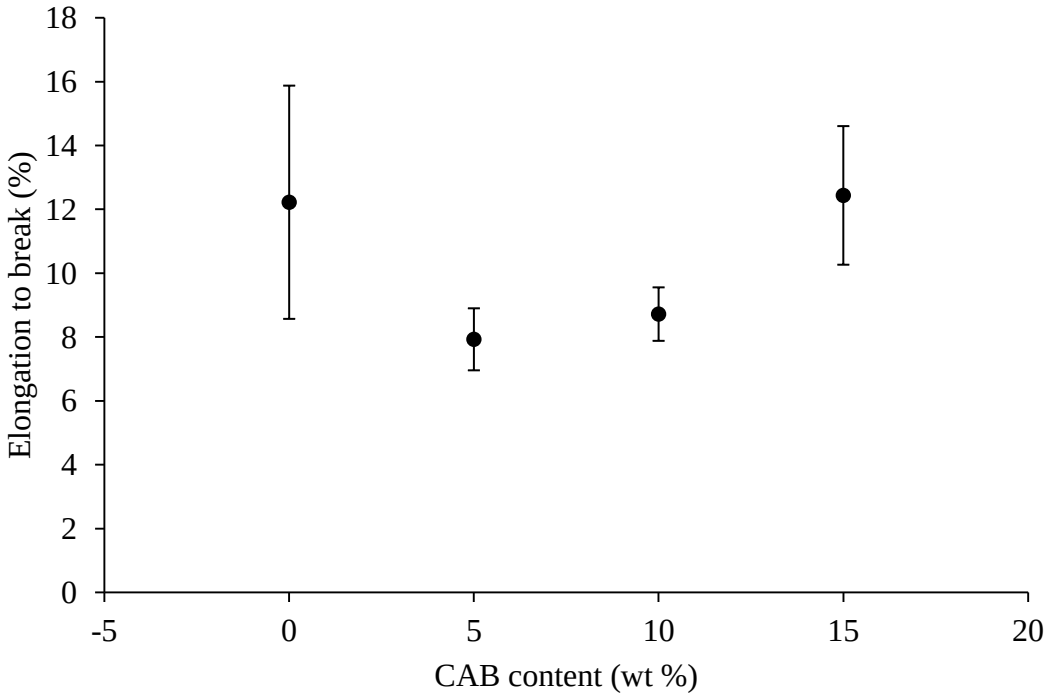

Figure 4.23.The effect of CAB content on the E_b of P(HB-co-HV)/ CAB blends prior to storage

This curve may result from increasing the ductile component within the blend. Wang et al (2002) showed that by increasing the CAB content up to 50 wt% the E_b of the material increased from 2 to 7 %. It is therefore reasonable to assume that further improvements would come as a result of increasing the CAB concentration further. The large error bars could result from the large variability found within P(HB-co-HV) due to a processing effect from an un-level hot press. This could have caused different parts of the sample to have cooled at different rates, thus affecting the crystallinity of each sample produced and leading to variable mechanical properties within the sample set. It could also be a product of machine error, or also loading error. Loading the sample in at an angle will affect the way it responds to tension, by the creation of stress concentrations which could lead to premature failure of the samples.

In addition to the increasing E_b, a decrease in Young's modulus (E) was observed indicating that the material is becoming less stiff with the addition of CAB (Figure 4.24). This could be occurring due to the reducing crystallinity with increasing CAB content. Crystallinity creates stiffness within materials and therefore the less crystalline the material, the higher the proportions of the ductile amorphous regions leading to the increasing E_b and the reducing Young's modulus.

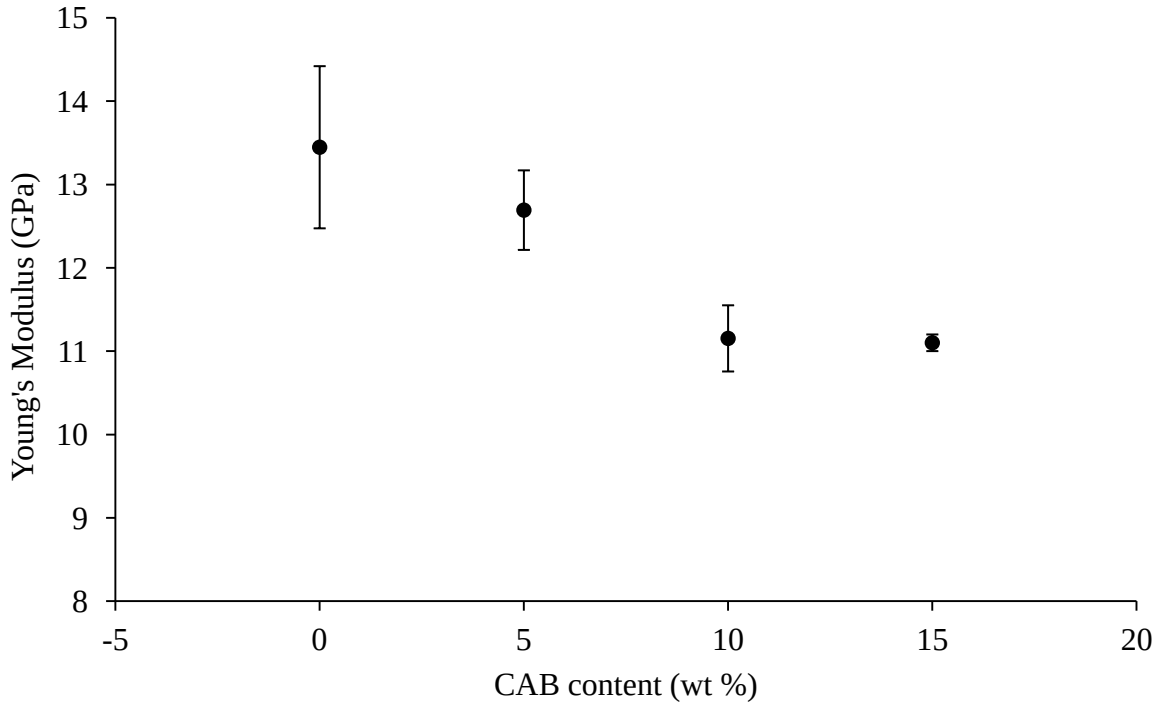

Figure 4.24.The effect of CAB content on the Young's Modulus of the P(HB-co-HV)/ CAB blends prior to storage

With this reduction in modulus, there is an accompanying increase in Ultimate Tensile Stress (UTS). This also relates to the crystallinity of the material as discussed above. The higher amorphous fraction present in more ductile materials means a greater stress is required to break the material as there are a higher proportion of amorphous chains that can stretch

under tension before failure (Figure 4.25). However, due to the large error bars present, these results could all be the same within error despite the apparent trend upwards with increasing CAB content.

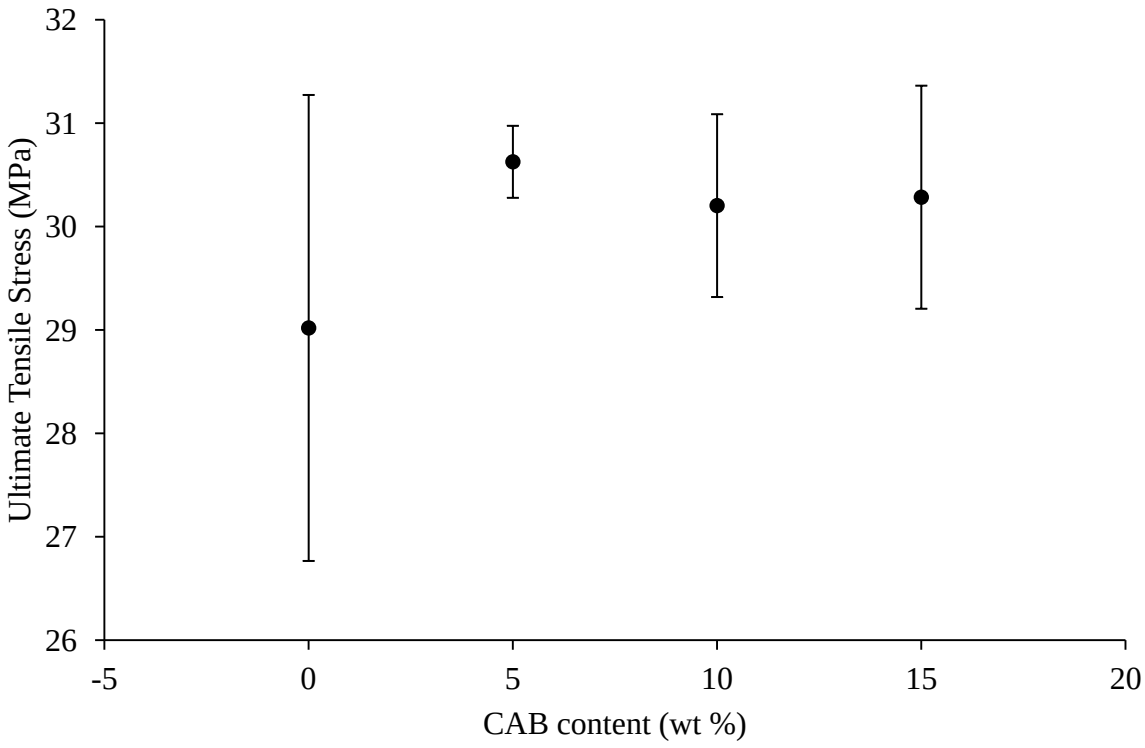

Figure 4.25. The effect of CAB content on the UTS of P(HB-co-HV)/ CAB blends prior to storage

Taking into account that toughness is strongly dependent on E_b, the pattern is similar to E_b as above with increasing CAB content. It shows a similar U shaped curve where the addition of 5 % CAB acts to reduce the toughness of the material, then further additions of CAB increase the toughness of the material to around the same value of P(HB-co-HV) (Figure 4.26). These results appear insignificant however due to the large error bars present which indicate the results could be similar values for each blend within experimental error. Table

4.10 summarises all of the results from mechanical testing of each sample set on day 0 prior to storage.

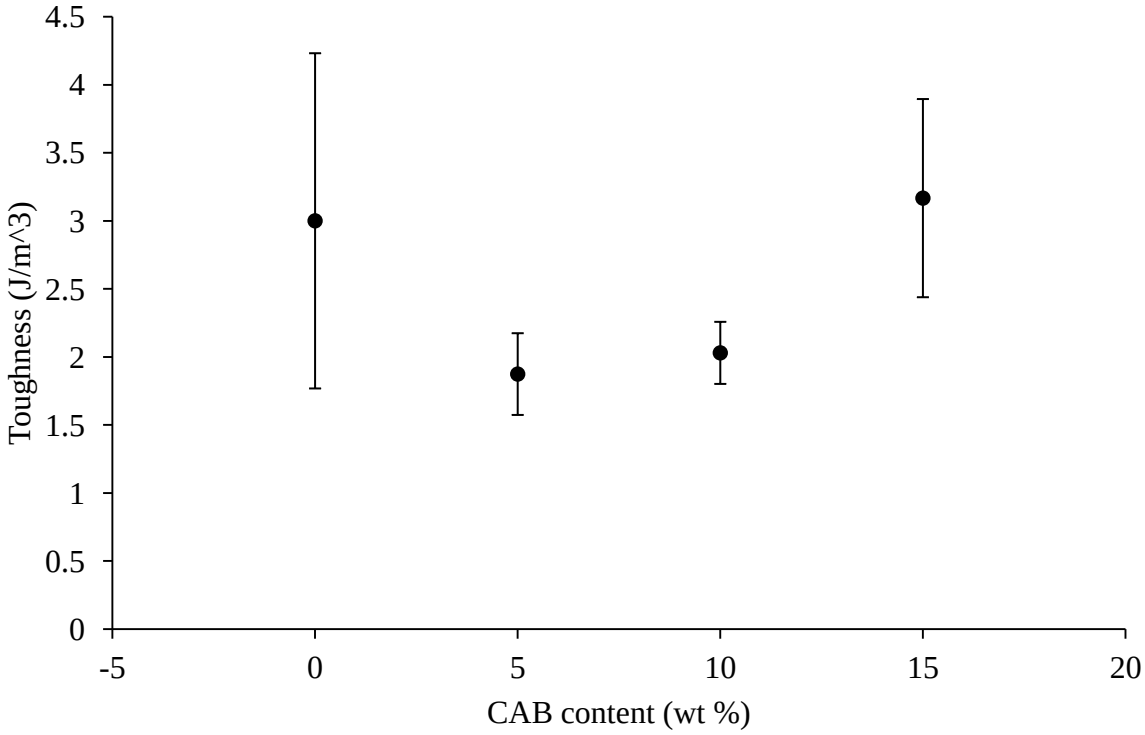

Figure 4.26. The effect of CAB content on the toughness of P(HB-co-HV)/CAB blends prior to storage

Table 4.10. A summary of the mechanical properties of the P(HB-co-HV)/CAB blends prior to storage

Sample	E_b (%)	UTS (MPa)	Young's Modulus (GPa)	Toughness (J/m^3)
P(HB-co-HV)	12.2 ± 3.7	29.0 ± 2.3	13.5 ± 1.0	3.0 ± 1.2
5 wt %	7.9 ± 1.0	30.6 ± 0.4	12.7 ± 0.5	1.9 ± 0.3
10 wt %	8.7 ± 0.8	30.2 ± 0.9	11.2 ± 0.4	2.0 ± 0.2
15 wt %	12.4 ± 2.2	30.3 ±1.1	11.1 ± 0.1	3.2 ± 0.7

4.1.3 Fourier transform Infra-Red Spectroscopy (FTIR)

Intermolecular hydrogen bonding has been previously reported in other work investigating P(HB-co-HV)/ CAB blends. FTIR is one of the best methods for determining any chemical changes occurring within the material on blending and therefore has been conducted to analyse the effect of blending CAB into P(HB-co-HV). The main region of interest is the carbonyl region as any shifts in this peak indicates interaction between the two components. It has previously been reported that with the presence of intermolecular hydrogen bonding, there is a shift of the carbonyl peak to higher wavenumbers (Suttiwijitpukdee et al. 2011). The effect of blending on the carbonyl peak is shown in Figure 4.27. Here it can be seen that there is a very slight shift of the peak to a higher wavenumber, indicating the possible presence of H-bonding (Table 4.11). This however may not be significant and is not composition dependent, suggesting minimal interactions of the blend components.

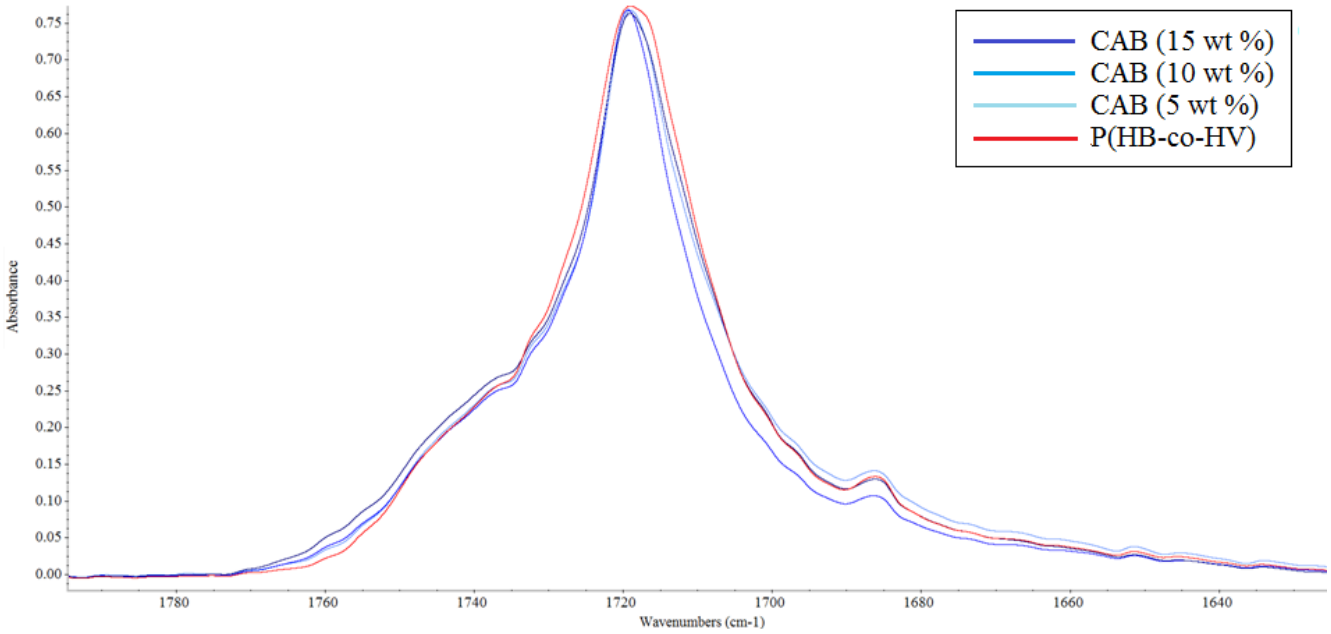

Figure 4.27. FTIR spectrum showing the effect of blending on the carbonyl peak

Table 4.11. Values for the position of the carbonyl peak in each blend

Sample	Wavenumber (cm^{-1})
P(HB-co-HV)	1717
5 % wt %	1719
10 wt %	1719
15 wt %	1718

Suttiwijitpukdee reported a new peak at 1738 cm^{-1} in blends containing 50 % of high molecular weight CAB which they suggested could be an indication of intermolecular hydrogen bonding, however this peak was not present in the current study.

Another interesting peak discussed by Suttiwijitpukdee et al. (2012) was that of the first overtone of the intramolecular hydrogen bonding peak for PHB in the region of 3435 – 3445 cm^{-1}. The dominant peak centred at around 3435 cm^{-1} has been previously reported to shift to higher wavenumbers with CAB content, brought about by intermolecular hydrogen bonding between the two components creating crosslinks (Suttiwijitpukdee, Sato et al. 2012). However, as can be seen from Figure 4.28, there is minimal shift with its addition. These are conflicting results to those obtained from Suttiwijitpukdee et al. (2012), who found this peak to shift from 3435 cm^{-1} to 3450 cm^{-1} with 50 % CAB. It is possible that upon further increasing the concentration of CAB within the blends, more prominent shifts would be observed, and therefore the seemingly low level of interaction could be a result of the low concentration of blend component, as was the case with the T_g behaviour. It is also possible that the number of hydroxyl groups available on the experimental CAB are not high enough to induce a significant effect, as there was only 1.5 wt % hydroxyl groups on the CAB used in this work. This was due to availability of materials.

The reduction in the peak at 3445 cm^{-1} which was assigned to the first overtone of the crystal peak of PHB for intramolecular hydrogen bonding within this same region could mean the CAB is reducing the ability of the P(HB-co-HV) to intramolecular hydrogen bond with itself in the crystalline regions. This could indicate that the CAB is trapped within the amorphous regions and preventing the P(HB-co-HV) from forming intra-molecular hydrogen bonds with itself during crystallisation. This could therefore be evidence for the presence of CAB hindering crystallisation and also retarding the rate of crystallisation as mentioned earlier within the DSC work (Section 4.1.1.1).

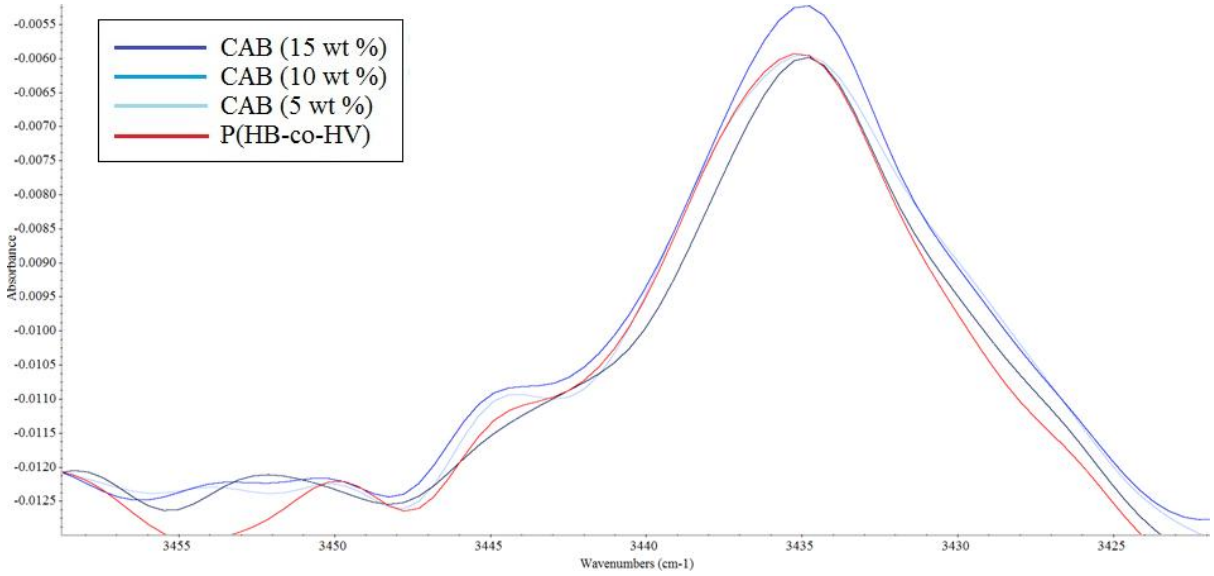

Figure 4.28. FTIR spectra of the PHB intramolecular hydrogen bonding region

Additionally, in a set of studies conducted by Suttiwijitpukdee et al. (2011) and Suttiwijitpukdee et al. (2012), a number of peaks were analysed in PHB/CAB blends. They assigned the wavenumber of 3485 cm^{-1} to intermolecular hydrogen bonding between the carbonyl group of the CAB units. It can be seen from Figure 4.29, that as the concentration of CAB is increased, the peak shifts to a higher wavenumber (from 3485 to 3486 cm^{-1} for blends containing CAB 15 wt%) and the magnitude of the peak is reduced. This indicates intermolecular hydrogen bonding is occurring, thus confirming some level of interaction within the blends.

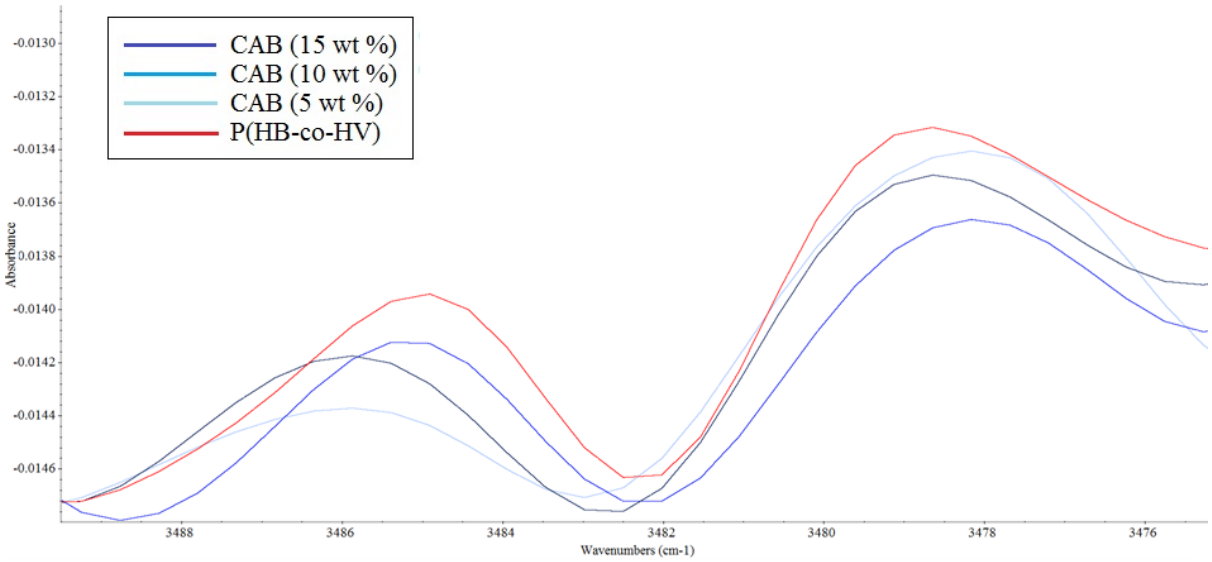

Figure 4.29. FTIR spectrumof the region assigned to intramolecular bonding within CAB

4.1.4 Morphology

4.1.4.1 Hot stage microscopy

Another way to determine miscibility is through visual inspection via microscopy techniques. This allows the level of mixing to be observed on a microscopic level and can be used to relate the mechanical and thermal properties. Hot stage microscopy was used to analyse the spherulite morphology of the base material and the resulting blends. Figure 4.30 shows the unblended P(HB-co-HV) in the melt state. It can be seen that the P(HB-co-HV) is heavily nucleated with Boron Nitride as outlined in Chapter 2, which is the reason for the rapid crystallisation during the isothermal experiments and melt crystallisation experiments. Boron Nitride (BN) is a very effective nucleating agent leading to a fine spherulitic texture as displayed in Figure 4.31. The BN particles are approximately 10 µm in size and evenly distributed throughout the sample. CAB is a 100 % amorphous material, and therefore could not be observed under polarised light microscope.

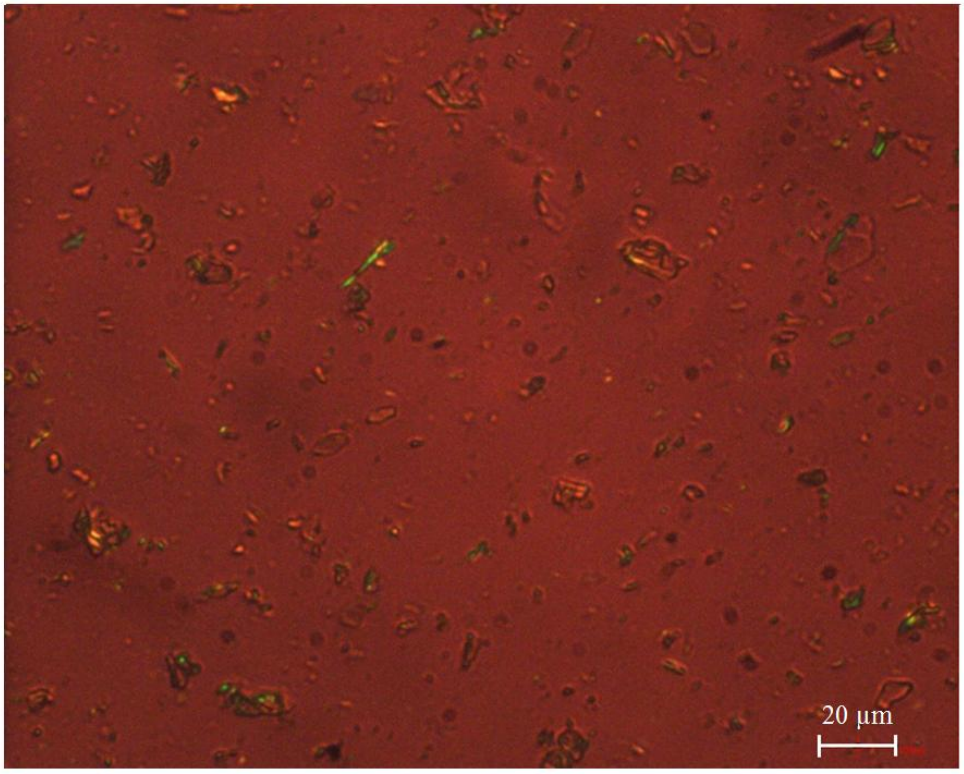

Figure 4.30. P(HB-co-HV) in the melt at 180 °C

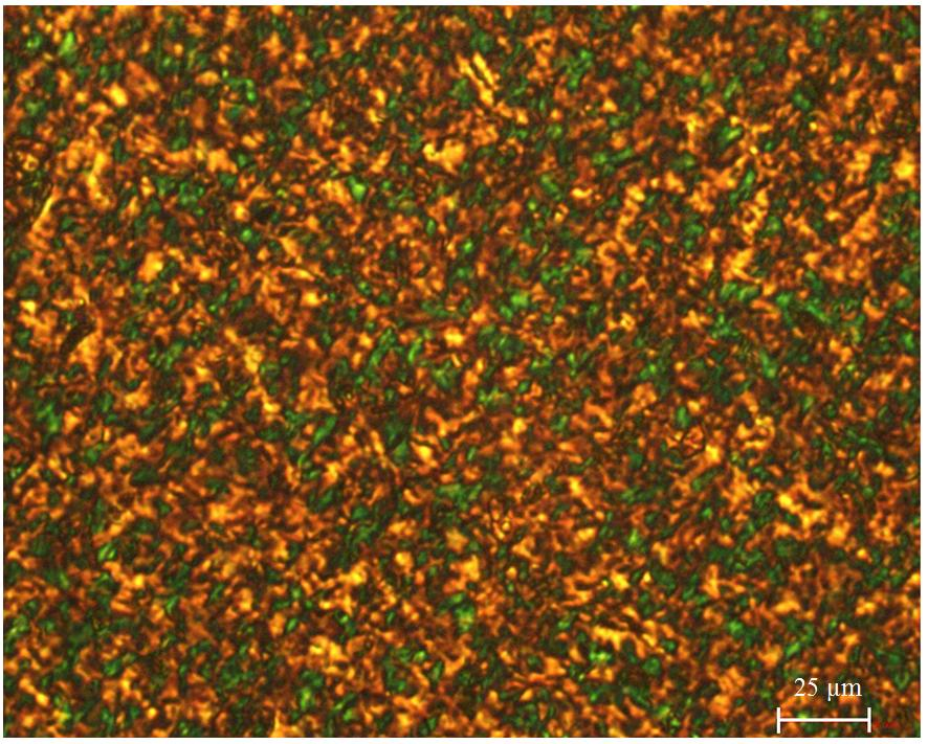

Figure 4.31. Fully crystallised P(HB-co-HV) analysed under hot stage. Sample cooled from 180 °C to 25 °C at 50 °C/min

The addition of CAB seems to create two distinct phases (Figure 4.32). In Figure 4.32a (5wt %), the blend is in the melt state and the two phases components are obviously visible suggesting no interaction between the two. As the material is cooled and spherulites start to form however, there is evidence of what is presumed to be amorphous CAB leaching out into P(HB-co-HV) at the edges (Figure 4.32b). This is observed at 115 ºC, which is above the T_g of CAB, and the T_c of the blend containing CAB (5 wt %)(109 ºC), allowing the flow between the two components to take place. If the two components were completely immiscible, this would not happen and they would stay completely separate from each other. This therefore suggests some level of interaction and therefore, also taking into account previous findings from this work, suggests that these two components are at least partially miscible.

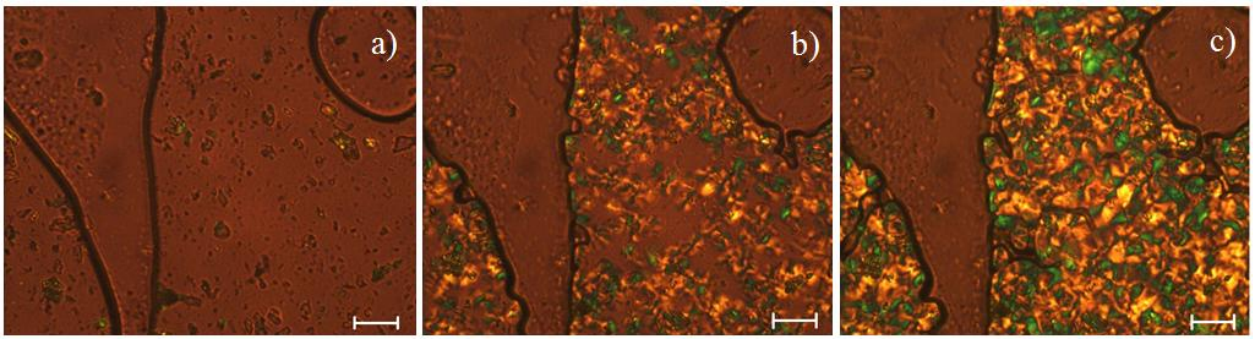

Figure 4.32. Cooling of P(HB-co-HV)/CAB (5 wt %) from the melt. a) melt state at 180 °C b) intermediate state at 115 °C and c) fully crystallised at 25 °C. Scale bars represent 25 µm.

This abstract leaching in CAB (5wt %) can be seen more clearly in Figure 4.33. If the two components were completely immiscible, the CAB would remain as a completely discrete and spherical droplet within the P(HB-co-HV) matrix. Instead, as the P(HB-co-HV) component crystallises, the CAB is able to incorporate itself into the P(HB-co-HV) and around crystal boundaries between spherulites.

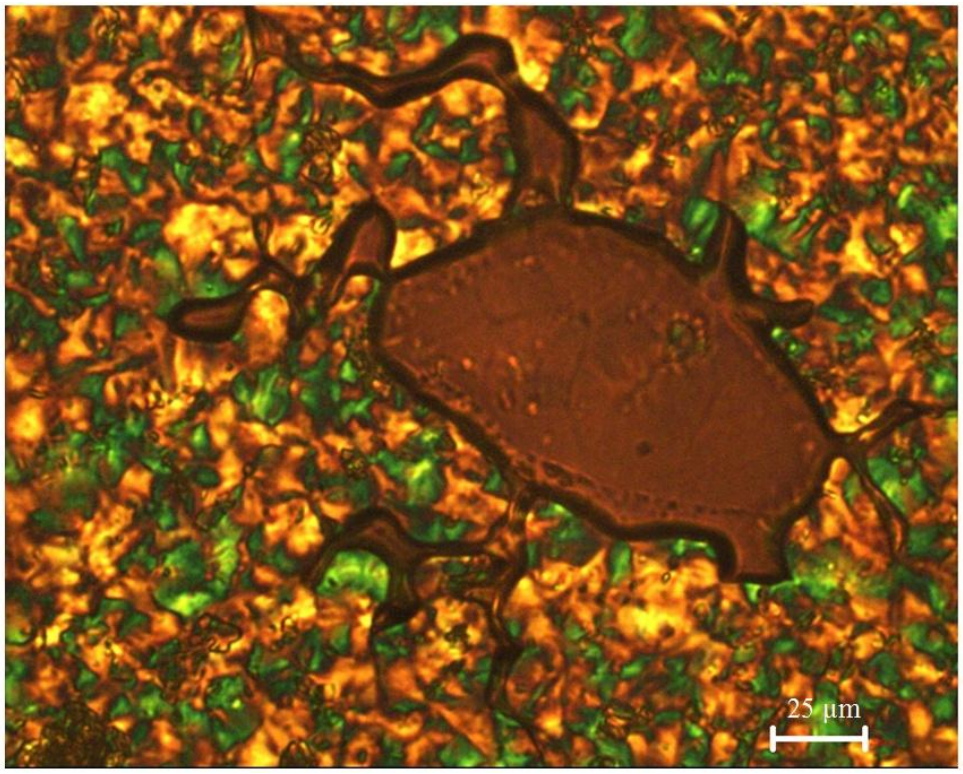

Figure 4.33. A CAB droplet leaching into the P(HB-co-HV)

These effects can be seen more clearly in CAB 10 wt % and 15 wt % compositions where the CAB appears to be located at the inter-spherulitic boundaries (Figure 4.34).This could indicate that CAB is being rejected by the P(HB-co-HV), and therefore getting trapped at the crystal growth front where it may act as a boundary to the crystallisation process. It is also very apparent that the presence of CAB has an effect on the spherulite size. What was an extremely fine spherulitic texture in the unblended P(HB-co-HV)(Figure 4.31) is now a coarser texture, where individual spherulites are more visible. This is in agreement with previous findings where CAB was observed to reduce the crystallisation rate of the blends, which results in larger spehrulites within the material. This also suggests that some of the CAB has been incorporated into the inter-lamellar regions of the spherulites and interaction is present, as larger spherulites are also observed in regions further away and not just those in direct contact with the CAB. These results agree with the isothermal and non-isothermal

crystallisation experiments. It seems that the presence of CAB is reducing the nucleation density, possibly by trapping some of the nucleating agent to render it ineffective, and interacting with the P(HB-co-HV) within the spherulites to slow the process down. It may therefore be deduced that the CAB is trapped in the interspehulitic regions but also in the interlamellar regions leading to such effects and observations. If there was no interaction between the two phases, the CAB portions would have no effect on the spherulite size, and this is therefore another argument for partial miscibility. The increase in spherulite size could therefore be the cause of the reduced mechanical properties within the blends through opposing the effects of the BN nucleating agent, thus producing fewer spherulites that aren't as mechanically stable.

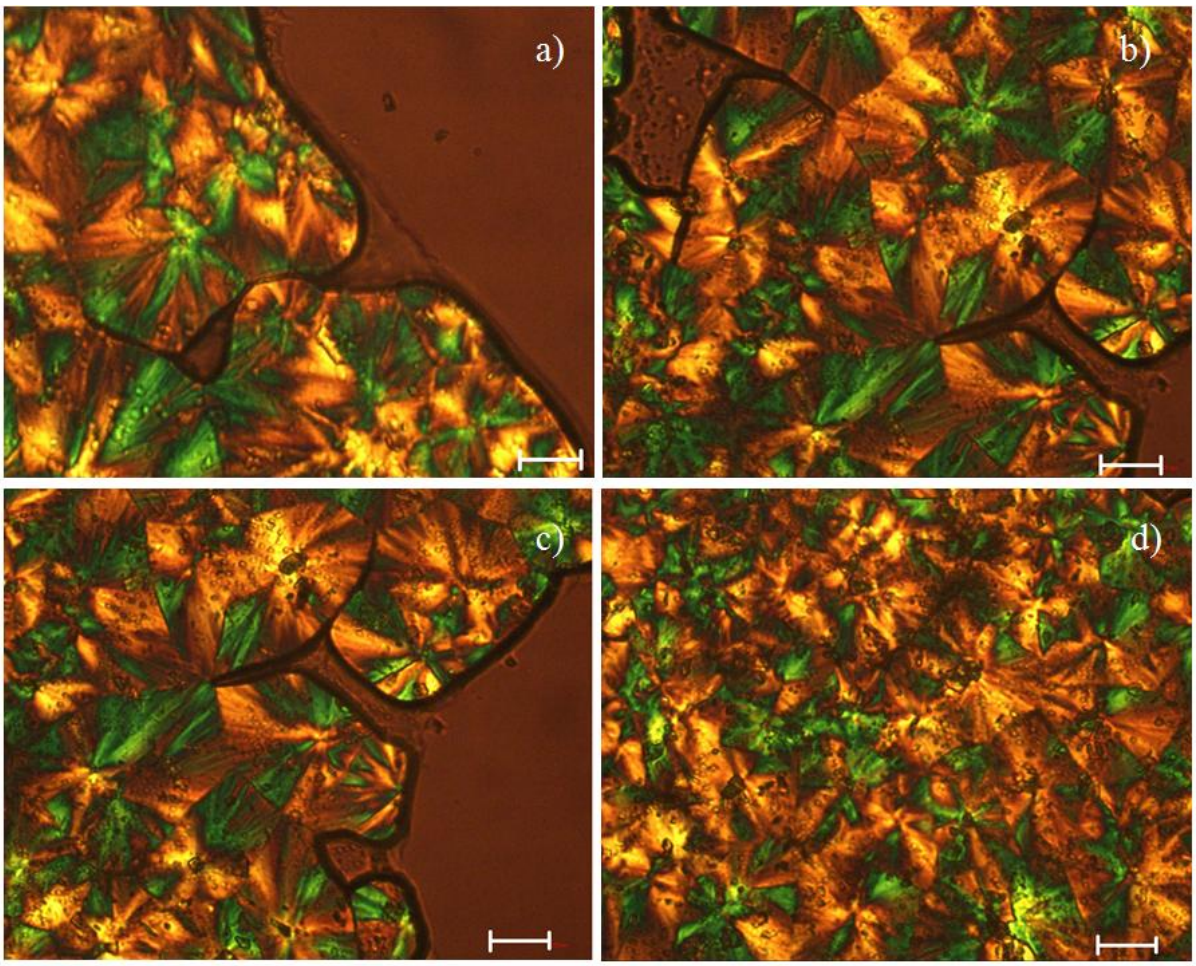

Figure 4.34.Optical microscopy of a) and d) CAB 10 wt % and b) and c) CAB 15 wt %. The scale bars represent 25 µm

4.1.4.2 Scanning Electron Microscopy (SEM)

SEM was used to analyse the fracture surface and assess if there is any evidence of a dual phase morphology. The fracture surfaces of the individual components can be seen in Figures 4.35 and 4.36.

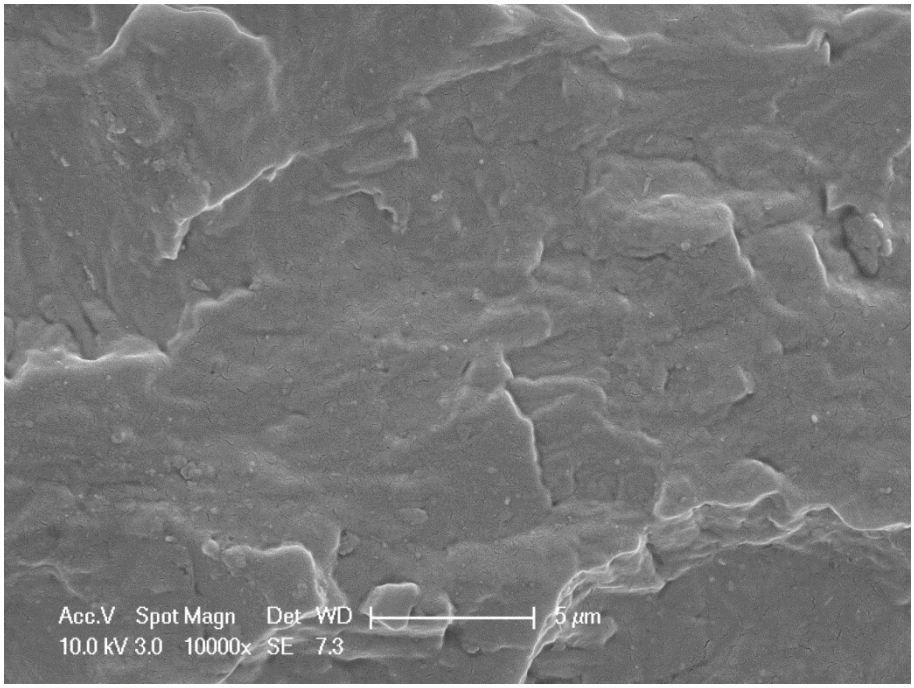

Figure 4.35. The fracture surface of P(HB-co-HV) under SEM at 10,000 x magnification

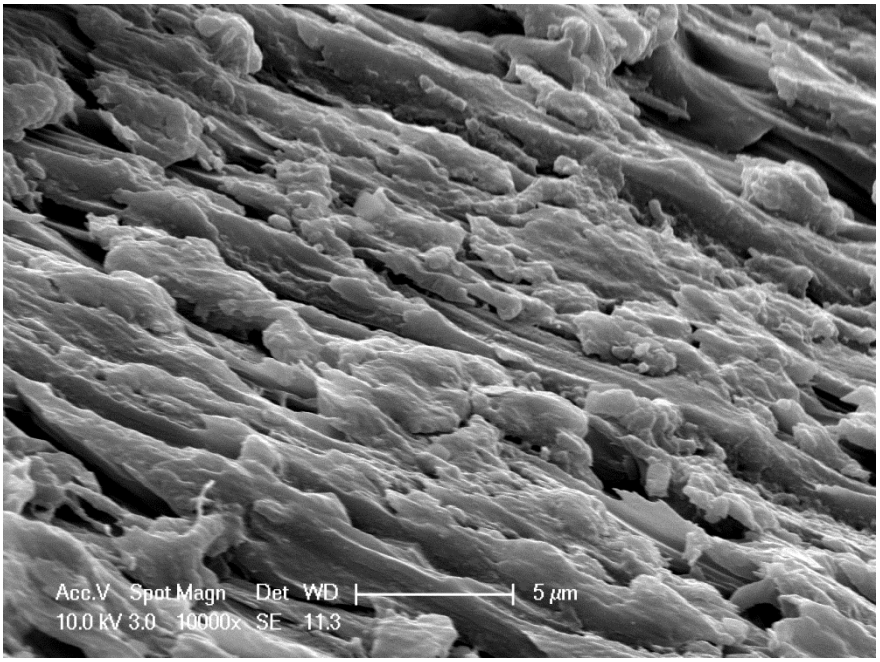

Figure 4.36. The fracture surface of CAB under SEM at 10,000 x magnification

It can be seen that the two components exhibit very different fracture surfaces. The fracture surface of P(HB-co-HV)(Figure 4.35) displays a brittle fracture mode with smooth surfaces. This agrees with the mechanical testing data indicating a brittle fracture mode and a low elongation to break. In contrast, the fracture surface of the unblended CAB demonstrates a ductile fracture surface with a rough morphology (Figure 4.36). This is due to its amorphous nature which gives unblended CAB its high value for E_b as earlier reported.

Upon blending, it is apparent that a brittle fracture surface is displayed, similarly to the mechanical testing results. However, it is now apparent that there are some features observed within the blends that are not present in the unblended material, namely craters which increase in size as the CAB concentration is increased (Figure 4.37). These range from 10 μm (Figure 4.37a) in 5 wt % CAB blends to approximately 100 μm (Figure 4.37c) with the addition of 15 wt % CAB.

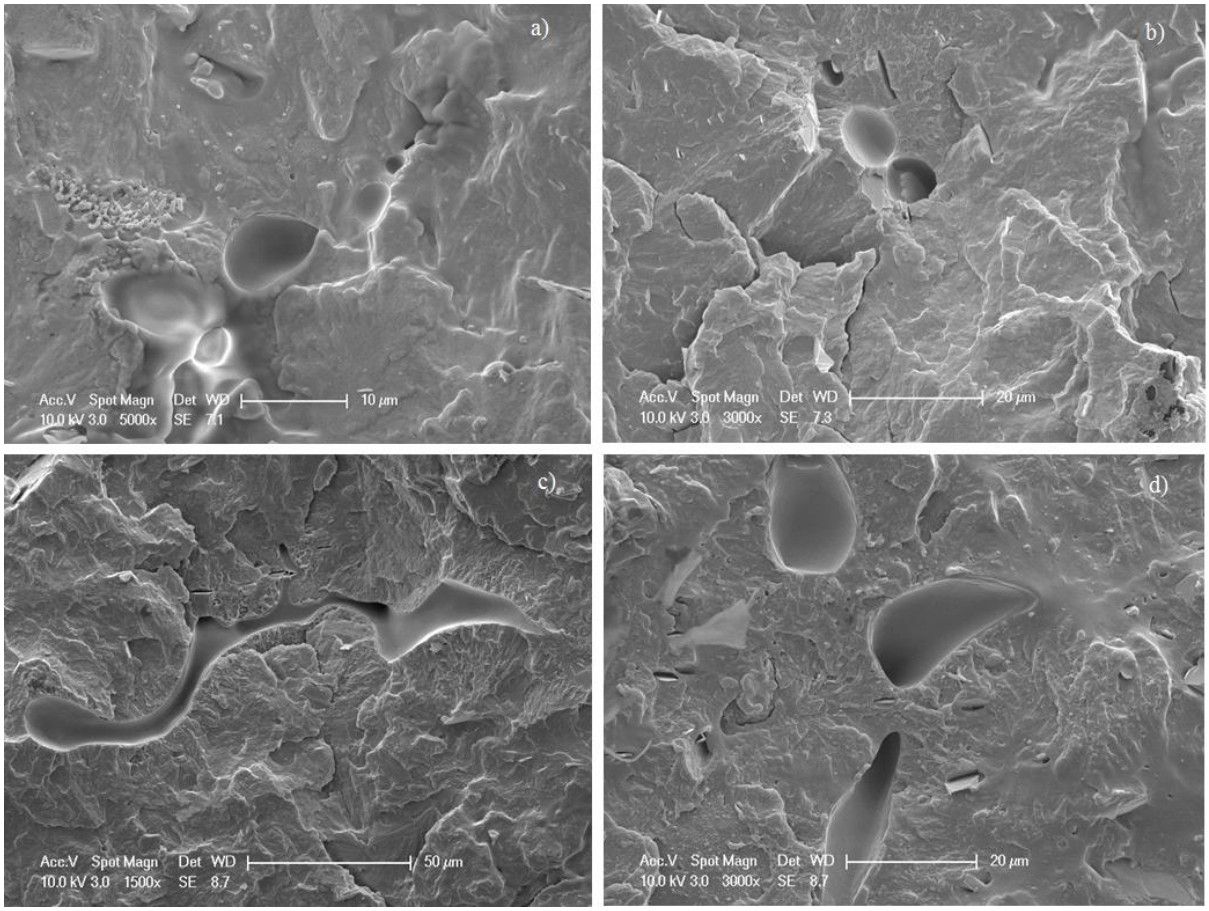

Figure 4.37. SEM images of CAB blends presenting pull out holes a) CAB 5 wt % (x 5,000) b) CAB 10 wt % (x 3,000), c (x 1,500) & d) 15 wt % (x 3,000)

These follow the same irregular shapes that were present in the optical microscopy images and appear smooth on the inside indicating the presence of a material which has since been pulled out. This indicates low interfacial adhesion as previously reported in the presence of starch within PHB/starch blends(Thiré, Ribeiro et al. 2006). It is therefore possible that CAB was coalescing and acting as an inclusion, resulting in the reduced E_b initially observed upon the addition of CAB. However, some interaction must occur for the E_b to increase again as more CAB is added. If no interaction was present at all, the mechanical properties and E_b of the material would be reduced further with increasing CAB content whereas the opposite trend is observed.

4.1.5 Effect of CAB on the materials properties over time

4.1.5.1 Thermal Properties

Monitoring changes to thermal properties is a good way of confirming the secondary crystallisation process. Indicators of the secondary process are an increase in melting temperature as the lamellar thicken during the process, and the formation of second peaks as smaller subsidiary lamellae form between the dominant lamellar stacks. It was proposed that due to the H-bonding capabilities of CAB, its presence would restrict the chain mobility required for secondary crystallisation thus stabilise the properties of P(HB-co-HV). To assess the effectiveness of CAB, the T_m and degree of crystallinity of each blend were analysed over time.

As can be seen from Figures 4.38 and 4.39, the presence of CAB in the blends did not have the desired effect on reducing the secondary crystallisation behaviour as the thermal properties were found to change over time. Figure 4.37 shows that despite reducing the initial T_m as discussed in Section 4.1.1.1, the T_m of all of the blends increased over time. The results of the whole study are summarised in Table 4.12. Interestingly, the greatest change in T_m was observed for the blend containing the most amount of CAB.

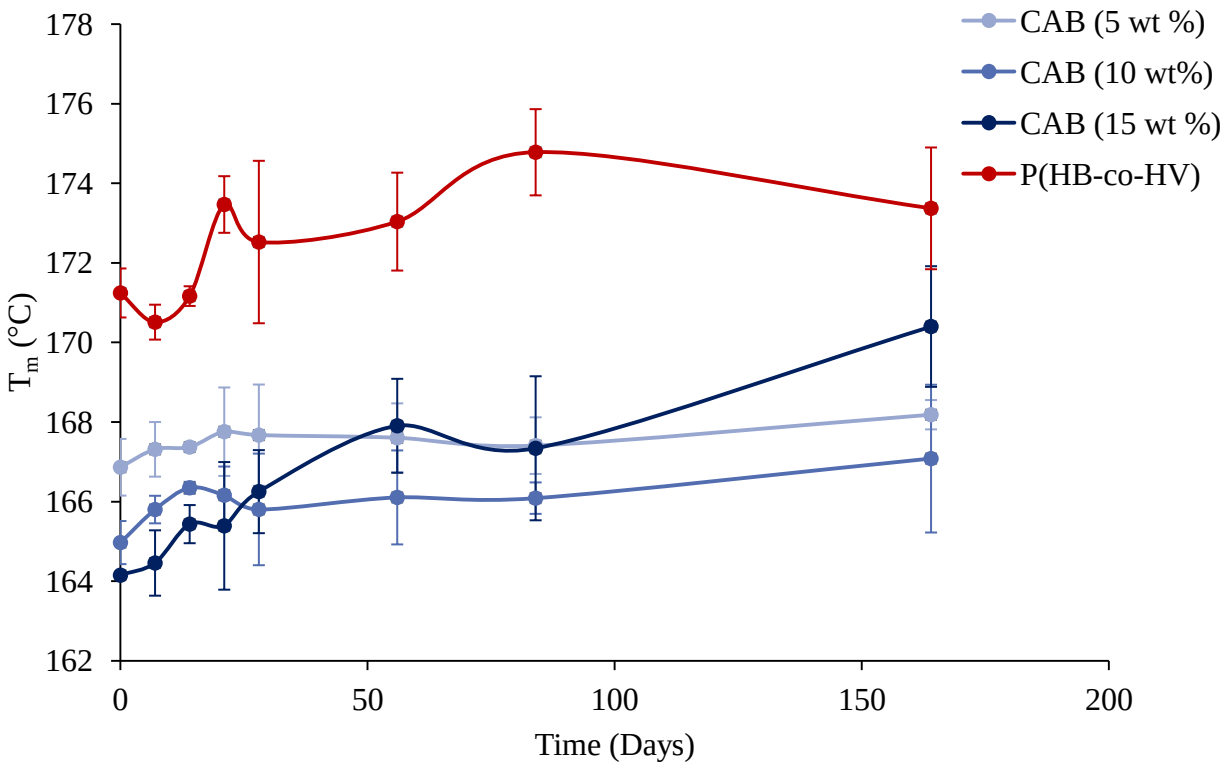

Figure 4.38. The effect of CAB content on the T_m of the blends over time

Table 4.12. A summary of the change in T_m over time for each blend

Sample	Day 0	Day 168	% change
P(HB-co-HV)	171.2	173.4	1.3
CAB (5 wt %)	166.9	168.2	0.8
CAB (10 wt %)	165.0	167.1	1.3
CAB (15 wt %)	164.2	170.4	3.8

The same trends can be observed in the degree of crystallinity study (Figure 4.39). The degree of crystallinity increased with time in each of the samples tested with the greatest change observed in blends containing the highest concentration of CAB.

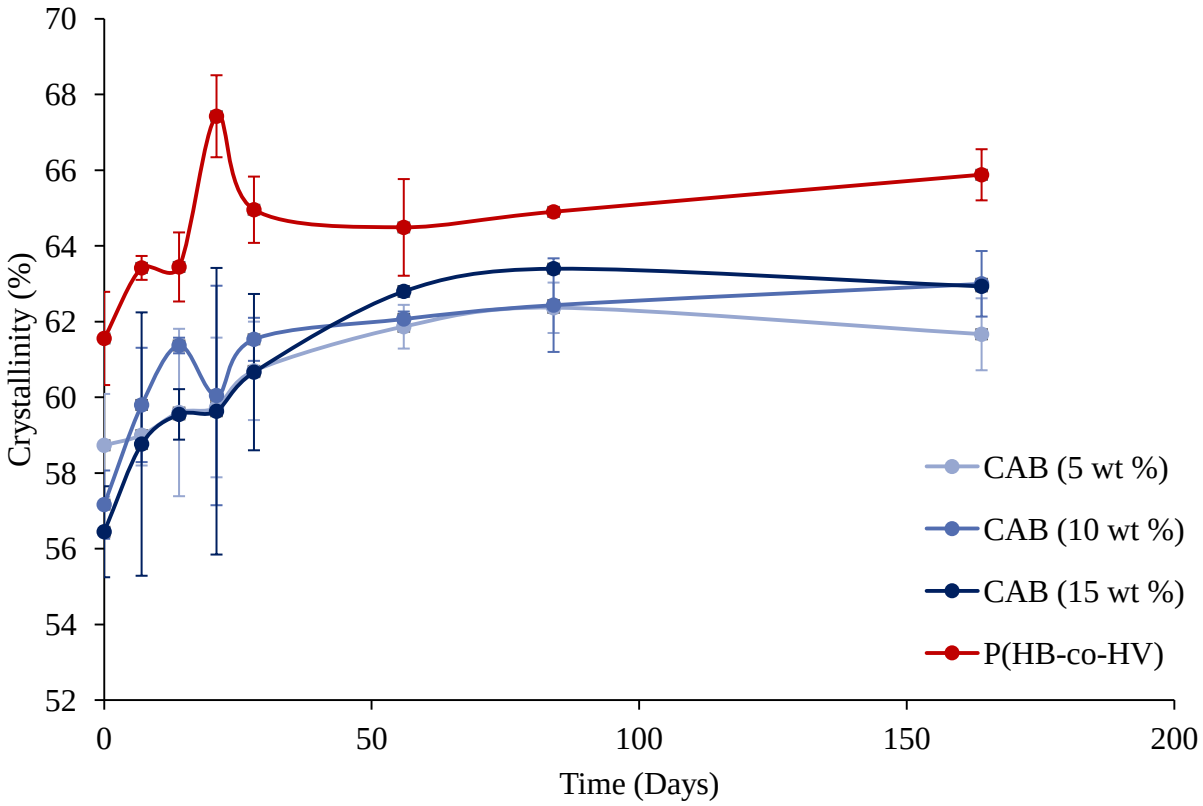

Figure 4.39. The effect of CAB content on the X_c of the blends over time

Table 4.13. A summary of the change in X_c over time for each blend

Sample	Day 0	Day 168	% change
P(HB-co-HV)	61.6	65.9	7.0
CAB (5 wt %)	58.7	61.7	5.1
CAB (10 wt %)	57.2	63.0	10.1
CAB (15 wt %)	56.5	62.9	11.3

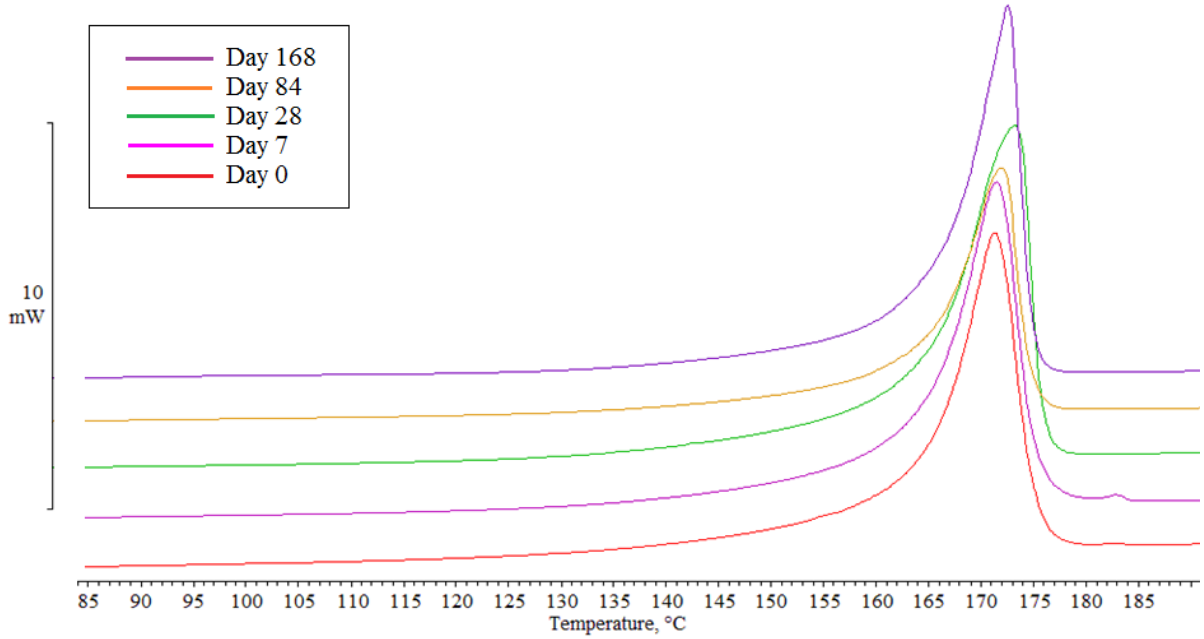

Figure 4.40. Change in the shape of the melting endotherm over time in the P(HB-co-HV) heated at 10 °C/min

Figure 4.40 shows the melting endotherms of pure P(HB-co-HV) over time. There is minimal change in the shape of the curves, just an increasing T_m as the secondary process ensues. The addition of 5 wt % CAB has minimal impact on the shape of the melting endotherms as illustrated in Figure 4.41. As the concentration of CAB is increased to 10 wt %, changes in the melting endotherms are apparent in the form of a high temperature shoulder appearing at days 7, 28 and 84 (Figure 4.42), The greatest changes are observed in the blends containing 15 wt % CAB (Figure 4.43).

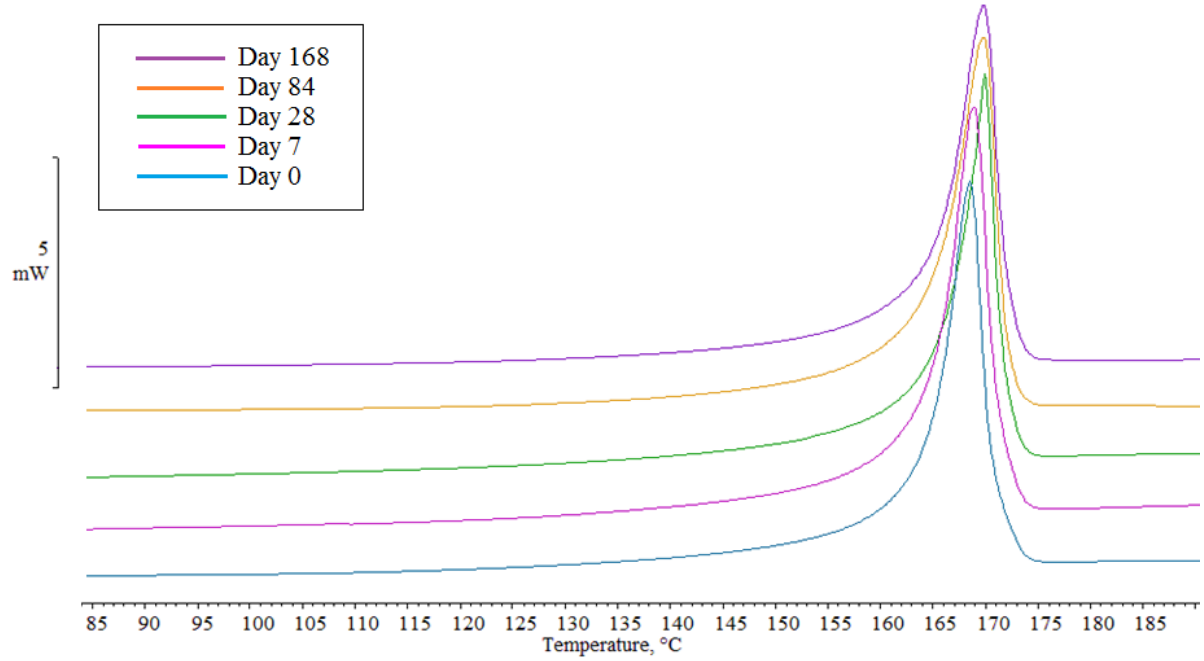

Figure 4.41. Change in the shape of the melting endotherm over time in the P(HB-co-HV)/ CAB 5 wt % blend heated at 10 ºC/ min

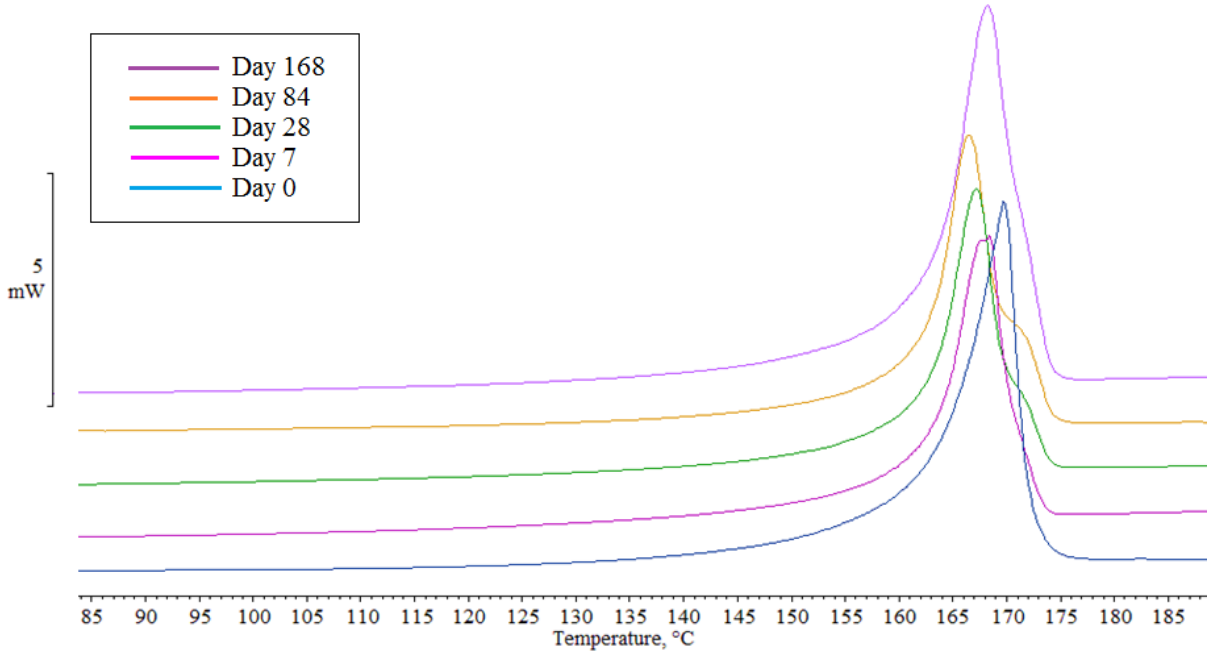

Figure 4.42. Change in the shape of the melting endotherm over time in the P(HB-co-HV)/ CAB 10 wt % blend heated at 10 °C/min

At this higher composition of CAB, a shoulder becomes apparent on the melting endotherms leading to double melting. This is subtly apparent at day 0, and then increases in magnitude as time progresses until it merges with the main endotherm after 28 days. Following this, a broad endotherm is displayed, and a new small endotherm forms at an even higher temperature at day 168.

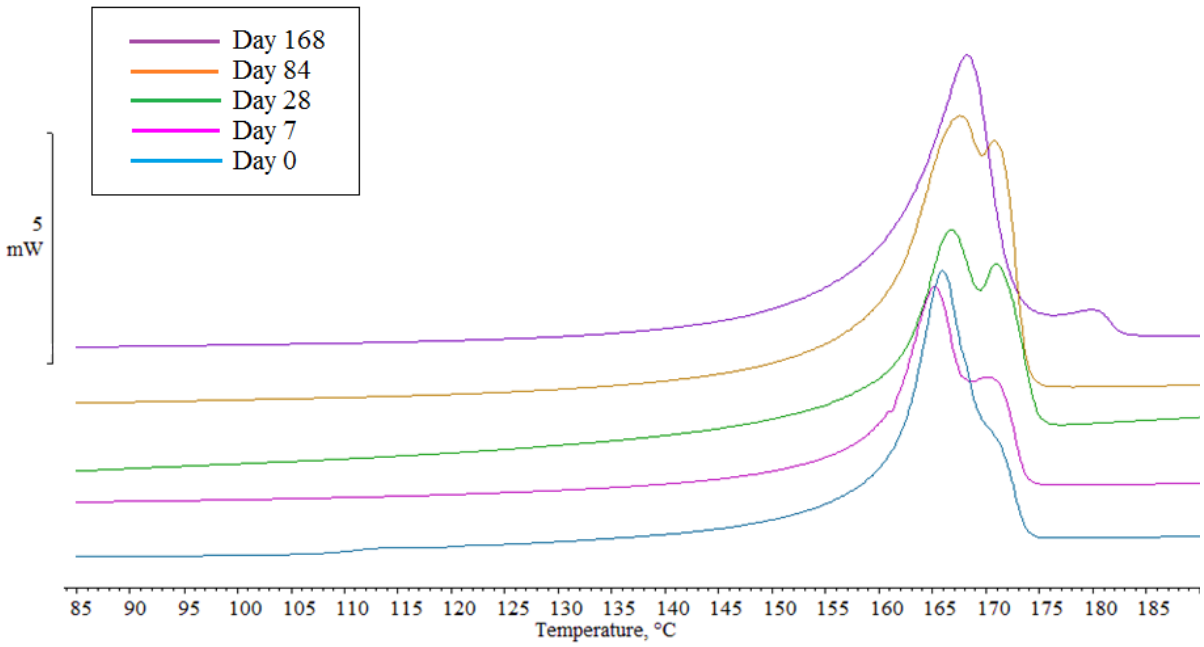

Figure 4.43. Change in the shape of the melting endotherm over time in the P(HB-co-HV)/CAB 15 wt % blend heated at 10 ºC/min

The formation of high temperature peaks could indicate one of two processes. It could be a result of secondary crystallisation, where lamellar thickening could act to increase the T_m of the main peak, while the shoulder increasing in magnitude over time could be a product of increasing crystal perfection of secondary crystals. It could also be due to phase separation, where the T_m of the blend gradually returns to the original T_m value of the unblended P(HB-co-HV) as the time study progresses.

4.1.5.2 Mechanical properties

The effect of secondary crystallisation on the mechanical properties was observed. It can be seen from Figures 4.43 to 4.46 that in conjunction with the thermal properties, the mechanical properties also change over time. Decreases in E_b (Figure 4.43) and toughness (Figure 4.44) while E (Figure 4.45) and UTS (Figure 4.46) increase, are characteristic behaviours of the secondary crystallisation process.

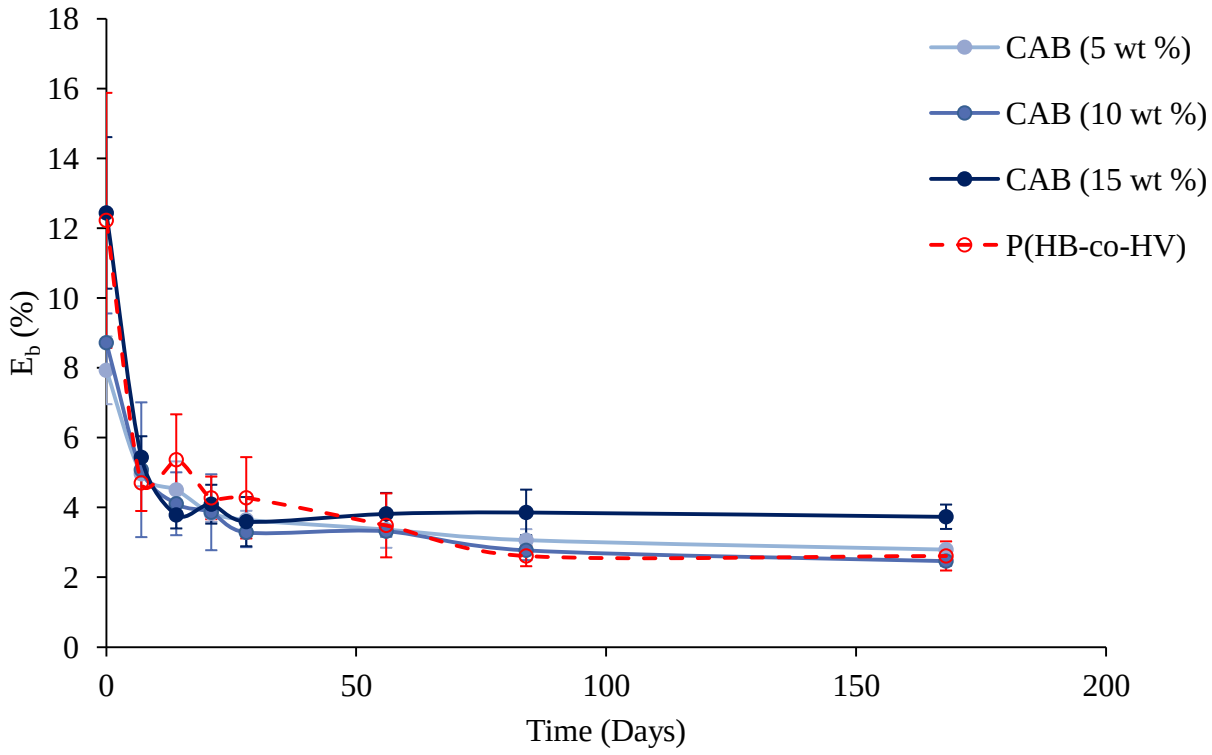

Figure 4.44.The effect of increasing CAB concentration on the E_b of the blends over time

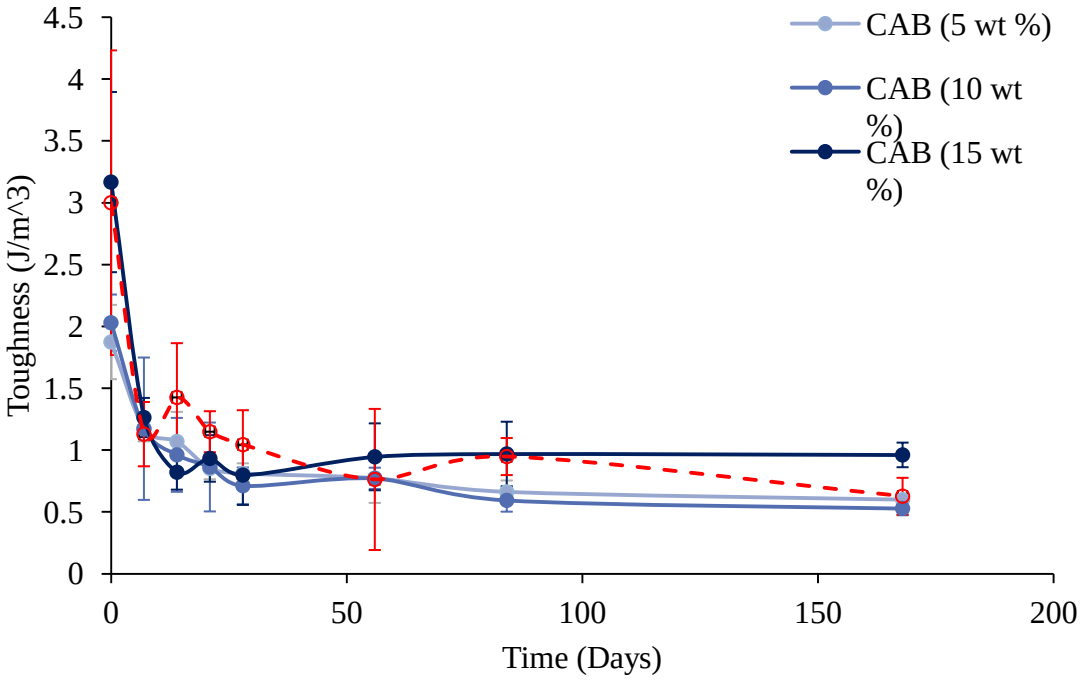

Figure 4.45.The effect of increasing CAB content on the toughness of the blends over time

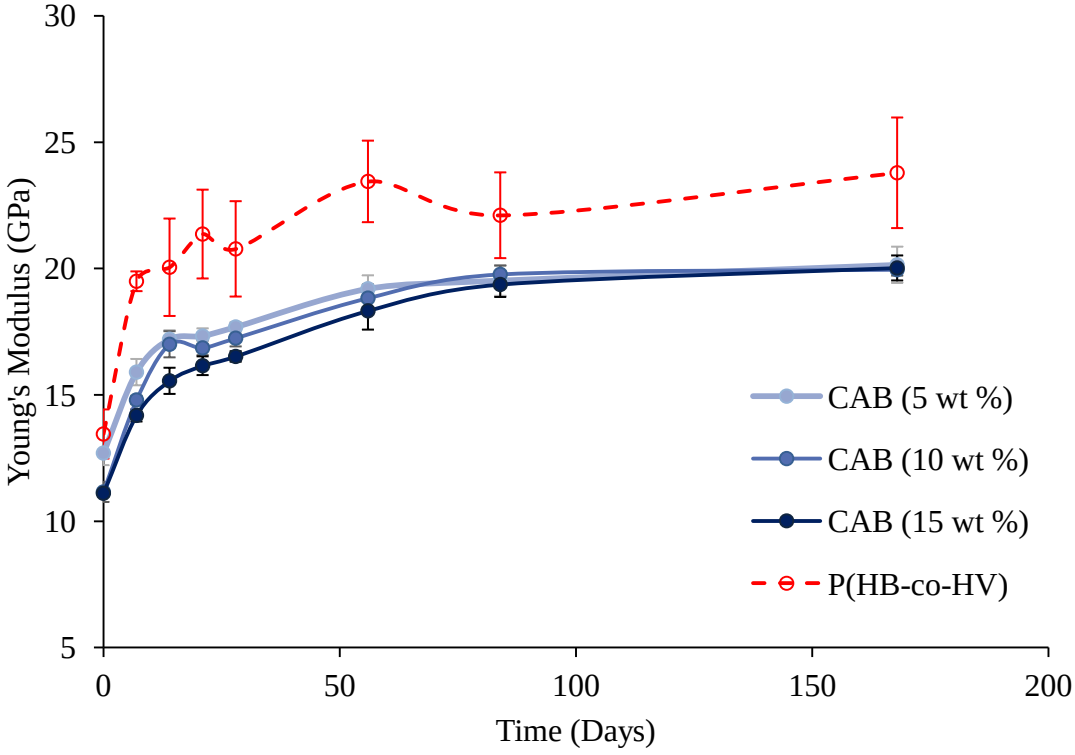

Figure 4.46.The effect of increasing CAB concentration on the E of the blends over time

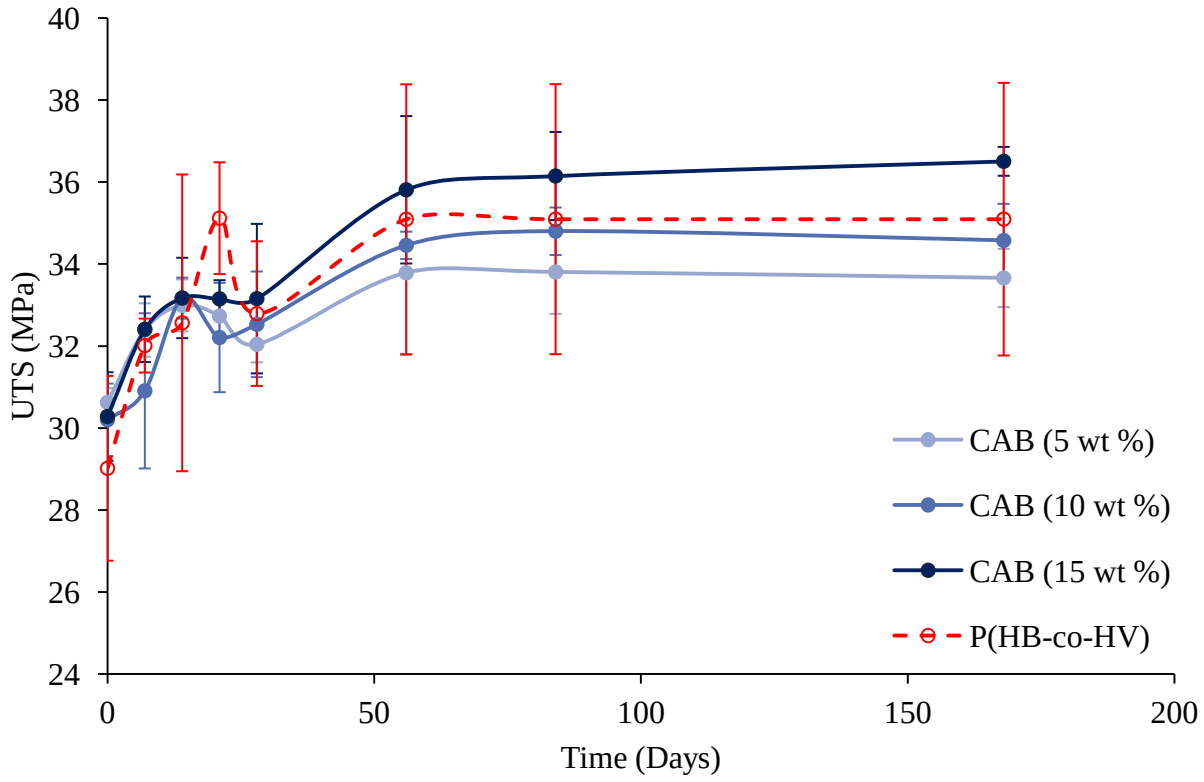

Figure 4.47.The effect of increasing CAB content on the UTS of the blends over time

Table 4.14. A summary of the percentage change in values following 168 days of storage at 25 ºC

	E_b (%)	Toughness (%)	E (%)	UTS (%)
P(HB-co-HV)	78.7	79.1	76.9	20.9
5 wt %	64.8	68.0	58.7	9.9
10 wt %	71.8	74.0	78.9	14.5
15 wt %	70.0	69.7	80.3	20.6

The overall percentage change of each property following 168 days of storage at room temperature is summarised above in Table 4.14. Although the overall change within the

blends is lower than the change occurring in the un-blended material, it is apparent that as the CAB content is increased from 5 to 15 wt %, there is a greater change occurring for each property over time, indicating that the secondary process occurs to a greater extent in samples containing higher percentages of CAB, approaching the change in the unblended material. Interestingly, this is the opposite effect to that observed in the P(HB-co-HV) saccharide blends, where less change was observed with increasing the concentration of the additive (Chapter 3).

4.2 Conclusions

In this work, P(HB-co-HV) was blended with 5, 10 and 15 wt % CAB. The blends were characterised and the effect of CAB on the secondary crystallisation behaviour reported. Based upon the evidence presented, it was concluded that this grade of CAB is interacting and having an effect on P(HB-co-HV) within the composition range explored, and was characterised as a partially miscible blend. Decreasing $T_{m,}$ T_c, and crystallinity of the P(HB-co-HV) component indicate a level of interaction between the two components. Furthermore, the leaching of the CAB component into the P(HB-co-HV) component suggests partial miscibility, as if the component were completely immiscible, the two phases would remain completely separate. Other evidence of interaction is the effect of CAB on the crystallisation behaviour of P(HB-co-HV), where it was observed that the process was slowed significantly with the presence of CAB. During isothermal crystallisation, at the same crystallisation temperature (140 ºC), $t_{1/2}$ is increased from 3 seconds in P(HB-co-HV) to 938 seconds in the blends containing 15 wt % CAB indicating that CAB has a significant effect on the crystallisation kinetics of P(HB-co-HV). This was also confirmed by a reduced value for T_c and slowing of the melt crystallisation transition confirmed with the addition of CAB.

The P(HB-co-HV) used in this work is filled with Boron Nitride (1 wt %) as identified by hot stage microscopy creating a very fine spherulitic texture. Upon the addition of CAB, there was a significant increase in spherulite size. This is in agreement with the slowing of the crystallisation process, and suggests that the CAB is affecting the nucleation and growth of crystals in the blends at all compositions. This could be another reason for the decreased mechanical properties observed in CAB blends by counteracting the BN nucleating agent within the samples, and another argument for interaction of the component materials.

However, there also appear to be arguments for the lack of miscibility within the system. Interestingly, the T_g (based upon E´) and Ea appear to reduce with CAB to values below those of P(HB-co-HV). This suggests that the presence of CAB is acting as an impurity that is disrupting the chains like a plasticiser making the transitions easier. This is an argument for lack of miscibility between the two components, as in miscible systems, the T_g of the two components will move towards each other. Thus, the T_g would be expected to increase towards that of CAB rather than decrease. In addition to this, minimal shift in the carbonyl peak is observed following blending, which would be expected in a miscible system. This indicates a lack of H-bonding which is a likely cause of the low percentage of hydroxyl groups present on the grade of CAB used in this work. Analysis of CAB with higher hydroxyl content could have yielded more positive results, and forms the basis for further investigation. Additionally, smooth pull out holes are present in SEM images which also suggests lack of miscibility and interfacial adhesion between the two phases. The shoulder on the samples containing higher percentages of CAB could have also been an indicator of phase separation of the two components..

Common properties used to determine the ductility of materials are E_b and toughness. These are reported to increase with the addition of CAB in previous studies, creating a more ductile material. However, in this work, with the addition of 5 % CAB, the mechanical properties are

initially reduced, but increase to above those of P(HB-co-HV) as the content is increased to 15 wt %. This indicates that there may be a critical limit below which the presence of CAB is detrimental to the mechanical properties of the material, indicating a potential window of miscibility. Similar behaviour is observed upon measuring the toughness of the samples. Furthermore, the Young's modulus and UTS increase with the addition of CAB. Based on findings reported on these blends, it is likely that upon further addition of CAB, further improvements to mechanical properties would be made as observed in other work.

The effect of CAB on the secondary crystallisation process of P(HB-co-HV)/CAB blends was reported for the first time in this work. From the increasing T_m, X_c, Young's modulus and UTS with reducing E_b and toughness over time, it can be concluded that CAB does not act to hinder the secondary crystallisation process within P(HB-co-HV). In fact, as the CAB content was increased there was a greater change within the properties of all thermal and mechanical properties, indicating that the addition of CAB somewhat encourages secondary crystallisation. In addition, a shoulder was observed to evolve on the melt endotherms in the 10 % CAB blends over time and became more significant in 15 % CAB blends. This could be indicative of the secondary process due to the melting out of more perfect crystals produced by secondary crystallisation, or phase separation of the two component materials. The melting of secondary crystals is the most likely explanation as the peak becomes more pronounced over time, eventually shifting to a higher melting temperature in the 15 wt % CAB blend, a behaviour linked to the secondary process.

Despite the addition of CAB being unsuccessful at hindering the secondary crystallisation behaviour, its use as an attempt to hinder the process through its ability to form H-bonds was used for the first time in this work. Controlling the secondary process in PHB based materials in of commercial importance for the future of sustainable polymeric products and therefore further work into other suitable materials to prevent this phenomenon should be considered.

4.3 References

Balaji, S., et al. (2013). "A review on production of poly β hydroxybutyrates from cyanobacteria for the production of bio plastics." Algal Research **2**(3): 278-285.

Buchanan, C. M., et al. (1992). "Cellulose acetate butyrate and poly(hydroxybutyrate-co-valerate) copolymer blends." Macromolecules **25**(26): 7373-7381.

Callister, W. D. and D. G. Rethwisch (2008). Fundamentals of Materials Science and Engineering. An Intergrated Approach. Asia, John Wiley and Sons.

El-Shafee, E., et al. (2001). "Miscibility, crystallization and phase structure of poly(3-hydroxybutyrate)/cellulose acetate butyrate blends." European Polymer Journal **37**(10): 2091-2104.

Gunaratne, L. M. W. K., et al. (2004). "Thermal history effects on crystallisation and melting of poly(3-hydroxybutyrate)." Thermochimica Acta **423**(1–2): 127-135.

He, Y., et al. (2004). "Hydrogen bonds in polymer blends." Progress in Polymer Science **29**(10): 1021-1051.

Kroh, L. W. (1994). "Caramelisation in food and beverages." Food Chemistry **51**(4): 373-379.

Ni'mah, H. and E. M. Woo (2013). "Configurational effects on the crystalline morphology and amorphous phase behavior in poly(3-hydroxybutyrate) blends with tactic poly(methyl methacrylate)." Journal of Applied Polymer Science **129**(6): 3113-3125.

Park, J. W., et al. (2005). "Uniaxial Drawing of Poly[(R)-3-hydroxybutyrate]/Cellulose Acetate Butyrate Blends and Their Orientation Behavior." Macromolecular Bioscience **5**(9): 840-852.

Park, J. W., et al. (2005). "Uniaxial drawing of poly[(R)-3-hydroxybutyrate]/cellulose acetate butyrate blends and their orientation behavior." Macromol Biosci **5**(9): 840-852.

Pizzoli, M., et al. (1994). "Crystallization Kinetics and Morphology of Poly(3-hydroxybutyrate)/Cellulose Ester Blends." Macromolecules **27**(17): 4755-4761.

Ramsay, B. A., et al. (1993). "Biodegradability and mechanical properties of poly-(beta-hydroxybutyrate-co-beta-hydroxyvalerate)-starch blends." Appl Environ Microbiol **59**(4): 1242-1246.

Sugisawa, H. (1966). "The Thermal Degradation of Sugars. II. The Volatile Decomposition Products of Glucose Caramel." Journal of Food Science **31**(3): 381-385.

Suttiwijitpukdee, N., et al. (2012). "Effects of Hydrogen Bond Intermolecular Interactions on the Crystal Spherulite of Poly(3-hydroxybutyrate) and Cellulose Acetate Butyrate Blends: Studied by FT-IR and FT-NIR Imaging Spectroscopy." Macromolecules **45**(6): 2738-2748.

Suttiwijitpukdee, N., et al. (2011). "Effects of Intermolecular Hydrogen Bondings on Isothermal Crystallization Behavior of Polymer Blends of Cellulose Acetate Butyrate and Poly(3-hydroxybutyrate)." Macromolecules **44**(9): 3467-3477.

Suttiwijitpukdee, N., et al. (2011). "Intermolecular interactions and crystallization behaviors of biodegradable polymer blends between poly (3-hydroxybutyrate) and cellulose acetate butyrate studied by DSC, FT-IR, and WAXD." Polymer **52**(2): 461-471.

Thiré, R. M. S. M., et al. (2006). "Effect of starch addition on compression-molded poly(3-hydroxybutyrate)/starch blends." Journal of Applied Polymer Science **100**(6): 4338-4347.

Tian, J., et al. (2005). "Kinetic Studies of Polyhydroxybutyrate Granule Formation in Wautersia eutropha H16 by Transmission Electron Microscopy." Journal of Bacteriology **187**(11): 3814-3824.

Wang, T., et al. (2003). "Crystallization behavior, mechanical properties, and environmental biodegradability of poly(β-hydroxybutyrate)/cellulose acetate butyrate blends." Journal of Applied Polymer Science **89**(8): 2116-2122.

Woo, K. S., et al. (2015). "Characteristics of the Thermal Degradation of Glucose and Maltose Solutions." Preventive Nutrition and Food Science **20**(2): 102-109.

Yamaguchi, M. and K. Arakawa (2006). "Effect of thermal degradation on rheological properties for poly(3-hydroxybutyrate)." European Polymer Journal **42**(7): 1479-1486.

Zhang, M. and N. L. Thomas (2010). "Preparation and properties of polyhydroxybutyrate blended with different types of starch." Journal of Applied Polymer Science **116**(2): 688-694.

Chapter 5
Influence of temperature on the secondary crystallisation behaviour of P(HB-co-HHx)

5.0 Introduction

Poly(3-hydroxybutyrate-co-3-hydroxyhexanoate) (referred to as P(HB-co-HHx) within this work) is a long chain length PHA commonly produced by *R. eutropha* bacteria (Dennis, McCoy et al. 1998). Due to its chemical structure, it is a more ductile material than its P(3HB) and P(3HB-co-3HV) counterparts. Its longer HHx pendant chain shown in Figure 5.1b creates steric hindrance and prevents close packing of chains required for crystallisation. As a result of this, the material possesses a lower degree of crystallinity resulting in a more ductile material. Furthermore, its reduced crystallinity also results in a more transparent material, and therefore it is an attractive substitute for film materials in food packaging.

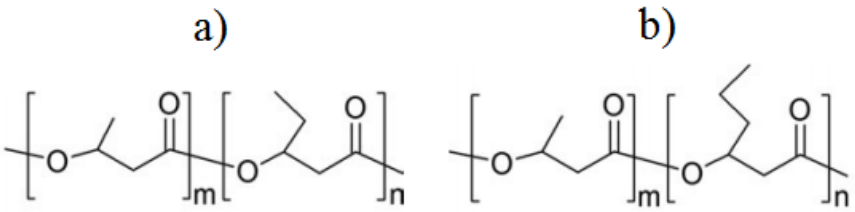

Figure 5.1. The chemical structures of a) P(HB-co-HV) and b) P(HB-co-HHx)

However, thermal instability is one of the key disadvantages of PHB based materials due to their narrow processing window, with degradation known to occur during processing at temperatures around the T_m (Grassie, Murray et al. 1984, Nguyen, Yu et al. 2002, Luo and Netravali 2003, Gonzalez, Irusta et al. 2005, Abe 2006, Ariffin, Nishida et al. 2008). A number of studies have reported the thermal degradation of PHB to occur exclusively by a non-radical random chain scission reaction (Grassie, Murray et al. 1984, Aoyagi, Yamashita

et al. 2002, Abe 2006). In this process, degradation proceeds with the formation of a 6 membered ring ester intermediate and C-C ester bond cleavage at hydroxybutyrate or hydroxyvalerate linkages with the elimination of β-hydrogen. This scission leads to reductions in molecular weight (M_w) of the material (Grassie, Murray et al. 1984, Nguyen, Yu et al. 2002, Bugnicourt, Cinelli et al. 2014). The reaction mechanism can be seen in Figure 5.2 below (Abe 2006).

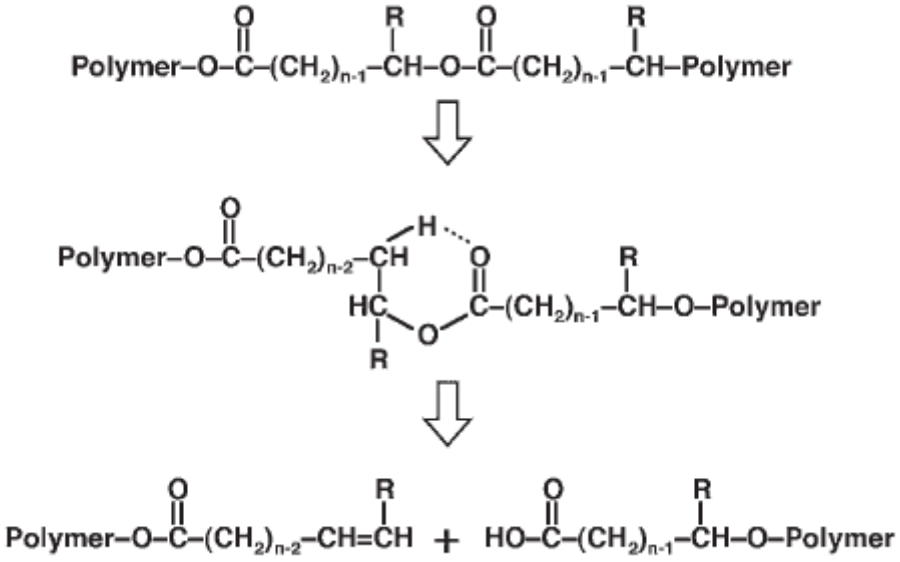

Figure 5.2. Cis-elimination reaction of polyesters as shown in Abe (2006)

The main component of PHB degradation products is trans-crotonic acid (Gonzalez, Irusta et al. 2005, Abe 2006, Ariffin, Nishida et al. 2008), with Arrifin et al. observing quantities of 67.7 % using gas chromatography. A further 3.1 % of the pyrolyzates was attributed to cis-crotonic acid with other oligomers of crotonic acid such as dimers and trimers possessing crotonyl end groups also present (29.9 %) (Ariffin, Nishida et al. 2008). These products have

been reported in a number of studies in the temperature range of 170 – 400 ºC (Kopinke, Remmler and Mackenzie, 1995; Grassie and Murray, 1983).

Thermal degradation is accompanied by a significant reduction in $M_{w,}$ which affects the thermal and mechanical properties of the material. In a study by Luo and Netravali (2003) from the first heating scan in DSC, T_m decreased from 145.2 to 142.2 ºC with a reduction in M_w from 287,000 to 37,000 g/mol. This occurs because reducing molecular weight reduced the lamellar thickness, leading to the crystals melting out at lower temperatures. Moreover, T_c was found to increase from 110.6 ºC to 114.6 ºC with the same decrease in M_w. This was attributed to faster rates of crystallisation at lower M_ws, as shorter chains can crystallise more readily. Furthermore, the melting enthalpy increases with lower M_w as a result of the increased crystallinity with decreasing M_w (Luo and Netravali 2003).

In contrast, M_w seems to have minimal effect on T_g in P(HB-co-HV). There are two ways that M_w can influence the T_g. Chain ends can acts as defects, and therefore, the presence of a higher proportion of chain ends at lower M_w can create more free volume, reducing the constraints on the chains and resulting in a reduction of T_g. But as previously discussed, P(HB-co-HV)'s with lower M_w have a higher crystallinity, and more crystals increase the constrains on the amorphous chains, raising T_g. It therefore appears that in the case of P(HB-co-HV)s, the effects largely cancel each other out, and thus, there is no distinct variation of T_g with M_w for the thermal treatment used in this paper (Luo, Grubb and Netravalia, 2002).

Regarding mechanical properties, Luo et al (2002) found a very strong dependence of UTS on M_w. The UTS and strain at break were found to decrease while the Young's modulus was found to increase with decreasing M_w. Decreasing M_w from 134,000 g/mol to 37,000 g/mol lead to a decrease of UTS from 28.2 MPa to 11.6 MPa. This data can be interpreted as a rapid loss of strength with reducing M_w as the chain entanglement network becomes less

established with the presence of shorter chains, causing the failure mode to change from ductile to brittle behaviour (Luo, Grubb and Netravalia, 2002).

In addition to thermal degradation, another factor that limits the commercial use of this polymer is that it undergoes secondary crystallisation, leading to ongoing embrittlement of the material. The extent of the secondary process however is affected by the concentration of HHx within the polymer chain, with higher proportions of HHx found to reduce the secondary process by the most (Alata, Aoyama et al. 2007).

There have been numerous studies analysing the thermal stability of PHB and P(HB-co-HV), but they have all focused on temperatures at or above the melting temperature of PHB. To the authors knowledge, there have been no sub T_m stability studies conducted on the properties of P(HB-co-HHx). Furthermore, the material is known to secondary crystallise at ambient temperature, however the effects of this at different storage temperatures have not thus far been analysed. Therefore, P(HB-co-HHx) with a HHx content of 33 wt % was used in this work to establish whether increasing the storage temperature has an effect on the secondary crystallisation process and whether the longer pendent group creates enhanced thermal stability and resistance to the secondary process at elevated temperatures over time. This will assess whether degradation occurs within the material below its T_m, and how it manifests itself through characterisation via DSC, mechanical testing and FTIR.

5.1 Results

5.1.1 Characterisation of P(HB-co-HHx)

5.1.1.1 Thermal Characterisation

Figure 5.3 shows the DSC heating run for P(HB-co-HHx), where a double melting endotherm is observed. This double melting behaviour has been commonly observed previously in PHB

and its copolymers analysed at slow heating rates, and occurs due to the melting, re-crystallisation and re-melting (MRR) model where the chains have enough time to recrystallize on heating (Hu, Zhang et al. 2007, Pan, Shan et al. 2013). Crystallisation produces primary crystals of lower degree of perfection or thinner lamellae, which can melt and re-crystallise during the subsequent heating scan to yield crystals of higher perfection or greater thickness which then melt out again at a higher temperature. The lower temperature endotherm on Figure 5.3 is the melting of unstable crystals formed through recrystallization on heating and the higher temperature peak represents the crystals formed through primary crystallisation.

As a focus of this study was to monitor changes in crystallinity throughout the secondary crystallisation process, it was necessary to obtain a single peak for analysis. This was achieved by introducing a faster heating rate which gave rise to a single melting endotherm (Figure 5.4), and thus it was possible to determine crystallinity. This is because the chains have less time to re-crystallise on heating at a faster rate. The melt crystallisation temperatures (T_c) (Figure 5.5) and behaviours were also monitored as they can be an indicator of thermal degradation occurring within the material. A summary of the properties obtained for P(HB-co-HHx) are provided in Table 5.1.

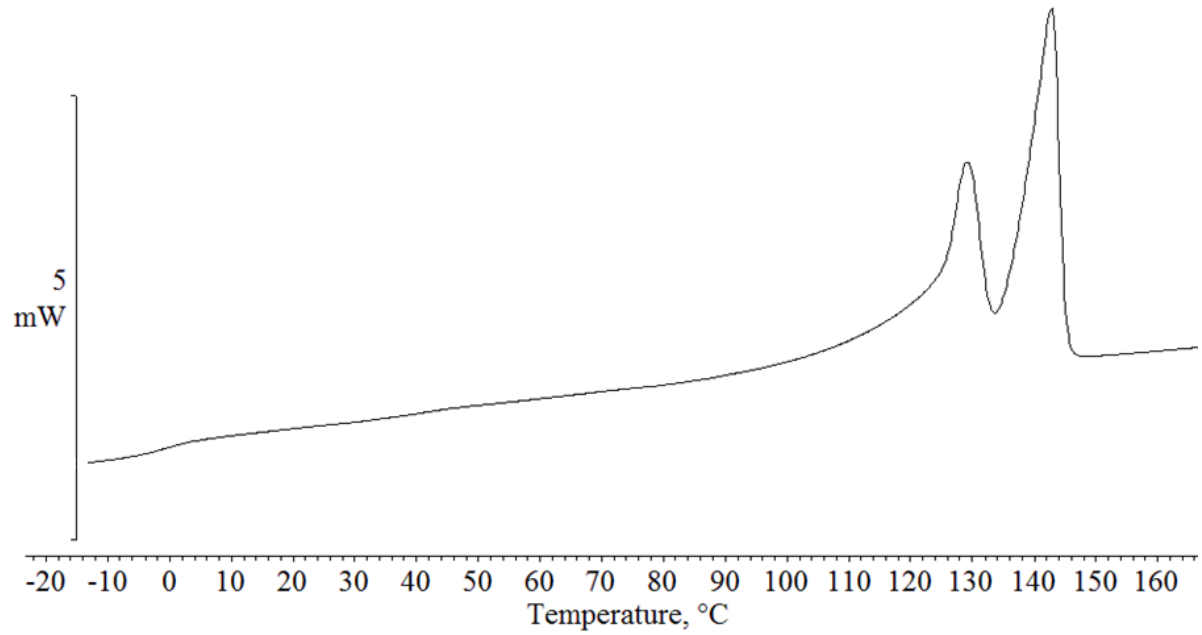

Figure 5.3. The T_m of P(HB-co-HHx) resulting from the above processing conditions obtained by heating at 10 ºC/min

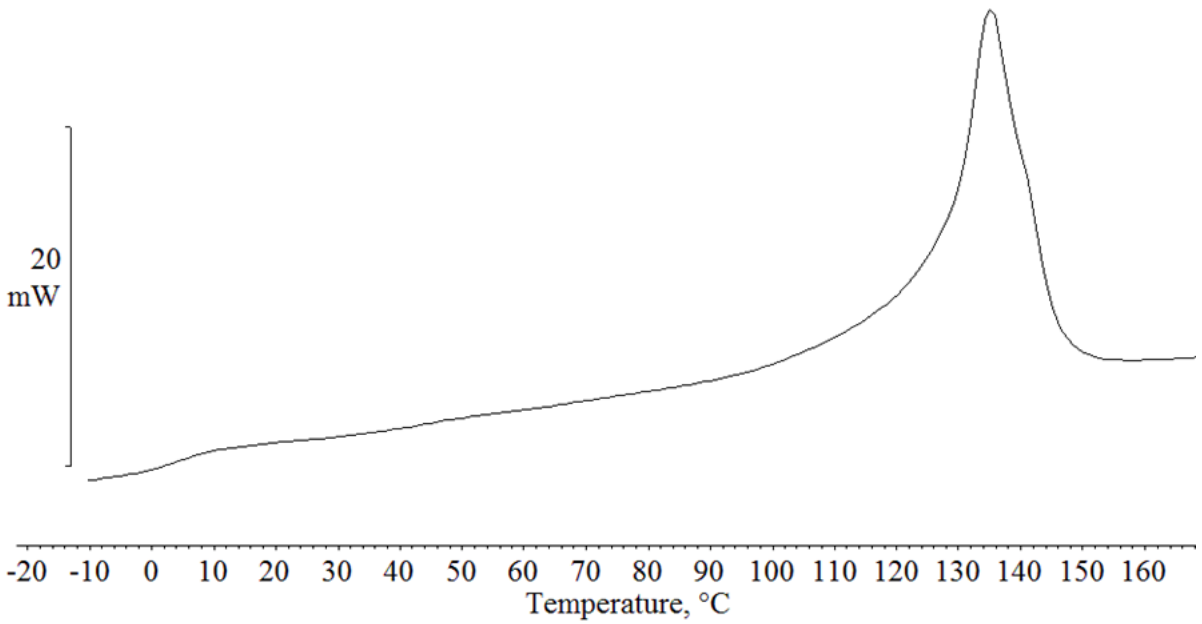

Figure 5.4. The T_m of P(HB-co-HHx) resulting from the above processing conditions obtained by heating at 50 ºC/min

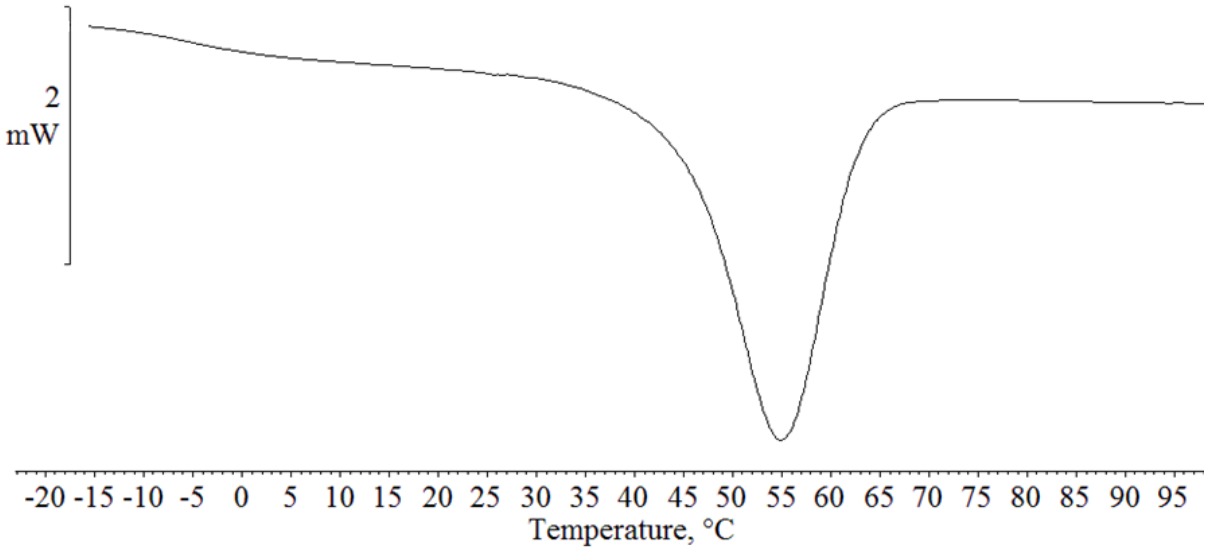

Figure 5.5. The T_c of P(HB-co-HHx) following processing at the above conditions by cooling at 10 ºC/min

Table 5.1. A summary of the thermal properties of the P(HB-co-HHx) material

Property	Value
T_{m1} (ºC)	128
T_{m2} (ºC)	142
T_m (50 ºC/min)(ºC)	134
T_c (ºC)	55
T_g (ºC)	-2
X_c (%)	39

5.1.1.2 Exploring Sample variability

Due to the large variability observed in mechanical properties in Chapters 3 and 4, a study on the variability in the mechanical properties was conducted within a single sample plaque for P(HB-co-HHx) to determine the sample variability and possible reason for error within results. Samples were cut from the plaque as illustrated below in Figure 5.6 and subjected to uniaxial tensile tests.

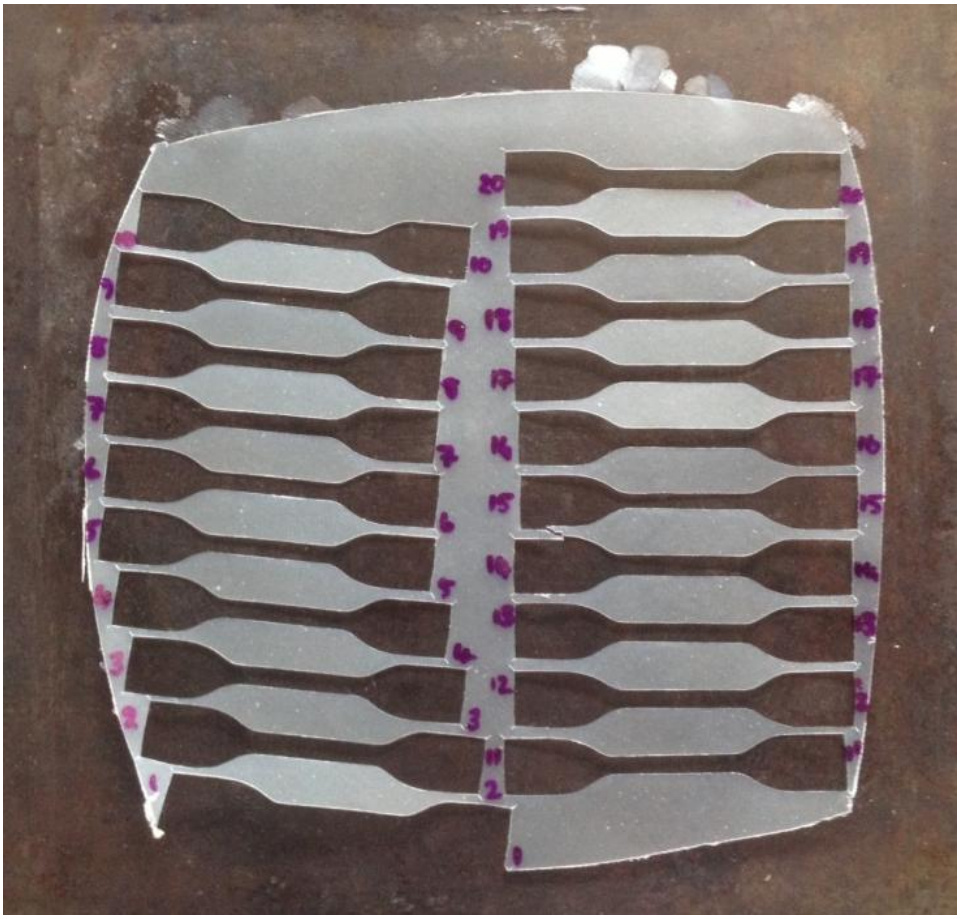

Figure 5.6. Locations of samples within the plaque

Figure 5.7 shows examples of sample variability within this plaque. The most noticeable difference was observed in elongation to break (E_b) of the material which ranges from 14 to 37 %. This could be due to a number of factors. There is an element of user error attaining

sample alignment within the clamps of the tensile apparatus as this is done manually. A test piece loaded at an angle could create stress concentrations and consequently lead to premature failure of the sample, rendering the results inaccurate. Another possibility could be that the hot press used to produce the samples does not heat or cool uniformly, leading to differing levels of crystallinity within the same sample, as well as different sample thicknesses. The degree of crystallinity, which is a product of the crystallisation conditions, is directly linked to the ductility of the material leading to its possible influence over the observed properties. Additionally, the polymer surface texture could also be a possibility (Gabaue 2000). It is therefore apparent that there may be a great deal of variability observed within the following studies, so this should be kept in mind when analysing results containing large error bars and anomalies in mechanical testing analysis.

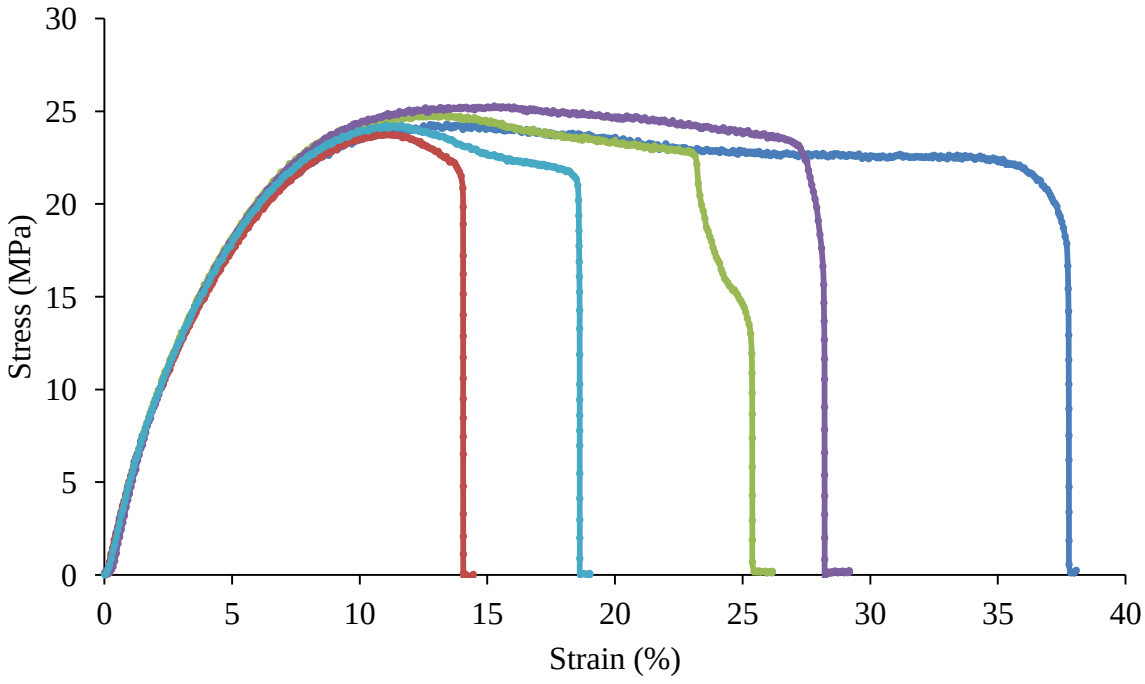

Figure 5.7. Inter-plaque variation within a sample plaque

As well as the differing values for E_b and UTS, the stress-strain behaviour preceding fracture also seems vary across all samples. All samples yield, but some present necking (dark blue curve) while others fracture after yielding (red). The green curve represents a sample that has torn, and continued to slowly tear before fracturing. Samples also displayed crazing before fracture. Crazes are zones of highly plastically deformed and oriented polymer that consist of numerous fibrils along the direction of the applied stress. Values for Young's modulus remain quite constant throughout the plaque locations represented by comparable gradients of the initial portion of the curves (Figure 5.7).

The effect of this for each individual property and its relation to where it came from in the plaque is shown in Figures 5.8-5.11. The possible effect of sample thickness was also considered alongside the variation in properties to see if this could also be a factor. It can be seen from Figures 5.8-5.11 that the thickness increases from the front of the sample plaque to the back, however all properties seem to be independent of sample thickness. This demonstrates uneven pressure applied during the hot pressing, which as previously mentioned is another factor which could have an effect on the mechanical properties of the material due to the potential of variable cooling rates throughout the samples.

From analysis of Figure 5.8, it can be seen that the samples increase in elongation to break (E_b) at the corners of the plaques, and is higher still in the corners on the right hand side of the plaque in samples 11-12 and 17-20 (Figure 5.8). This seems to be independent of the sample thickness. Very similar behaviours are also observed for toughness, as this property is highly dependent on the elongation to break of the material (Figure 5.10).

The effect of sample location on UTS is illustrated in Figure 5.10, where it is observed that the regions producing the highest values are the front left corner and the rear right corner of the plaque. The regions possessing the highest UTS align with the regions with the highest

E_b. This is because tensile stress and E_b depend on similar properties of the material. Both require the ability of polymers chains to be able to slip past one another under tension.

The Young's modulus distribution throughout the sample is shown in Figure 5.11. It can be seen that the Young's modulus is independent of thickness, and increases from left to right and front to back, creating samples with higher values for modulus in the far right hand corner. From this set of studies, it is apparent that there is large sample variation within the same sample plaques produced at exactly the same conditions, which could be a product of the uneven pressure distribution of the hot press. The corners of the samples appear to produce better mechanical properties than the middle of the plaques, with values for all properties increasing from front left to back right. As the properties seem independent of sample thickness, it is likely that variation in samples could be brought about by differential cooling in the hot press, giving rise to differing rates of crystallisation within the sample. The plates were cooled from the rear of the press which could have led to this effect. This distribution inevitably gives rise to a broad range of properties within the samples which could to large error bars within the work and so should be taken into account upon analysis.

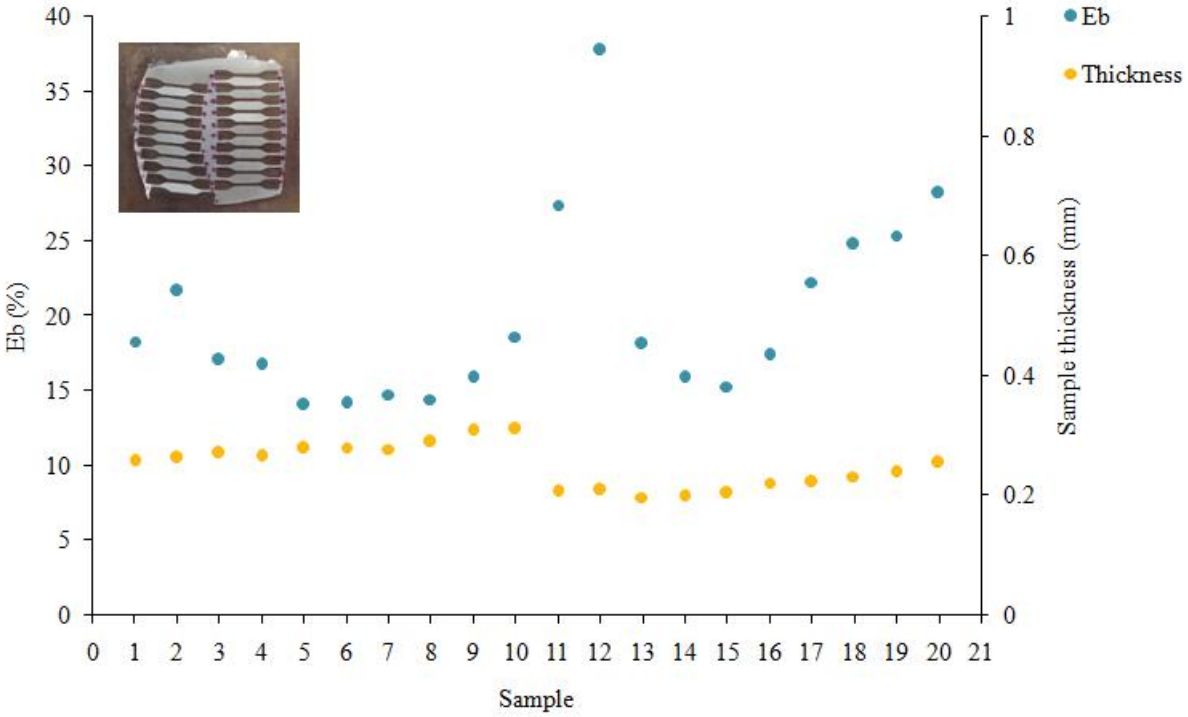

Figure 5.8. Variability in elongation to break within the same sample plaque

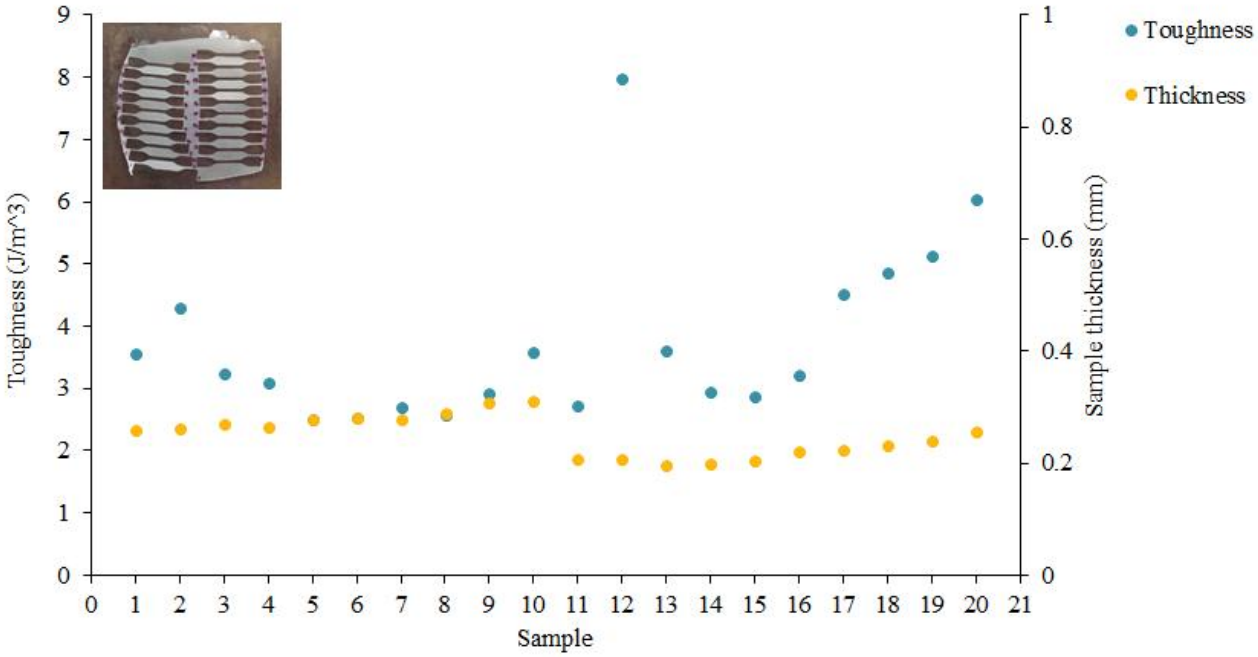

Figure 5.9. Variability in toughness within the same sample plaque

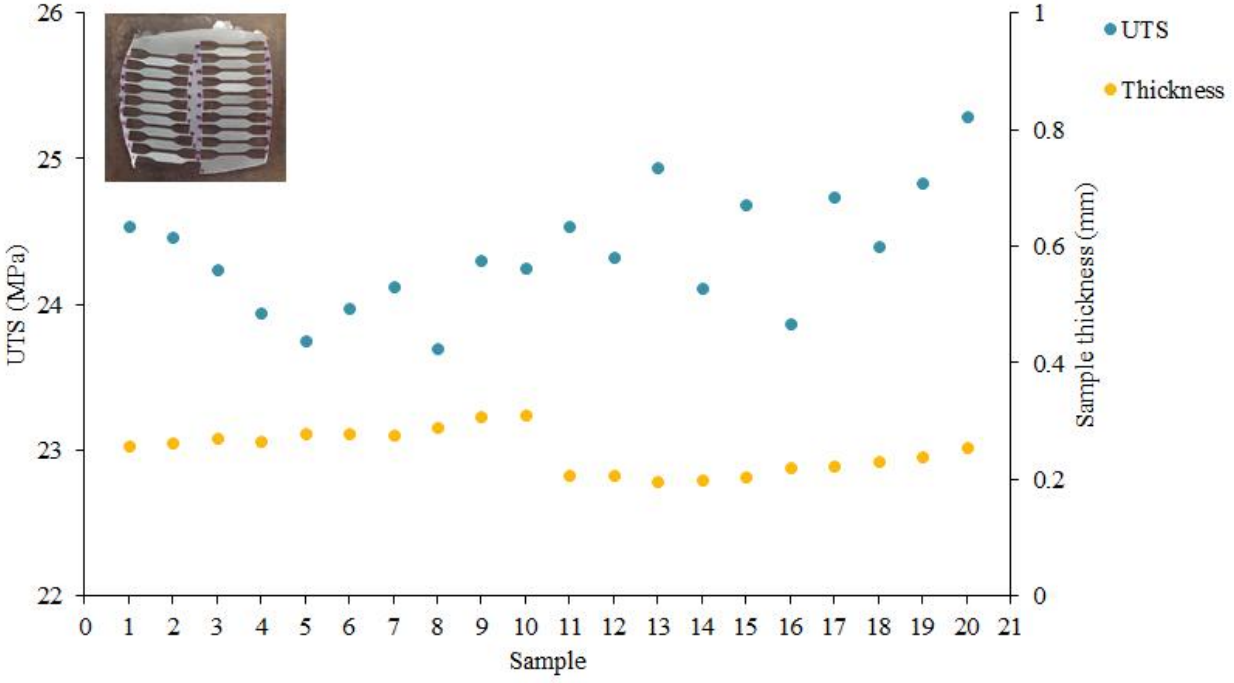

Figure 5.10. Variability in UTS from within the same sample plaque

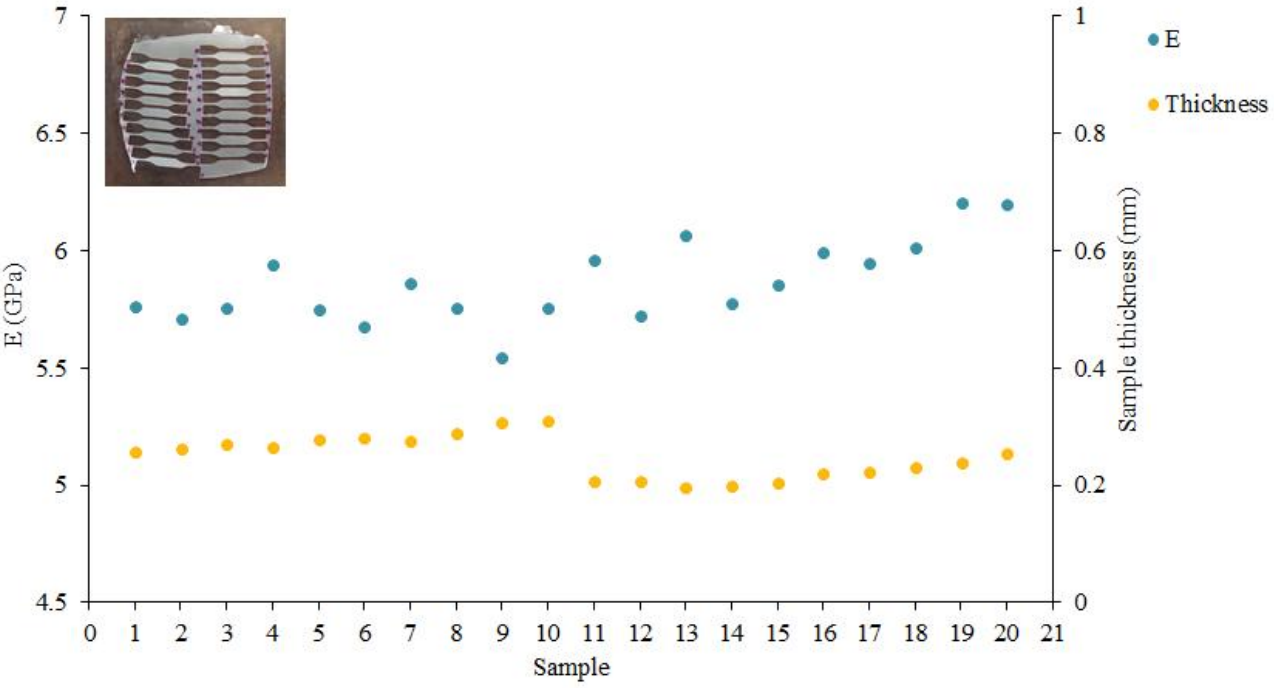

Figure 5.11. Variability of Young's Modulus within the same sample plaque

5.1.2 Effect of storage temperature on P(HB-co-HHx) over time

5.1.2.1 Thermal Properties

5.1.2.1.1 Melting

The effect of storage of P(HB-co-HHx) at different temperatures on the thermal properties was established by DSC. The samples were stored below the T_g at -22 ºC, just above the T_g at 7 ºC, at room temperature, and then at elevated temperatures of 50, 75 and 100 ºC. The properties were analysed immediately following production of the sample plaques, termed 'Day 0' and then at set intervals over 28 days as outlined in Chapter 2. Upon removal from each storage condition, the samples were rested at ambient temperature (25 ºC) for 10 minutes to allow them to reach room temperature, as temperature is known to influence mechanical properties (Callister and Rethwisch 2008).

Upon heating at 10 ºC/min, P(HB-co-HHx) displays double melting behaviour as observed previously in Figure 5.5. The effect of thermal storage on both of the melting endotherms was analysed and can be seen in Figure 5.12. From these results, it can be seen that there is no significant change in the melting points of the material stored at -22 ºC and 7 ºC. However, as the storage temperature is increased from 25 ºC upwards, the melting temperatures begin to increase over time with increasing storage temperature. The greatest change is observed in samples stored at 100 ºC for both endotherms illustrated by the red lines. Due to time constraints and equipment availability in the quick succession of time points it was not possible to conduct repeats in order to obtain average values in this study, but singular values allow general trends to be observed. The dashed lines connecting the points are there for clarity of trends and to draw the reader's eye through the results.

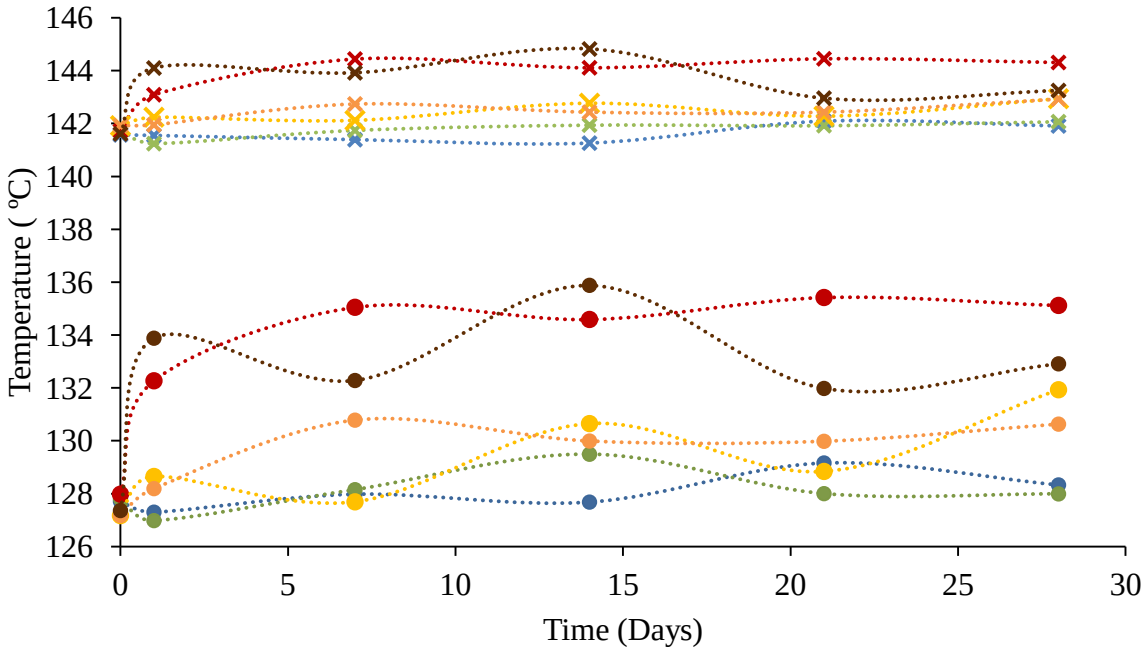

Figure 5.12. Effect of storage temperature on the T_{m1} and T_{m2} over 28 days in samples stored at -22 ºC (blue), 7 ºC (green), 25 ºC (yellow), 50 ºC (orange), 75 ºC (brown) and 100 ºC (red)

These changes in T_m occur as a result of increasing crystallinity as secondary crystallisation progresses. Secondary crystallisation occurs via a lamellar thickening mechanism (Kolb, Wutz et al. 2001, Sics, Ezquerra et al. 2001). Thicker lamellae possess a higher T_m as they are more crystalline and therefore more chain interactions are present in the form of intramolecular hydrogen bonds. It therefore requires more energy to disorder the chains resulting in the increased values for T_m. The greatest change in T_m is observed for samples stored at the higher temperatures (Figure 5.12), as a result of there being more energy in the system, which increases the mobility of the polymer chains, and therefore increased likelihood of the chain interactions required for crystallisation. Secondary crystallisation therefore occurs more quickly in samples stored at higher temperatures leading to increasing values for crystallinity over time as observed in (Figure 5.12).

In response to the occurrence of a greater amount of secondary crystallisation occurring in samples stored at higher temperatures, a change in degree of crystallinity is expected. The

changes in crystallinity over time at each storage temperature can be seen in Figure 5.13. From this, it is observed that samples stored at -22 ºC and 7 ºC show minimal change to crystallinity over time. However, as the storage temperature is increased to room temperature and above, a significant increase in crystallinity is observed. By 28 days of storage there is minimal effect of temperature on the final crystallinity, but in the higher temperatures the samples increase in crystallinity at faster rates between days 0 and 1. A greater amount of secondary crystallisation can occur in samples held at higher temperatures due to greater chain mobility. This acts to increase chain perfection in already formed crystals (lamellar thickening), leading to increasing T_m of the material, but also encourages the formation of thinner, less perfect crystals that also appear in the melting endotherms upon annealing.

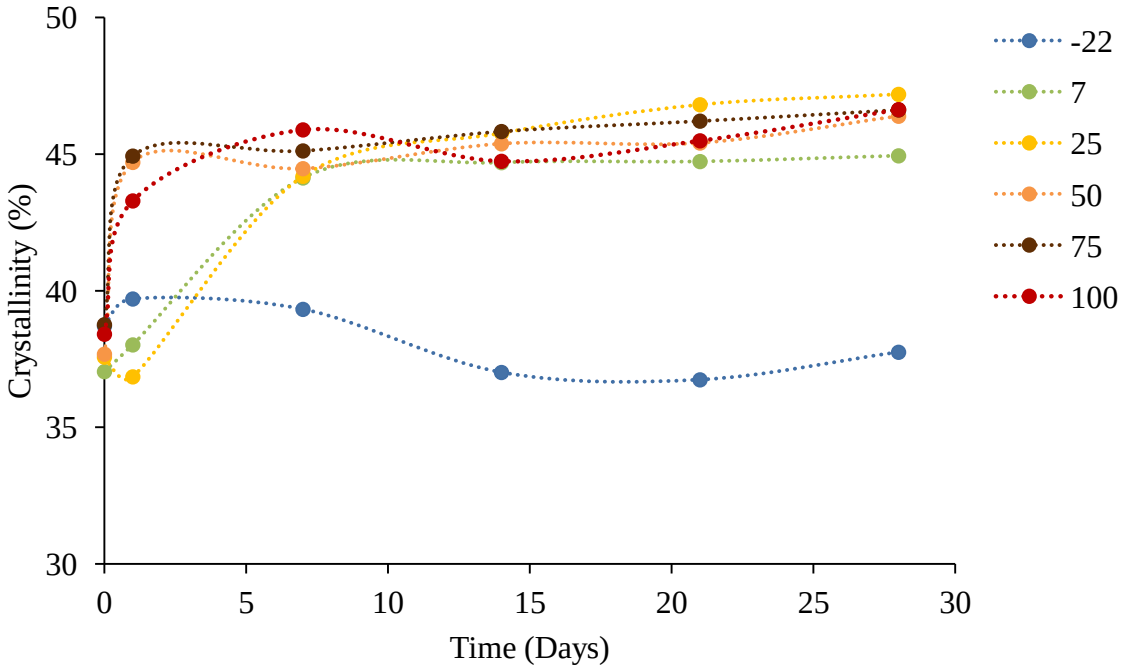

Figure 5.13. Change in crystallinity over time at each storage temperature

This is also true for the T_g of the material, as observed in Table 5.2, where the T_g is seen to increase as a function of storage temperature. The increase in the T_g of the samples stored at 25 ° C are in agreement with previously published results where T_g increased following storage of PP(HB-co-HHx) over 60 days (Alata, Aoyama et al. 2007). An increase in the T_g indicates progressive constraint of the amorphous regions which is a characteristic trait of the secondary crystallisation process as the amorphous regions are consumed.

Table 5.2. Change in T_g over time at each storage temperature

Temperature (ºC)	Day 0	Day 28
-22	-1.72	-2.25
7	-2.07	-1.85
25	-2.03	-1.50
50	-2.09	-0.28
75	-2.02	-1.85
100	-2.26	1.36

Upon further analysis of the melting endotherms, it is apparent that both endotherms are affected by the secondary process and change as secondary crystallisation progresses. The DSC traces for samples stored at -22 ºC and 100 ºC are shown below for comparison (Figures 5.14 and 5.15). Over the 28 day time period, minimal change in the shape of the endotherms can be observed for the samples stored at -22 ºC (Figure 5.14). However, analysis of the melting endotherms for samples stored at elevated temperatures shows significant changes in the shape and intensity of each endotherm as time proceeds. These effects are the most

significant in the samples stored at the highest temperature (100 ºC), and occur within the first day following storage of the material in all cases (Figure 5.15).

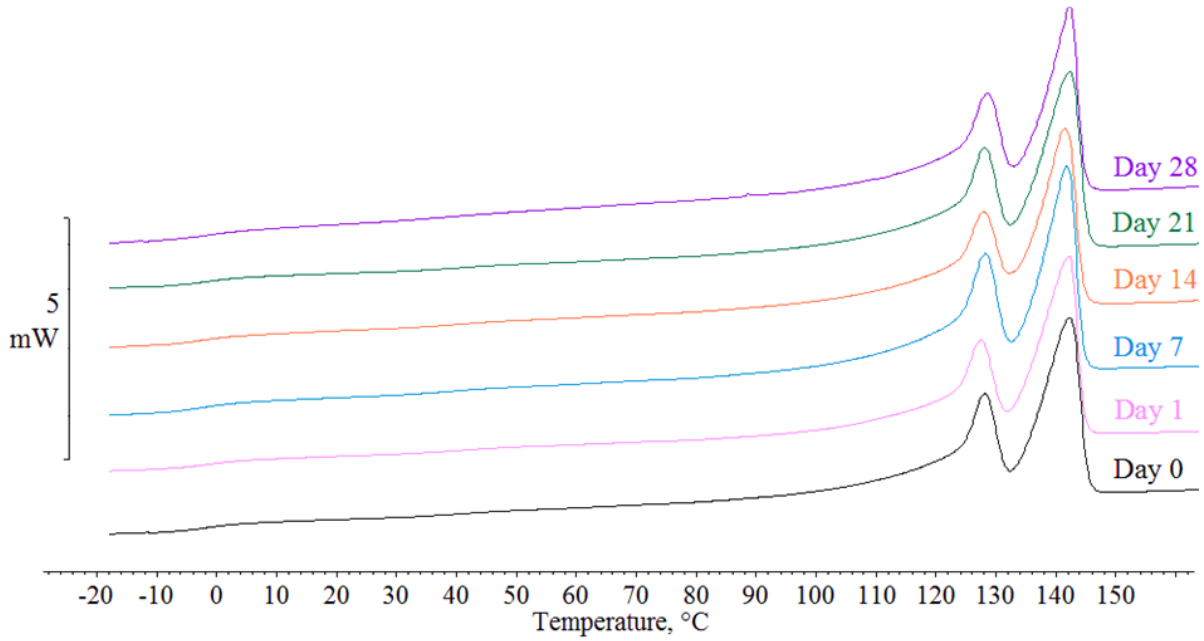

Figure 5.14. Melting temperatures of P(HB-co-HHx) stored at -22 ºC over time

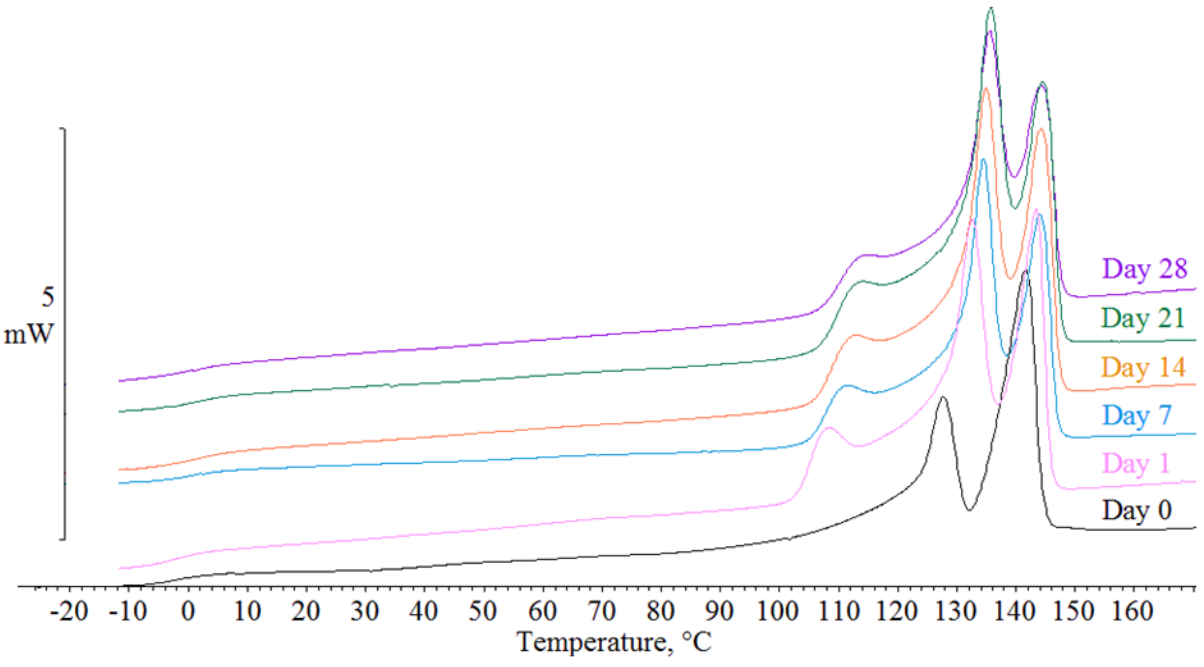

Figure 5.15. Melting temperature of P(HB-co-HHx) over time at 100 ºC

The melting endotherms in Figure 5.15 show the emergence of a low temperature shoulder after just one day of storage at 100 ºC. The emergence of this peak has been previously reported by Hu et al. (2007), who proposed that this was an annealing peak caused by the melting of imperfect crystallites, brought about by sub T_m annealing as a secondary process following primary crystallisation (Hu, Zhang et al. 2007). This theory suggests that t annealing produces an alternative crystallite structure (lamellar insertion) that corresponds to the formation of a lower melting peak, in addition to the lamellar thickening that occurs within the material upon storage over time. This indicates that both of the secondary crystallisation mechanisms (lamellar thickening and lamellar insertion) could be working together at higher temperatures, leading to the increased rates of secondary crystallisation observed at these temperatures.

This shoulder observed in Figure 5.15 remains throughout the 28 days, and shifts to higher temperatures over time. This occurs due to increasing crystal perfection with increasing storage time at that temperature as the secondary crystallisation process proceeds causing the crystals to melt out at an increasingly high temperature. This is proposed due to a partial melting experiment conducted by Hu et al, (2007) where, following isothermal crystallisation at 60 ºC and subsequent partial melting and annealing of the smaller crystals at 90 ºC, the annealing peak (labelled IIa in Figure 5.16) shifts to a higher temperature over time where the imperfect crystals increase in perfection and melt out at a higher temperature. A similar effect was seen in the samples stored at 50 ºC and 75 ºC, but occurs to the greatest extent and in samples stored at 100 ºC.

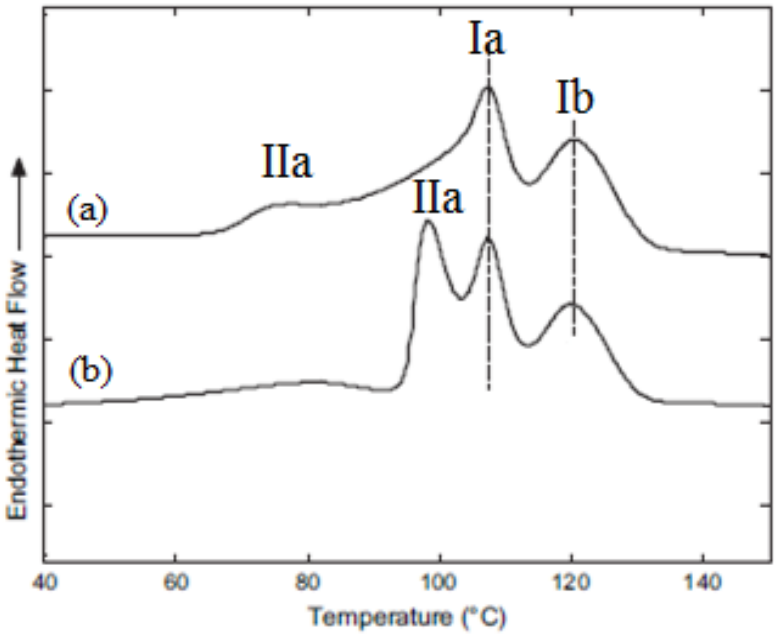

Figure 5.16. DSC experiment examining the effect of partial melting on the annealing peak in P(HB-co-HHx) for samples a) isothermally crystallised at 60 ºC and b) partially melted at 90 ºC for 10 mins following isothermal crystallisation at 60 ºC

Comparisons of the position of this annealing peak within P(HB-co-HHx) were observed (Figure 5.17). From this, it is apparent that with increasing storage temperature, a shift in the position of the shoulder was observed (Figures 5.17 and 5.18). Figure 5.17 shows an example melting endotherm for each storage temperature following 28 days of storage. It can be clearly seen that a shoulder begins to emerge at around 50-60 ºC for samples stored at 25 ºC, suggesting the annealing peak could relate to secondary crystallisation. As the storage temperature was increased to 50 ºC, the position of the shoulder increased to 70-80 ºC. This then increased further to 90-100 ºC for samples stored at 75 ºC, and finally to 110-120 ºC for samples stored at 100 ºC. The approximate linear relationship between storage temperature and position of the shoulder can be observed in Figure 5.18. The appearance of this shoulder has been previously attributed to an annealing peak, which materialises following the secondary crystallisation process upon storage at temperatures above the T_g (Janigová, Lacík et al. 2002, Hu, Zhang et al. 2007). These results agree with the data obtained in this work, as

the shoulder cannot be observed in the samples stored below the T_g at -22 ºC, but becomes apparent in the samples stored at 7 ºC and above. It is the most prominent in the samples stored at 100 ºC due to a greater amount of secondary crystallisation taking place within these samples, thus there are a larger amount of secondary crystals to melt out. The shift occurs as a result of increasing chain mobility at higher storage temperatures which leads to a greater reorganisation of amorphous material at a faster rate. The greatest change is observed within the first day following storage as there is the largest amount of amorphous material present for reorganisation. As time proceeds, the changes occur to a lesser extent as the amorphous regions are consumed and therefore there is less available to reorganise and crystallise.

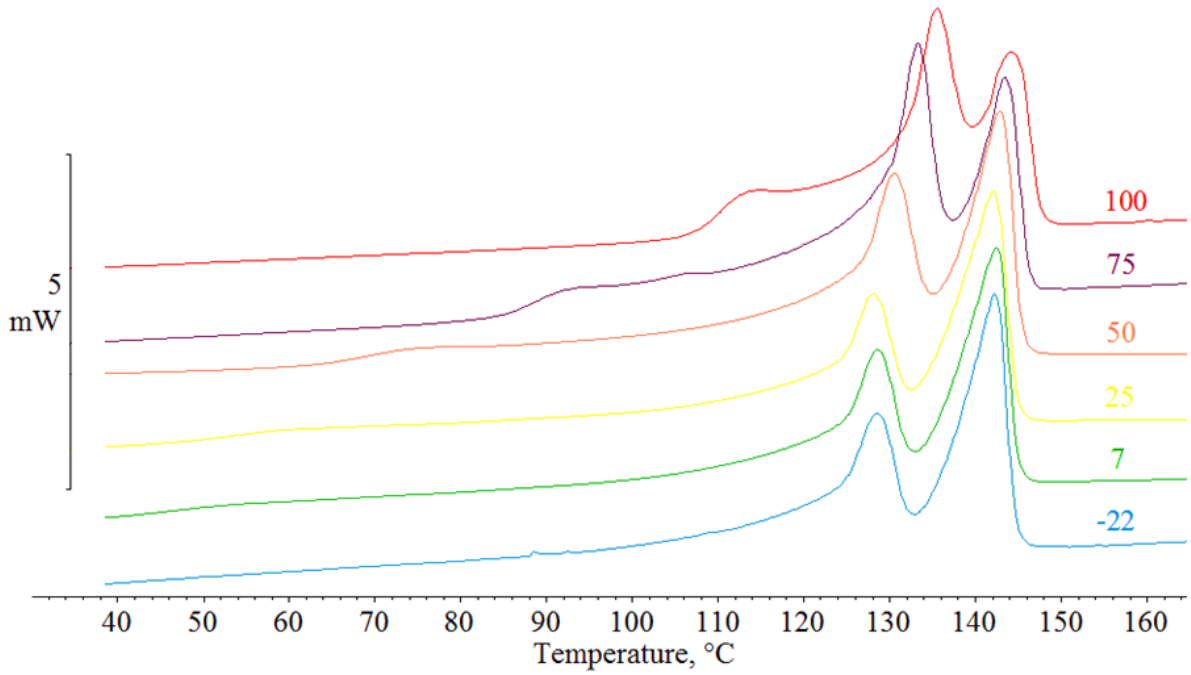

Figure 5.17. Final melting endotherms following 28 days at each storage temperature

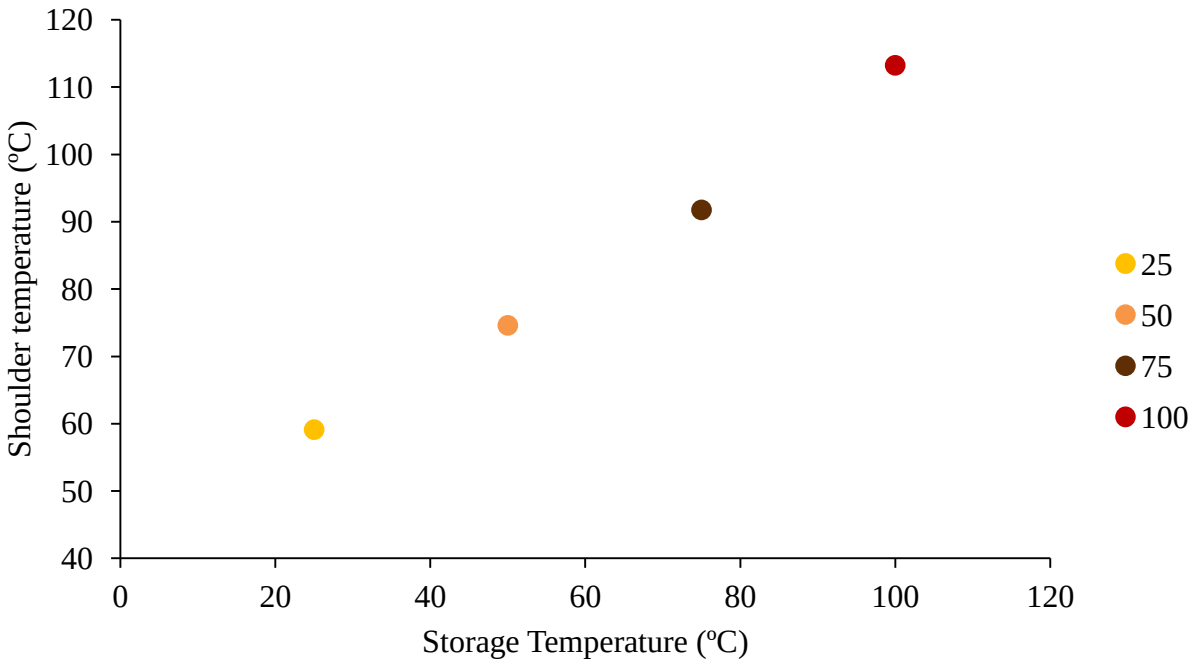

Figure 5.18. Effect of storage temperature on the appearance of a shoulder at 25 ºC and above following 28 days of storage

Another noticeable change occurring upon high temperature storage is the peak height of the two endotherms. In Figure 5.19, following storage at -22 ºC, the shape of the endotherms remain reasonably constant with the lower temperature peak being the smaller peak, and the higher temperature peak being the larger peak. The former is attributed to re-crystallised crystals upon heating, and the latter attributed to the melting of the crystals produced during primary crystallisation. Following storage at 100 ºC, the peak heights reverse whereby the lower temperature peak becomes larger than the higher temperature peak. This effect can be observed within the first day of storage at 100 ºC, and at the 14 day time point of storage at 75 ºC. This produces peaks that are of greater magnitude than the originally dominant primary peak. The shift in magnitude and temperature following storage at high temperatures is indicative of increased crystal perfection brought about by the annealing, and an increased number of imperfect crystallites possibly brought about by chain scissions.

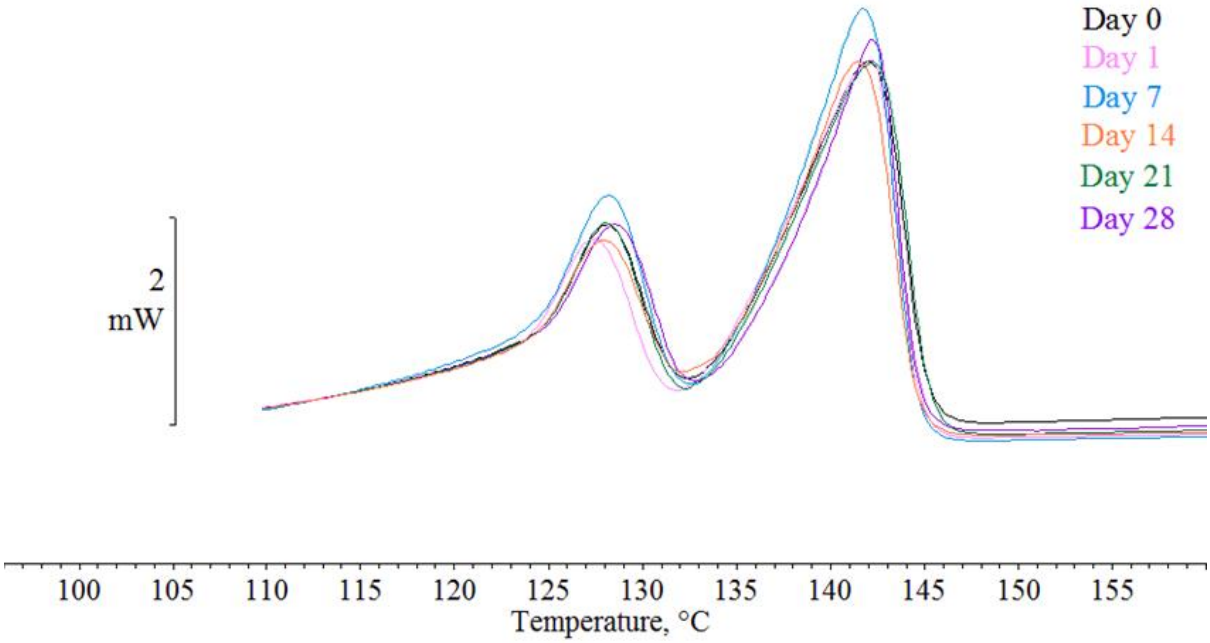

Figure 5.19. Change in the shape of the melting endotherm following storage of P(HB-co-HHx) at -22 ºC over 28 days

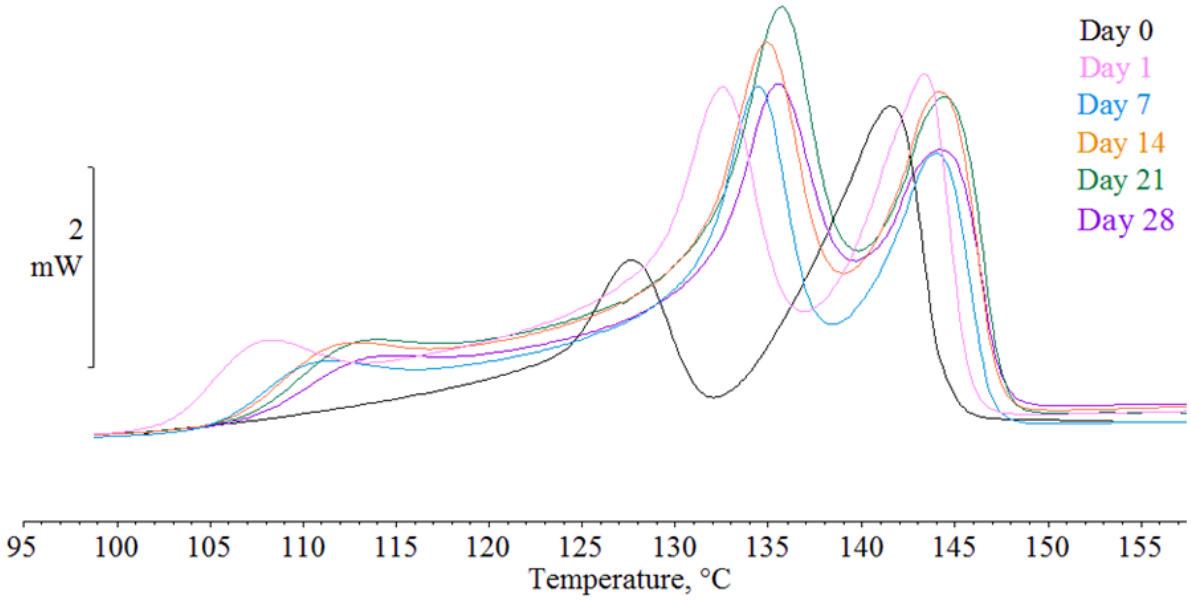

Figure5.20. Change in shape of the melting endotherm following storage of P(HB-co-HHx) at 100 ºC for 28 days

As expected in these studies, minimal changes occur in the samples stored below the T_g of the material, and therefore, the chains have no mobility which is required for the crystallisation process. It can therefore be concluded from these figures that the secondary crystallisation process does not occur at temperatures below the T_g, but as the temperature is increased above the T_g, the chains have increasing mobility, making the secondary crystallisation process easier where it occurs at a faster rate and to a greater extent due to more energy in the system. This confirms that samples stored in the freezer (which was a strategy employed to store samples that were not able to be tested immediately) are prevented from secondary crystallising.

5.1.2.1.2 Melt crystallisation

Melt crystallisation is a useful property to determine crystallisation behaviour of samples and can also indicate degradation within the samples. The results from the change in T_c temperature over time are shown below in Figure 5.21. The T_c of the samples remains relatively constant up to 50 ºC. This indicates that although the secondary crystallisation is enhanced at these temperatures, the samples are showing no signs of degradation. However, at temperatures of 75 ºC and above, a decrease in the T_c is observed over time with the largest effect occurring in the samples stored at 100 ºC.

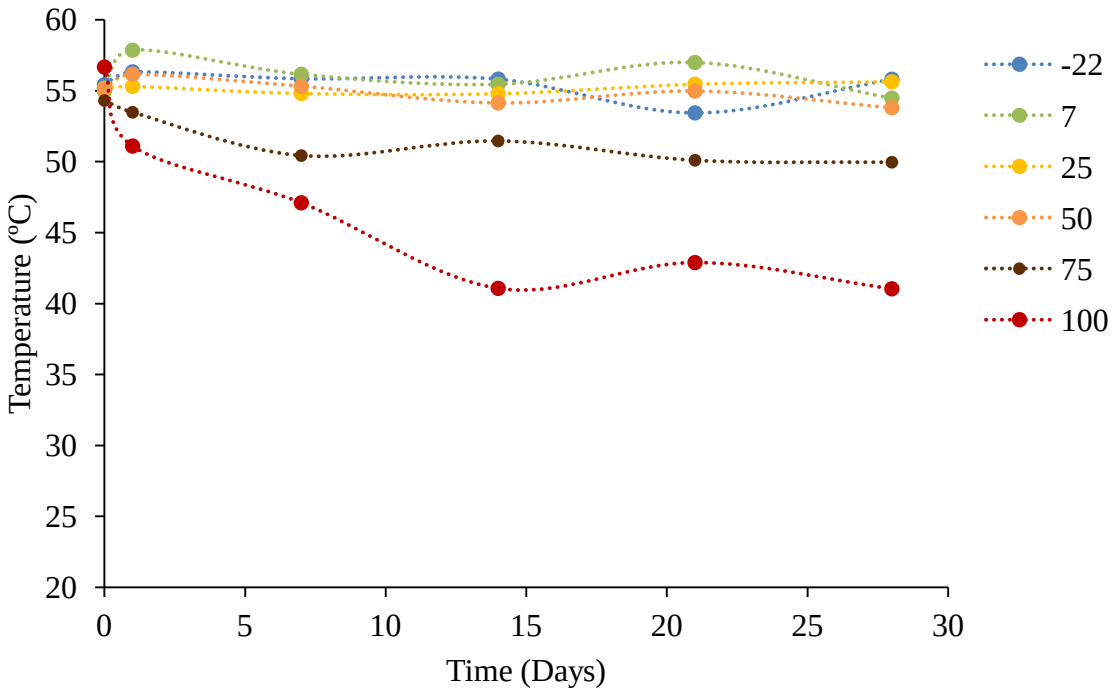

Figure 5.21. Change in T_c over time at each storage temperature

Visual examples of the shift and change in shape of the T_c curves are shown seen in Figure 5.22 and 5.23 comparing samples stored at -22 ºC and 100 ºC have been made. It can be observed that there is minimal change in samples stored at -22 ºC over 28 days as expected, however, in samples stored at 100 ºC, as well as the shift in T_c values, crystallisation also slows generating a broader crystallisation exotherm which could indicate degradation of the material.

There are conflicting theories on the behaviour of T_c in response to thermal degradation. In a paper by Luo and Netravali (2003), an increase in the value for T_c was observed from 110.6 ºC to 114.6 ºC as a result of a reduced M_w allowing ease of crystallisation upon cooling from the melt. However decreasing T_c (Janigová, Lacík et al. 2002, Di Lorenzo, Sajkiewicz et al. 2009) and increasing crystallisation time (El-Hadi, Schnabel et al. 2002) have previously been reported in PHB as a sign of thermal degradation. This was attributed to a decreasing

molar mass induced by chain degradation (Di Lorenzo, Sajkiewicz et al. 2009). The decreasing T_c with increasing temperature in this study therefore seems to conclusively indicate sub T_m thermal degradation of P(HB-HHx) at temperatures below its T_m.

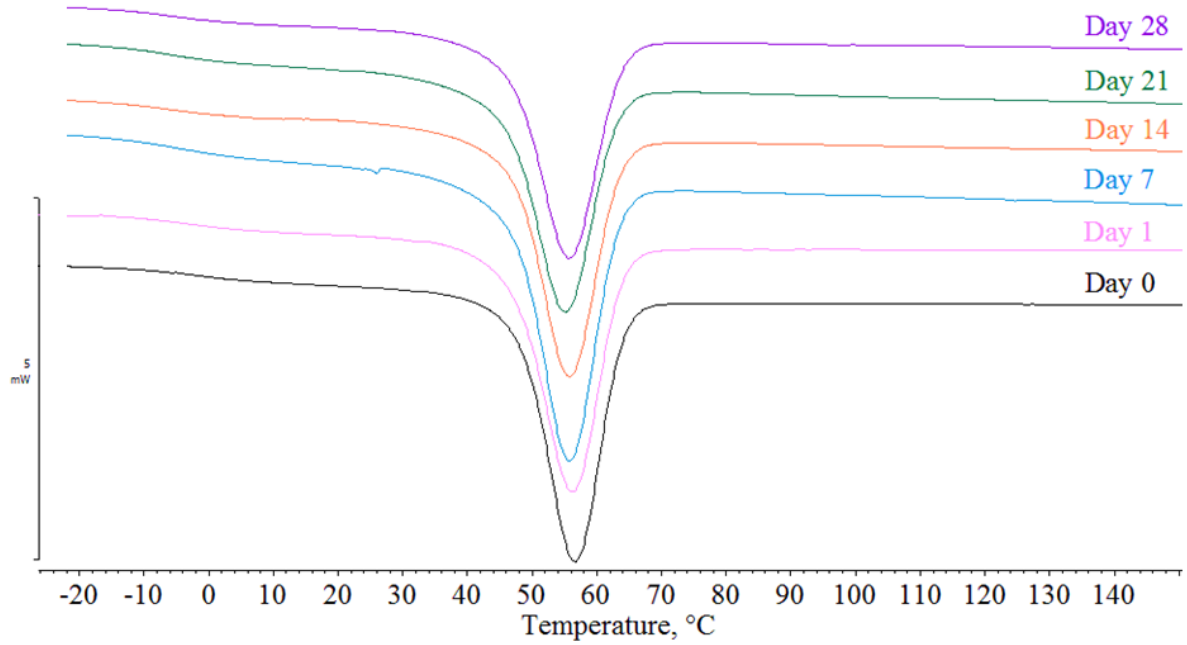

Figure 5.22. T_c of P(HB-co-HHx) following storage at -22 ºC over time

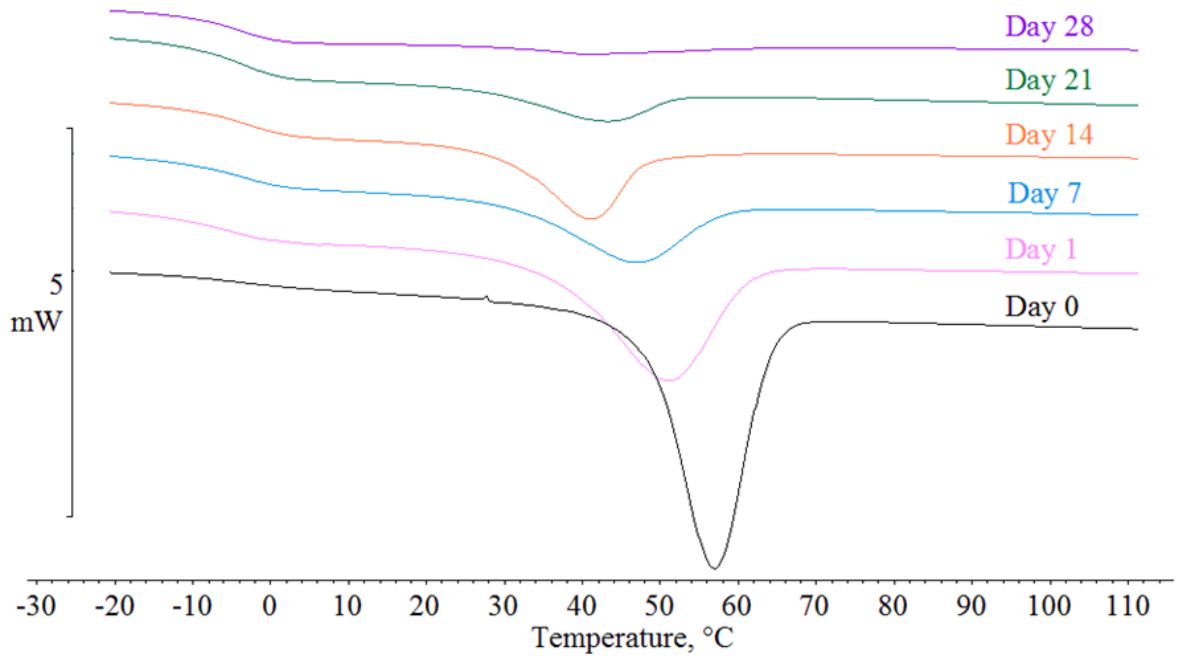

Figure 5.23. T_c of P(HB-co-HHx) following storage at 100 ºC over time

Figure 5.24 draws comparisons on the T_c curves from samples stored at each temperature stored for 28 days. It is apparent that with increasing storage temperature, the peak width increases while the peak height decreases. Figure 5.25 shows the effect of storage temperature on the enthalpy of crystallisation (ΔH_c). It can be seen that higher storage temperatures of 75 ºC and 100 ºC, leads to a decrease in ΔH_c decreases while samples stored between -22 ºC and 50 ºC produce similar values. This drop is most apparent in samples stored at 100 º C where the resulting peak is negligible (Figure 5.26). The exotherms begin to reduce in magnitude and begin to broaden at 25 ºC and 50 ºC, however, the onset of crystallisation and values for ΔH_c remain constant. This implies that as the storage temperature begins to increase, the broadening of the crystallisation exotherm is the result of an increasing molecular weight distribution

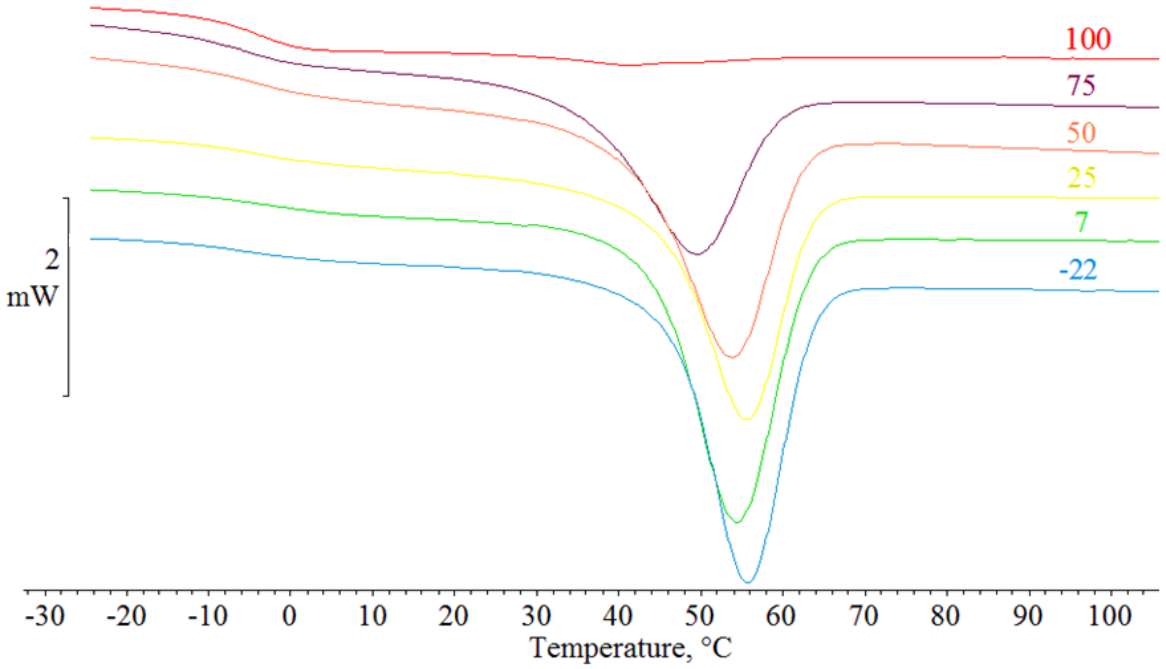

Figure 5.24. Effect of storage temperature on T_c of P(HB-co-HHx) following storage for 28 days

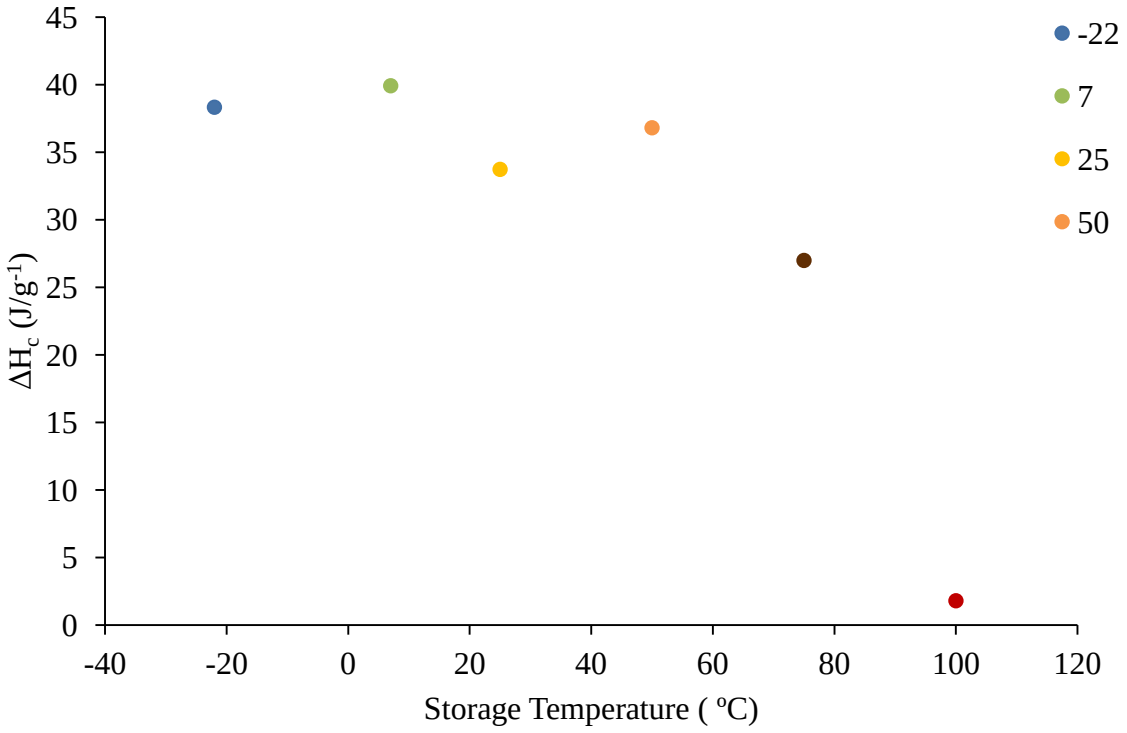

Figure 5.25. Effect of storage temperature on the ΔH_c of P(HB-co-HHx) following storage at each temperature for 28 days

5.1.2.1.3 Chemical changes

Increasing crystallinity can also be confirmed by changes observed by FTIR spectra. Figure 5.26 shows the carbonyl region over time in samples stored at -22 ºC, and peaks in the fingerprint region relating to amorphous and crystalline peaks are examined (Figure 5.27). It can be observed that there is minimal difference in spectra over the 28 day time period in samples stored at this temperature. In contrast, samples stored at 100 ºC show increased crystallinity following storage over 28 days. The carbonyl peak at this temperature (Figure 5.28) becomes sharper, and decreases on the amorphous side of the peak (1740 cm^{-1}) while the position of the peak does not shift over time . Furthermore, an increased intensity of the crystalline band at 1225 cm^{-1} with a decreasing intensity of the amorphous band at 1180cm^{-1} indicates an increase in crystallinity over the time frame observed (Figure 5.29) .. Samples stored at 25 ºC (Figures 5.30 and 5.31) present intermediate results between the those from samples stored at -22 ºC and samples stored at 100 ºC.

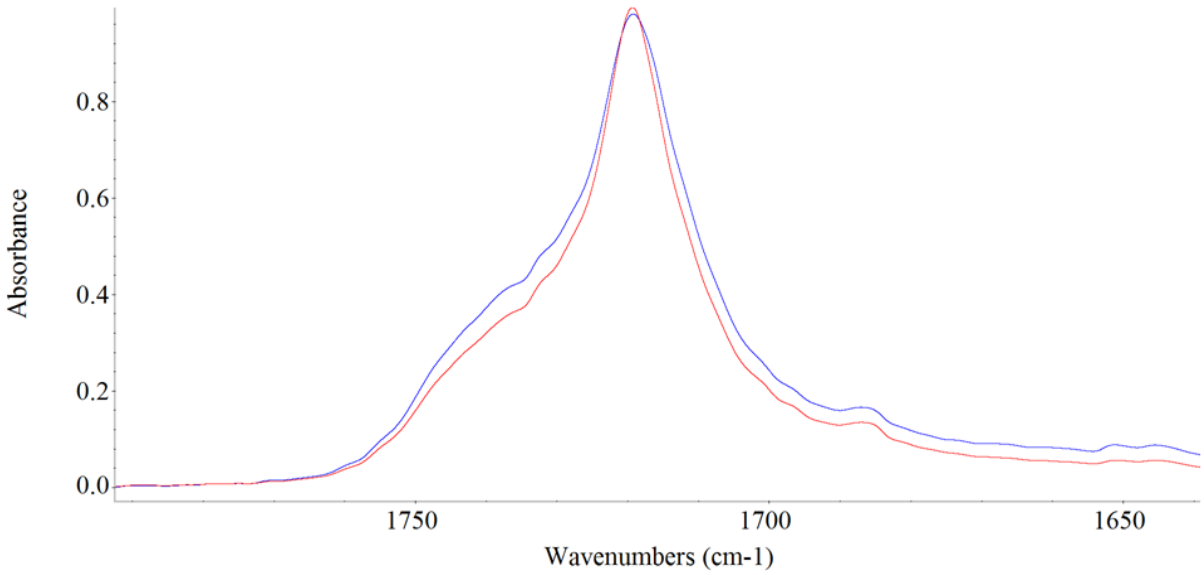

Figure 5.26. FTIR Spectra of the carbonyl peak for samples stored at -22 ºC over time. Day 0 (blue) Day 28 (red)

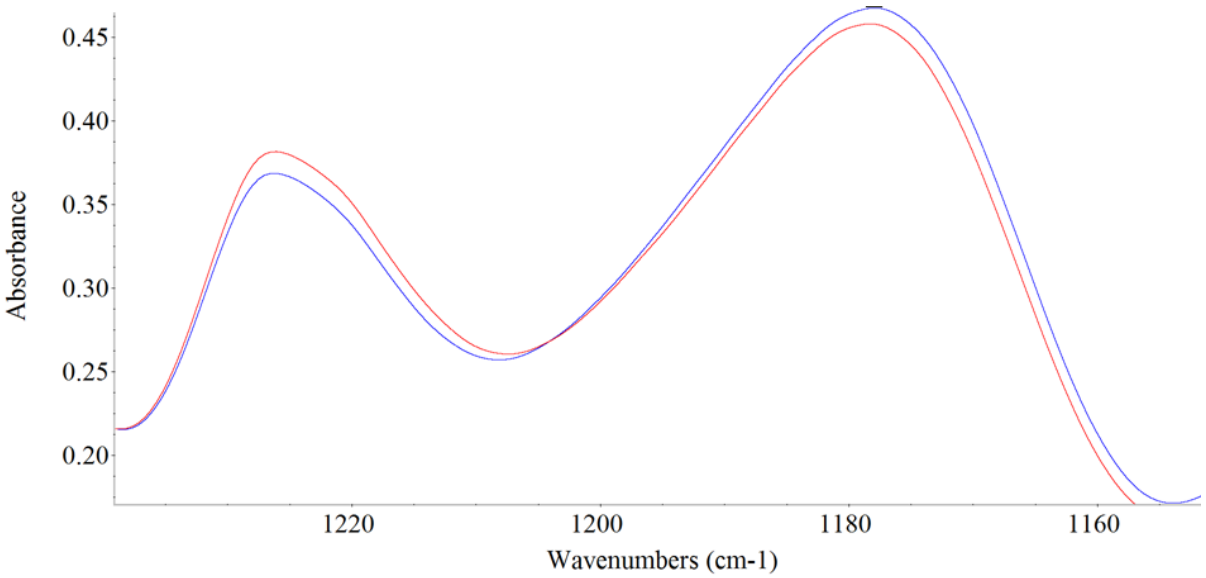

Figure 5.27. FTIR Spectra of the 1230 - 1160 cm^{-1} range located within the fingerprint region for samples stored at -22 ºC over 28 days . Day 0 (blue) Day 28 (red)

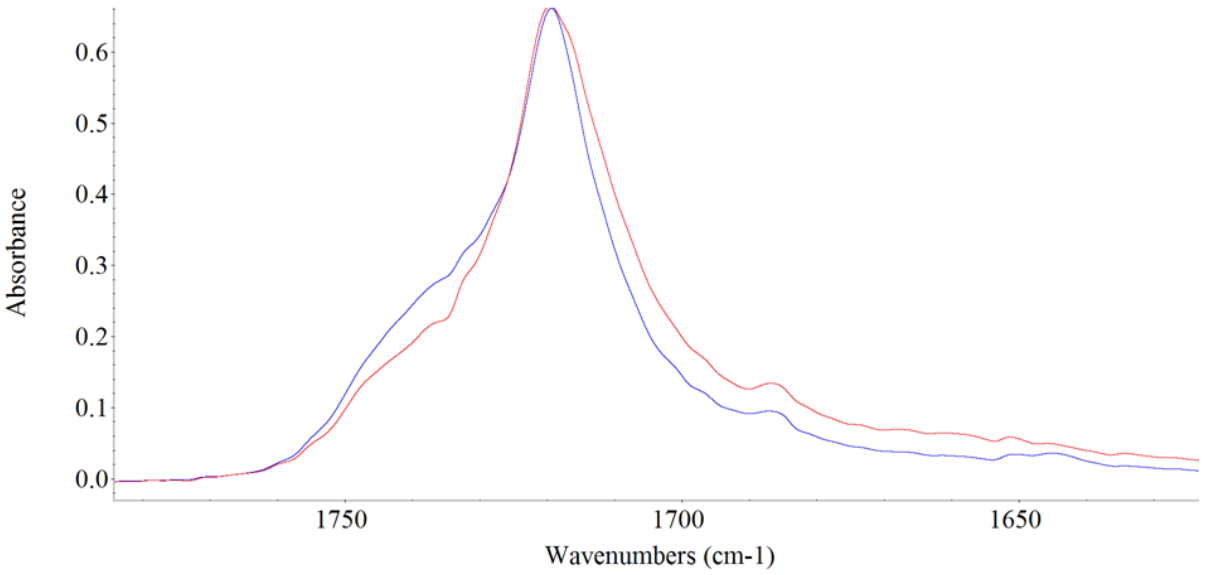

Figure 5.28. FTIR spectra of the carbonyl peak for samples stored at 100 ºC over time. Day 0 (blue) Day 28 (red)

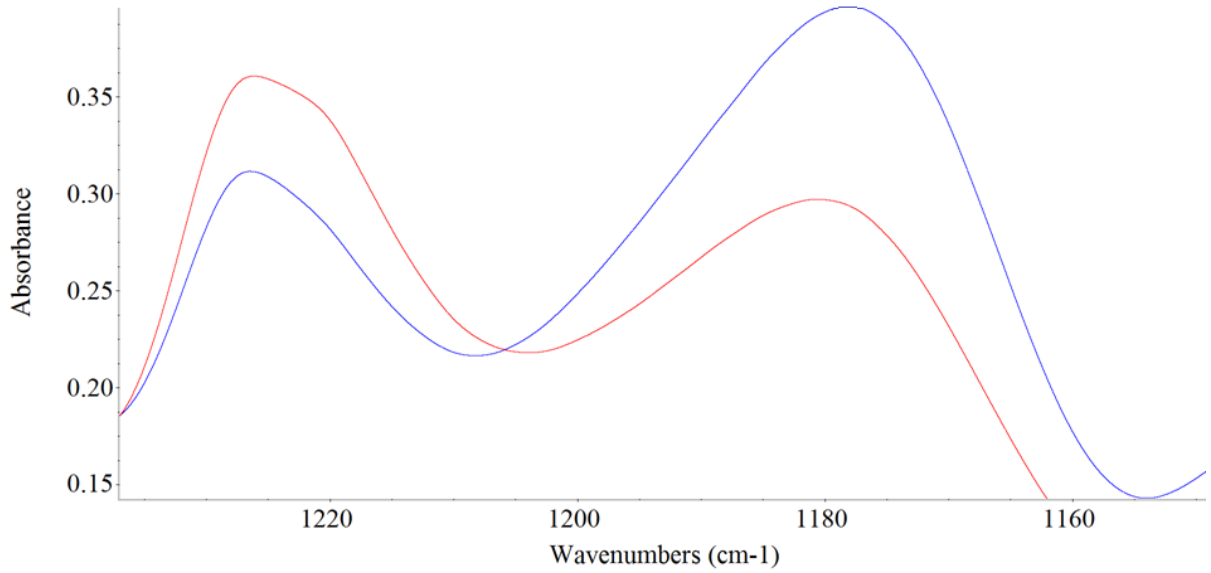

Figure 5.29. FTIR spectra of the 1240 - 1150 cm^{-1} range located within the fingerprint region for samples stored at 100 ºC over 28 days. Day 0 (blue) Day 28 (red)

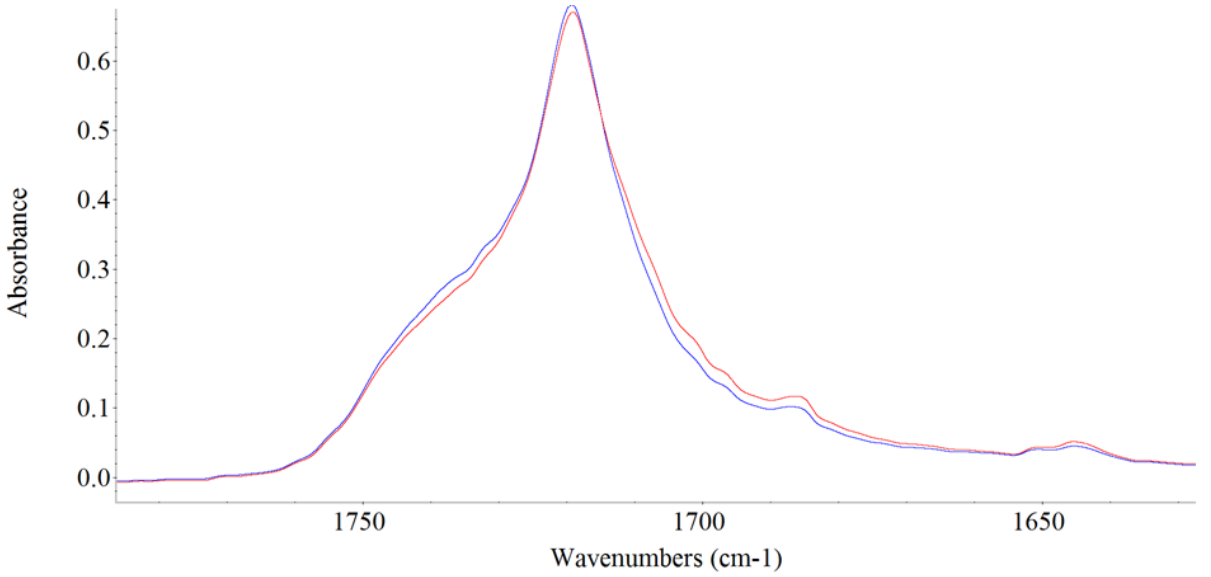

Figure 5.30. FTIR spectra of the carbonyl peak for samples stored at 25 ºC over time. Day 0 (blue) Day 28 (red)

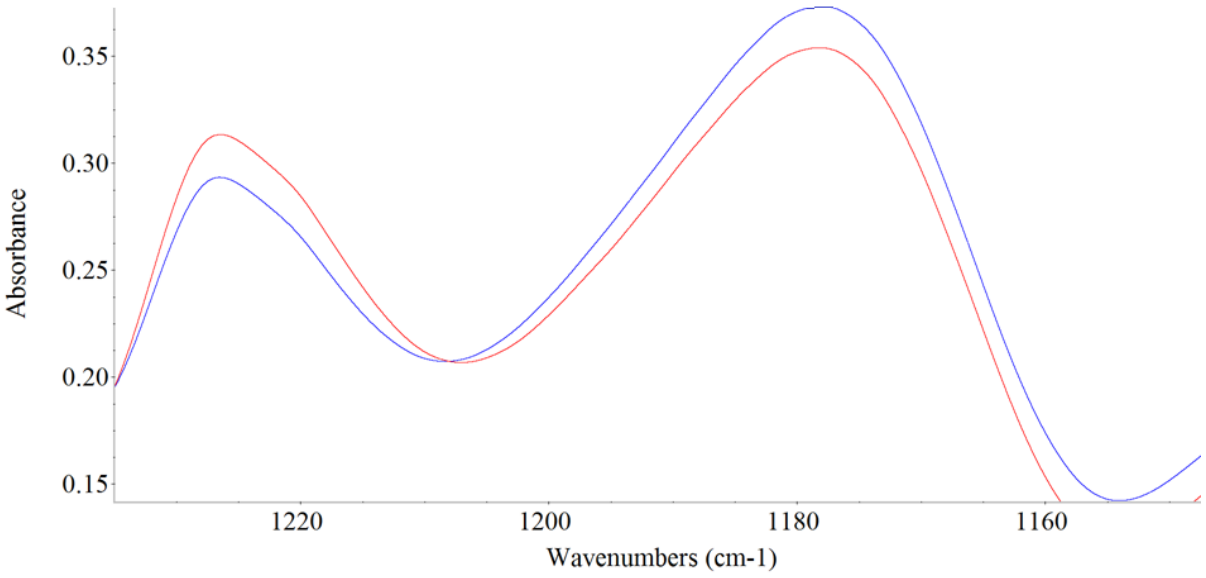

Figure 5.31. FTIR spectra of the 1230-1160 cm^{-1} range located within the fingerprint region for samples stored at 25 ºC over 28 days. Day 0 (blue) Day 28 (red)

Previous studies have shown the occurrence of a split carbonyl peak upon thermal degradation of P(HB-co-HHx). This has not been observed in this study however a shoulder begins to emerge at the top of the carbonyl following 28 days of storage as shown in Figure 5.28. Spectra from the other time points have been omitted from the analysis for clarity of the change between day 0 and 28 at each temperature but possess intermediate findings.

5.1.2.1.4 Visual inspection

The increase in crystallinity can also be observed macroscopically by obvious visual changes within the samples over time. Figure 5.32 shows samples stored at -22 ºC and 100 ºC for 28 days. It is apparent that while storage at -22 ºC shows no change compared to the day 0 material, storage at 100 ºC leads to a more opaque appearance clearly indicated by the disappearance of the purple line observed through the sample.

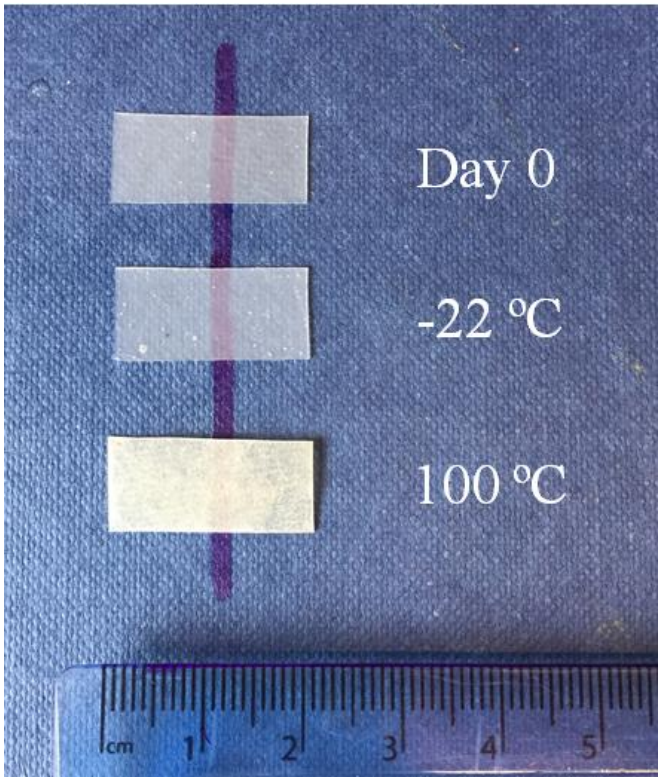

Figure 5.32. Effect of high temperature storage on the appearance and opacity of P(HB-co-HHx). Comparisons between samples post processing prior to storage (Day 0) and those stored at -22 ºC and 100 ºC for 28 days

5.1.2.2 Mechanical Properties

In order to investigate the effect of high temperature storage on the mechanical properties of P(HB-co-HHx), the samples were subjected to tensile testing. Elongation to break (E_b) has been found to be one of the properties that is strongly affected by the secondary crystallisation process (Figure 5.33). It is apparent that the sample stored below the T_g shows minimal changes over time (Figure 5.34). Any variations in the material at this temperature can be explained by sample variability and are within error. At 7 ºC, just above the T_g, a clear reduction in E_b over time can be observed, with the effect increasing as the storage temperature increases. The varying set of starting values obscure clear trends within the data sets for each temperature. Therefore the percentage change from original starting values was

also calculated for each set of samples in order to draw comparisons (Figures 5.34, 5.36, 5.38, 5.40).

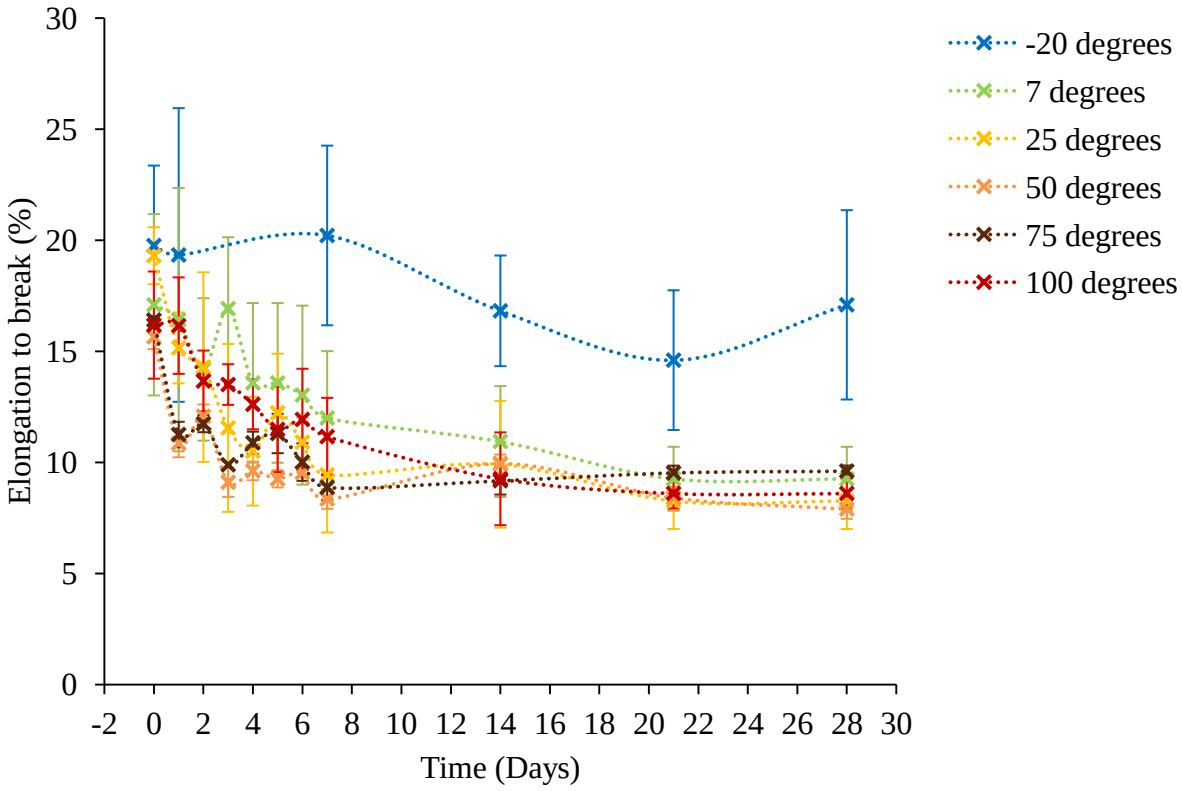

Figure 5.33. Change in elongation to break over time at each storage temperature

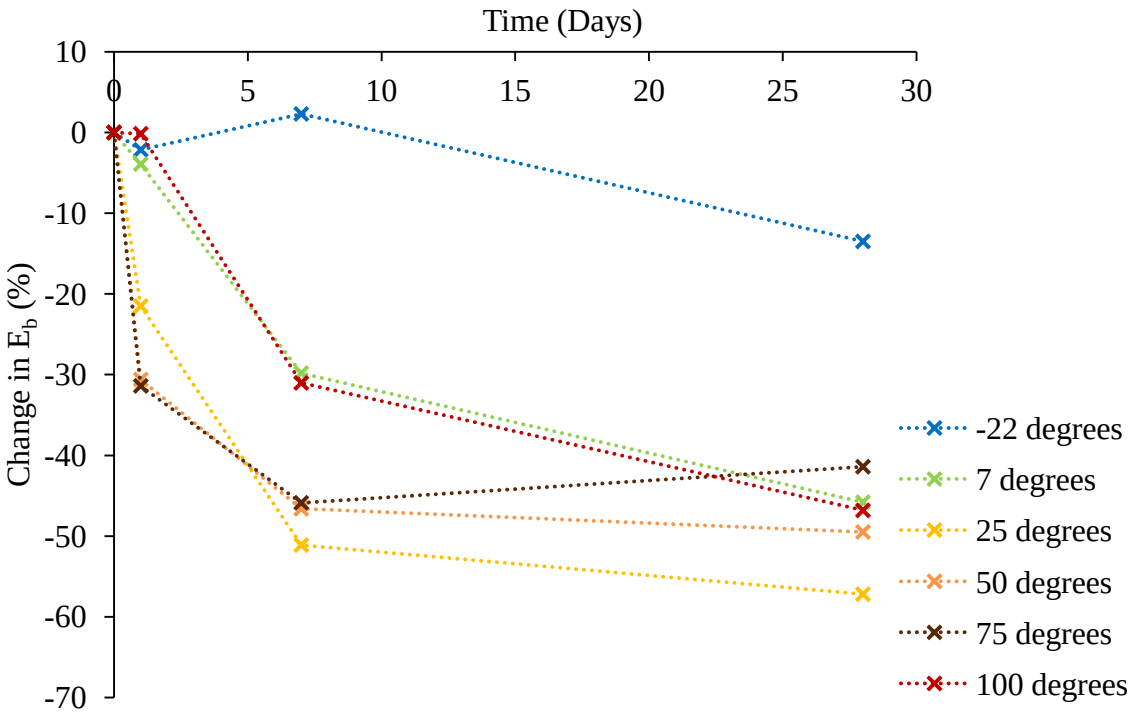

Figure 5.34. Percentage change in elongation to break over time at each storage temperature

It is evident that only minimal change occurs in the samples stored at -22 ºC, but as the storage temperature is increased above the T_g, a significant change of E_b over time can be observed (Table 5.3). The material stored at room temperature displays the greatest difference with a 57.2 % change from its original starting value, however all final values are similar to each other and within error. This indicates that the storage temperature doesn't significantly impact the end values of E_b of the material above the T_g, just the rate at which it gets to those values. This conflicts with the findings of Alata et al. (2007), who showed minimal changes to the properties of P(HB-co-HHx) in samples containing increasing HHx content (above 10 mol %) at room temperature.

Table 5.3. Initial and final values for E_b at each storage temperature after 28 days

Storage Temperature	Day 0	Day 28	% change
-22	19.8	17.1	13.5
7	17.1	9.3	45.8
25	19.3	8.3	57.2
50	15.7	7.9	49.5
75	16.4	9.6	41.4
100	16.2	8.6	46.9

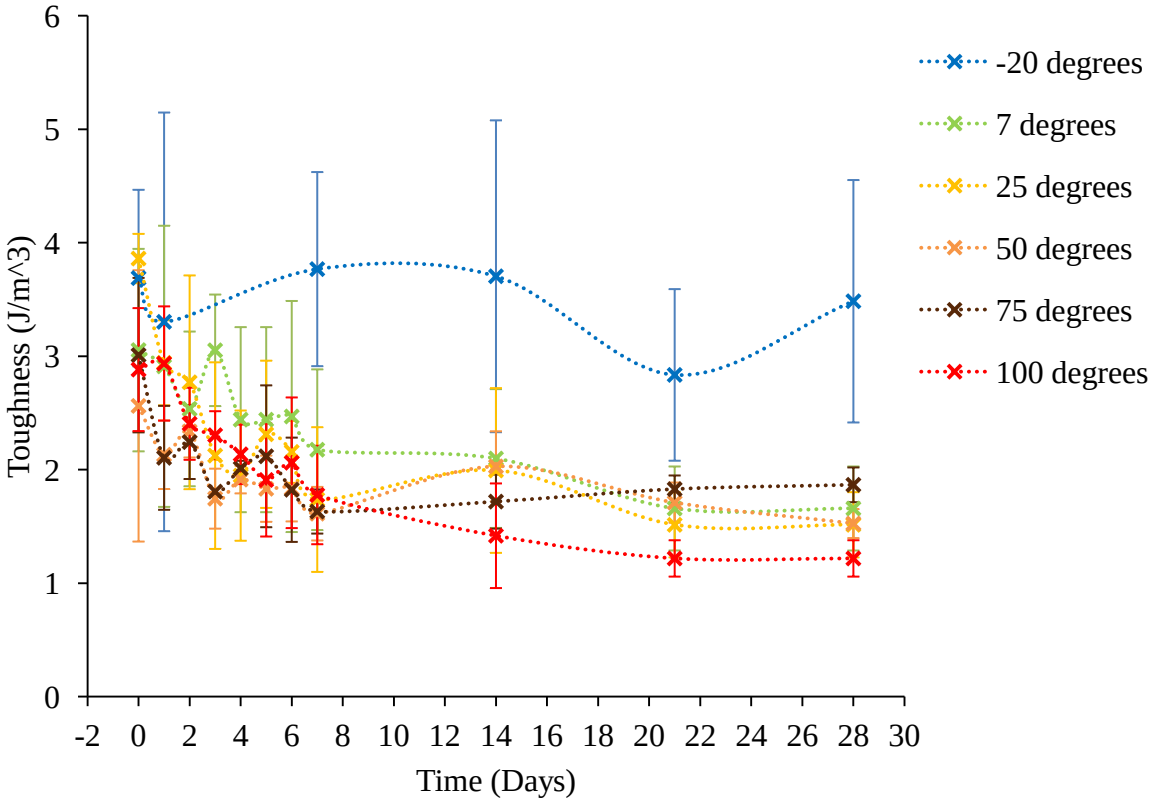

Figure 5.35. Change in Toughness over time at each sample temperature

Toughness is heavily dependent on the elongation to break, and they therefore show similar patterns of behaviour over time (Figure 5.35). Samples stored below the T_g exhibit negligible change over time, while samples stored above the T_g (7 ºC and upwards) display a reduction in toughness. This is because the secondary crystallisation process occurs, resulting in a less ductile material, in which the chains are less flexible as a result of the increased crystallinity, and therefore cannot absorb as much energy before fracture. These results are also reflected in Figure 5.36 and Table 5.4 and reflect similar results to Figure 5.34 and Table 5.3 to compare the behaviour of the material across all storage temperatures.

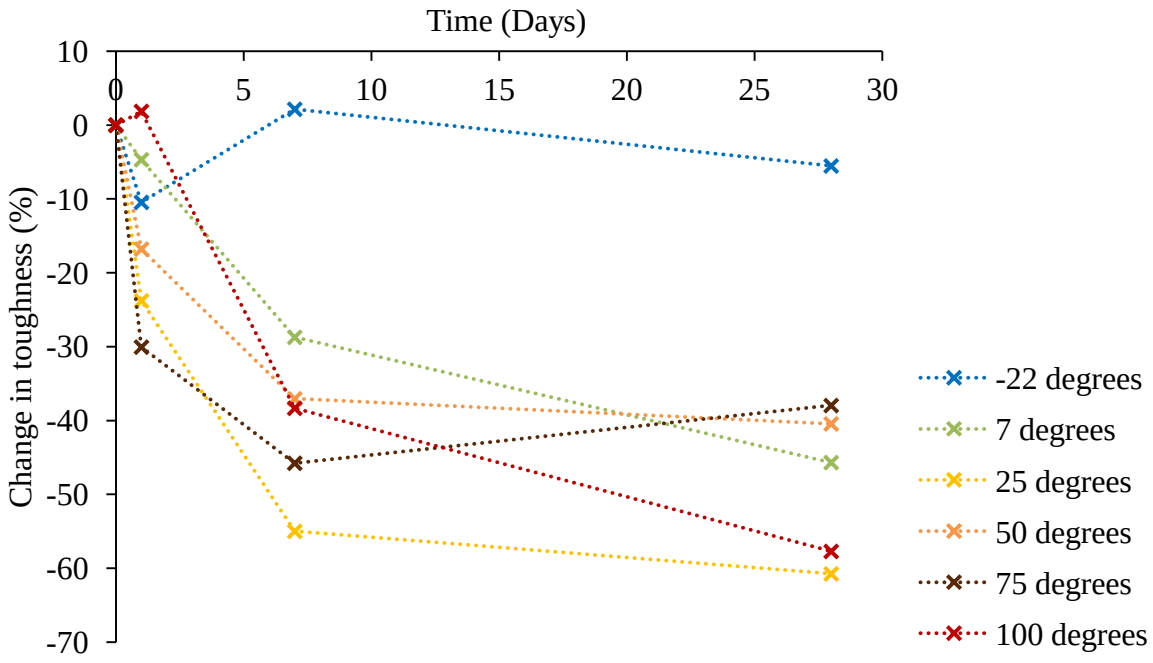

Figure 5.36. Percentage change in Toughness over time at each storage temperature

Table 5.4. Initial and final values for toughness at each storage temperature after 28 days

Storage Temperature	Day 0	Day 28	% Change
-22	3.7	3.5	5.5
7	3.1	1.7	45.7
25	3.9	1.5	60.8
50	2.6	1.5	40.4
75	3.0	1.9	38.0
100	2.9	1.2	57.7

Figure 5.37 shows the change in Young's Modulus over time at each storage temperature. From this graph, it can be seen that in samples stored at -22 ºC, showed minimal change over time as expected. As the temperature is increased to 7 ºC, the Young's Modulus starts to increase as the material secondary crystallises. This is because Young's Modulus relates to the stiffness of the material and as the material secondary crystallises the chains become more constrained leading to an increased stiffness of the material. As the temperature is increased, the Young's modulus of the material increases at a faster rate and to a greater extent up to 50 ºC where the increasing temperature leads to increased chain mobility and thus a faster secondary crystallisation process occurring (Figure 5.37).

However, as the storage temperature is increased to 75 ºC, the Young's modulus begins to change by less, occurring at a slower rate and to a lesser extent. There is another step down in E again in samples stored at 100 ºC. This therefore means that at storage temperatures of 75 ºC and above, the stiffness of the material still increases due to the secondary process, but not

as much as those stored at lower temperatures which could be another indicator of degradation within the material at 75 ºC and above. This is because, with thermal degradation of the material, chain scissions occur, leading to lower molecular weight material. It could therefore be the case that there are two conflicting processes occurring with secondary crystallisation acting to increase the stiffness of the material, but the chain scission as a result of degradation reducing the M_w of the material thus reducing the stiffness of the material. These results link with previous DSC melt crystallisation results showing that the T_c of the material isn't significantly affected until the material is stored at 75 ºC. It therefore seems fitting that degradation could be the cause of these results.

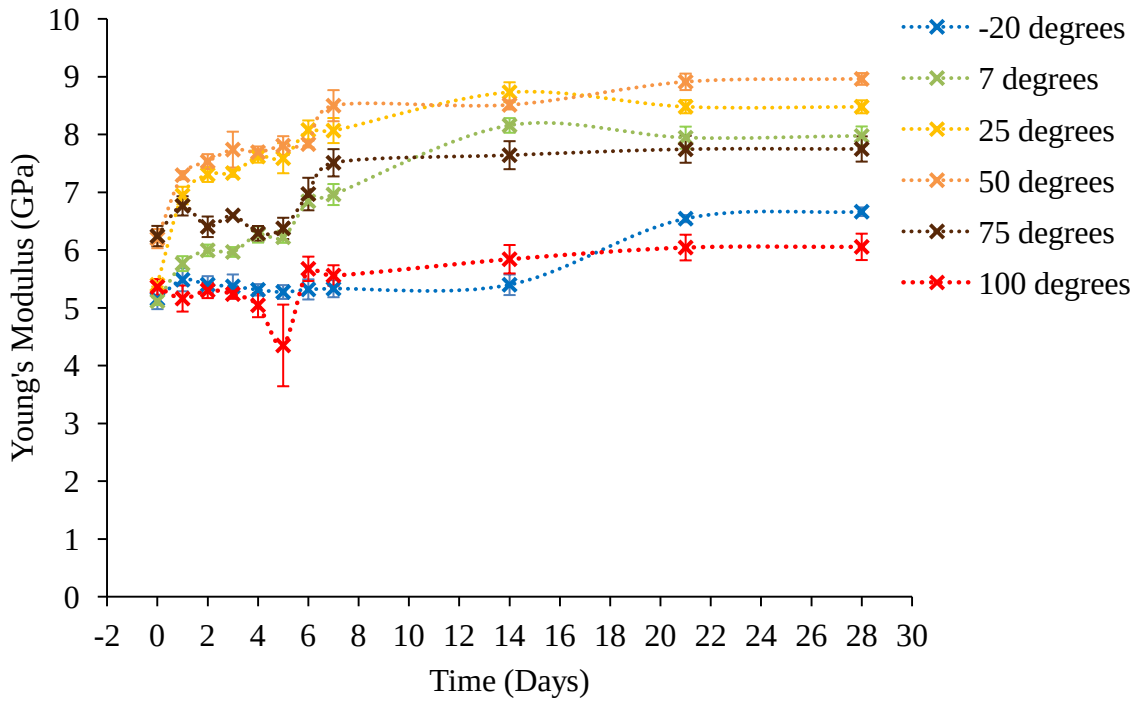

Figure 5.37. Change in E over time at each storage temperature

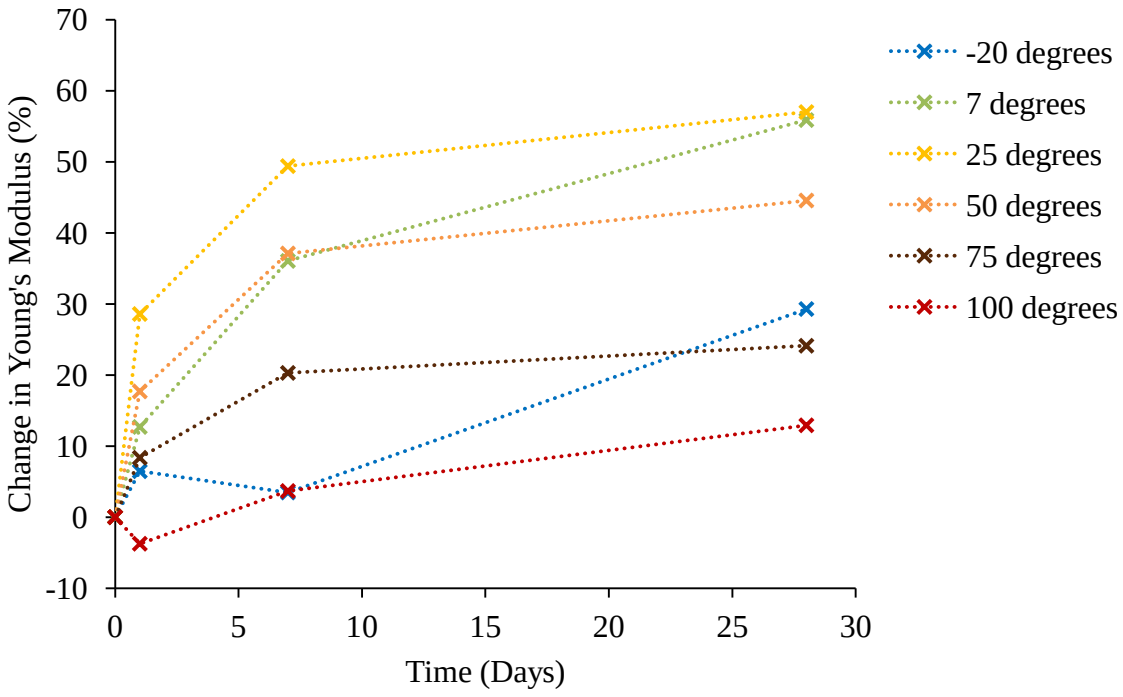

Figure 5.38. Percentage change in E over time at each storage temperature

Interestingly, when analysing the percentage change of the material over time at each storage temperature, it appears that the samples stored at 100 ºC change by the least amount and therefore results in this figure alone could be misleading. It is likely that with the two conflicting processes occurring within the material that the net change in stiffness is low, but it is important to note that this does not mean that the storage at 100 ºC has no effect on the material. Table 5.5 summarises the overall change within the material at each storage temperature.

Table 5.5. Initial and final values for Young's modulus at each storage temperature after 28 days

Storage Temperature	Day 0	Day 28	% change
-22	5.2	6.7	29.3
7	5.1	8.0	55.89
25	5.4	8.5	57.0
50	6.2	9.0	44.6
75	6.2	7.8	24.1
100	5.4	6.1	12.9

A similar result to the change in Young's modulus is also observed with UTS (Figure 5.39). At all sample storage temperatures, the UTS increases as time proceeds. The rate and extent of the change increases up to 50 ºC, and subsequently begins to decrease again at 75 and 100 ºC. This again can be linked to degradation of the material, whereby shorter chains with lower molecular weight will lead to reduced values for UTS. The molecular weight is reduced as a result of degradation, leading to fewer chain entanglements and therefore lower sample strength.

A similar effect on the percentage change for UTS can be compared to the Young's Modulus with an initial increase as the storage temperature increases up to 50 ºC followed by a less distinct change at temperatures above 75 ºC due to conflicting processes of degradation and secondary crystallisation occurring within the material (Figure 5.44 and Table 5.6).

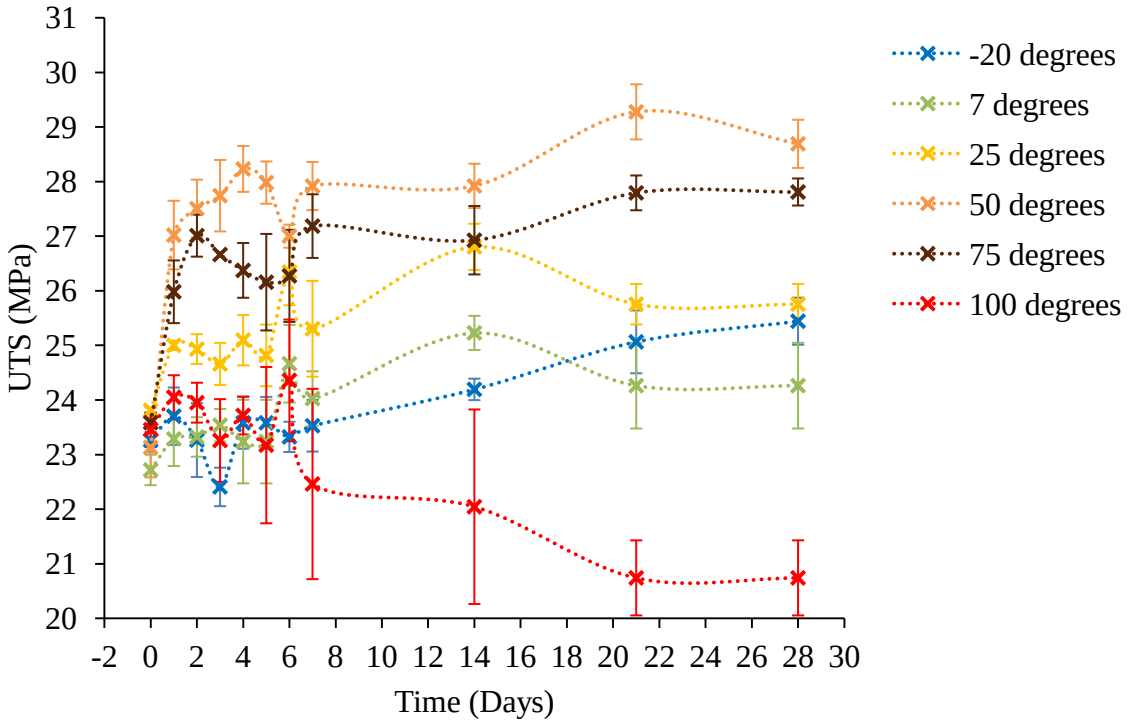

Figure 5.39. Change in UTS over time at each storage temperature

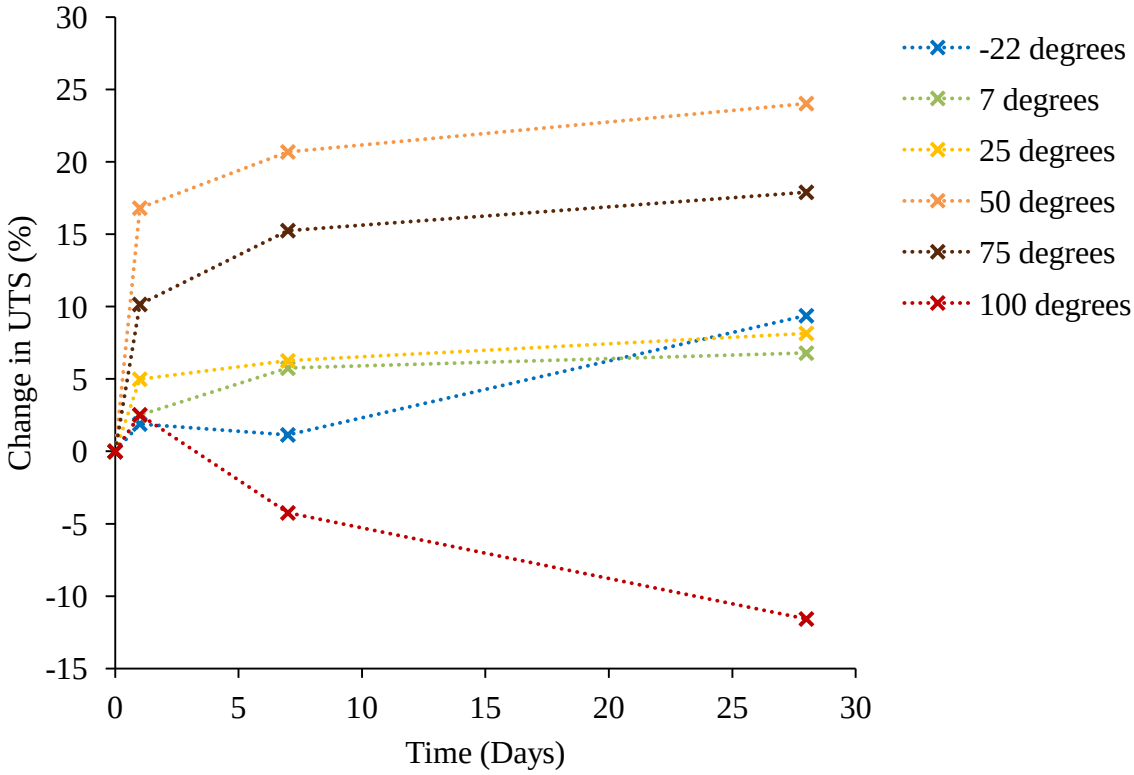

Figure 5.40. Percentage change in UTS over time at each storage temperature

Table 5.6. Initial and final values for UTS at each storage temperature after 28 days

Storage Temperature	Day 0	Day 28	% change
-22	23.3	25.4	9.4
7	22.7	24.3	6.8
25	23.8	25.8	8.2
50	23.1	28.7	24.0
75	23.6	27.8	17.9
100	23.5	20.7	-11.6

5.2 Conclusions

P(HB-co-HHx) (33 wt % HHx) was stored at -22, 7, 25, 50, 75 and 100 ºC to assess the effect of storage temperature on the secondary crystallisation process. Upon DSC analysis, P(HB-co-HHx) was observed to be a semi-crystalline material presenting double melting behaviour due to the melt-recrystallisation-remelting model. There is a large amount of variability in mechanical properties within the sample plaque, with the most likely cause attributed to differential cooling produced by un-even hot press plates and unilateral injection of coolant, leading to variable crystallinity within the sample plaque. This could have been analysed in more detail through DSC experiments to assess crystallinity values throughout the plaque in a similar manner to confirm this theory. Sample thickness appeared to show minimal effect on the mechanical properties of the material.

The P(HB-co-HHx) used within this work secondary crystallises at temperatures above its T_g . Characteristic effects of secondary crystallisation such as increasing T_m, X_c, Young's modulus and UTS, while E_b and toughness decreased in samples stored above the T_g of the material were reported due to the chains having sufficient mobility to re-organise. P(HB-co-HHx) displayed these characteristic behaviours at 7 ºC and above, where the rate and extent of the change for each property increased with increasing storage temperature. The greatest change occurs within 1 day of storage of the materials at each temperature while the amorphous fraction is at its highest. The change in mechanical properties is highest in samples stored at room temperature, as higher temperatures begin to degrade the material, consequently leading to conflicting effects of secondary crystallisation and degradation on the properties.

A low temperature shoulder appears on melting endotherms in samples stored at 25 ºC and above, further highlighting the secondary process. The position of this shoulder increases approximately linearly as a function of storage temperature following 28 days as a result of crystals of increasing perfection being formed at higher temperatures. This shoulder along with the increasing values for T_m at temperatures above the T_g indicate that both secondary crystallisation mechanisms (lamellar thickening and lamellar insertion) are occurring within P(HB-co-HHx) at elevated temperatures over time leading to the significant increase in values for degree of crystallinity and T_{m1} and $T_{m2.}$ It is important to note however that due to time constraints and availability of machinery, trends observed whilst monitoring the T_ms and crystallinity of the material were taken from one repeat, and therefore more repeats would be required to draw more accurate conclusions.

The samples appear to display sub-T_m degradation, a phenomenon not previously reported in PHB copolymers, upon storage of the material at 75 and 100 ºC. This is indicated by T_c shifting to a lower temperature, whilst values for UTS and Young's modulus declined A

reduction in T_c has previously been reported to occur due to reductions in molar mass following thermal degradation, but also likely to occur due to changes in the chemical structure of P(HB-co-HHx), making the intramolecular interactions required for crystallisation more difficult to form. Investigations into M_w via GPC would be required to analyse the possibility of chain scission and M_w distribution within the samples, and pyrolysis experiments should be considered to monitor degradation products of this copolymer in order to fully understand its degradation mechanism.

5.3 References

Abe, H. (2006). "Thermal degradation of environmentally degradable poly(hydroxyalkanoic acid)s." Macromol Biosci **6**(7): 469-486.

Alata, H., et al. (2007). "Effect of Aging on the Mechanical Properties of Poly(3-hydroxybutyrate-co-3-hydroxyhexanoate)." Macromolecules **40**(13): 4546-4551.

Aoyagi, Y., et al. (2002). "Thermal degradation of poly[(R)-3-hydroxybutyrate], poly[ε-caprolactone], and poly[(S)-lactide]." Polymer Degradation and Stability **76**(1): 53-59.

Ariffin, H., et al. (2008). "Determination of multiple thermal degradation mechanisms of poly(3-hydroxybutyrate)." Polymer Degradation and Stability **93**(8): 1433-1439.

Bugnicourt, E., et al. (2014). "Polyhydroxyalkanoate (PHA): Review of synthesis, characteristics, processing and potential applications in packaging." Express Polymer Letters **8**(11): 791-808.

Callister, W. D. and D. G. Rethwisch (2008). Fundamentals of Materials Science and Engineering. An Intergrated Approach. Asia, John Wiley and Sons.

Dennis, D., et al. (1998). "Formation of Poly(3-hydroxybutyrate-co-3-hydroxyvalerate) by PHA synthase from Ralstonia eutropha." Journal of Biotechnology **64**: 177-186.

Di Lorenzo, M. L., et al. (2009). "Optimisation of melting conditions for the analysis of crystallization kinetics of poly(3-hydroxybutyrate)." e-polymers.

El-Hadi, A., et al. (2002). "Correlation between degree of crystallinity, morphology, glass temperature, mechanical properties and biodegradation of poly (3-hydroxyalkanoate) PHAs and their blends." Polymer Testing **21**(6): 665-674.

Gabaue, W. (2000). The determinations of Uncertainties in Tensile Testing. Austria.

Gonzalez, A., et al. (2005). "Application of pyrolysis/gas chromatography/Fourier transform infrared spectroscopy and TGA techniques in the study of thermal degradation of poly (3-hydroxybutyrate)." Polymer Degradation and Stability **87**(2): 347-354.

Grassie, N., et al. (1984). "The thermal degradation of poly(-(d)-β-hydroxybutyric acid): Part 1—Identification and quantitative analysis of products." Polymer Degradation and Stability **6**(1): 47-61.

Hu, Y., et al. (2007). "Multiple melting behavior of poly(3-hydroxybutyrate-co-3-hydroxyhexanoate) investigated by differential scanning calorimetry and infrared spectroscopy." Polymer **48**(16): 4777-4785.

Janigová, I., et al. (2002). "Thermal degradation of plasticized poly(3-hydroxybutyrate) investigated by DSC." Polymer Degradation and Stability **77**(1): 35-41.

Kolb, R., et al. (2001). "Investigation of secondary crystallization of polymers by means of microbeam X-ray scattering." Polymer **42**(12): 5257-5266.

Luo, S. and A. N. Netravali (2003). "A study of physical and mechanical properties of poly(hydroxybutyrate-co-hydroxyvalerate) during composting." Polymer Degradation and Stability **80**(1): 59-66.

Nguyen, S., et al. (2002). "Thermal Degradation of Poly(3-hydroxyalkanoates): Preparation of Well-Defined Oligomers." Biomacromolecules **3**(1): 219-224.

Pan, P., et al. (2013). "Crystallization kinetics of bacterial poly(3-hydroxylbutyrate) copolyesters with cyanuric acid as a nucleating agent." Journal of Applied Polymer Science **129**(3): 1374-1382.

Sics, I., et al. (2001). "On the relationship between crystalline structure and amorphous phase dynamics during isothermal crystallization of bacterial poly(3-hydroxybutyrate-co-3-hydroxyvalerate) copolymers." Biomacromolecules **2**(2): 581-587.

Chapter 6
Conclusions and Further Work

6.1 Conclusions

In this work, P(HB-co-HV) (3wt%) and P(HB-co-HHx) (33 wt % HHx) were studied. P(HB-co-HV) was melt blended with glucose, fructose, maltose, and melezitose with three different concentrations based upon calculated crosslink ratios 87.94, 41.66, and 25.78, while CAB was added at 5, 10 and 15 wt %. Characterisation techniques including DSC, FTIR, DMTA, rheology, mechanical testing, SEM and Hot Stage Microscopy were used to analyse these blends. The secondary crystallisation behaviour of P(HB-co-HV)/CAB and saccharide blends, along with sub-T_m degradation of P(HB-co-HHx) were reported for the first time in this work.

Caramelisation occurred in all saccharide blends, resulting in brown coloured material, with the degree of colour change linked to the respective caramelisation temperature of each saccharide. Crosslinking between saccharides and P(HB-co-HV) did not seem to occur as expected, and the additives were found to have a detrimental effect on the initial mechanical properties of P(HB-co-HV), particularly at high concentrations. It can be concluded that the reduction in properties occurred as a result of hydrolytic degradation of the P(HB-co-HV) component, induced by the production of water during the caramelisation process of the saccharide during melt blending. This produced lower M_w chains which, in turn, acted to decrease the mechanical, thermal and rheological properties of the blends. Furthermore, the P(HB-co-HV) saccharide blends did not prevent the secondary crystallisation process from occurring as intended, however a chain length and compositional effect were observed on the process. As the chain length and composition of additive increased, the percentage change in

materials properties reduced, resulting in melezitose (trisaccharide), at the highest concentration being the most effective additive at resisting change. However, it should be noted that as high concentrations of additives reduced initial mechanical properties, the reduced percentage change over time offers no real advantage. One of the aims of this study was to investigate the commercial merit of the P(HB-co-HV)/saccharide blends, however, results have shown that these are not commercially viable options.

CAB was found to be partially miscible with P(HB-co-HV) within the composition range explored (0,5,10,15 wt % CAB). Decreasing T_m and crystallinity of the P(HB-co-HV) component indicate a level of interaction between the two components. Furthermore, leaching of the CAB component into the P(HB-co-HV) component suggests partial miscibility. Additional evidence of interaction was the effect of CAB on the crystallisation behaviour of P(HB-co-HV), showing a significant reduction in the rate of crystallisation with its addition . This was observed visually through hot stage microscopy where spherulite size had increased significantly as a result, with further confirmation through the reduction in T_c obtained by DSC, where the onset of crystallisation was delayed and the crystallisation process took longer as CAB content increased. The change in crystallisation behaviour was attributed to exclusion of CAB into the interlamellar amorphous regions while P(HB-co-HV) crystallised, with more CAB taking longer to expel. This lead to initial reductions in E_b, as larger spherulites are less mechanically stable, however values began to increase again as the ductile component of the blend was increased. Further increases would be expected at higher compositions of CAB.All additives blended with P(HB-co-HV) were found to secondary crystallise and therefore their presence did not hinder the process. This was characterised by increasing values for T_m, X_c, Young's modulus and UTS while the E_b and toughness of the materials decreased over time. In addition, the appearance and development of bimodal peaks on CAB 10 and 15 wt % blends over time confirms the presence of different crystal

morphologies resulting from the secondary process. Unlike the P(HB-co-HV)/saccharide blends, the properties were found to change to a greater extent in blends containing the highest concentrations of additives, indicating that in this instance CAB was acting to accelerate the process.There was minimal evidence of H-bonding occurring within the blends which was attributed to low hydroxyl content of the CAB. It is likely that with increased hydroxyl content, greater H-bonding will occur, leading to greater effects on the secondary crystallisation process. This should be addressed in further work to assess the success of this H-bonding mechanism on secondary crystallisation.

Analysis of inter-plaque variation in P(HB-co-HHx) presented high levels of variability in mechanical properties within the same sample plaque. This was attributed to un-even hot press plates and unilateral injection of coolant leading to variable crystallinity within the same sample. As all samples were produced by this hot press method throughout this work, it is likely that this has a strong influence on large errors presented in mechanical properties throughout.

In order to assess the effect of storage temperature on the secondary crystallisation process, P(HB-co-HHx) was stored at -22, 7, 25, 50, 75 and 100 ºC. Upon DSC analysis, the melting endotherm from heating at 10 ºC/min gave rise to a bimodal melting endotherm associated with the MRR model. Both of these peaks were measured and monitored throughout the study. Characteristic behaviours of secondary crystallisation such as increasing T_m (1 and 2), X_c, Young's modulus and UTS, with decreasing E_b and toughness were observed for P(HB-co-HHx) stored above the Tg (-2 ºC) over 28 days. . Therefore, such effects of secondary crystallisation were apparent following storage at 7 ºC, and occurred to the greatest extent at 25 ºC. A new low temperature endotherm forms following storage at 25 ºC and above, with the position of the endotherm increasing as the storage temperature increases. This indicates the formation of a new crystalline morphology that increases in perfection with increasing

storage temperature, further highlighting the effect of storage temperature at accelerating the secondary process. As expected, the greatest change in materials properties occurs within 1 day of storage of the materials at each temperature while the amorphous fraction is at its highest, with higher temperatures causing changes to occur at a greater rate due to there being more energy in the system creating more chain mobility and thus increased likelihood of chain interactions

The samples appear to display sub T_m degradation upon storage at 75 ºC and above, however further investigations into M_w are required to confirm this. Values for T_c, Young's modulus and UTS began to reduce at these temperatures where the secondary crystallisation process was competing with chain scissions resulting from thermal degradation. Visual discolouration of samples stored at 100 ºC provides additional evidence of degradation. This indicates that the degradation process in P(HB-co-HHx) occurs well below its melting temperature, which has not been reported to date in PHB copolymers and therefore provides a basis for further investigation.

6.2 Further Work

Due to availability of resources, the CAB available only contained 1.5 wt % hydroxyl groups. This functional group is fundamental to the H-bonding mechanism desired in this work. It would therefore be advantageous to analyse a series of CAB grades with varying quantities of hydroxyl groups, in order t to assess the effect of increasing the number of hydroxyl groups within CAB on the success of the H-bonding mechanism, and the resulting effect on the secondary crystallisation process. It is proposed that the addition of CAB with a higher proportion of hydroxyl groups per repeat unit could be more effective at reducing the secondary crystallisation process by creating more sites for crosslinking within the material, and thus have a greater influence on restricting chain mobility to prevent crystallisation.

It would also be advantageous to assess the secondary crystallisation process of CAB blends at higher percentages within the blends. Previous studies found that ther presence of CAB improved the properties of PHB (>20 wt %) therefore analysis of its influence on the secondary crystallisation process may also be beneficial. Another line of investigation could be the incorporation of thermoplastic starch into the blend to assess its ability to reduce secondary crystallisation within P(HB-co-HV). This has been found to significantly improve properties of PHB, however the secondary crystallisation behaviour of these blends is unknown and therefore is a possible avenue for future work.

Currently there are no studies assessing the thermal degradation of the P(HB-co-HHx) copolymer. Therefore, studies to investigate this further in terms of molecular weight studies by GPC would help to improve knowledge within this area, as well as pyrolysis experiments to assess any differences in degradation products and gain a better understanding of the degradation process. It would also be beneficial to look at higher temperatures above the T_m, and the response to this from other PHB copolymers for comparison.